ABSTRACT

Title of Document: **CARBON AND NITROGEN SOURCES AND CYCLING IN PLANKTONIC MARINE ECOSYSTEMS**

David P. Keller, Ph.D., 2010

Directed By: Professor Raleigh R. Hood

Marine-Estuarine-Environmental Sciences

Carbon and nitrogen are involved in many important biological and environmental processes and can even influence the global climate (i.e. CO_2 as a greenhouse gas). In this dissertation the role of dissolved organic matter (DOM) in marine C and N cycling is studied. Research is also presented that looks at phytoplankton as potential sources of C and N in the upper Chesapeake Bay estuary food web.

To better understand DOM cycling a model was constructed to simulate dissolved organic carbon (DOC) and nitrogen (DON) cycling in marine surface waters. Using the model DOM cycling was simulated in the context of: (1) a steady-state comparison of idealized oceanic, coastal, and estuarine ecosystems, (2) the seasonal cycle in eutrophic waters, and (3) a focus on the roles of viruses and microzooplankton. The results suggest that DOM cycling is intricately tied to the biomass concentration, ratio, and productivity of phytoplankton, zooplankton, viruses, and bacteria. The first set of simulations highlights the importance of certain

processes in each ecosystem. The second set of simulations shows how DOM cycling, particularly the sources of DOM, changes seasonally. The third set of simulations highlights differences in the top-down and bottom-up roles of viruses and microzooplankton and their subsequent effect on DOM cycling and trophic interactions.

To better understand C and N cycling in the upper Chesapeake Bay the biomass distribution and floral composition of the phytoplankton community was studied during the winter and spring to determine if phytoplankton could play an important role in the estuarine turbidity maximum (ETM) food web. This research suggests that the general distribution of phytoplankton in the upper Bay is somewhat like a classic estuarine "salt wedge" diagram with two distinct phytoplankton communities separated by a zone of increased mortality due to salinity stress and ETM entrapment. High concentrations of phytoplankton pigment degradation products were often observed in the ETM suggesting that this is an area of high phytoplankton mortality and/or an area where phytoplankton derived particulate organic matter was being concentrated. These results suggest that phytoplankton have the potential to play an important role in C and N cycling and the ETM food web.

CARBON AND NITROGEN SOURCES AND CYCLING IN PLANKTONIC MARINE ECOSYSTEMS

By

David Peter Keller

Dissertation submitted to the Faculty of the Graduate School of the
University of Maryland, College Park, in partial fulfillment
of the requirements for the degree of
Doctor of Philosophy
2010

Advisory Committee:
Professor Raleigh R. Hood, Chair
Associate Professor Byron C. Crump
Assistant Professor Elizabeth W. North
Associate Professor K. Eric Wommack
Associate Professor Patrick C. Kangas, Dean's Representative

Acknowledgements

This dissertation would not have been possible without the support of my adviser, Dr. Raleigh R. Hood. I am very grateful for his patience and tireless efforts to help me succeed. I would also like to thank my committee: Drs. Byron C. Crump, Elizabeth W. North, K. Eric Wommack, and H. Rodger Harvey. Each one of them contributed to this dissertation and my development as a graduate student. I greatly appreciate their time and dedication.

I would also like to thank my colleagues from both the DOMINO and BITMAXII programs for their support, discussions, and shared expertise. Dr. Danielle Winget was especially helpful in sharing data with me from the Microbial Observatory for Virioplankton Ecology (MOVE). I would also like to thank Dr. Anne Thessen for identifying Chesapeake Bay phytoplankton for me.

I would also like to thank the National Science Foundation for funding the DOMINO (OCE-0221825) and BITMAXII (OCE-0453905) programs that have supported the majority of my research. My dissertation work would also not have been possible without funding from Horn Point Laboratory for travel, a small research grant, and two teaching assistantships.

Table of Contents

List of Tables

List of Figures

Abbreviations

DOM	Dissolved organic matter
CDOM	Colored dissolved organic matter
DOC	Dissolved organic carbon
DON	Dissolved organic nitrogen
HMW	High molecular weight
LMW	Low molecular weight
DIC	Dissolved inorganic carbon
DIN	Dissolved inorganic nitrogen
DIP	Dissolved inorganic phosphorus
ETM	Estuarine turbidity maximum
UV	Ultraviolet
HPLC	High performance liquid chromatography
CTD	Conductivity temperature depth
PC	Particulate carbon
PN	Particulate nitrogen
POC	Particulate organic carbon
PON	Particulate organic nitrogen
CBP	Chesapeake Bay Program
MOVE	Microbial Observatory for Virioplankton Ecology
TSS	Total suspended solids
PAR	Photosynthetically active radiation
Chl *a*	Chlorophyll *a*

Introduction

Carbon and nitrogen are key elements that are necessary for life on this planet. These elements also play important roles in a number of environmental processes and can even influence the global climate (i.e. CO_2 as a greenhouse gas). Due to their chemical properties these elements can be found in many states and are transferred frequently between environmental pools and living organisms. Primary production by plants is one of the most important drivers of these transfers and plays an especially important role in the global C cycle. While understanding the C cycle has been of particular interest recently because of the link to climate change, C cycling cannot be understood without looking at other elements because primary production is usually not limited by C, but by N, P, or other elements (Elser et al., 2007; Saito et al., 2008). Thus there is a biologically driven link between C and N cycling.

Marine phytoplankton contribute to roughly half (48%) of the biosphere's net primary productivity (Behrenfeld et al., 2006b; Carr et al., 2006) and thus have a large influence on global biogeochemical cycling. Phytoplankton production is very dynamic with the annual mean productivity of 45-50 Gt C being carried out by phytoplankton with a biomass of ~ 1 Gt C (Carr et al., 2006) and an estimated to turn over time (i.e. replacement time) of two to six days (Behrenfeld and Falkowski, 1997). Most of this rapid turn over is due to sinking, grazing, (Behrenfeld et al., 2006b) or other biological processes like cell lysis (Fuhrman, 1999). As a result of these processes much of the C and N that is fixed by phytoplankton flows through marine food webs.

Unfortunately, the interactions between the environment, nutrients, and marine food webs are often so complex that determining exactly how C and N are being

transferred is very difficult. In some planktonic food webs zooplankton grazing appears to control phytoplankton abundance and primary production (top-down control) while in other systems phytoplankton production appears to be regulated by the availability of light and nutrients (bottom-up control) (Glibert, 1998). Further complicating our understanding of these systems are measurements which show that in many aquatic ecosystems respiration exceeds local primary production (Del Giorgio and Williams, 2005; Thorp and Delong, 2002), indicating that the system is net heterotrophic. In addition, there are also many marine communities whose heterotrophic biomass exceeds their autotrophic biomass (Gasol et al., 1997). The food webs and sources of organic matter in these heterotrophic ecosystems are often very different from autotrophic ecosystems, even though they are both ultimately driven by primary production. For example, Cole and Caraco (2001) suggest that the net heterotrophy measured in the Hudson river is driven in part by very old (>1000 years) organic matter of terrestrial origin. Compared to a classic autotrophic system where local primary production supplies the organic matter that drives the food web it is easy to see how these types of differences can affect C and N cycling. Furthermore, some systems such as the Chesapeake Bay, USA are dominantly autotrophic in the spring and become more heterotrophic as the year progresses (Bronk et al., 1998), which adds a seasonal component to C and N cycling. Despite decades of study to address the role that biology plays in these cycles there is still much to learn about marine C and N cycling. The research presented in this dissertation focuses on the role that dissolved organic matter (DOM) plays in the food web and in C and N cycling and also looks at food web sources of C and N in estuaries like the Chesapeake Bay.

Dissolved Organic Matter Cycling

Fifty percent, or more, of the carbon fixed by phytoplankton eventually flows through the DOM pool where much of it is consumed by bacterioplankton (del Giorgio and Cole, 1998; Ducklow and Carlson, 1992). Thus, interactions between the food web and pools of DOM must be understood to fully constrain marine C and N cycling. However, these interactions are complex and involve a number of chemical and biological processes (Fig. I, adapted from Carlson (2002)). Processes that produce marine DOM include extracellular release by phytoplankton (Baines and Pace, 1991; Nagata, 2000), grazer mediated release (i.e. sloppy feeding) and excretion (Møller, 2005; Møller and Nielsen, 2001; Nagata and Kirchman, 1991; Steinberg et al., 2000; Steinberg et al., 2002), release via cell lysis (both viral (Wommack and Colwell, 2000) and bacterial (Carlson, 2002)), the solubilization of particles (Smith et al., 1992), and bacterial transformation and release (Tanoue et al., 1995). In coastal and estuarine waters DOM may also originate from terrestrial sources (Hopkinson et al., 1998; Mannino and Harvey, 2000). DOM is removed from marine waters mainly by bacterial consumption (Azam et al., 1983) but can also be removed by eukaryotic uptake (Berman and Chava, 1999; Mulholland et al., 2002), phototransformation (Benner and Biddanda, 1998; Smith and Benner, 2005), and sorption onto particles (Druffel et al., 1996).

A significant amount of research has been conducted to understand DOM cycling in marine systems and there are now accurate estimates of many of the biological, chemical, and physical processes involved (Hansell and Carlson, 2002). However, despite decades of work there are still some fundamental aspects of DOM cycling that are poorly understood. Limited data exist on the distribution of DOM throughout the oceans

and our understanding of its spatial and temporal variability is based on relatively few measurements at key oceanic sites. Furthermore, a mechanistic understanding of the processes that control this variability is often lacking (Hansell, 2002). Understanding the complexities of DOM cycling has been particularly difficult because the composition of DOM in surface waters has only been characterized at the molecular level for 4 to 11% of the DOC and 7 to 14% of the DON, while in deep water only 1-3% of the DOC and 4-9% of the DON has been characterized as recognizable biochemicals (Benner, 2002). Methodological limitations have also made it difficult to quantify rates of DOM production and removal and our knowledge of some processes is based on extremely small and largely inadequate datasets. An incomplete understanding of the ecology and physiology of many microbial organisms has also made it difficult to quantify the role of biology in DOM cycling.

Models are one of best tools available for understanding the complex, and often un-measurable, interactions that drive these cycles. However, models to date have not included enough detail to fully constrain the role of biology and DOM in marine C and N cycling. Early ecosystem models that included DOM such as the models of Fasham et al. (1990) and Taylor and Joint (1990) included labile DOM and heterotrophic bacteria as state variables, but no slow-turnover DOM pools. Considering that most marine DOM is very old and resistant to biological degradation (Benner, 2002) these representations were not very realistic even though they provided us with valuable insights into C and N cycling. More recent models such as the model of Anderson and Williams (1999) have focused on the longer-lived pools of DOM and the processes that produce DOM. However, many of these models have run into problems describing the turnover rates of

these pools and some of the fundamental processes that produce, transform, and consume the DOM (Christian and Anderson, 2002).

Turnover rates of DOM have been particularly difficult to model because the correlation between molecular weight (used to measure and classify DOM) and lability is very weak. Bacteria cannot directly take up high-molecular weight organic matter because it is too large to be transported across their cell membranes. However, bacteria can take up low-molecular weight organic matter and so must enzymatically hydrolyze high-molecular weight organic matter into simple monomers in order to utilize them. Thus, in principal high-molecular weight organic matter should be utilized more slowly than low-molecular weight organic matter (Christian and Anderson, 2002). However, high-molecular weight material can be highly bioreactive, while low-molecular weight organic matter which comprises the bulk of oceanic DOM is often taken up very slowly or not at all by bacteria (Amon and Benner, 1996). Therefore, many researchers have categorized DOM as labile, semi-labile, and refractory on the basis of turnover rates with labile material turning over in a matter of minutes or days, semi-labile material turning over in weeks to months, and refractory material turning over in years or not at all. While this classification is useful from some perspectives it makes it difficult to compare observations of DOM, which are often reported in terms of molecular weight, with models that classify DOM according to its bioavailability. Furthermore, the bioavailability of DOM has been applied differently in the literature with the semi-labile pool, as defined above, described as both labile (e.g., Six and Maier-Reimer (1996)) and refractory (e.g. Levy et al. (1998)). In addition, few models have included a long-lived

refractory pool, even though this pool comprises most of the DOM in marine waters (Christian and Anderson, 2002).

Simulating the individual processes that produce, transform, and remove DOM has been difficult for a number of reasons. Many biogeochemical models have not included enough biological state variables to fully constrain some processes such as viral lysis. Modeling efforts have also been limited by a lack of data for parameterization and validation (Christian and Anderson, 2002). Furthermore, some of the most fundamental processes, like phytoplankton extra cellular release, still lack an adequate numerical description (Flynn et al., 2008).

Since experimental and observational research on DOM cycling is ongoing models must be constantly created or revised to account for new discoveries. Much of the most recent research on processes such as sloppy feeding, viral lysis, and viral decay has yet to be included in ecosystem modeling studies. Large sets of data are available for a number of marine ecosystems and many of them have yet to be used in numerical simulations of DOM cycling. In addition to working with available data, new models must also be developed to generate theoretical predictions that can be used to guide future experimental research.

Sources of Carbon and Nitrogen in Estuaries and Turbidity Maxima

Estuaries are an important transition zone between terrestrial and aquatic systems and thus have carbon and nitrogen cycles with linkages to each system. Because of the linkages between terrestrial and aquatic systems the structure and dominant pathways of energy flow through an estuarine food web are strongly influenced by the amount of

terrestrial organic matter and nutrients that flow into it and the physical process that occur when freshwater mixes with saltier estuarine water.

In some estuaries the food web appears to be primarily autotrophic with zooplankton grazing directly on riverine or estuarine phytoplankton (Winkler et al., 2003). However, in many estuaries, and the rivers that flow into them, turbidity limits light and consequently phytoplankton biomass and productivity are low (David et al., 2006; Thorp and Delong, 2002). Measurements often indicate that these regions are heterotrophic as well (Kemp et al., 1997a; Smith and Kemp, 1995; Thorp and Delong, 2002). Additionally in some estuaries, turbidity and hydrodynamic processes may play an especially important role in the food webs due to the formation of an estuarine turbidity maximum (ETM). ETMs are common physical features that are typically located at the heads of coastal plain estuaries near the freshwater/saltwater interface (Schubel, 1968). As the name implies they are characterized by high suspended sediment concentrations that result from a combination of the system's gravitational circulation, stratification, tidal asymmetry, topography, wind, waves, flocculation, and sediment characteristics (Sanford et al., 2001). The hydrodynamic processes that form ETMs also tend to trap particulate matter and may permanently bury much of the terrestrial material that enters the estuary (Schubel and Pritchard, 1986). Despite these conditions, these regions often have high secondary productivity (David et al., 2006). In many estuaries a persistent maxima in zooplankton biomass occurs in the ETM region (David et al., 2006; Roman et al., 2001). In addition to being an important area for zooplankton, many ETMs have also been shown to be nurseries area for a number of juvenile fish species (Winkler et al. 2003, Shoji et al. 2005, North and Houde 2003, Laprise and Dodson 1989). Much

less is known about the lower trophic levels of the food web and the sources of organic matter that support this secondary productivity.

So why is secondary productivity often high in ETMs? Previous studies have indicated that in some ETMs the food web depends mainly on the allochtonous input of organic matter to fuel a detritus based food chain (Heinle and Flemer, 1975; Hummel et al., 1988). In this type of heterotrophic food web organic detritus provides an important link between primary and secondary production with particle-attached bacteria acting as an essential link for the transfer of C and N through the food chain (Hummel et al., 1988). However, other studies have hypothesized that the decrease in chlorophyll through the ETM frontal zone may result from grazing on riverine phytoplankton by zooplankton in the ETM region (indicating an autotrophic food web; (Winkler et al., 2003)). Thorp and Delong (2002) also describe a food web where the primary, annual energy source supporting higher trophic levels is autochthonous primary production that enters food webs via algal-grazer and decomposer pathways with the decomposers being responsible for the system's heterotrophic state and secondary production being supported by the algal-grazer. In addition to the previously mentioned types of C and N transfer, other processes such as cellular death/lysis, aggregation, and sinking may also be important. Furthermore, freshwater flow and tidal cycles may play an important role by influencing the delivery of organic material, the organic content of the detritus, the degree of stratification in the salt-front region, and the ETM trapping efficiency (Sanford et al., 2001; Schubel and Pritchard, 1986). Despite this knowledge of the food web in some ETMs, in many estuaries the sources of organic matter that support high secondary ETM productivity are not well understood and require more study.

Research Objectives and Approaches

The overall goal of the research presented in this dissertation is to expand our knowledge of how the flow of C and N through planktonic food webs and the environment *controls* and is *regulated* by the biology of different marine ecosystems. Initially my research focuses mostly (Chapters 1, 2, and 3) on the cycling of DOM as it is one of the least well-understood aspects of C and N cycling. Then I focus (Chapter 4) on aspects of estuarine C and N cycling by studying the upper Chesapeake Bay, which is the region where the ETM is located. Both numerical modeling approaches and field observations are used in these studies. Below is a summary of the general objectives and approaches for each chapter. Note that chapters presented in this document were originally written as separate manuscripts with a coauthor, Raleigh R. Hood, and have been combined here for this dissertation.

Chapter 1: *A Steady-State Model Comparison of Dissolved Organic Matter Cycling in Idealized Oceanic, Coastal, and Estuarine Surface Waters*

The many processes involved in DOM cycling occur in most aquatic systems, but the importance of each often varies substantially from one environment to another. For example, the planktonic biomass in estuaries is often dominated by larger species of phytoplankton and zooplankton whereas smaller species tend to make up most of the biomass in oceanic waters. Therefore, sloppy feeding, which occurs as a result of large zooplankton (i.e. copepods) feeding on other large plankton, is likely more important as a source of DOM in estuaries than in oceanic waters. Clearly, DOM cycling must be specifically studied and understood in the different types of marine systems (e.g.,

estuarine, coastal and the open ocean) if we are to understand the role of marine waters in global C and N cycling. The numerical model presented in this chapter facilitates the study of these differences by incorporating the most recent experimental research on DOM cycling into a new mass based model that constrains both the C and N cycles. One of the main objectives of this study was to further our understanding of the role that the planktonic community structure plays in DOM and C and N cycling. To test the new model and study these cycles in different types of marine ecosystems steady-state simulations were run for idealized oceanic, coastal, and estuarine surface waters. A detailed sensitivity analysis was also performed to better understand the model behavior in each system and to better constrain some of the poorly understood process involved in DOM cycling. When possible model results were validated with published research.

Chapter 2: *Modeling the Seasonal Autochthonous Sources and Cycling of Dissolved Organic Carbon and Nitrogen at Station CB3.3C in the Upper Chesapeake Bay*

Planktonic productivity, biomass, and community structure can change significantly on an annual basis in temperate aquatic systems in response to seasonal fluctuations in light and temperature. These biological changes, along with the other environmental effects of seasonality, can have a profound effect on C and N cycling. The study presented here examined the effects of these annual changes by building on the steady-state modeling research conducted in Chapter 1. Much of this research is focused on understanding how the autochthonous sources of DOM change seasonally. Data from multiple monitoring programs was used to parameterize and force the model to respond to seasonal changes in the environment (i.e. light, temperature, etc.) at a station in the

Chesapeake Bay. A sensitivity analysis was also performed to better understand the role of some poorly constrained processes in seasonal DOM cycling. When possible the model was validated with model skill assessment metrics.

Chapter 3: *Modeling the Food Web Dynamics and Biogeochemical Impact of Viruses and a Microzooplankton Grazer on Batch Cultures of the Prymnesiophyte Phaeocystis globosa*

Viruses and microzooplankton are both so small that they are very difficult to work with experimentally. Consequently there is little published data that quantifies how they affect C and N cycling. However, the measurements that have been taken of their activities indicate that they both can play very important roles in marine food webs and biogeochemical cycles (Sherr and Sherr, 2002; Suttle, 2007). In this study I modified the model that I used in Chapters 1 and 2 to better understand the roles that viral lysis and microzooplankton grazing processes play in DOM and C and N cycling. Since so little is known about these organisms I simulated non-axenic batch culture experiments with the prymnesiophyte *Phaeocystis globosa* to isolate and compare the biogeochemical effects of viruses and microzooplankton on an important primary producer. Another major objective of this research was to study the differences between the top-down (mortality) and bottom-up (nutrient regeneration) effects of viruses and microzooplankton on a simple *P. globosa* based food web. Originally this research was going to be conducted in conjunction with actual live culture experiments that could be used to validate and improve the model. However, due to technical difficulties these experiments did not occur. Therefore, the results of these simulations are theoretical although comparisons

were made to published studies of *P. globosa* interactions with viruses and microzooplankton when possible.

Chapter 4: *Phytoplankton Biomass Distribution and Floral Composition in the Upper Chesapeake Bay in the Winter and Spring: Influences of Estuarine Physics and Turbidity Maximum Entrapment*

Little is known about the dietary sources of C and N that support high zooplankton biomass and a larval fish nursery in the ETM region of the Chesapeake Bay during the spring. Since phytoplankton are the base of the food web in many aquatic systems the objective of research presented in this chapter was to examine the biomass distribution and floral composition of the phytoplankton community in the upper Chesapeake Bay during the winter and spring to determine if phytoplankton play an important role in the ETM food web. To achieve this goal fluorometry, high performance liquid chromatography (HPLC), and microscopy were used in conjunction with krigging techniques to describe the distribution and composition of phytoplankton along the main channel of the upper Bay during the winter and spring. This methodology also allowed for the identification of areas of high phytoplankton mortality via the presence of pigment degradation products and phytoplankton derived detritus. Analyses were also conducted to infer the role of hydrodynamic processes, including ETM entrapment, in phytoplankton transport, community formation, and mortality. These results were then used to assess the potential for phytoplankton to be an important component of the ETM food web.

Figures

Figure I. Schematic representation of the various DOM production and consumption processes in marine systems.

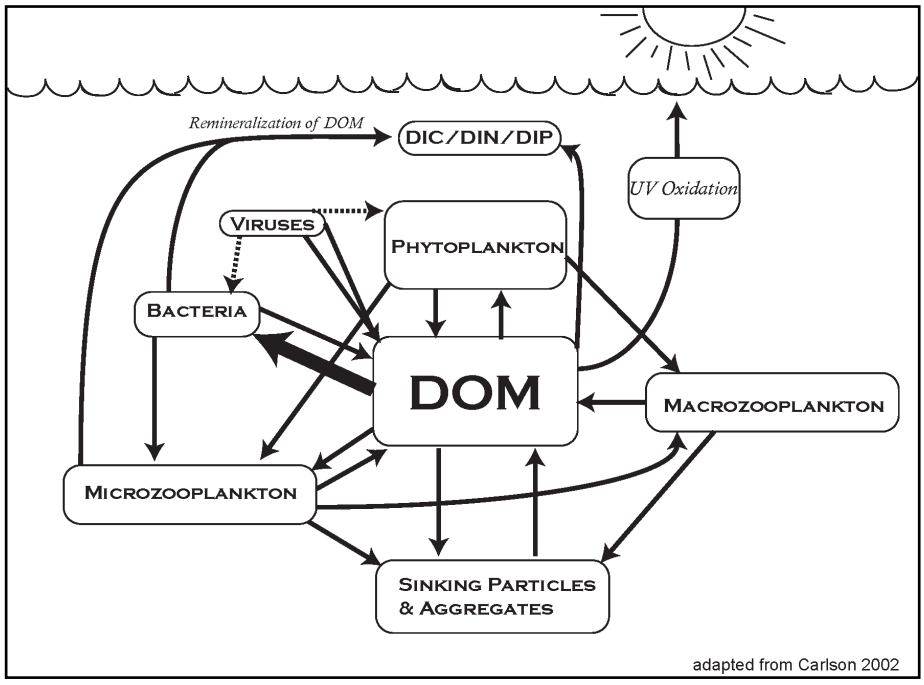

Chapter 1: A Steady-State Model Comparison of Dissolved Organic Matter Cycling in Idealized Oceanic, Coastal, and Estuarine Surface Waters

Abstract

Dissolved organic matter (DOM) constitutes one of the Earth's largest reservoirs of bioreactive elements (C, N, P, etc.), yet the composition and cycling of DOM is still poorly understood. As a result, most marine ecosystem and biogeochemical models include highly simplified representations of DOM cycling, if at all. In this paper we investigate the cycling of dissolved organic carbon (DOC) and nitrogen (DON) in idealized oceanic, coastal, and estuarine surface waters using a new mass-based ecosystem model that includes an unprecedented level of detail in the DOM pools and sources and sinks. Important features of the model are: (1) carbon and nitrogen are incorporated by means of a set of fixed and varying C:N ratios; (2) DOM is separated into labile, semi-labile, and refractory pools for both C and N; and (3) the production and consumption of DOM is treated in detail. Our model runs are able to reproduce DOM and planktonic biomass concentrations, uptake rates, and production rates (including DOM) that fall within ranges reported for oceanic, coastal, and estuarine systems. We show that DOM cycling is intricately tied to the biomass concentration, distribution, and production of phytoplankton, zooplankton, and bacteria. The model suggests that the relative importance of the different plankton groups in controlling DOM cycling is very different in oceanic, coastal and estuarine waters. In the oceanic runs bacteria are particularly important for mediating DOM cycling because they are the primary agents that control nutrient recycling and supply. In contrast, in the estuarine runs zooplankton have the most influence on DOM production due to the impact of their grazing and excretion, with grazing processes being particularly important. In addition, DOM cycling is generally less dependant on interactions between phytoplankton, zooplankton, and

bacteria in the estuarine case because estuaries have so much DOM loading from terrestrial sources. The coastal runs are somewhere in between, i.e., small zooplankton and bacteria both have a strong influence on DOM cycling because they are both important agents that control nutrient recycling and supply. Furthermore, in the oceanic and coastal cases the concentrations of labile, semi-labile and refractory DON and DOC vary little in response to parameter variations even though the relative importance of the different sources and sinks changes substantially. This result is consistent with the general observation that DOM concentrations in oceanic and coastal waters are relatively constant in time and space even though the composition of the plankton (and the sources and sinks) varies. In contrast, in the estuarine runs the concentrations of labile, semi-labile and refractory DON and DOC concentrations are much more sensitive to changes in the parameter values even though the total concentration of DOC and DON does not change much.

Introduction

One of the Earth's largest reservoirs of bioreactive elements such as C, N, P is dissolved organic matter (DOM) in the ocean. Dissolved organic carbon (DOC) is particularly important because the amount of carbon in the ocean, estimated to be 685 Gt of organic C, is approximately equal to the amount of inorganic carbon, mostly CO_2, in the atmosphere (Hansell and Carlson, 1998). Because of interactions between atmospheric, oceanic, and terrestrial pools of carbon, small changes in oceanic carbon cycling can potentially affect global carbon cycling and atmospheric CO_2 concentrations (Carlson, 2002). A significant amount of research has been conducted to understand DOM cycling in the oceans and we now have estimates of many of the biological,

chemical, and physical processes involved (Hansell and Carlson, 2002). However, despite decades of work there are still some fundamental aspects of DOM cycling that are poorly understood.

Marine DOM exists in a continuum of sizes and states of bioavailability. Because of limitations in methods used to analyze DOM and the usefulness of a size based distinction for understanding the sources and transformations of DOM, it is often operationally defined as either high-molecular-weight (HMW) DOM or low-molecular-weight (LMW) DOM. Furthermore, even though most DOM is composed of compounds containing multiple elements, it is often classified as pools consisting of a single element such as DOC. Limited data exist on the distribution of DOM throughout the oceans and our understanding of its spatial and temporal variability is based on relatively few measurements at key oceanic sites (Hansell, 2002). The composition of DOM in surface waters has only been characterized at the molecular level for 4 to 11% of the DOC and 7 to 14% of the DON, while in deep water only 1-3% of the DOC and 4-9% of the DON has been characterized as recognizable biochemicals (Benner, 2002). Because most DOM compounds have not yet been characterized, DOM is instead often classified as labile, semi-labile, or refractory based on its ability to resist biological degradation. Studies have shown that most of the DOM in the ocean, most of which is in the deep ocean (>70%), is old (4000-6000 years) and very resistant to biological degradation (i.e. refractory) (Bauer et al., 2002; Benner, 2002). Dissolved organic matter that is not resistant to biological degradation (i.e. labile) is quickly consumed by heterotrophic bacteria (Nagata, 2000) and represents less than 1% of the total DOM pool (Carlson and Ducklow, 1995). A more biologically resistant fraction of DOM (i.e. semi-labile), often

accumulates seasonally and is estimated to have a turn-over time of weeks to a few years (Carlson, 2002; Hansell, 2002; Repeta and Aluwihare, 2006). Since bacterial production can be high in surface waters (Ducklow, 1999) and because the concentration of labile DOM is low (Carlson and Ducklow, 1995; Cherrier and Bauer, 2004), logic dictates that in the absence of a large non-marine source, labile and semi-labile DOM is being produced in significant quantities through either chemical, physical, or biological processes.

In the euphotic zone, the focus of this paper, several processes are responsible for DOM production. These include extracellular release by phytoplankton, grazer-mediated release and excretion, release via cell lysis (both viral and bacterial), solubilization of particles, and bacterial transformation and release. In addition, rivers and atmospheric deposition can add significant quantities of DOM to coastal and estuarine waters (Bronk, 2002). Physical processes such as upwelling and mixing can also act as a source of DOM in surface waters by bringing DOM from deeper waters to the surface.

Dissolved organic matter in surface waters is removed through several biotic and abiotic processes. Biotically, free-living heterotrophic bacterioplankton are the dominant consumers of DOM in the ocean (Nagata, 2000). In addition to bacteria, some phytoplankton also have the ability to take up DOM to supplement their metabolic needs (Mulholland et al., 2003). Abiotically, photochemical processes, through UV excitation, directly and indirectly remove and transform DOM (Mopper and Kieber, 2002). Dissolved organic matter may also be removed from surface waters by physical processes such as downwelling or mixing. In addition, DOM can also potentially form gels that

may aggregate to form particulate organic matter (POC) (Verdugo et al., 2004) which may sink out of surface waters.

The many processes involved in DOM cycling occur in most aquatic systems, but the importance of each varies substantially from one environment to another. For example, the planktonic biomass in estuaries is often dominated by larger species of phytoplankton and zooplankton whereas smaller species tend to make up most of the biomass in oceanic waters. Therefore, sloppy feeding, which occurs as a result of large zooplankton feeding on other large plankton, is likely more important as a source of DOM in estuaries than in oceanic waters. Clearly, DOM cycling must be specifically studied and understood in the different types of marine systems (e.g., estuarine, coastal and the open ocean) if we are to understand how it relates to global elemental cycling.

Models can be a powerful tool for determining the magnitude and importance of processes that are difficult to measure and observe in the field. Numerical simulations are also valuable for integrating data and running long term simulations. In this paper we describe a modeling study of DOM cycling where our aim is to develop a model that can determine the magnitude, rates, and importance of processes that control DOM production, transformation, and loss in estuarine, coastal, and oceanic surface waters. We specifically focus on the roles that phytoplankton extra-cellular release, non-grazing mortality, bacterial and phytoplankton viral lysis, and grazer-mediated sloppy feeding, egestion, and excretion play in the production of DOM. In addition, we explore how DOM is transformed and removed by chemical and biological processes and how this relates to the overall production of DOM.

Our findings show that in an ecosystem context the cycling of DOM is intricately tied to the biomass, distribution, and production of phytoplankton, zooplankton, and bacteria. Because these components differ between estuarine, coastal and open ocean systems, so does their role in DOM cycling. Our model results suggest that in oceanic surface waters bacteria are extremely important in DOM cycling because they act as the primary source of recycled nutrient (ammonium) for phytoplankton growth and organic matter production, which is the primary source of DOM in oceanic waters. In coastal surface waters bacteria similarly play an important role but zooplankton become more important and influence DOM cycling through grazing impacts and regeneration of nutrients. Our results suggest that in estuarine waters zooplankton grazing impacts are important in determining how planktonic DOM production and cycling occurs, but because estuaries have so much DOM from terrestrial sources DOM cycling is generally less dependant on interactions between phytoplankton, zooplankton, and bacteria.

Model Description

The model of Anderson and Williams (1998) provided the basic structure for the ecosystem model that we developed and used in this study. However, there are a few significant departures from their model: DOM is divided into labile, semi-labile, and refractory pools, zooplankton and phytoplankton have two size classes, sediment is not included, and two virus compartments have been added along with a dissolved inorganic carbon (DIC) pool. The processes that occur in this model are considered to occur in the upper portion of the water column in typical temperate estuarine, coastal, and oceanic waters. A complete list of model parameters along with the literature sources and justifications for their selection can be found in Appendix A. The model equations are in

Appendix B.

The model includes 18 state variables that span the herbivorous and microbial food webs, with compartments for large phytoplankton (P_L), small phytoplankton (P_S), large zooplankton (Z_L), small zooplankton (Z_S), bacteria (B), phytoplankton viruses (V_P), bacteriophages (V_B), ammonium (A), nitrate (N_n), detritus (D_N and D_C), dissolved inorganic carbon (DIC), and labile (L_C and L_N), semi-labile (S_C and S_N), and refractory (R_C and R_N) DOM. Figure 1.1 is a schematic diagram that shows the flow of nitrogen and in some instances carbon between the model compartments. Nitrogen is the basic unit for simulation and mass balance. However, carbon has been accounted for by allowing the state variables to have fixed or varying C:N ratios. Close attention has been paid to the formulation of the interactions between these two elements. Thus, both the carbon and nitrogen cycles have been constrained. Phytoplankton are divided into two size classes to reflect the physiological differences between larger and smaller species (i.e. diatoms versus cyanobacteria). Zooplankton are similarly divided into two size classes to reflect the differences between larger and smaller species (i.e. macrozooplankton versus microzooplankton). A chemostat-like formulation (see Appendix B) is used to add nutrients to the system to simulate different nutrient loading regimes, i.e., estuarine, coastal, and open ocean systems.

Phytoplankton

The light- and nitrogen-dependant growth rate of phytoplankton is described by an exponential saturation function with photoinhibition for light dependence (Platt et al., 1980) and a non-dimensional Michaelis-Menten hyperbolic saturation function is used to describe nitrogen (ammonium, nitrate, and labile DON) dependence. This formulation

allows phytoplankton cells to take up ammonium and potentially labile DON preferentially, resulting in nitrate uptake inhibition in the presence of significant concentrations of ammonium (Christian et al., 2002; Harrison et al., 1996) and labile DON. Phytoplankton are also assumed to use DIC in combination with nutrients at a fixed C:N ratio for production (Anderson and Pondaven, 2003). A constant fraction of phytoplankton production is exuded as DOM, and "extra" DOC is also excreted in proportion to production (Anderson and Williams 1998). The "natural" mortality of phytoplankton produces DOM and detritus, and is modeled by a simple linear equation.

Zooplankton

Use of food by zooplankton for growth is based on a stoichiometric model (Anderson and Hessen, 1995) that operates on the basis of a food-threshold elemental ratio, below which C limits growth and above which N limits growth. This formulation accounts for the respiration of DIC, the egestion of feces to detritus, and the excretion of ammonium and DOM. The model also allows for the assignment of "preferences" for different forms of organic nitrogen (Hood et al., 2001). The production of DOM and detritus as a result of large zooplankton sloppy feeding is based on a predator-to-prey size ratio (Møller, 2005) that determines the amount of DOM and detritus produced. The "natural" mortality of zooplankton produces DOM and detritus.

Bacteria

The cycling of C and N by bacteria is described by Anderson and Williams' (1998) stoichiometric model. This formulation describes the adaptive capability of bacteria and assumes that labile DOC and DON are the primary growth substrates, with

ammonium supplementing DOM only when the C:N of DOM is high. Thus, bacteria act as either remineralizers or consumers of ammonium, depending on the relationship between their fixed C:N ratio and that of the DOM they consume. The "natural" mortality of bacteria produces DOM and is modeled by a simple linear equation.

Viruses

Viruses that infect phytoplankton and bacteria are considered to be a component of DOM even though they are treated as separate pools for the purpose of this model. The infection of phytoplankton and bacteria by viruses is modeled so that a certain percentage of the viral host is lysed on a daily basis (see description in Appendixes A and B). Viral infection and subsequently lysis of the host produces new viruses, detritus, and DOM. The number of new viruses produced per lysis event was calculated using average burst size data (Wommack and Colwell, 2000). Viral decay or loss is formulated using a power function (Fischer et al., 2004) with destroyed viral material returning to the DOM pool.

Dissolved Organic Matter

Dissolved organic matter has separate state variables for C and N which are divided into labile, semi-labile, and refractory pools (Anderson and Williams, 1999). Dissolved organic matter is produced by phytoplankton excretion and leakage, zooplankton sloppy feeding, zooplankton excretion, phytoplankton and bacteria mortality, viral lysis of phytoplankton and bacteria, and detritus decay. Labile DOM is consumed directly by bacteria and potentially by phytoplankton. Semi-labile DOM requires ectoenzyme hydrolysis by bacteria to become available (labile) for consumption.

A Michaelis-Menten kinetic formulation (Anderson and Williams 1999) describes bacterial hydrolysis of semi-labile DOM, with semi-labile DOM entering the labile and refractory DOM pools upon hydrolysis. Refractory DOM is considered unavailable for consumption by bacteria and phytoplankton.

Photochemical processes are assumed to be the only means of turnover for refractory material in estuarine and coastal waters where refractory DOM is transformed into labile DOM. These formulations were used because some research has shown that UV radiation tends to make terrestrially derived refractory material from coastal and estuarine environments more available for use by bacteria (Mopper and Kieber, 2002). In oceanic water where there is almost no terrestrially derived DOM, photooxidation studies have shown that recently produced DOM can become less available to bacteria (Benner and Biddanda, 1998; Obernosterer et al., 2001). Because there is also refractory DOM in oceanic waters which may become more bioavailable due to UV exposure (Mopper and Kieber, 2002), we have assumed that the processes balance each other so our formulation for the oceanic model runs does not have DOM becoming more or less bioavailable due to photochemistry. In all model runs, photochemical processes are also responsible for the conversion of DOC to dissolved inorganic carbon. Recent research (Koopmans and Bronk, 2002) has shown that in humic-rich surface waters photochemical processes can release ammonium from more refractory DON, so for the estuarine model runs we also allowed some DON to be photooxidized to produce ammonium.

Detritus, DIC, and Nutrients

Detritus is produced by mortality, lysis, zooplankton egestion, and sloppy feeding. Detritus is consumed by zooplankton and broken down by chemical leaching and

bacterial consumption. Dissolved inorganic carbon is produced by heterotrophic respiration and through photochemical processes acting on DOM. Phytoplankton assimilate DIC during growth. Ammonium and nitrate are taken up as a nitrogen source by phytoplankton. Bacteria are also capable of taking up ammonium. Heterotrophic processes produce ammonium. Nitrification converts ammonium into nitrate at a fixed rate following the formulation of Anderson and Williams (1998). For simplicity, urea is treated as ammonium in our model because of the ability of phytoplankton to utilize it even though urea is actually a component DON.

Model Parameters

We parameterized the model differently for the oceanic, coastal, and estuarine runs in order to reflect the differences between these systems. Model parameterization is described in detail in Appendix A. The tuning of the carbon biomass (mmol C m^{-3}) of phytoplankton, zooplankton, and bacteria for the oceanic, coastal, and estuarine model runs was based on the carbon biomass of bacteria and phytoplankton in the Sargasso Sea, the coastal waters of southern California, USA, and Chesapeake Bay, USA and the relative biomass ratios described by Gasol et al. (1997). However, because Gasol et al. did not differentiate between large and small phytoplankton for the oceanic run we allowed small phytoplankton biomass to be 80% of the total phytoplankton biomass following typical oceanic size based biomass and production distributions (Malone, 1980). In the coastal and estuarine runs small phytoplankton biomass was assumed to be less than 50% of the total phytoplankton biomass.

The chemostat formulated inflow of nutrient and DOM for each system was set to be representative of the limited supply of new nutrients in open ocean water, the

moderate supply of new nutrients in coastal waters, and the high supply rate of new nutrients often found in estuarine waters. In all of the model runs the rate at which material flowed into the system was 0.01 cm s^{-1}. The concentrations of inflowing ammonium were 0.1, 2, and 50 μM N for the oceanic, coastal, and estuarine model runs. The concentrations of inflowing nitrate were 0.2, 2, and 85 μM N for the oceanic, coastal, and estuarine model runs. Inflowing DOM in the oceanic model run had a C:N ratio of 14 and the inflowing DON concentration was 10 μM N. This C:N ratio was used to account for the flux of DOM from deeper water to the surface and from adjacent surface waters and was based on the mean oceanic C:N ratio reported by Bronk (2002). Inflowing DOM in the coastal model run had a C:N ratio of 17 and the DON concentration was 15 μM N. This C:N ratio was used to account for the flux of DOM from deeper water to the surface and from adjacent coastal waters and was set based on the mean coastal C:N ratio reported by Bronk (2002). Inflowing DOM in the estuarine simulation had a C:N ratio of 10 and the DON concentration was 100 μM N. This C:N ratio was used to simulate the flux of DOM into an estuary from both terrestrial and estuarine sources and was based on DOM measurements from the mesohaline portion of Chesapeake Bay, USA (Bronk 2002).

The model was integrated numerically over time with Stella™ software using a fourth-order Runge-Kutta scheme. A 6 hour time step was used and the model runs were allowed to reach a steady state. We analyzed the sensitivity of the model to various parameters that are directly related to DOM cycling by allowing them to vary within ranges reported in the literature. The results of the parameter variation runs were then normalized to biomass for the sensitivity analysis. The parameters that we varied were

the viral infection rates (Ψ_{P_L} , Ψ_{P_S} , and Ψ_B), the amount of DOM produced by sloppy feeding (ω_{P_L} , ω_{Z_L} , and ω_D), the rate of detritus decay ([redacted]), non-grazing mortality rates (S_{P_L} , S_{P_S} , S_{Z_L} , S_{Z_S} , and S_B), the rate of viral decay (υ), the amount of DOM produced by zooplankton excretion (κ_Z and σ_Z), the amount of DOM produced by phytoplankton exudation (α), bacterial growth efficiency (gge_b), and the zooplankton growth coefficients (ge_{Z_L} and ge_{Z_S}). We varied viral infection from 50% and 20% mortality per day for bacteria and 10% and 0% per day for phytoplankton. We allowed the amount of DOM produced from sloppy feeding to vary by ± 0.10 (dimensionless). We let the rate of detritus decay vary from + 0.05 to -0.05 d^{-1} (χ_{D_N}) and 0.039 d^{-1}(χ_{D_C}). Non-grazing mortality was varied from 10% per day to 0% per day. We varied the rate of viral decay from 1.0 to 0.01 h^{-1}. We also varied the amount of DOM produced by zooplankton excretion, the amount of DOM produced by phytoplankton exudation, bacterial growth efficiency, and the zooplankton growth coefficients by ± 0.10 (dimensionless).

Results and Discussion

Open Ocean Model Run

Oceanic Planktonic Biomass

The oceanic biomass distribution (Fig. 1.2 a) reflects the tuning of the model to the relative oceanic planktonic biomass ratios found by Gasol et al. (1997) and the large and small phytoplankton biomass distribution from Malone (1980), i.e., the carbon biomass is dominated by bacteria (35%) and small phytoplankton (25%) and to a lesser

extent by large and small zooplankton (15% and 18%, respectively). By contrast, large phytoplankton constitute a relatively small fraction (7%) of the oceanic plankton biomass.

The sensitivity analysis (Fig. 1.3) reveals that the biomass of plankton is not very sensitive to parameter variations in sloppy feeding, detritus decay, zooplankton excretion, zooplankton growth efficiency, and phytoplankton exudation. Planktonic biomass is only moderately sensitive to parameter variations in mortality and bacterial growth efficiency (Fig 1.3 d, h). We expect plankton to be sensitive to variations in their mortality rates because they represent a direct loss of biomass. These results show, however, that the relative magnitude of these terms is not large. Moderate sensitivity to variations in bacterial growth efficiency appears to be related to the role bacteria play in remineralizing nutrients (see below). Planktonic biomass is very sensitive to variations in viral infection and the parameters (infection rate and the viral decay rate) involved in regulating infection (Fig 1.3 a, e). Phytoplankton and bacteria are sensitive to changes in viral infection because it can be a large source of mortality, especially for bacteria, that can potentially limit their abundance and production.

Bacteria remineralize nutrients which phytoplankton depend upon so changes in the abundance or production of bacteria as a result of varying parameters like their growth efficiency or rate of viral infection will either increase or decrease the amount of nitrogen available for phytoplankton growth. Thus, in an oceanic environment where nitrogen limits phytoplankton growth the abundance and production of phytoplankton will be substantially regulated by the bacterial abundance and how much remineralization is occurring. Some feedback from these processes also occurs because some of the DOM

that bacteria use to grow comes from mortality, phytoplankton exudation, and viral lysis so a change in DOM from these sources as a result of changing planktonic biomass and production due to parameter variations can impact bacterial abundance and production as well. Zooplankton can potentially regulate the biomass of their prey through grazing pressure. However, this was not the case in the oceanic model runs as variations in the growth efficiency of zooplankton did not have much effect on the biomass or productivity of other plankton (Fig. 1.3 i). All of these results highlight the role of bacteria and viruses in determining the ecosystem dynamics of the oceanic model runs.

Other State Variables

The steady state concentrations of DOC and DON (Fig. 1.4 a, b) are within the range (DOC (μM): 60 – 90; DON (μM): 3.5 – 7.5) of measured total DOC and DON concentrations typically found in oceanic surface waters (Benner, 2002). The range bars represent the maximum and minimum values that model runs produce when the parameters mentioned above are varied over observed ranges. The small variation in the range of steady state DOM concentrations is partially because of the stabilizing effect of a constant flux of DOM into the model system and partially because of the dynamics of the model's DOM cycling (see section below). Ammonium and nitrate concentrations are both 0.02 mmol N m^{-3} at steady state, detritus consists of 0.26 mmol C m^{-3} and 0.04 mmol N m^{-3}, bacterial virus concentrations are 0.021 mmol N m^{-3}, and phytoplankton virus concentrations are 0.016 mmol N m^{-3}.

Oceanic Production

Our main run oceanic bacterial production rates (Table 1.1) are within the range of values (BP (mg C m^{-3} d^{-1}): 0.01- 122, avg. 12-15) that have been reported in the

literature but are lower than typically found (Ducklow and Carlson, 1992). Our primary production rates (Table 1.1) are within the range of values that has been measured at a number of oceanic sites (Table 1.2) (Behrenfeld et al., 2006a) which experience conditions similar to the steady state conditions of the model. However, we should note that there is a wide range of primary production rates reported in the literature for oceanic waters and our rates are at the low end of this range. The low bacterial and primary production rates and high bacterial production to primary production ratio is likely the result of the model being tuned to the biomass distributions found by Gasol et al. (1997), which represent a mean biomass distribution from samples taken at different times of the year. While this mean biomass ratio may reflect the overall mean for the system it is likely different from ratios that would be measured at any one time in the field. This makes tuning the model to the mean biomass ratio useful for looking at the system as a whole over a long time scale but difficult to compare to reported measurements of productivity that include a plankton biomass ratio as most of these have not been reported as a seasonal mean. Therefore, we conducted an additional model run with the phytoplankton and bacteria biomasses tuned to a Sargasso Sea mean biomass distribution (Ducklow, 2001) to show that the model is capable of producing a bacterial production to primary production ratio that falls within the range typically observed in oceanic surface water. For this run (Table 1.1) bacterial production is 19% of total primary production which is within the range of 10-30% typically found in oceanic waters (Fuhrman, 1992).

Oceanic Uptake and Regeneration

The total uptake (mmol N m^{-3} d^{-1}) of ammonium and nitrate by phytoplankton (Table 1.3) is within the range (NH_4^+: 0.0009 – 0.0482; NO_3^-: 0.0002 – 0.24) reported for

the South Atlantic Ocean (Metzler et al., 1997). The uptake of DIC by phytoplankton reflects the fixed C:N ratio of phytoplankton which dictates that for every mole of nitrogen taken up 7.5 moles of carbon must be taken up as well. Uptake of DON by bacteria (Table 1.3) corresponds with bacterial production (Table 1.1), which is a measure of assimilated DOM that becomes bacterial biomass.

Ammonium is regenerated by bacteria and zooplankton at 0.034 mmol N m^{-3} d^{-1}, of which 88% is derived from bacteria. This regeneration occurs at almost the same rate at which ammonium is being assimilated by phytoplankton (Table 1.3). Thus, these model results compare well with rates of ammonium regeneration and assimilation that have been extensively measured at sea (Glibert et al., 1988; Varela et al., 2005) and usually shown to be almost the same.

Oceanic DOC Production

The largest source of dissolved organic carbon is phytoplankton exudation (45 nmol C m^{-3} d^{-1}) (Fig 1.5 a), which is mostly (88%) from small phytoplankton, and is within the large range of reported phytoplankton exudation rates (0-24 mmol C m^{-3} d^{-1}) (Carlson, 2002). Even when parameter variations are run phytoplankton exudation is the dominant source of DOC with the exception of the run where the bacterial growth efficiency is increased (DOC from viral lysis was the dominant source for this run). Most of the DOC from viral lysis comes from the lysis of bacteria so it is not surprising that an increase in bacterial production due to an increase in bacterial growth efficiency increases the amount DOC from viral lysis. While phytoplankton exudation is the largest individual source of DOC, total production of DOC (102.5 nmol C m^{-3} d^{-1}) was

dominated (56%) by heterotrophic processes which is consistent with other modeling studies (Christian and Anderson, 2002).

Oceanic DON Production

The production of DON (12.5 nmol N m^{-3} d^{-1}), which is well within the large range of reported DON release rates (Bronk, 2002), derives from a variety of sources such as phytoplankton exudation, lysis, viral decay, and detritus decay that are nearly equal in magnitude (Fig. 1.5 b). The ratio of DON release to gross N uptake is 49% which is within the range and close to the mean (41.4 %) of reported DON release to gross N uptake ratios reported for oceanic waters (Bronk, 2002). The smallest source of DON is from sloppy feeding by large zooplankton, which is not surprising considering that smaller forms of phytoplankton and zooplankton dominate these waters. Dissolved organic nitrogen from viral decay does not really represent an addition of DON to the pool as viruses are already a component of DON. However, we include this as a source because previous research has often overlooked how much DON is derived from decayed viral material.

The sensitivity of the sources of DON to parameter variations is shown in figure 1.6. In most of the variations the amount of DON produced by these sources is related to the effect that a parameter variation has on the mass (Fig. 1.3) and production of the source (i.e. lower the biomass or lower production and less DON is produced). Dissolved organic nitrogen release by phytoplankton exudation (Fig. 1.6 g) is sensitive to variations in the viral infection rate, viral decay rate, the exudation parameter (α), and the growth efficiency of bacteria. Viral infection of phytoplankton, which is controlled by the infection rate and the viral decay rate, can be large source of mortality for phytoplankton

so variations in these parameters will affect their biomass (Fig. 1.3) and rate of production. Viral infection can also be a large source of mortality for bacteria, which provide ammonium for phytoplankton growth through remineralization so the effect of viral lysis on bacteria must also be taken into account because the amount of ammonium they produce can affect phytoplankton growth and consequently exudation. Sensitivity to the exudation parameter (α) is expected as this parameter regulates how much assimilated nitrogen is allocated toward phytoplankton growth and how much is exuded as DON. The biomass of phytoplankton (Fig. 1.3 h) and the rates of primary production are sensitive to changes in growth efficiency of bacteria because this parameter partially controls the rate at which ammonium is remineralized by bacteria. In addition, because small phytoplankton produce more DOM per unit biomass than large phytoplankton, parameter variations that shift the distribution of phytoplankton in favor of small phytoplankton will increase the amount of DOM produced by phytoplankton exudation.

Zooplankton excretion of DON is sensitive (Fig. 1.6 e) to the parameters involved in viral infection because, as explained in the section on planktonic biomass, variations in viral infection can increase or decrease the biomass of zooplankton (Fig. 1.3). Variations in the zooplankton excretion parameters have little effect on zooplankton biomass (Fig. 1.3) and the amount of DON from zooplankton excretion is so small in the main run (Fig. 1.5 b) that changes in DON from excretion have a negligible effect. Dissolved organic nitrogen from mortality is sensitive (Fig. 1.6 c) only to an increase in the mortality rates of plankton. The production of DON from sloppy feeding is not sensitive (Fig. 1.6 b) to any of the parameter variations because very little sloppy feeding occurs in oceanic waters due to the low biomass of large zooplankton and large phytoplankton. Dissolved

organic nitrogen from detritus decay is only sensitive (Fig. 1.6 f) to variations in the rate of detritus decay.

Dissolved organic nitrogen from viral lysis is sensitive (Fig. 1.6 a) to parameter variations in the rate of viral infection and the rate of viral decay. Parameter variations that affect bacterial biomass and production are especially important in determining DON production from lysis because 86% of the DON from lysis comes from bacteria in the main run. The viral decay rate determines how many viruses are present to infect phytoplankton and bacteria. If the decay rate is high then fewer viruses are present so the rate of infection decreases and vice versa. The production of DON from viral decay is sensitive (Fig. 1.6 d) to variations in the viral infection rate, the mortality rate, the viral decay rate, and the growth efficiency of bacteria. The infection rate determines the production of viruses so changes in it will determine how many viruses are around to decay. Increases in the mortality rate result in fewer phytoplankton and bacteria that can be infected by viruses so fewer viruses are produced, which reduces the amount of viruses present to decay. The viral decay parameter directly determines the rate at which viruses decay so it is not surprising that DON from viral decay is sensitive to this parameter. Variations in the growth efficiency of bacteria affect the amount of DON from viral decay because this parameter affects bacterial production and biomass, and bacterial lysis is a major source of new viruses that ultimately decay.

Oceanic DOM Inflow Sensitivity

The concentrations of DOC and DON (Fig. 1.4 a, b) do not vary much in response to changes in the model parameters so additional runs were performed to see if the chemostat-like inflow of DOM into the system stabilizes the concentration of DOM and

how this inflow impacts the dynamics of DOM cycling. In a model run where there is an inflow of ammonium and nitrate but not DOM (Fig. 1.7), there is 62 and 27 % less refractory DOC and DON in the system, 32 % less semi-labile DOC, 38 % more semi-labile DON, and labile DOM concentrations that are almost the same. The reduction in refractory DOM is as we had expected because most refractory DOM is very old and very little is being produced by planktonic processes. The increase in semi-labile DON and decrease in semi-labile DOC in the run where there is no DOM inflow occured because the DOM that supplies the semi-labile pool in this run is all being "freshly" produced, instead of being partially supplied by inflow, and has a lower C:N ratio than the inflowing DOM in the main run. Thus, there is an increase in the semi-labile DON concentration and a decrease in the semi-labile DOC concentration as the pools of DOM adjust to reflect the lower C:N ratios of the DOM sources. This shift in the C:N ratio is not seen in the labile DOM pools because labile DOM is taken up almost as fast as it is being produced. The refractory DOM pools show this trend as well with the DON concentration not decreasing as much as the DOC concentration when there is no inflow. However, the trend is not as pronounced in the refractory pools because very little refractory DOM is "freshly" produced.

The total planktonic biomass at steady state is almost the same, 1.11 mmol C m^{-3} with DOM inflow and 1.10 mmol C m^{-3} with no DOM inflow. However, the biomass distribution changes dramatically (Fig. 1.7 a) when there is no DOM inflow. Specifically, the biomass of large zooplankton more than doubles, the biomass of small zooplankton declines, the biomass of large phytoplankton increases, the biomass of small phytoplankton declines, and bacterial biomass declines. This shift in the biomass

distribution is likely caused by a combination of less loss, especially for large zooplankton, due to the chemostat-like outflow of material and a reduction in the amount of labile DOM available for bacteria, who strongly influence the biomass and productivity of other plankton through nutrient remineralization.

The change in the biomass distribution affects how DOM is cycled (Fig 1.8). The largest source of DOC (Fig. 1.8 a) and 47% of total DOC production is still phytoplankton exudation. However, because phytoplankton production declines by 48% and the biomass of small phytoplankton declines, the amount of DOC from exudation is reduced by 57%. Dissolved organic carbon from every other source except sloppy feeding also declines by at least half when compared to the main run. Dissolved organic carbon from sloppy feeding increases slightly because the biomass of large zooplankton increases.

The production of DON decreases for every source except for sloppy feeding (Fig. 1.8 b). Dissolved organic nitrogen from viral lysis is reduced by 82% because the biomass of bacteria is lower and production by both phytoplankton and bacteria is less. The biomass of large zooplankton increases and as a result DON from sloppy feeding increases. The decreased biomass of small zooplankton, small phytoplankton, and bacteria along with a decrease in primary production and bacterial production reduces the amount of DON produced by mortality. Less viral infection, primarily because of reduced bacterial biomass and production, results in the production of fewer viruses so not as much DON is produced from viral decay. The amount of DON produced by zooplankton excretion is less even though the biomass of large zooplankton more than doubles. This is probably due to the decline in the biomass and production of small

zooplankton which produce more DON than large zooplankton. Less DON is exuded by phytoplankton because phytoplankton production decreases by almost half. Not as much detritus is produced because less mortality and lysis occurs so the amount of DON produced by detritus decay is less.

Oceanic Summary

Our oceanic model run is able to reproduce DOM and biomass concentrations, uptake rates, and production (biological and DOM) rates that fall within ranges reported for open ocean systems. This suggests that the model captures the flow of carbon and nitrogen through the different biological and chemical states that are involved in DOM cycling. The model shows that DOM cycling in an oceanic environment is intricately tied to the biomass concentration, distribution, and production of phytoplankton, zooplankton, and bacteria. The concentrations of DOC and DON vary little during the parameter variation runs. Thus it appears that when one source of DOM increases another source of DOM decreases by a similar amount keeping the total concentration of DOM about the same. These results suggest that DOC and DON concentrations are "robust" quantities in open ocean systems which may help to explain the fact that these concentrations are relatively constant in space and time. In addition, these results indicate that DOM production and biomass concentrations and distributions are very sensitive to viral infection, and that bacterial biomass and production is also very important in determining how DOM cycling occurs. The sensitivity analysis also indicated that bacterial recycling of nutrients controls the biomass and production of phytoplankton and zooplankton, indicating more of a bottom-up control of the ecosystem. However, as Thingstad (2000) points out the concept of top-down and bottom-up control

cannot be readily separated in steady-state models of recycling systems and as discussed by Glibert (1998) these two processes are always in a dynamic balance. In addition, our model does not include the necessary components (physics or a 3-D context) which would be needed to understand the relative roles of top-down or bottom-up controls. Nevertheless, our sensitivity analysis does provide us with some valuable information that highlights the central role of bacteria and viruses in oceanic plankton dynamics and DOM cycling.

Coastal Model Run

Coastal Planktonic Biomass

The coastal biomass distribution (Fig. 1.2 b) reflects the tuning of the model to the relative coastal planktonic biomass ratios found by Gasol et al. (1997) which is substantially different from the oceanic biomass ratios in that the bacteria to phytoplankton ratio is approximately 0.62 to 1 instead of 1 to 1, the large zooplankton to phytoplankton ratio is approximately 0.87 to 1 instead of 0.51 to 1, and the small zooplankton to phytoplankton ratio is approximately 0.27 to 1 instead of 0.54 to 1. In addition, instead of having the small phytoplankton biomass be 80% of the total phytoplankton biomass the small phytoplankton biomass is set to be slightly less than 50% of the total phytoplankton biomass. In the sensitivity analysis the biomass of plankton is not very sensitive (Fig. 1.9) to variations in the detritus decay rate and the zooplankton excretion parameters. Planktonic biomass is only moderately sensitive (Fig. 1.9) to parameter variations in phytoplankton exudation, bacterial growth efficiency, zooplankton growth efficiency, and sloppy feeding. Planktonic biomass is very sensitive (Figs. 1.9) to variations in viral infection, viral decay, and mortality. As discussed in the

oceanic results, variations in these latter parameters that affect the biomass and production of bacteria also change the rate of ammonium regeneration. This in turn affects the growth of phytoplankton and the zooplankton that graze on them. The coastal model run sensitivity analysis (Fig. 1.9) shows that these same dynamics are occurring in this system as well. However, unlike the oceanic model run small zooplankton contribute significantly to ammonium regeneration (see below) in the coastal run so changes in their biomass or production can also potentially affect the planktonic biomass distribution. But small zooplankton production and biomass remain relatively constant during the model sensitivity runs while bacteria do not, which makes the coastal model behave much like the oceanic model.

Competition between large and small phytoplankton is evident in all of the parameter variations runs with the coastal model. Parameter variations often have the effect of giving either large or small phytoplankton competitive advantage for nutrients, which results in a decrease in the biomass of one size class and an increase in the biomass of the other size class. Even if the parameter variation increases mortality for both size classes the biomass of one will often increase or stay the same while the biomass of the other declines. In some of the runs large phytoplankton are even driven to extinction because small phytoplankton become substantially better competitors.

In model runs where the viral infection rate and the viral decay rate are allowed to vary (Figs. 1.9 a and e) the biomass of small phytoplankton stays almost the same while the biomass of large phytoplankton changes significantly. Interestingly, the biomass of small phytoplankton is relatively stable even though they experience substantial changes in mortality rates and the availability of regenerated nutrients with the parameter

variations. When the rate of viral infection increases a combination of increased mortality and competition with small phytoplankton drive large phytoplankton to extinction. In the absence of large phytoplankton the small phytoplankton have no competition for nutrients and they grow faster, thus balancing out the increased mortality from viral infection and the decrease in regenerated ammonium. When the infection rate is reduced the biomass of large phytoplankton increases. Thus competition with large phytoplankton for nutrients keeps the small phytoplankton biomass the same even though they experience less mortality and have more regenerated ammonium available.

Competition between large and small phytoplankton is also evident when the parameter that controls sloppy feeding is varied (Fig. 1.9 b). In these runs the biomass of small zooplankton and bacteria does not change very much whereas the biomass of large zooplankton and phytoplankton varies considerably. Large zooplankton are sensitive to changes in the sloppy feeding parameter because increasing or decreasing this parameter affects how much of a large prey item is consumed for growth versus being lost during the feeding process. Thus a decrease in the sloppy feeding parameter increases the growth of large zooplankton, which leads to an increase in the amount of grazing on large phytoplankton. Subsequently, the biomass of large phytoplankton declines. The increased mortality that large phytoplankton experience gives small phytoplankton a competitive advantage so their biomass increases. When the sloppy feeding parameter is increased the opposite scenario occurs, i.e., the biomass of large zooplankton and small phytoplankton decreases and the biomass of large phytoplankton increases.

As expected all plankton are sensitive (Fig. 1.9 d) to variations in their mortality rate. Interestingly, due to competition between large and small phytoplankton the

biomass of large phytoplankton decreases regardless of whether their mortality rate increases or decreases. In contrast, the biomass of small phytoplankton always increases. Evidently, the combination of increased or decreased mortality along with the subsequent change in nutrients regenerated by bacteria always favors small phytoplankton. Small zooplankton biomass also increases regardless of whether their mortality rate increases or decreases because the biomass of their primary prey, small phytoplankton, always increases. In all of the other parameter variation runs (Fig. 1.9 c, f, g, h, and i) competition between phytoplankton is evident because whenever one size class increases the other decreases and vice versa.

As mentioned above, a combination of grazing pressure, mortality, and the availability of nutrients from bacterial remineralization determines whether small or large phytoplankton do better or worse when a parameter is varied. The competition that is observed between large and small phytoplankton in the parameter variations runs is consistent with the general observation that, in temperate coastal waters, the biomass distribution of large and small phytoplankton varies seasonally as different environmental conditions favor one size class of phytoplankton over another (Malone, 1980).

Other State Variables

The steady state concentrations of DOC and DON (Fig. 1.4) are within the range of measured total DOC and DON concentrations (DON (μM): 9.9 ± 8.1; C:N DOM pool: 17.7 ± 4.3) typically found in coastal surface waters (Bronk, 2002). As in the oceanic model run, the variation in the range of steady state DOM concentrations during parameter variation runs is small partially because of the stabilizing effect of a constant inflow of DOM into the model system and partially because of the dynamics of the

model's DOM cycling. These dynamics are evident in that there is a tendency during the parameter variation runs for other DOM sources to increase when one source decreases thus keeping the overall concentration of DOM relatively stable. This likely occurs because of the feedback between the model variables and because the system is at steady state, nitrogen limited, and must conserve mass.

In addition, at steady state concentrations of ammonium and nitrate are 0.02 and 0.05 mmol N m^{-3}, detritus consists of 0.45 mmol C m^{-3} and 0.13 mmol N m^{-3}, bacterial virus concentrations are 0.04 mmol N m^{-3}, and phytoplankton virus concentrations are 0.02 mmol N m^{-3}.

Coastal production

As in the oceanic model run, production by coastal phytoplankton and bacteria (Table 1.1) are within the range of values reported in the literature (BP (mg C m^{-3} d^{-1}): 0.2- 2184, avg. 25-119; PP (mg C m^{-3} d^{-1}) at 60% irradiance in August off the Delaware Coast: 2.43-312, median 18.89) but lower than the typical average (Behrenfeld et al., 2006a; Ducklow and Carlson, 1992). The lower than average production rates and the high bacterial to primary production ratio is again likely a result of how we tuned the model biomass distribution (see oceanic production section).

Coastal uptake and regeneration

The total uptake (mmol N m^{-3} d^{-1}) of ammonium and nitrate by phytoplankton (Table 1.3) is within the range (NH_4^+: 0.031 – 1.38; NO_3^-: 0.0014 – 0.26) reported for studies in the South Atlantic coastal shelf (Metzler et al., 1997). The uptake of DIC by phytoplankton reflects the fixed C:N ratio of phytoplankton which dictates that for every mole of nitrogen taken up 7.5 moles of carbon must be taken up as well. Uptake of DOC

and DON by bacteria (Table 1.3) corresponds with bacterial production (Table 1.1), which is a measure of assimilated DOM that becomes bacterial biomass.

Ammonium is regenerated by bacteria and zooplankton at 0.04 mmol N m^{-3} d^{-1}, of which 37 % is derived from bacteria, 48% is from small zooplankton, and 15% is from large zooplankton. This rate of regeneration is much less than the rate at which ammonium is assimilated by phytoplankton (Table 1.3) indicating that regenerated nutrients alone cannot sustain this abundance of coastal phytoplankton at a steady state.

Coastal DOC production

Dissolved organic carbon is produced at 407.5 nmol C m^{-3} d^{-1} with the largest individual source of DOC being phytoplankton exudation (202.5 nmol C m^{-3} d^{-1})(Fig. 1.5 c), which is mostly (70%) from small phytoplankton. This rate of DOC production from phytoplankton exudation, which accounts for 50% of total DOC production, is within the large range of reported exudation rates (0-24 mmol C m^{-3} d^{-1}) (Carlson, 2002). The other 50% of DOC is produced by excretion, mortality, lysis, sloppy feeding, viral decay, and detritus decay. None of these sources stands out as particularly important (Fig. 1.5 c) although DOC from viral decay and detritus decay is less than from the other sources. Phytoplankton exudation of DOC is clearly the most important individual source of DOC in this model of coastal waters. Phytoplankton exudation also remains the most important source of DOC even when the parameters involved in DOM production are allowed to vary. DOC is also converted to DIC at a rate of 30 nmol C m^{-3} d^{-1} which is important because it acts to turnover less bio-available forms of DOC.

Coastal DON production

DON is produced at 760 nmol N m^{-3} d^{-1} which is within the range of coastal DON production reported in the literature (see table IV in Bronk (2002)). The DON release to gross N uptake ratio is 55% which is within the range of reported DON release to gross N uptake ratios (Bronk, 2002). The production of DON (Fig. 1.5 d) is derived from a variety of sources such as phytoplankton exudation, zooplankton excretion, mortality, viral lysis, viral decay, and detritus decay. The largest individual source is phytoplankton exudation and the smallest source is zooplankton excretion. The magnitude of dissolved organic nitrogen derived from mortality, viral lysis, sloppy feeding, viral decay, and the decay of detritus is similar. In addition, refractory DON is converted to labile DON through photooxidation at a rate of 10 nmol N m^{-3} d^{-1} which is important because this is the only mechanism to prevent refractory DON from accumulating. In some of our early model test runs where we turned off photooxidation we could not get the model to achieve a steady state as everything was eventually converted to refractory DOM.

The sensitivity of DON sources to parameter variations is shown in Figure 1.10. The production of DON from viral lysis is only moderately sensitive (Fig. 1.10 a) to variations in the viral infection rate, the mortality rate, the viral decay rate, and the growth efficiency of bacteria. Since most of the DOM from lysis comes from bacterial lysis (92% in the main coastal run) it is not surprising that the production of DON from viral lysis is also sensitive to parameters that affect the biomass (Fig. 1.10) and production of bacteria. If bacterial biomass or production increases then so does the amount of DON from lysis and vice versa.

The production of DON from sloppy feeding is not very sensitive (Fig. 1.10 b) to parameter variations when normalized to large zooplankton and phytoplankton biomass. The production of DON from mortality is sensitive (Fig. 1.10 c) only to variations in the mortality rates of the plankton. Zooplankton excretion of DON is not very sensitive (Fig. 1.10 e) to parameter variations because the biomass of small zooplankton, who produce most of the excreted DON, does not vary much during the parameter variation runs. When their biomass does increase during the mortality variation runs (Fig. 1.9 d), the increase in biomass is offset by a bigger decrease in the biomass of large zooplankton. This is in contrast to oceanic runs where the amount of DON produced by zooplankton excretion was sensitive to the parameters involved in viral infection (Fig. 1.6 e). This example highlights one of the main differences between the oceanic and coastal model runs. In the oceanic simulation the plankton dynamics were very dependant on the interactions between bacteria and other plankton, while in the coastal model run bacteria exerted less control on the biomass and productivity of other plankton and the role of grazers became more important. The production of DON from the decay of detritus is sensitive (Fig. 1.10 f) only to variations in the decay rate of detritus.

Dissolved organic nitrogen from phytoplankton exudation is sensitive (Fig. 1.10 g) to variations in the viral infection rate, the mortality rate, the viral decay rate, and the exudation parameter. Small phytoplankton produce most (69% in the main run) of the DON from exudation, so parameter variations that affect their biomass or production have the largest influence on this source of DON. Thus, the competition between large and small phytoplankton that was discussed in the section above plays an important role in determining how much DON is produced by exudation. An increase in the viral

infection rate increases DON production even though the biomass of large phytoplankton declines and the biomass of small phytoplankton stays about the same. This is because small phytoplankton production increases by 27% because there is less competition from large phytoplankton. Thus, the increased mortality experience by small phytoplankton is offset by increased growth. Decreasing viral infection reduces the amount of DON from phytoplankton exudation even though the total biomass of phytoplankton increases. This is because competition between phytoplankton then results in a decrease in small phytoplankton production thus decreasing the amount of DON from exudation.

The production of DON from the decay of viruses, which is dependant on the abundance of viruses, is sensitive (Fig. 1.10 d) to variations in the infection rate, the mortality rate, the viral decay rate, the zooplankton excretion parameters, the phytoplankton exudation parameter, and the growth efficiency of bacteria. DON from viral decay is only moderately sensitive to variations in the rate of viral infection, which will increase or decrease the abundance of viruses. Interestingly, DON from viral decay is not sensitive to a decrease in the mortality rate but is very sensitive to an increase in the mortality rate. An increase in the mortality rate causes the biomass of bacteria and large phytoplankton to decline while the biomass of small phytoplankton increases slightly (Fig. 1.9 d). This results in fewer viruses being produced so fewer viruses to decay. As expected, variations in the rate of viral decay causes the amount of DON from viral decay to change substantially. Variations in the zooplankton excretion parameters and the phytoplankton exudation parameter have very little affect on planktonic biomass (Figs. 1.9 f and g) but they do impact phytoplankton and bacterial production so the amount of DON from viral decay is moderately sensitive to variations in these parameters.

Variations in the growth efficiency of bacteria affect the amount of DON from viral decay because bacterial lysis is the largest source of viruses, i.e., changes in this parameter affect the biomass and production of bacteria and therefore also the production of viruses and their decay to DON.

Overall the sensitivity of coastal DON sources to parameter variations show a very similar response, with the exception of DON from zooplankton excretion, when compared to the sensitivity of oceanic DON sources to the same parameter variations. However, even though the pattern is similar the magnitude of the response of some DON sources is different. The increase or decrease in DON from viral lysis and viral decay is less in the coastal runs than in the oceanic runs (Figs. 1.6 a, d and 1.10 a, d). Given that these variations are normalized to the biomass of each system this shows that viruses play a less important role in coastal DON production than they do in oceanic DON production. In addition, coastal DON sources were much more sensitive to variations in phytoplankton exudation than in the oceanic runs (Figs. 1.6 and 1.10 g). This is likely due to competition between large and small phytoplankton.

Coastal DOM Inflow Sensitivity

Figure 1.11 compares the biomass of plankton and the concentration of DOC and DON at steady state for the main run and a case where external DOM loading is turned off. Except for large zooplankton the biomass of plankton is almost the same in both runs. When there is no DOM loading the concentrations of refractory DOC and DON both decline and are affected the most, whereas the concentrations of labile DON and DOC remain largely unchanged. The effect on the semi-labile pools is intermediate, but semi-labile DON concentrations increase and semi-labile DOC concentrations decrease.

As in the oceanic model run, this increase in semi-labile DON and decrease in semi-labile DOC is because all of the semi-labile DOM is being "freshly" produced and has a lower C:N ratio. Whereas in the main run the semi-labile DOM pools are supplied by inflowing DOM with a high C:N ratio and "freshly" produced DOM. Thus, overall the DOM loading acts mostly to stabilize the concentration of the more refractory DOM and to keep the C:N ratio of the pools higher whereas the more labile components are maintained to a greater extent by ecosystem recycling.

As in the rest of sensitivity analysis, the production of DOC and DON (Fig. 1.12) in these runs depends on how the external DOM load affects the biomass or production of the plankton that directly produce or indirectly play a significant role in the internal production of DOM. For example, when there is no DOM loading the biomass and production of large zooplankton increases which results in an increase in the amount of DOC and DON produced by sloppy feeding.

Coastal Summary

Our model is able to reproduce DOM and biomass concentrations, uptake rates, and production (biological and DOM) rates that fall within ranges reported for coastal surface waters. Like the oceanic model runs, the coastal model runs show that DOM cycling in a coastal environment is intricately tied to the biomass concentration, ratio, and production of zooplankton, phytoplankton, and bacteria. There were also some important abiotic processes occurring as well such as photooxidation, which was our only mechanism for turning over refractory DOM in coastal waters. Like the oceanic runs, the DOC and DON concentrations are robust quantities, i.e., they do not vary much during the parameter variation runs because there are compensatory changes in the various

source and sink terms. But in marked contrast to the oceanic case, competition between large and small phytoplankton plays a large role in DOM production and cycling in the coastal runs. Any changes that increase the biomass and production of small phytoplankton tend to result in a decrease in the biomass and production of large phytoplankton and vice versa. This suggests the potential for substantial temporal changes in the sources and sinks for DOM cycling in coastal waters, i.e., seasonally, even though absolute concentrations may not change very much. Zooplankton play a more important role in nutrient cycling in the coastal run (compared to the oceanic case) because small zooplankton are responsible for more than half of the ammonium regeneration. Phytoplankton are, therefore, less dependant on bacteria for regenerated ammonium. As a result, the production of DOM is less sensitive than in the oceanic model runs to parameter variations that affect bacteria. Because small zooplankton must graze on other plankton in order to regenerate nutrients they exert both a "top down" and "bottom up" control on the ecosystem dynamics. Thus, indicating that DOM production in coastal waters is determined by more of a balance between "top down" and "bottom up" control than in the oceanic model runs where the regeneration of nutrients by bacteria (bottom-up control) was the most important process. However, as noted in the oceanic section it is difficult to draw conclusions about top-down vs. bottom-up control in steady-state modeled ecosystems. Nonetheless, there are obvious differences between the oceanic and coastal model runs that highlight the importance of both grazing and the regeneration of nutrients in the coastal model runs.

Estuarine Model Run

Estuarine Planktonic Biomass

The estuarine biomass distribution (Fig. 1.2 c) reflects the tuning of the model to the relative coastal planktonic biomass ratios found by Gasol et al. (1997). The coastal ratios are used for the estuarine runs because estuarine planktonic biomass distribution data comparable to Gasol et. al. (1997) are not available. However, unlike the coastal model run we used a higher zooplankton to phytoplankton ratio for the large zooplankton biomass in order to reflect the abundance of large zooplankton in estuarine waters. Thus, instead of using the mean value, as we did in the coastal run, reported for the zooplankton to phytoplankton ratio (0.87:1) in Gasol et. al (1997) we used the mean plus the standard deviation (0.18) to set the large zooplankton to phytoplankton biomass ratio. The biomass of plankton in figure 1.2 c was set so that bacterial biomass was within the range typically found in August in the mesohaline region of the Chesapeake Bay, USA. The biomass of other plankton was then tuned based on the biomass ratio discussed above.

The sensitivity of plankton biomass to parameter variations is shown in figure 1.13. Large zooplankton are sensitive to parameter variations in viral infection, sloppy feeding, mortality, viral decay, and the growth efficiency of zooplankton. In contrast, small zooplankton biomass is not particularly sensitive to parameter variations. This does not mean that small zooplankton are unaffected by parameter variations as their productivity often changed in response to parameter variations without changing their biomass. Large phytoplankton are sensitive to parameter variations in viral infection, sloppy feeding, mortality, viral decay, and the growth efficiency of zooplankton. Small phytoplankton are moderately sensitive to parameter variations in viral infection, sloppy

feeding, mortality, viral decay, and the growth efficiency of zooplankton. Bacteria are sensitive only to parameter variations in the viral infection and decay rates.

As in the coastal model runs, competition between large and small phytoplankton is clearly evident in the parameter variation runs (Fig. 1.13), i.e., parameter changes that increase the biomass of one phytoplankton size class usually decrease the biomass of the other size class and vice versa. For example, when the mortality rates are varied (Fig. 1.13 d) for zooplankton, phytoplankton, and bacteria the biomass of large phytoplankton always increases and the biomass of small phytoplankton always decreases. Competition between bacteria and phytoplankton may also occur because bacteria are nitrogen limited in the estuarine case (see below). However, if competition between phytoplankton and bacteria is occurring it is not readily apparent in figure 1.13.

Large phytoplankton and bacteria are sensitive to variations in viral infection (Fig. 1.13 a) and viral decay rates (fig. 1.13 e) because these parameters are a source of mortality for large phytoplankton and bacteria. Large zooplankton are sensitive to variations in these parameters because large phytoplankton are an important prey item for them so their biomass and productivity depends partially on the biomass and productivity of large phytoplankton who are sensitive to viral infection. Small phytoplankton are moderately sensitive (loss of biomass) only to increases in viral infection and decreases in the viral decay rate, both of which act to increase their mortality. Their biomass seems to be mostly unaffected by parameter variations that reduce their mortality from viral infection (i.e. decreased rate of viral infection or an increased rate of viral decay). However, although their biomass does not change much when these sources of mortality are reduced their productivity decreases by 27%, due to increased competition with large

phytoplankton and increased grazing, thus offsetting the impacts of reduced mortality from viral infection.

Large zooplankton and phytoplankton are sensitive to parameter variations in sloppy feeding (fig. 1.13 b) because large zooplankton are very abundant and productive in estuarine runs. Thus, increases or decreases in the sloppy feeding parameter have an effect on large zooplankton and their primary prey, large phytoplankton. The effect of sloppy feeding on large phytoplankton then influences competition between large and small phytoplankton.

Plankton are sensitive to variations in the mortality rate (fig. 1.13 d) because mortality represents a direct loss of biomass. However, aside from the competition between large and small phytoplankton, variations in mortality do not affect plankton quite as we expected. While the biomass of all plankton, except large phytoplankton, decreases with increased mortality their biomass does not increase with decreased mortality. Instead it either stays the same or decreases slightly. Productivity decreases as well for all plankton except large phytoplankton when the rate of mortality decreases. It is not clear to us why this occurs as we had expected that a reduction in mortality would increase the biomass and productivity of all of the plankton.

Large zooplankton and large and small phytoplankton are sensitive to variations in the zooplankton growth efficiency because zooplankton play an important role in estuarine plankton dynamics as both grazers and regenerators of nutrients. Thus a decrease in the growth efficiency of zooplankton decreases the biomass of large zooplankton and reduces the grazing pressure on phytoplankton. And although this may slightly reduce the availability of regenerated nutrients it still benefits phytoplankton,

especially small phytoplankton who are then able to out compete large phytoplankton. An increase in the growth efficiency of zooplankton has the opposite effect.

As this sensitivity analysis and other data presented below shows, the plankton dynamics in the estuarine case differ from the oceanic and coastal plankton runs because the role of bacteria changes from a source of nutrients for phytoplankton uptake to a potential competitor. As a result, bacteria do not play such a key a role in determining the biomass and distribution of the other plankton groups in the estuarine case. Rather, zooplankton-mediated grazing plays a key role. This of course also means that the regeneration of nutrients by zooplankton must be important as well. Of course as in the oceanic and coastal runs viral lysis still plays an important role as a source of mortality for both bacteria and phytoplankton. These dynamics are evident in the parameter variation runs (Fig. 1.13) where the plankton are generally less sensitive to parameter variations that affect mostly bacteria (bacterial growth efficiency; Fig. 1.13 h) and the regeneration of nutrients (zooplankton excretion, fig. 1.13 f) and are more sensitive to parameter variations that affect zooplankton grazing (sloppy feeding, zooplankton growth efficiency; Fig. 1.13 b, i) and viral lysis (Fig. 1.13 a, e). This does not imply that bacteria or regenerated nutrients do not play an important role in estuarine plankton dynamics. Rather, it just means that that they are not as important as zooplankton grazing or viral lysis in determining the biomass concentration, distribution, and production of other plankton groups. All of these results point to more of a "top down" control of the plankton dynamics in our estuarine model runs.

Other State Variables

The steady state concentrations of ammonium and nitrate are 0.07 and 0.45 mmol N m^{-3}, detritus consists of 3.84 mmol C m^{-3} and 1.45 mmol N m^{-3}, bacterial virus concentrations are 0.32 mmol N m^{-3}, and phytoplankton virus concentrations are 0.27 mmol N m^{-3}.

The steady state concentrations of DOC and DON (Fig. 1.4 e, f) are within the range of measured total DOC and DON concentrations typically found in estuarine surface waters (Bronk, 2002; Carlson, 2002). Note, however, that in contrast to the oceanic and coastal runs, there are relatively large variations in the DOM concentrations that arise when the model parameters are varied. These variations appear to be due to the transfer of DOM between refractory and semi-labile pools as the overall concentration of DOM does not change substantially (total DOC range 264-296 mmol C m^{-3}, total DON range 30-35 mmol N m^{-3}). Thus, in the estuarine case it appears that the DOM pool is particularly sensitive to the parameter variations.

Estuarine Production

Primary production in the Chesapeake Bay ranges from 240 to 564 mg C m^{-3} d^{-1} (Ducklow, 2001) and our rate of primary production (Table 1.1) falls within this range. Our bacterial estuarine production rates (Table 1.1) are higher than the average values (50-73 mg C m^{-3} d^{-1}) reported for estuarine systems (Ducklow, 2001; Ducklow and Carlson, 1992). However, our model is tuned to reproduce the high bacterial biomass typically found in the mesohaline portion of the Chesapeake Bay, USA and our bacterial productivity falls within the range (1.20 – 600 mg C m^{-3} d^{-1}) of values reported for the Chesapeake Bay (Ducklow, 2001). As in the coastal and oceanic cases, the high bacteria

to primary production ratio is likely due, in part, to tuning the model to the biomass distribution from Gasol et al. (1997) (see oceanic production section). In addition, bacterial production in the estuarine run is different from the other systems in that it is not constrained as much by DOM produced within the system (i.e. estuaries have a high rate of external DOM loading from terrestrial sources and bacterial production may occasionally exceed local primary production (Ducklow, 2001)).

Estuarine Nitrogen Uptake and Regeneration

The total uptake (mmol m^{-3} d^{-1}) of ammonium and nitrate by plankton (Table 1.3) is within the range (see Fig. 2 in (Bronk et al., 1998)) reported for the Chesapeake Bay estuary. Note that large phytoplankton take up more nitrate than small phytoplankton, even though their productivity is lower, which is consistent with research (Stolte et al., 1994) that shows that large phytoplankton, such as diatoms, are better competitors for nitrate. As in the previous runs, the uptake of DIC by phytoplankton reflects the fixed C:N ratio of phytoplankton. In contrast to the coastal and oceanic runs, in the estuarine case bacteria are unable to meet their nitrogen requirement through the uptake of DON alone and consequently they take up ammonium (Table 1.3). Because bacteria need to retain and use ammonium as a nitrogen source they stop regenerating it. Thus, as we pointed out above, all of the regenerated ammonium (0.87 mmol N m^{-3} d^{-1}) is supplied by zooplankton with small zooplankton producing 66% of it. In addition, photooxidation of DON produces ammonium at a rate of 20 nmol N m^{-3} d^{-1}. Overall, the uptake of ammonium by phytoplankton and bacteria exceeds the amount supplied by regeneration indicating that regenerated nutrients alone cannot sustain production in the estuarine case. This result is consistent with ammonium regeneration and uptake measurements taken in

the Chesapeake Bay estuary during August (the month to which our biomasses were tuned) which show that the ammonium regeneration to gross ammonium uptake ratio was 0.86 (Bronk et al., 1998). In the run where there is no external DOM loading (see section below) the plankton survive on regenerated nutrients alone but their biomass and productivity are much lower.

Estuarine DOC Production

Dissolved organic carbon is produced at a rate of 13.17 mmol C m^{-3} d^{-1}. As in the coastal case, the largest source (48%) of dissolved organic carbon (Fig. 1.5 e) was phytoplankton exudation (6.34 mmol C m^{-3} d^{-1}) with 59% of it coming from small phytoplankton. This is within the large range of reported exudation rates (0-24 mmol C m^{-3} d^{-1}) (Carlson, 2002). Even when the model parameters are varied, phytoplankton exudation is always the largest source DOC which is also what we observe in the coastal run. Sloppy feeding and viral lysis are also important sources of DOC representing 33% of total DOC production. In addition, refractory DOC is converted to labile DOC through photooxidation at a rate of 170 nmol C m^{-3} d^{-1}. As noted in the coastal section, photooxidative processes are important because they allow refractory material to be turned over and prevent it from accumulating.

Estuarine DON Production

Dissolved organic nitrogen is produced at 1.57 mmol N m^{-3} d^{-1} which is within the range of estuarine DON production (0 – 39.12 mmol N m^{-3} d^{-1}) reported in the literature (Bronk et al., 1998; Lomas et al., 2002). The production of DON (Fig. 1.5 f) is derived from a variety of sources with phytoplankton exudation, viral lysis, sloppy feeding, and viral decay the largest. As in the coastal run, the largest individual source of DON is

phytoplankton exudation which is 29% of the total DON production. The smallest source of DON is from mortality. However, DON production from individual sources varies over a large range when the model parameters are changed (see range bars in Fig. 1.5). As in the oceanic and coastal cases, the amount of DON produced by most of these sources during the parameter variation runs is related to the effect that a parameter variation has on the biomass and production of the source. DON is also converted from refractory DON to labile DON through photooxidation at a rate of 30 nmol N m^{-3} d^{-1}.

The sensitivity of DON sources to parameter variations is shown in figure 2.14. The production of DON from lysis (Fig. 1.14 a) is moderately sensitive to parameter variations in the viral infection rate and the viral decay rate. Bacteria, the source of 85% of the DON from lysis in the main run, are sensitive to parameter variations in viral infection rate and the viral decay rate so it is not surprising that DON from lysis is sensitive to these parameter variations. The production of DON from sloppy feeding (Fig. 1.14 b) is not sensitive to parameter variations with the exception of an increase in the mortality rate. In the run where the mortality rate is increased the biomass of large zooplankton decreases (Fig. 1.13 d) so less sloppy feeding occurs. The production of DOM from mortality is sensitive (Fig. 1.14 c) only to variations in the mortality rates of plankton. The production of DON from viral decay (Fig. 1.14 d; note the different scale) is very sensitive to parameter variations in the viral decay rate. The production of DON from zooplankton excretion is not sensitive to parameter variations (Fig. 1.14 e) because the biomass of small zooplankton, who excrete 73 % of the DON in the main run, is not sensitive to parameter variations (Fig. 1.13). The production of DON from the decay of detritus is only sensitive (Fig. 1.14 f) to parameter variations in the rate of decay. The

production of DON from phytoplankton exudation is sensitive (Fig. 1.14 g) to parameter variations in viral infection, sloppy feeding, mortality, viral decay, exudation, and the growth efficiency of zooplankton. The production of DON from phytoplankton exudation is sensitive to these parameters because of competition between phytoplankton. Small phytoplankton exude more DON than large phytoplankton (60% in the main run) even if their biomass is lower so parameter changes that shift the biomass distribution of phytoplankton as a result of competition changes how much DON is exuded.

Overall the sensitivity of estuarine DON sources to parameter variations show a somewhat mixed response when compared to the sensitivity of oceanic and coastal DON sources to the same parameter variations (Figs. 1.6, 1.10, and 1.14). Parameter variations in mortality, viral lysis, and the decay of detritus show similar sensitivity trends in all three types of model runs while other variations like zooplankton excretion affect sources differently in the different model runs. The sensitivity of DON sources to variations in zooplankton excretion was low in the estuarine and coastal model runs but high for several sources in the oceanic model run. In addition unlike the oceanic and coastal runs, the estuarine model runs show that only DON from viral decay is sensitive to variations in the viral decay rate. DON sources are also affected much more by changes in phytoplankton exudation in the estuarine run than they are in the oceanic and coastal runs. Furthermore, in the estuarine model runs variations in sloppy feeding have a larger effect on a DON source (mortality) than they do on any DON source in the coastal or oceanic runs.

Estuarine DOM Inflow Sensitivity

Here also, we performed addition model runs to examine the effect of DOM loading, which in the estuarine case represents a substantial addition of organic nutrients into the system. Figure 1.15 compares the planktonic biomass and the concentration of DOC and DON at steady state for the main run and a run where there is no DOM loading. Surprisingly, when there is no DOM loading the biomass of plankton is almost the same or slightly higher than the main run. This is likely because bacteria are not remineralizing the DOM anyway so phytoplankton are not dependant on it as a remineralized source of nutrients for growth and are thus mostly unaffected by not having inflowing DOM.

The concentrations of labile and semi-labile DOC and DON are all relatively unchanged with no DOM loading. The concentration of refractory DOC and DON are reduced with no DOM which is not surprising given that the DOM inflow acts mostly to keep the concentrations of refractory DOM high. The internal production of DOM (Fig. 1.16) is determined by how variations in the external DOM flux (and the loss terms associated with running the model like a chemostat) affect the biomass and production of plankton. For example, if the biomass and production of phytoplankton is reduced then the production of DOM from phytoplankton exudation is reduced. When there is no DOM loading the production of DOM (Fig. 1.16) increased slightly from every source except the decay of detritus because the biomass and productivity of all of the plankton groups increased slightly.

Estuarine Summary

As in the coastal and oceanic cases, our model can be tuned to reproduce DOM and biomass concentrations, uptake and production rates (biological and DOM) that fall within ranges reported for estuarine surface waters. However, here also the model has a tendency to overestimate the ratio of bacteria to phytoplankton production. In this case high external DOM loading contributes to this problem because it increases bacterial production. Note also that even though the model is actually tuned to generate the coastal biomass distributions, with the exception of the large zooplankton to phytoplankton ratio, the results are different from the coastal case because the forcing and parameterization are not the same. These differences include lower light availability and substantially higher DOM and DIN loading.

Like the oceanic and coastal cases, the estuarine model runs show that DOM cycling in an estuarine environment is intricately tied to the biomass concentration, ratio, and production of zooplankton, phytoplankton, and bacteria. In addition, viral lysis plays an important role in the estuarine DOM cycling just as it did in the oceanic and coastal runs. Furthermore as in the coastal runs, competition between phytoplankton also plays a large role in DOM production and cycling in the estuarine runs. However, the estuarine runs are different from the other two cases because zooplankton play a particularly important role in the ecosystem dynamics and nutrient cycling, i.e., they not only exert top-down control of biomass through grazing, but also bottom-up control of phytoplankton growth through the regeneration of nutrients. And while both top-down and bottom-up controls are important drivers of the plankton dynamics in any system our analysis shows that in the estuarine model runs grazing had more of an influence on the

plankton dynamics and DOM cycling than the regeneration of nutrients by zooplankton. Thus, highlighting the role of zooplankton in the production of estuarine DOM.

Another important difference compared to the coastal and oceanic cases is that bacteria act as consumers of ammonium instead of a source for phytoplankton growth in the estuarine runs. Bacteria may even be competing with phytoplankton for nutrients. Because bacteria do not regenerate ammonium in these runs their role in determining the planktonic biomass concentration, distribution, and productivity at steady state is not as important as in the oceanic and coastal model runs. However, even though bacteria do not play as large a role in the plankton dynamics they still play a major role in DOM cycling by consuming DOM and contributing to it through viral lysis and mortality. Abiotic processes such as photooxidation, which is our only mechanism for turning over refractory DOM in estuarine waters, is also important in these runs.

Summary and Conclusions

In this paper we describe a new model formulation that is designed to simulate and investigate DOM cycling in pelagic marine systems. This model includes a representation of DOM in terms of refractory, semi-labile and labile constituents for both DON and DOC. In addition, sources and sinks for DOM from multiple phytoplankton and zooplankton size classes and bacteria are included in the model, along with an explicit representation of the impacts of viruses and viral infection. The effects of light on DOM lability are also included in the model. As such, the level of detail in the DOM pools and cycling in this model are unprecedented.

The model was broadly tuned and parameterized to provide steady state solutions for idealized oceanic, coastal and estuarine systems with the explicit goal of comparing

the DOM cycling dynamics in these different environments. These three different model implementations were generated by tuning the model to reproduce broad differences in the observed biomass distributions as defined by Gasol et al. (1997) and Malone (1980) under different forcing conditions (i.e., light availability and nutrient/DOM loading). The model results are analyzed using classic sensitivity analysis methods to characterize how the model behaves differently in oceanic, coastal and estuarine conditions.

We show that the model is able to reproduce the Gasol et al. (1997) biomass distributions in our oceanic, coastal and estuarine runs. Through comparisons with available data we demonstrate that the model generates reasonable DOM concentrations and also uptake and production rates (for phytoplankton, bacteria and DOM) that fall within ranges reported for oceanic, coastal, and estuarine systems. Thus we conclude that our detailed treatment of DOM cycling captures the flow of carbon and nitrogen through the different biological and chemical states that are involved in DOM cycling. Differences in the forcing and parameterizations in the oceanic, coastal and estuarine runs give rise to significant differences in DOM cycling that are intricately tied to differences in the biomass concentration, distribution, and production of phytoplankton, zooplankton, and bacteria. Abiotic processes such as photooxidation which differed from system to system also played an important role in DOM cycling by altering the bioavailability of some DOM and acting as a turnover mechanism for different pools of DOM.

In the oceanic model runs where nutrients are the most limiting, phytoplankton and zooplankton populations are sustained by bacterial nutrient regeneration. Thus, bacteria are the key to understanding how DOM cycling occurs in this system. Any parameter changes that increase or decrease bacteria biomass or production generally also

increase or decrease the biomass and productivity of phytoplankton and zooplankton as well. This in turn impacts DOM production derived from phytoplankton and zooplankton.

In the coastal model runs small zooplankton and bacteria both play a key role in regenerating nutrients that sustain phytoplankton production. Because there are two sources regenerating ammonium for phytoplankton growth, DOM production is less sensitive to parameter changes that affect the bacteria specifically and also changes that affect plankton dynamics in general. Competition between large and small phytoplankton is also evident in this environment. This suggests the potential for substantial temporal changes in the sources and sinks for DOM cycling in temperate coastal waters, i.e., seasonally, as commonly observed.

In the estuarine model runs, where nutrients are abundant, zooplankton play a particularly important role in controlling phytoplankton growth through a combination of grazing and ammonium regeneration, with grazing being particularly important. Thus, zooplankton have a strong influence on DOM production from phytoplankton and zooplankton. Unlike in the oceanic and coastal systems, bacteria do not have much influence on the plankton dynamics because they become nitrogen limited and take up ammonium instead of regenerating it. In addition, because there is so much DOM entering the system from external sources, bacteria are less dependant on the production of DOM by other planktonic sources. However, bacteria still play a large role in DOM cycling by consuming and contributing to it. Competition between phytoplankton also plays an important role in DOM production and cycling in the estuarine runs.

As our analysis shows the cycling of DOM in each system is strongly dependant on the structure and composition of the planktonic food web. Thus, the relative magnitude of sources and sinks of DOM in each system is mostly tied to the plankton dynamics, with the exception of DOC (and often DON) production from phytoplankton exudation which is always the dominant source. Figure 1.17 shows schematic diagrams which highlight the differences in DOC and DON production in oceanic, coastal, and estuarine model runs. In the oceanic model runs where bacteria are important DOM production was associated with processes that affected bacteria such as viral infection. In the coastal model runs where bacteria and small zooplankton are both important the magnitude of DOM production is similar for most of the sources, reflecting the importance of both top-down controls and bottom-up controls. In the estuarine model runs where grazing is a very important process DOM production from grazing is much more important than in the oceanic and coastal model runs. However, the production of DOM from the viral infection of bacteria is also still important in the estuarine runs because bacterial biomass is high even though bacteria did not have much of an overall effect on other plankton. Despite the differences between these systems there are a few general trends that we observed in all three systems: 1) as previously mention, DOC (and often DON) production is always dominated by phytoplankton exudation; 2) viral lysis is always an important source of DOM; and 3) as shown in the sensitivity analyses the production of DOM from a particular source can vary in magnitude by a considerable amount. The last result (3) has important implications for the cycling of DOM and even for the composition of the communities that utilize the DOM because the quality or bio-availability of DOM is different for each DOM source. However, we cannot elaborate

much further on this point, except to say that more research is needed in this area, because our parameterization which partitions DOM production to the labile, semi-labile, and refractory pools is poorly constrained for most of the sources.

In both the oceanic and coastal runs the concentrations of DOC and DON do not vary much when the model parameters are changed even though the production of DOM from a particular source may vary considerably. Thus it appears that when one source of DOM increases another source of DOM decreases by a similar amount keeping the total concentration of DOM about the same. These results suggests that the absolute DOC and DON concentrations are "robust" quantities in open ocean and coastal systems even though the sources and sinks may change substantially. This may help to explain the fact that DOM concentrations in these environments are relatively constant in space and time. In contrast, in the estuarine case the model generates much more variability in DOC and DON concentrations when the model parameters are changed, indicating that the model is more sensitive to parameter variations in the estuarine runs.

While many of our results compare well to measured marine processes it is difficult to make too many detailed predictions about DOM cycling because our model is currently run to a steady state which makes it hard to compare to marine waters, which are never at steady state. In addition, the model lacks physical processes and a 3-D context both of which play a large role in determining plankton dynamics. Nonetheless, the results of this comparative modeling study are broadly consistent with our conceptual understanding of how ecosystem dynamics and DOM cycling differ between oceanic, coastal and estuarine systems. Furthermore, the model does make some specific predictions about 1) the role of bacteria and zooplankton in nutrient and DOM cycling; 2)

the degree of competition between large and small phytoplankton species and their role in DOM production; 3) the effect of viruses on the plankton dynamics and DOM cycling; and 4) the inherent variability of DOM concentrations in oceanic, coastal and estuarine waters. These predictions can be viewed as testable hypotheses that can be used to help guide future field studies.

The development of this model has also revealed important gaps in our knowledge of key processes that influence DOM cycling in marine waters. Some of the model parameters, especially those related to viral infection and decay, had to be estimated using assumptions that may not be valid. And some processes, such as photochemical effects and the decay of detritus are modeled using simple linear equations and may not adequately describe these processes. Photochemical effects in particular are difficult to model as much of the information on these processes is contradictory, i.e. in some reports they are considered to be DOM sources and in others they are sinks (Mopper and Kieber, 2002). In addition, some parameters such the partitioning of DOM to labile, semi-labile, and refractory pools were poorly constrained. These poorly constrained parameters and processes can also help guide future research.

Tables

Table 1.1. Phytoplankton and bacterial production for oceanic, coastal, and estuarine model runs. The steady state value for the main run is in bold typeface. The range over which production varied during the sensitivity analysis is shown in parenthesis.

	Production (mg C m^{-3} d^{-1})			
	Oceanic	**Sargasso Sea**	**Coastal**	**Estuarine**
Large Phytoplankton	**0.25** (0 - 3.39)	**2.81**	**3.83** (0 - 5.62)	**155** (0 - 356)
Small Phytoplankton	**2.46** (0.78 - 3.01)	**11.82**	**8.32** (5.05 - 14.03)	**227** (0 - 410)
Total Phytoplankton	**2.71** (1.27 - 4.48)	**14.63**	**12.15** (10.33 - 14.12)	**382** (321 - 443)
Bacteria	**2.57** (0.29 - 2.90)	**2.79**	**7.20** (3.45 - 10.42)	**176** (98 - 238)

Table 1.2. Primary production at 60% irradiance from the OPPWG data set for oceanic regions that experience conditions similar to the steady state conditions of the model.

Examples of Typical Oceanic Primary Production		
(mg C m^{-3} d^{-1})	Latitude	Longitude
2.75	12.00	-140.00
6.68	12.00	-140.00
2.17	9.00	-140.00
2.35	9.00	-140.00
4.51	-12.00	-140.00
3.80	-12.00	-140.00
2.73	9.00	-140.00
6.65	-12.00	-140.00
4.87	-46.00	66.83
3.77	-45.23	66.50
4.34	-46.00	66.50
1.09	-12.82	-21.40
1.23	-14.07	-23.02
3.95	-13.49	-22.17
2.32	-13.14	-21.80

Table 1.3. Rates of carbon and nitrogen uptake by phytoplankton and bacteria for the main oceanic, coastal, and estuarine model runs. Phytoplankton and bacteria are unable to take up some substrates which are designated by NA.

Uptake		mmol N m^{-3} d^{-1}			mmol C m^{-3} d^{-1}	
		NH_4^+	NO_3^-	DON	DIC	DOC
Oceanic	Large Phytoplankton	0.0025	0.0015	NA	0.0295	NA
	Small Phytoplankton	0.0315	0.0075	NA	0.2920	NA
	Total Phytoplankton	0.0339	0.0089	NA	0.3215	NA
	Bacteria	0	NA	0.0585	NA	0.1453
Coastal	Large Phytoplankton	0.0400	0.0400	NA	0.4400	NA
	Small Phytoplankton	0.0882	0.0437	NA	0.9894	NA
	Total Phytoplankton	0.1282	0.0837	NA	1.4294	NA
	Bacteria	0	NA	0.1323	NA	0.5998
Estuarine	Large Phytoplankton	0.8000	1.6800	NA	18.4800	NA
	Small Phytoplankton	1.9200	1.6400	NA	26.8400	NA
	Total Phytoplankton	2.7200	3.3200	NA	45.3200	NA
	Bacteria	0.1854	NA	2.6797	NA	14.6123

Figures

Figure 1.1. Diagram of the ecosystem model showing the flow of nitrogen and carbon between the model compartments. Symbols as described in the text.

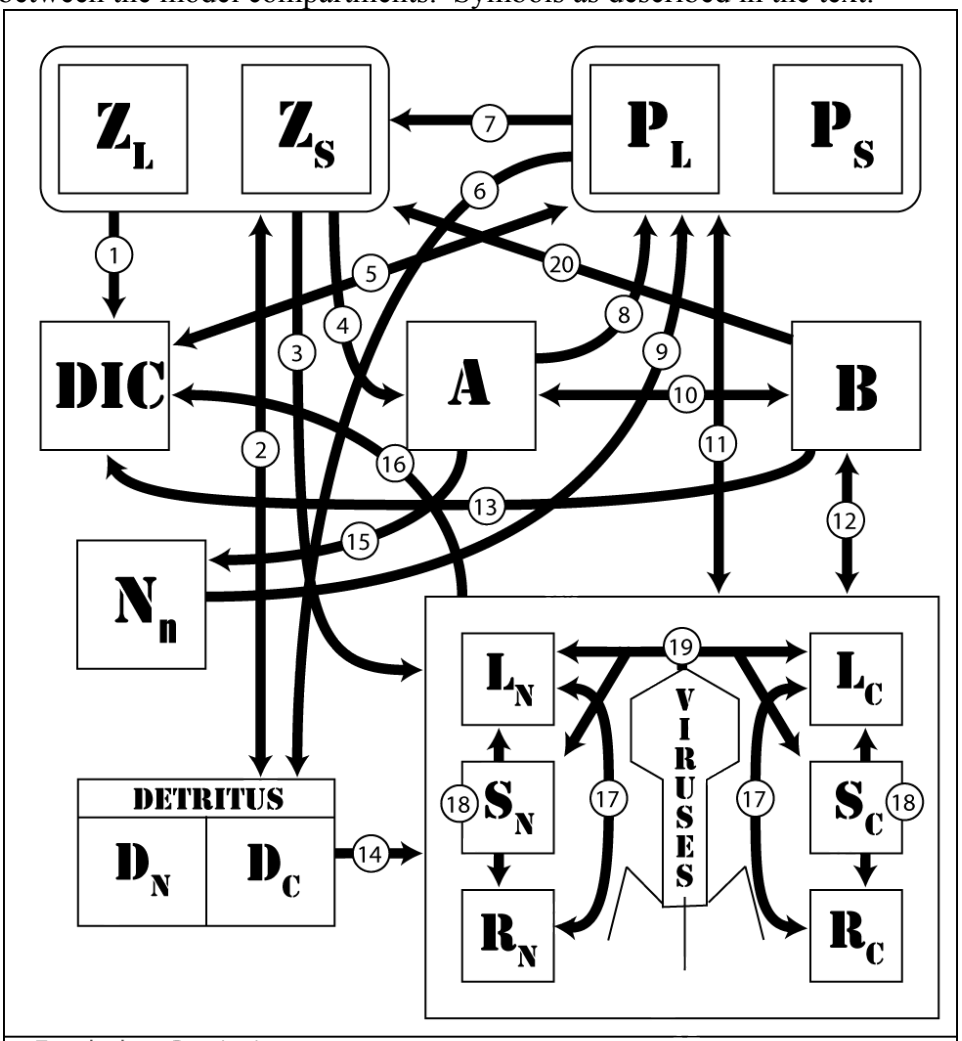

1. Zooplankton Respiration
2. Grazing, egestion, and mortality
3. Zooplankton excretion and mortality
4. Zooplankton excretion
5. Phytoplankton uptake and respiration
6. Phytoplankton mortality
7. Zooplankton grazing on phytoplankton
8. Phytoplankton ammonium uptake
9. Phytoplankton nitrate uptake
10. Uptake or excretion of ammonium
11. Uptake, exudation, mortality, and viral lysis
12. Uptake, mortality, and viral lysis
13. Bacterial respiration
14. Detritus decay
15. Nitrification
16. Photooxidation of DOC
17. Photooxidation of DOM
18. Hydrolysis of semi-labile DOM
19. Viral decay
20. Zooplankton grazing on bacteria

Figure 1.2. Steady state biomass (mmol C m^{-3}) of large and small phytoplankton, large and small zooplankton, and bacteria for the main (a) oceanic, (b) coastal, and (c) estuarine model runs.

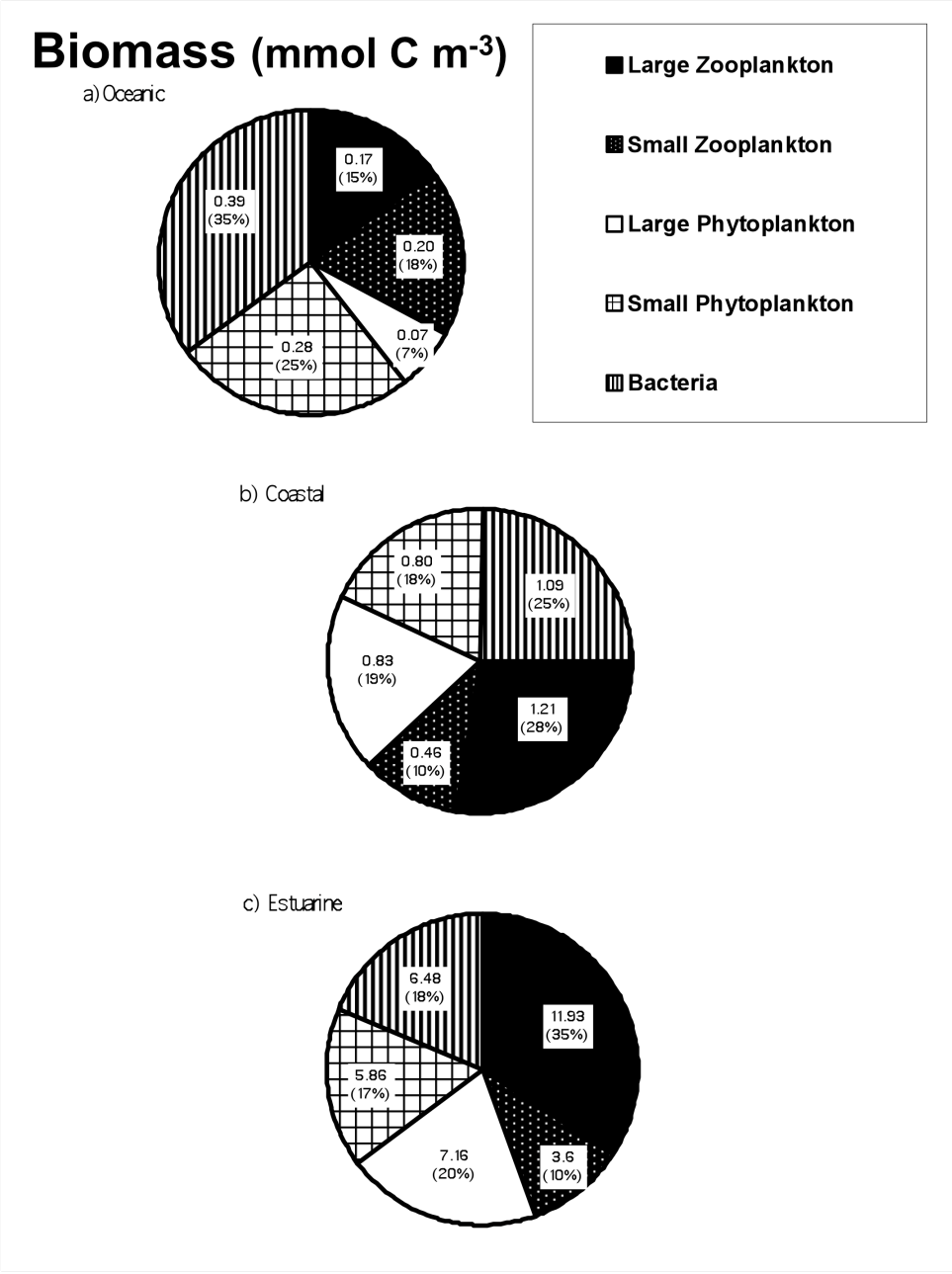

Figure 1.3. Sensitivity of oceanic zooplankton (Lrg. and Sm. Zoo), phytoplankton (Lrg. and Sm. P), and bacterial (B) biomass (mmol C m^{-3}) to parameter variations. The y-axis scale represents normalized deviations from the main oceanic model run biomass concentration (i.e. -0.1 mmol C m^{-3} represents a biomass decrease of 0.1 mmol C m^{-3} for the parameter variation run). Parameter decreases are in black (■) and parameter increases are in white (□). (a) infection rate variation run; (b) sloppy feeding parameter variation run; (c) detritus decay rate variation run; (d) mortality rate variation run; (e) viral decay rate variation run; (f) zooplankton excretion parameter variation run; (g) phytoplankton exudation parameter variation run; (h) bacterial growth efficiency variation run; (i) zooplankton growth efficiency variation run.

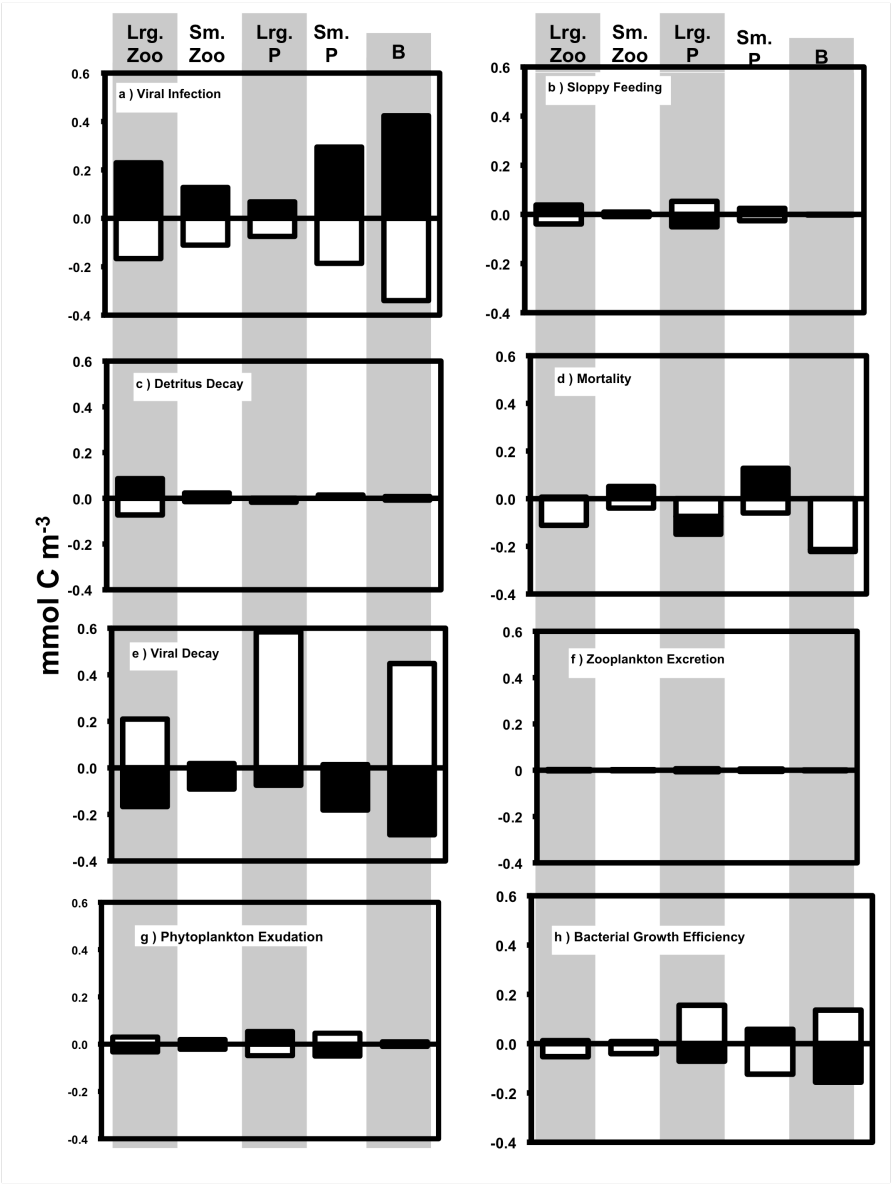

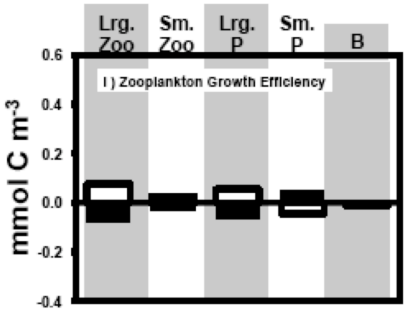
Lrg. Zoo
Sm. Zoo
Lrg. P
Sm. P
B
I) Zooplankton Growth Efficiency
mmol C m-3
0.6
0.4
0.2
0.0
-0.2
-0.4

Figure 1.4. Dissolved organic matter concentrations in terms of bioavailability at steady state for the oceanic, coastal, and estuarine model runs. (a) oceanic DOC concentrations; (b) oceanic DON concentrations; (c) coastal DOC concentrations; (d) coastal DON concentrations; (e) estuarine DOC concentrations; (f) estuarine DON concentrations. The bars represent the range over which the DOM concentrations varied during the parameter variation runs.

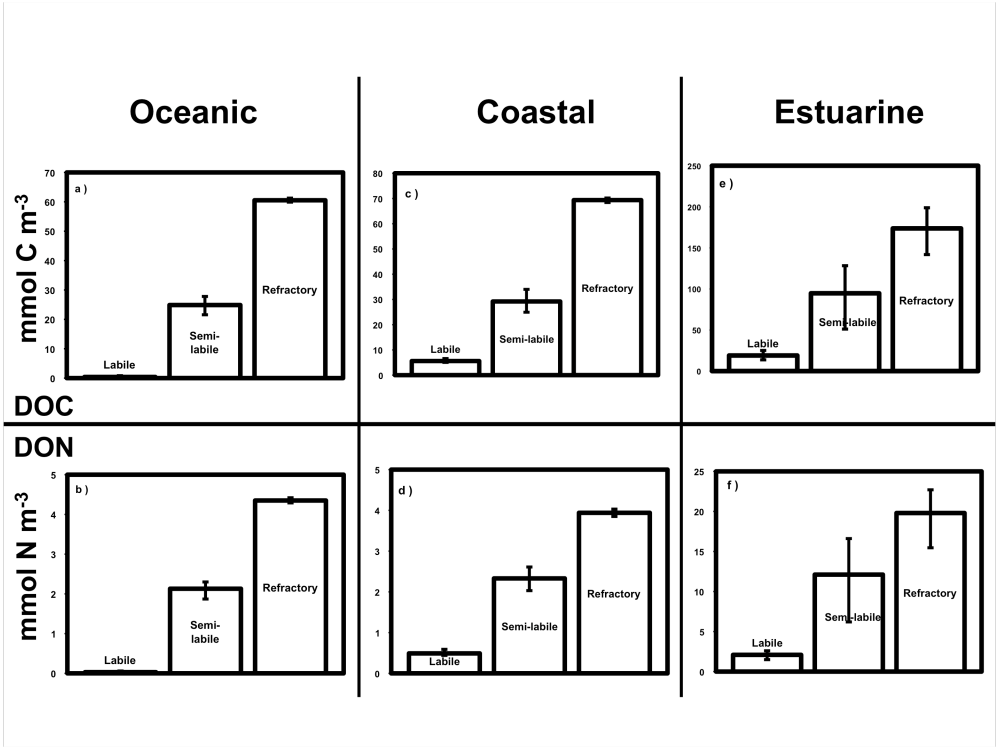

Figure 1.5. Dissolved organic matter production (nmol C or N m^{-3} d^{-1}) from phytoplankton exudation (PE), zooplankton excretion (ZE), mortality (M), viral lysis (L), sloppy feeding (SF), viral decay (VD) and detritus decay (D) at steady state for the oceanic, coastal, and estuarine model runs. (a) oceanic DOC production; (b) oceanic DON production; (c) coastal DOC production; (d) coastal DON production; (e) estuarine DOC production (in mmol C m^{-3} d^{-1}); (f) estuarine DON production. The bars represent the range over which DOM production varied during the parameter variation runs.

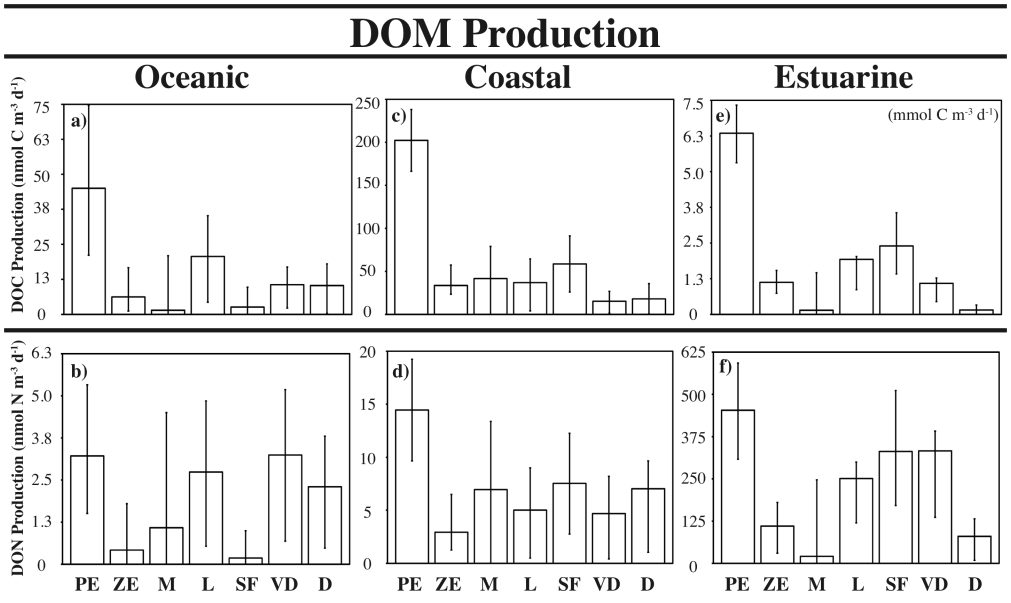

Figure 1.6. Sensitivity of oceanic DON production sources to parameter variation runs. The x-axis shows the different parameter variation runs: infection rate (Ψ_i) variation run; sloppy feeding parameter (ω) variation run; detritus decay rate (χ_D) variation run; mortality rate (S_i) variation run; viral decay rate (υ) variation run; zooplankton excretion parameter (κ_Z and σ_Z) variation run; phytoplankton exudation parameter (α) variation run; bacterial growth efficiency (gge_B) variation run; zooplankton growth efficiency (ge_Z) variation run. The y-axis scale represents normalized deviations from the main oceanic model run production rate at steady state (i.e. -0.1 nmol N m^{-3} d^{-1} represents a production decrease of 0.1 nmol N m^{-3} d^{-1} for the parameter variation run indicated on the x-axis). Parameter decreases are in black (■) and parameter increases are in white (□). (a) DON from viral lysis; (b) DON from sloppy feeding; (c) DON from mortality; (d) DON from viral decay; (e) DON from zooplankton excretion; (f) DON from detritus decay; (g) DON from phytoplankton exudation.

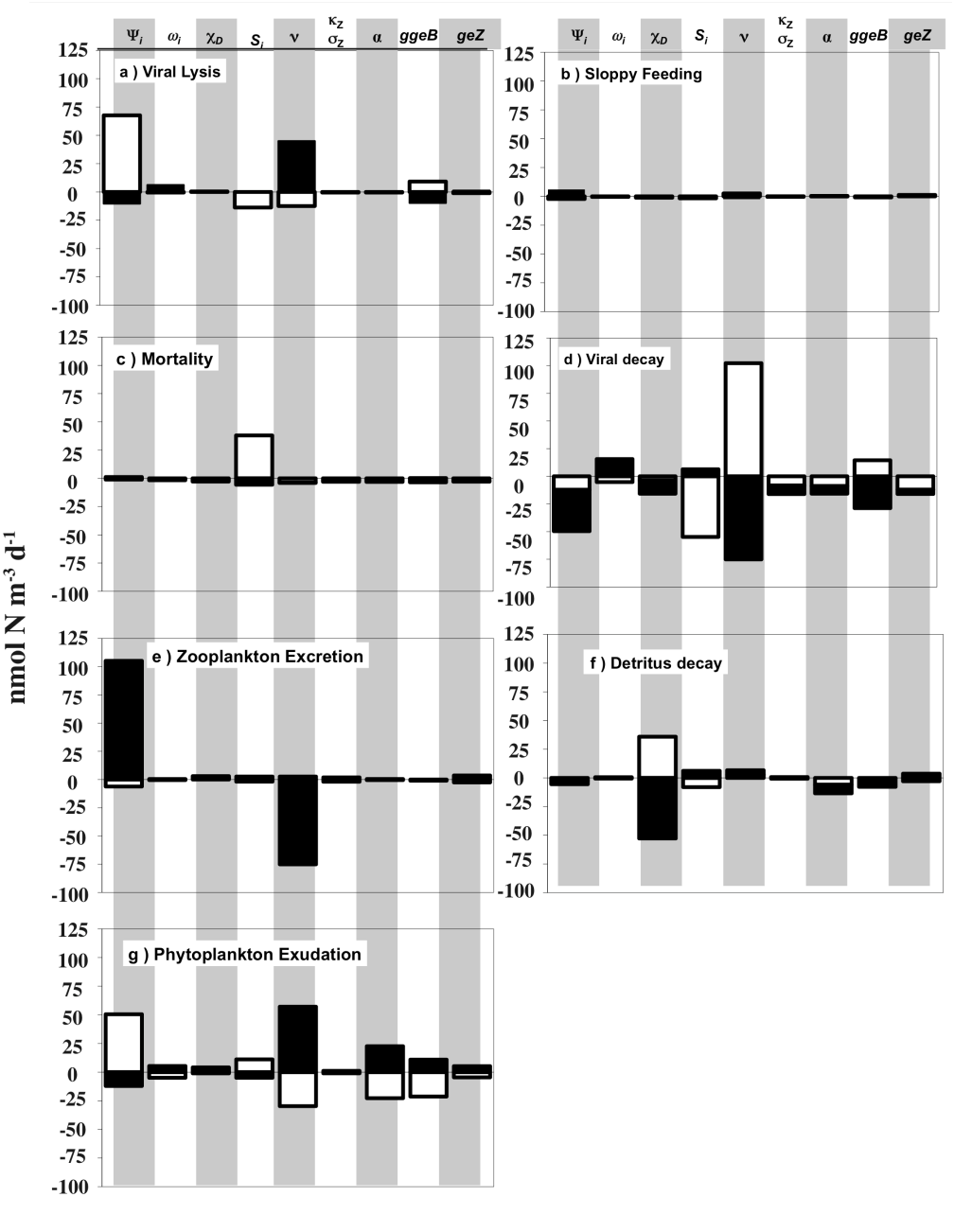

Figure 1.7. Biomass and DOM concentration comparison between the main oceanic model run and an oceanic run where DOM inflow was zero. The run were DOM inflow is zero is in black (■) and the main run is in white (□). (a) Zooplankton (lrg. and sm. zoo), phytoplankton (lrg. and sm. phyto), and bacteria biomass (mmol C m^{-3}); (b) DOC concentrations (mmol C m^{-3}); (c) DON concentrations (mmol N m^{-3}).

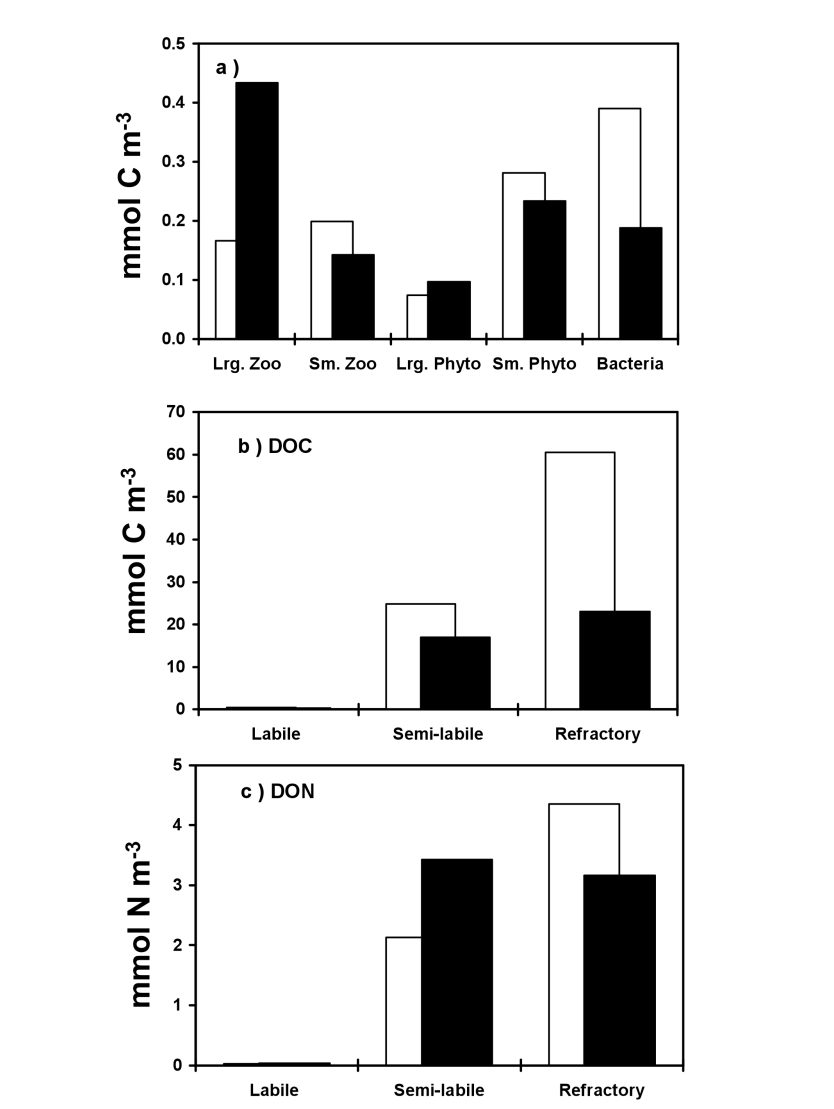

Figure 1.8. A comparison of DOC and DON production (nmmol C or N m^{-3} d^{-1}) at steady state between the main oceanic model run and an oceanic run where DOM inflow was zero. The run where DOM inflow was zero is in black (■) and the main run is in white (□). The sources of DOM on the x-axis are viral lysis (Lysis), sloppy feeding (SF), natural mortality (Mort.), viral decay (V. Decay), zooplankton excretion (Excret.), phytoplankton exudation (Exud.), and the decay of detritus (D. Decay). (a) DOC production; (b) DON production.

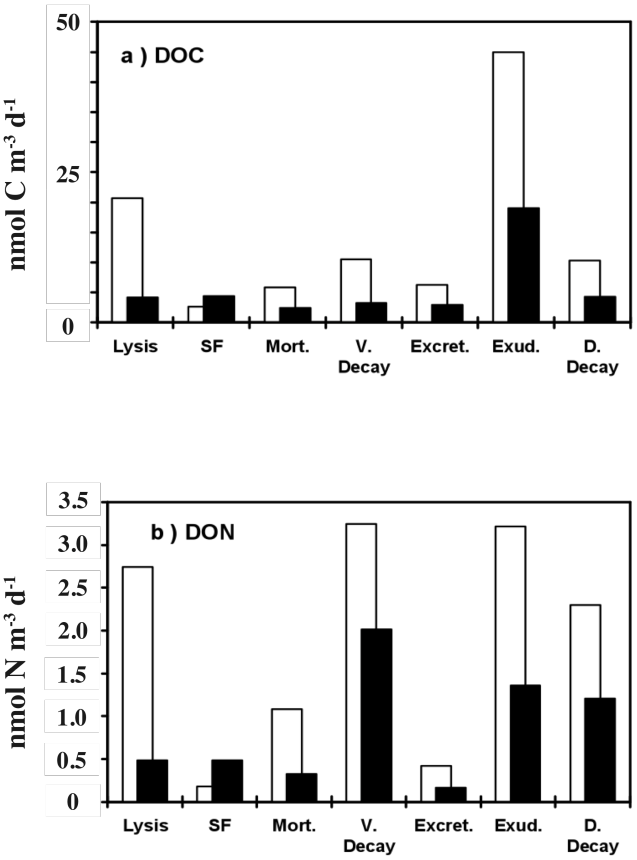

Figure 1.9. Sensitivity of coastal zooplankton (lrg. and sm. zoo), phytoplankton (lrg. and sm. P), and bacterial (B) biomass (mmol C m^{-3}) to parameter variations. The y-axis scale represents normalized deviations from the main oceanic model run biomass concentration (i.e. -0.1 mmol C m^{-3} represents a biomass decrease of 0.1 mmol C m^{-3} for the parameter variation run). Parameter decreases are in black (■) and parameter increases are in white (□). Parameter varied: (a) viral infection rate; (b) sloppy feeding; (c) detritus decay rate; (d) mortality rate; (e) viral decay rate; (f) zooplankton excretion; (g) phytoplankton exudation; (h) bacterial growth efficiency; (i) zooplankton growth efficiency.

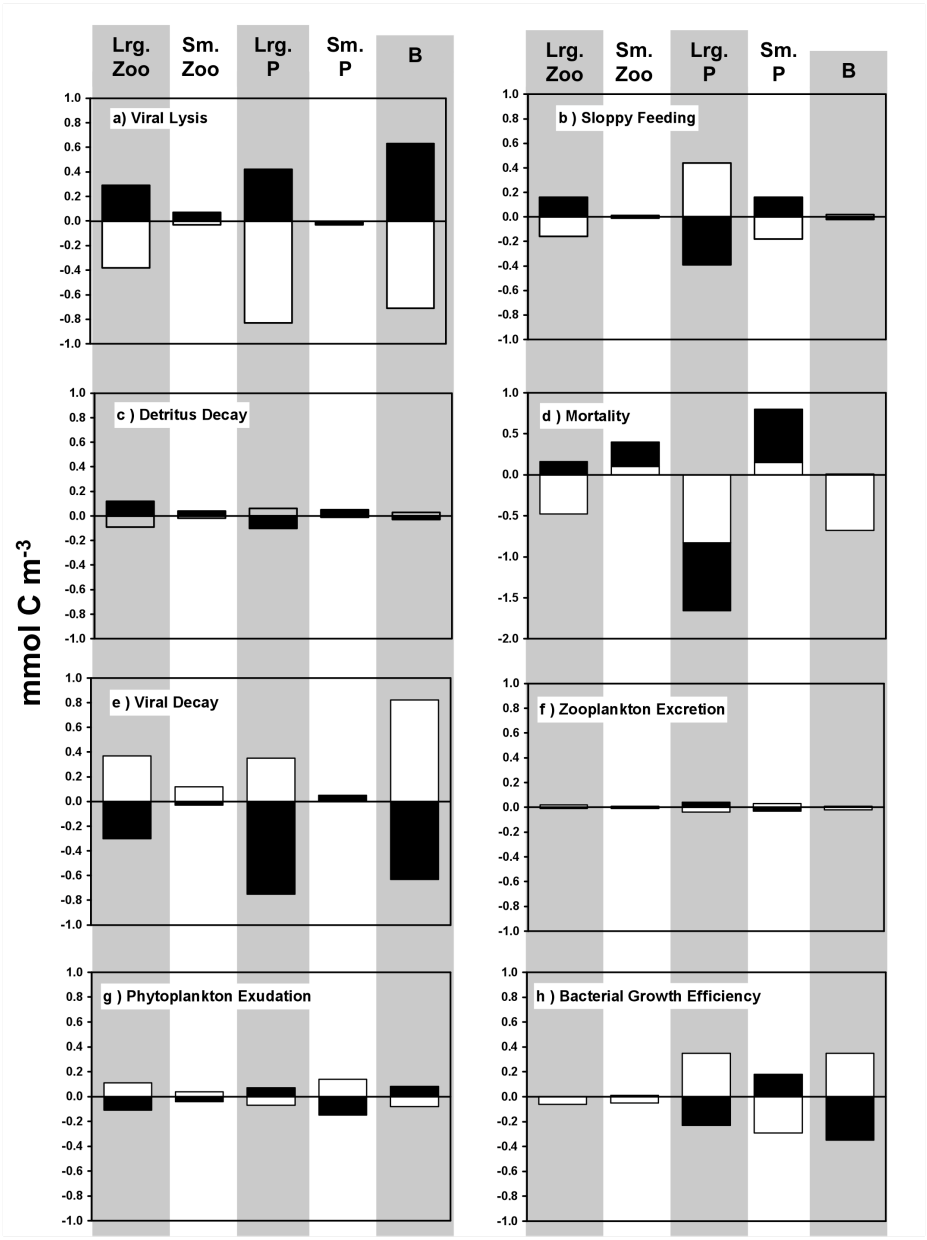

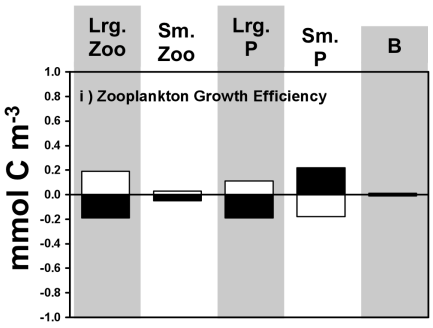
Lrg. Zoo
Sm. Zoo
Lrg. P
Sm. P
B
i) Zooplankton Growth Efficiency
mmol C m-3
1.0
0.8
0.6
0.4
0.2
0.0
-0.2
-0.4
-0.6
-0.8
-1.0

Figure 1.10. Sensitivity of coastal DON sources to parameter variation runs. The x-axis shows the different parameter variation runs: infection rate (Ψ_i) variation run; sloppy feeding parameter (ω) variation run; detritus decay rate (χ_D) variation run; mortality rate (S_i) variation run; viral decay rate (υ) variation run; zooplankton excretion parameter (κ_Z and σ_Z) variation run; phytoplankton exudation parameter (α) variation run; bacterial growth efficiency (gge_B) variation run; zooplankton growth efficiency (ge_Z) variation run. The y-axis scale represents normalized deviations from the main oceanic model run production rate at steady state (i.e. -0.1 nmol N m^{-3} d^{-1} represents a production decrease of 0.1 nmol N m^{-3} d^{-1} for the parameter variation run indicated on the x-axis). Parameter decreases are in black (■) and parameter increases are in white (□). (a) DON from viral lysis; (b) DON from sloppy feeding; (c) DON from mortality; (d) DON from viral decay; (e) DON from zooplankton excretion; (f) DON from detritus decay; (g) DON from phytoplankton exudation.

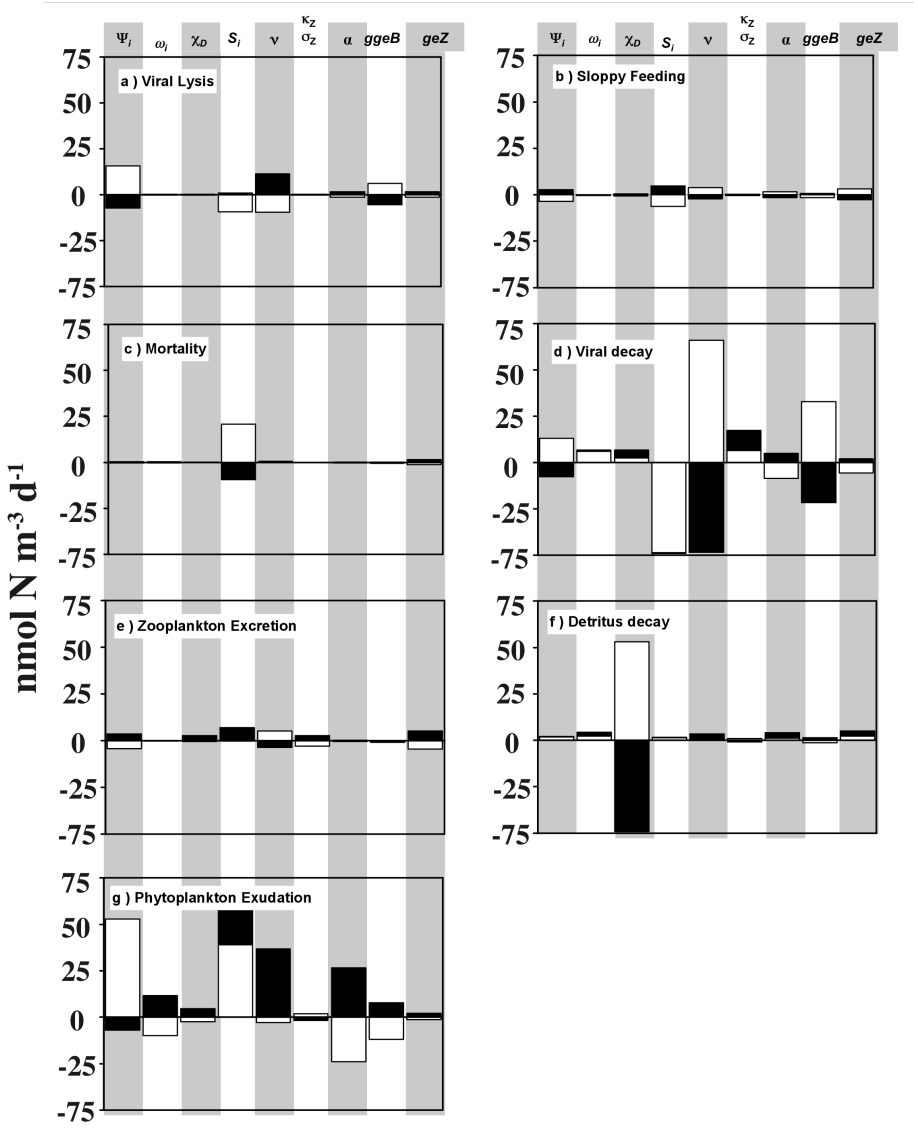

Figure 1.11. Biomass and DOM concentration comparison at steady state between the main coastal model run and a coastal run where DOM inflow was zero. The main run is in white (□) and the run where DOM inflow is zero is in black (■). (a) Zooplankton (lrg. and sm. zoo), phytoplankton (lrg. and sm. phyto), and bacteria biomass (mmol C m^{-3}); (b) DOC concentration (mmol C m^{-3}); (c) DON concentration (mmol N m^{-3}).

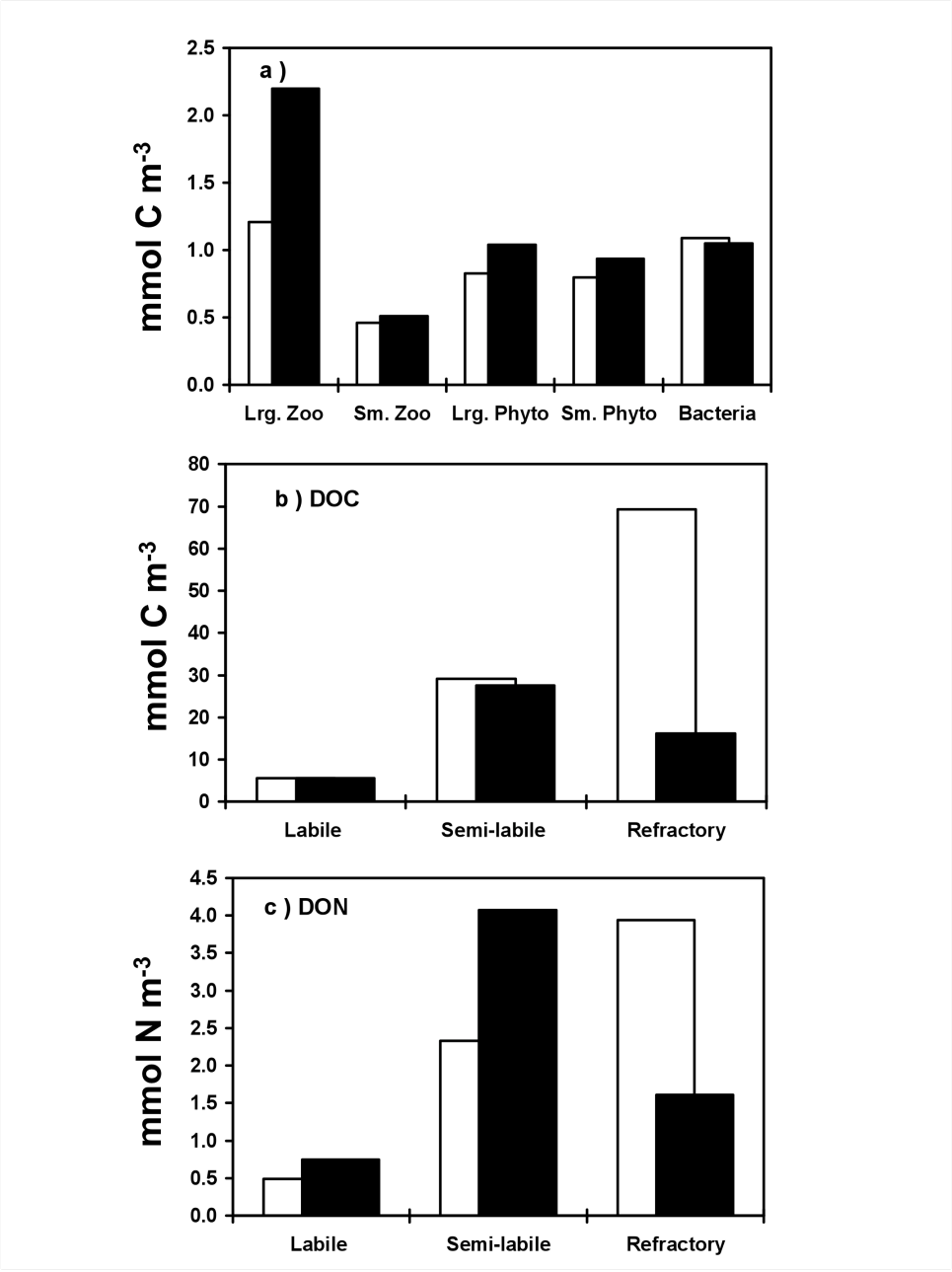

Figure 1.12. A comparison of DOC and DON production (nmol C or N m^{-3} d^{-1}) at steady state between the main coastal model run and a coastal run where there was no DOM inflow. The run where there was no DOM inflow is in black (■) and the main run is in white (□). The sources of DOM on the x-axis are viral lysis (Lysis), sloppy feeding (SF), natural mortality (Mort.), viral decay (V. Decay), zooplankton excretion (Excret.), phytoplankton exudation (Exud.), and the decay of detritus (D. Decay). (a) DOC production; (b) DON production.

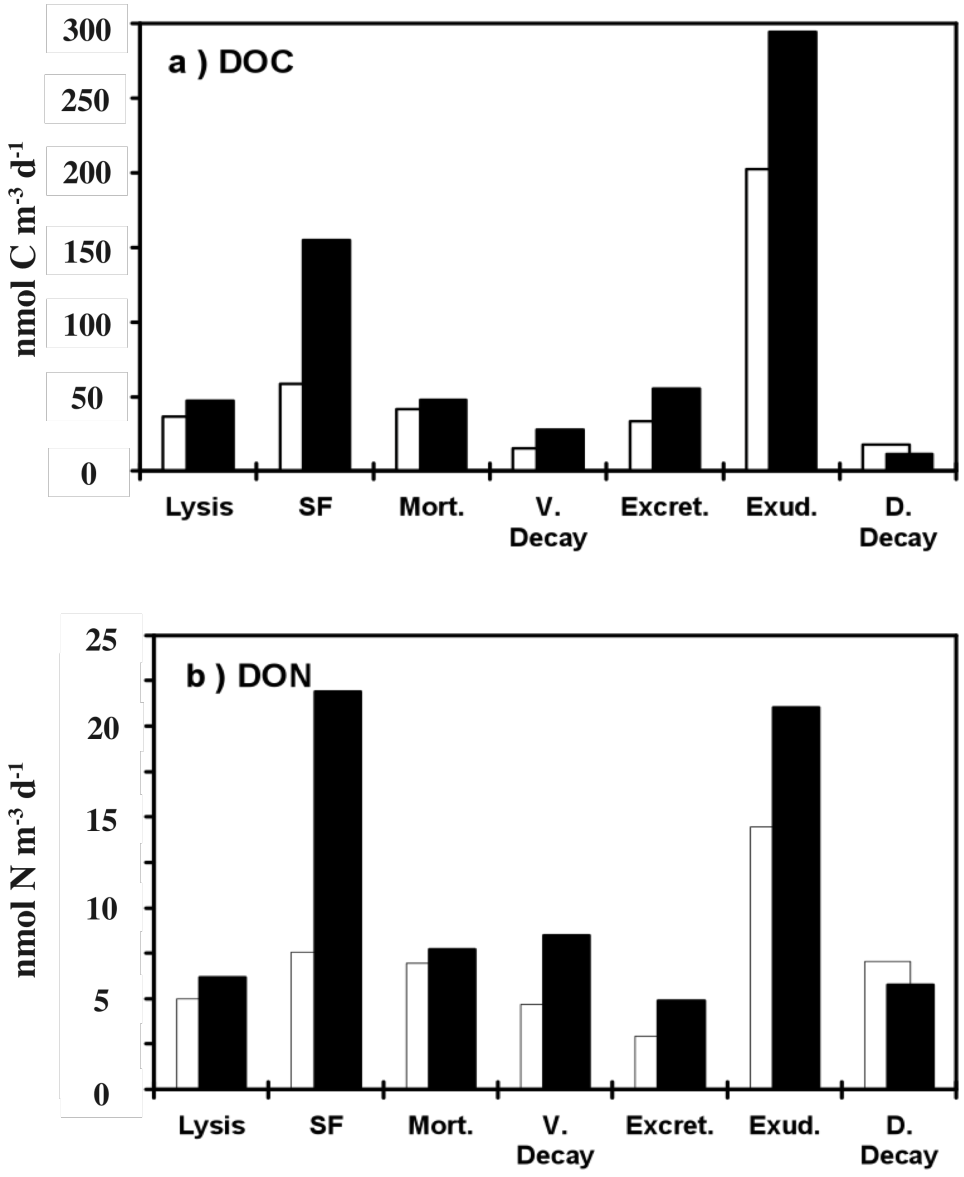

Figure 1.13. Sensitivity of estuarine zooplankton (Lrg. and Sm. Zoo), phytoplankton (Lrg. and Sm. P), and bacterial (B) biomass (mmol C m^{-3}) to parameter variations. The y-axis scale represents normalized deviations from the main oceanic model run biomass concentration (i.e. -0.1 mmol C m^{-3} represents a biomass decrease of 0.1 mmol C m^{-3} for the parameter variation run). Parameter decreases are in black (■) and parameter increases are in white (□). (a) infection rate variation run; (b) sloppy feeding parameter variation run; (c) detritus decay rate variation run; (d) mortality rate variation run; (e) viral decay rate variation run; (f) zooplankton excretion parameter variation run; (g) phytoplankton exudation parameter variation run; (h) bacterial growth efficiency variation run; (i) zooplankton growth efficiency variation run.

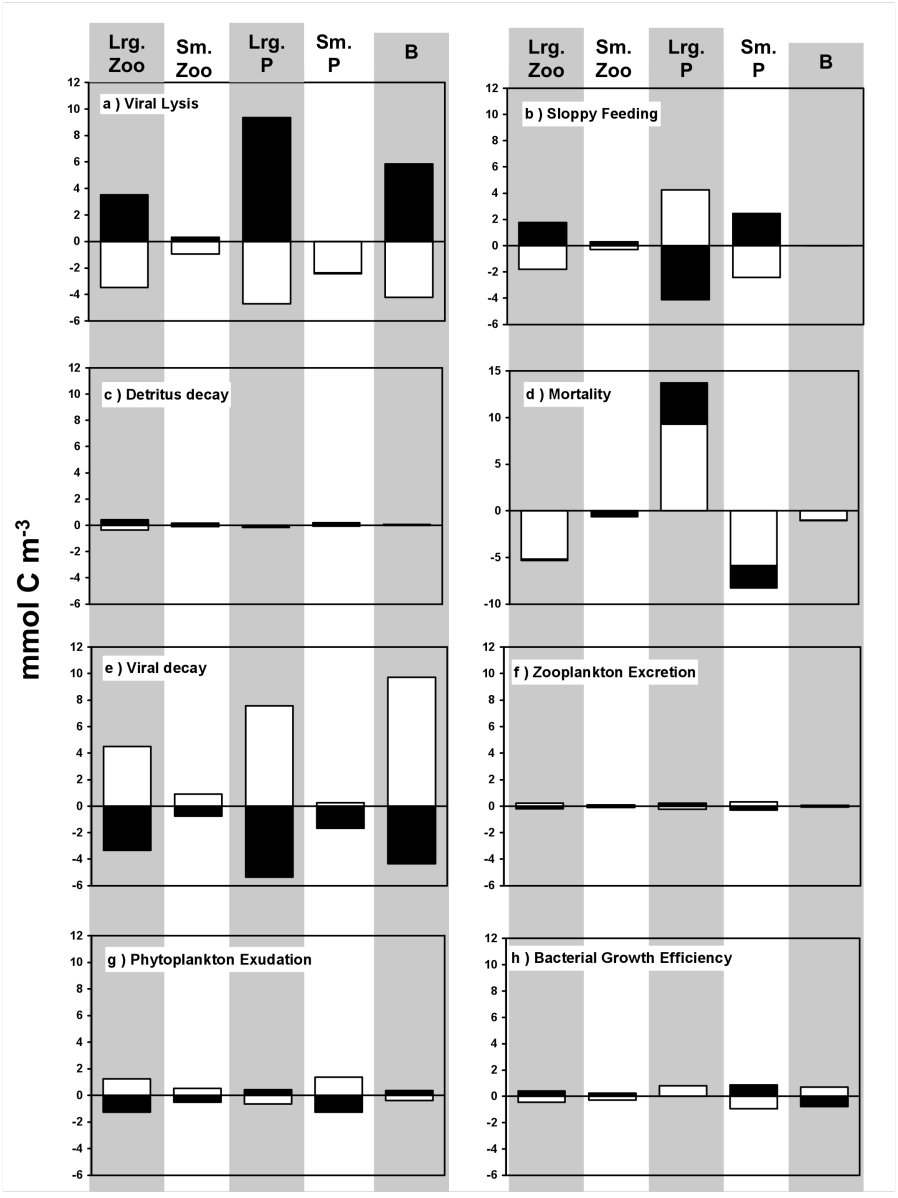

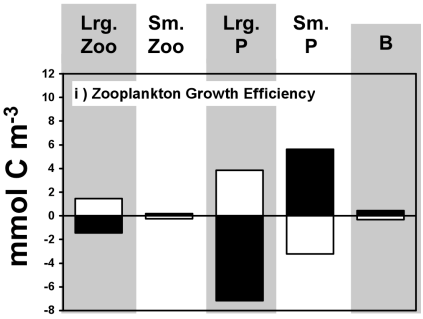
Lrg. Zoo
Sm. Zoo
Lrg. P
Sm. P
B
i) Zooplankton Growth Efficiency
mmol C m-3
12
10
8
6
4
2
0
-2
-4
-6
-8

Figure 1.14. Sensitivity of estuarine DON production sources to parameter variation runs. The x-axis shows the different parameter variation runs: infection rate (Ψ_i) variation run; sloppy feeding parameter (ω) variation run; detritus decay rate (χ_D) variation run; mortality rate (S_i) variation run; viral decay rate (υ) variation run; zooplankton excretion parameter (κ_Z and σ_Z) variation run; phytoplankton exudation parameter (α) variation run; bacterial growth efficiency (gge_B) variation run; zooplankton growth efficiency (ge_Z) variation run. The y-axis scale represents normalized deviations from the main oceanic model run production rate at steady state (i.e. -0.1 nmol N m^{-3} d^{-1} represents a production decrease of 0.1 nmol N m^{-3} d^{-1} for the parameter variation run indicated on the x-axis). Parameter decreases are in black (■) and parameter increases are in white (□). (a) DON from viral lysis; (b) DON from sloppy feeding; (c) DON from mortality; (d) DON from viral decay; (e) DON from zooplankton excretion; (f) DON from detritus decay; (g) DON from phytoplankton exudation.

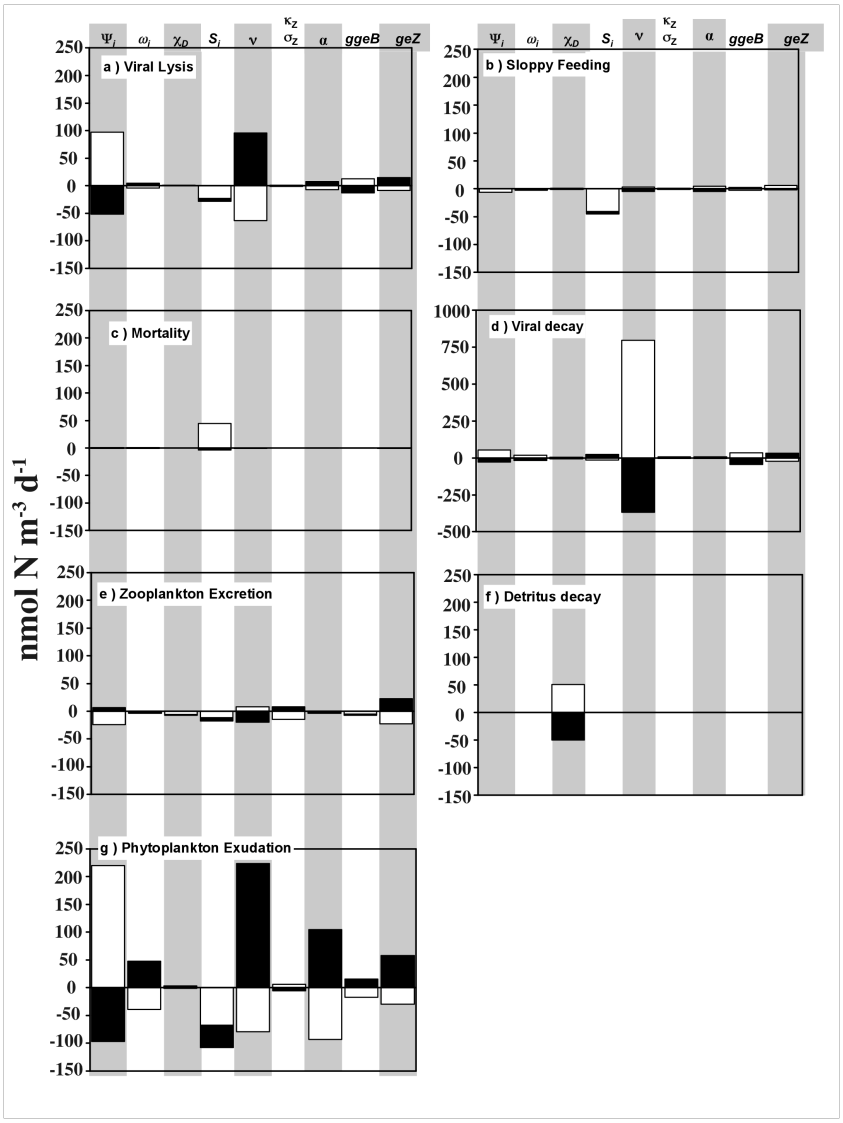

Figure 1.15. Biomass and DOM concentration comparison at steady state between the main estuarine model run and an estuarine run where DOM inflow was zero. The main run is in white (□) and the run where DOM inflow was zero is in black (■). (a) Zooplankton (lrg. and sm. zoo), phytoplankton (lrg. and sm. phyto), and bacteria biomass (mmol C m^{-3}); (b) DOC concentration (mmol C m^{-3}); (c) DON concentration (mmol N m^{-3}).

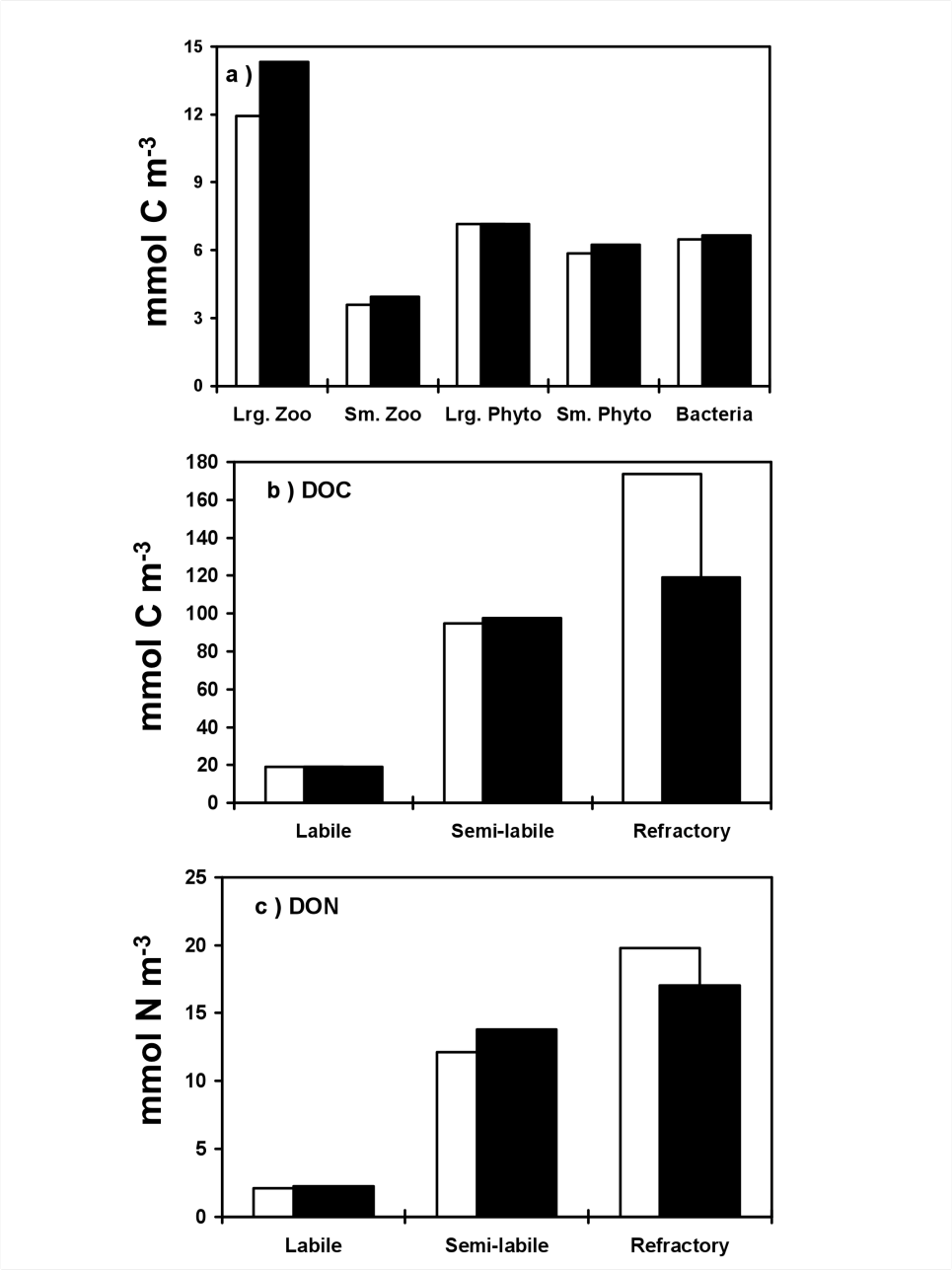

Figure 1.16. A comparison of DOC and DON production (mmol C or nmol N m^{-3} d^{-1}) at steady state between the main estuarine model run and an estuarine run where DOM inflow was zero. The run where DOM inflow was zero is in black (■) and the main run is in white (□). The sources of DOM on the x-axis are viral lysis (Lysis), sloppy feeding (SF), natural mortality (Mort.), viral decay (V. Decay), zooplankton excretion (Excret.), phytoplankton exudation (Exud.), and the decay of detritus (D. Decay). (a) DOC production; (b) DON production.

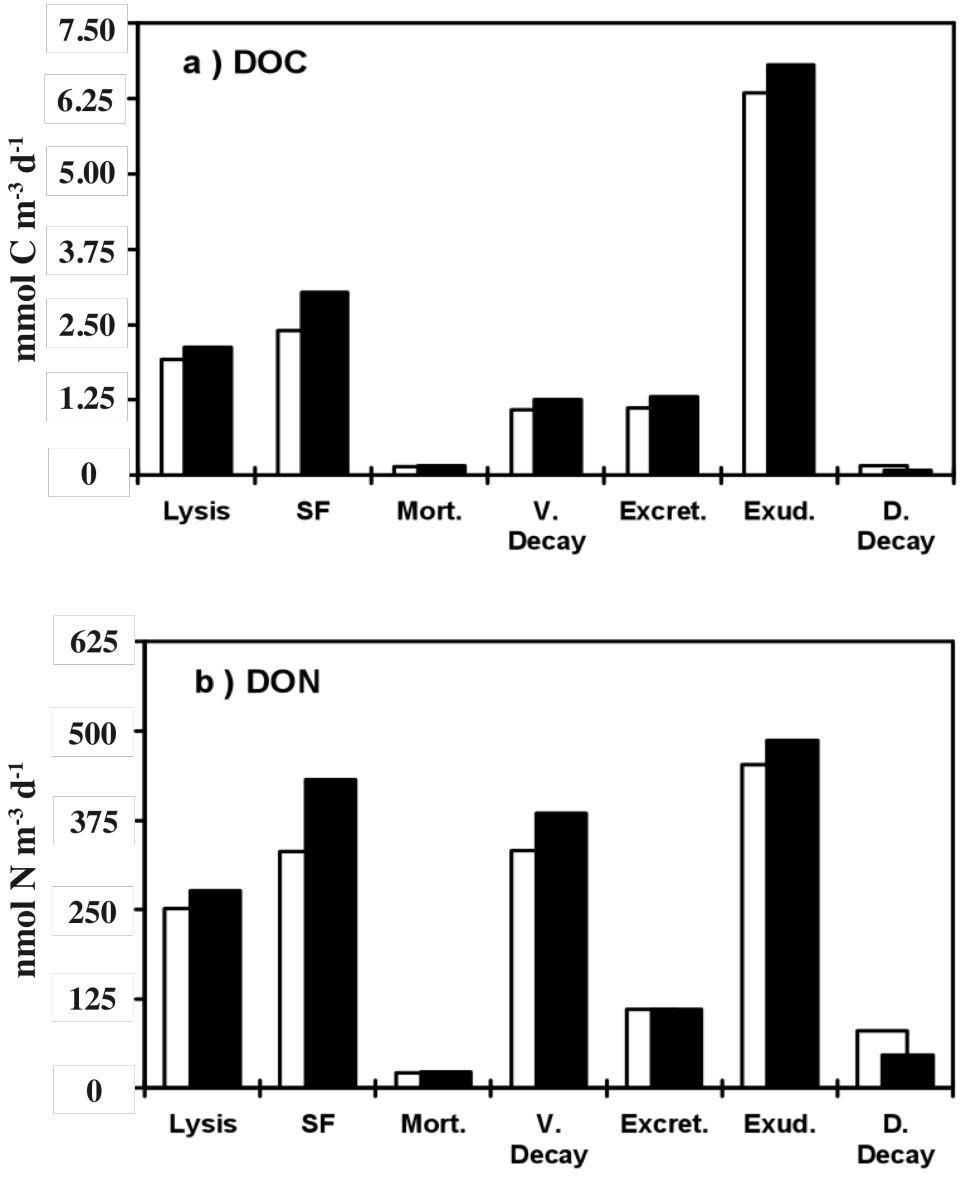

Figure 1.17. Conceptual diagrams of DOC and DON production in the oceanic, coastal, and estuarine model runs. The thickness of the arrows is an indication of the magnitude of the DOM production processes. Only pathways that produce significant amounts of DOC or DON are included. Schematic diagram adapted from (Carlson 2002).

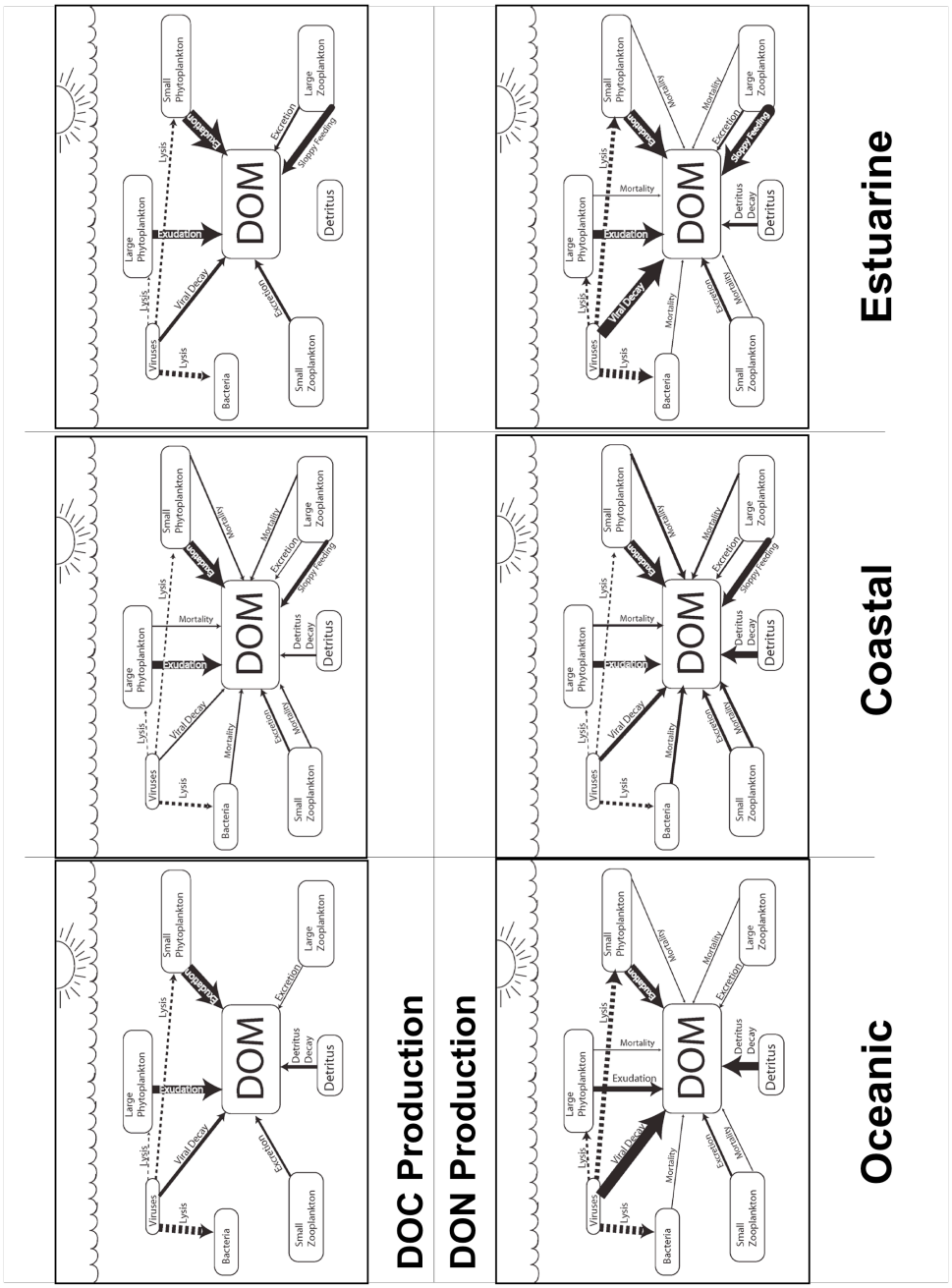

Chapter 2: Modeling the Seasonal Autochthonous Sources and Cycling of Dissolved Organic Carbon and Nitrogen at Station CB3.3C in the Upper Chesapeake Bay

Abstract

In this paper we investigate the seasonal cycling and production of dissolved organic carbon (DOC) and nitrogen (DON) in the euphotic zone at a station in the upper Chesapeake Bay using a new mass-based ecosystem model that includes an unprecedented level of detail. Important features of the model are: (1) carbon and nitrogen are incorporated by means of a set of fixed and varying C:N ratios; (2) DOM is separated into labile, semi-labile, and refractory pools for both C and N; (3) the production and consumption of DOM is treated in detail; and (4) seasonal observations of light, temperature, nutrients, and surface layer circulation are used to physically force the model. The model reasonably reproduces the mean observed seasonal concentrations of nutrients, DOM, plankton biomass, and chlorophyll *a*. The results suggest that, in addition to allochthonous sources of DOM, estuarine DOM cycling is intricately tied to the biomass concentration, ratio, and productivity of phytoplankton, zooplankton, viruses, and bacteria. During peak spring productivity phytoplankton exudation and sloppy feeding are important sources of DOM. In the summer when productivity peaks again, sources of DOM are more diverse and, in addition to phytoplankton exudation, include viral lysis and the decay of detritus. The potential importance of viral decay as a source of bioavailable DOM from within the bulk DOM pool is also discussed. The results also highlight the importance of some poorly constrained processes and parameters. Some potential improvements and remedies are suggested. Sensitivity studies on selected parameters are also reported.

Introduction

In many mid-Atlantic estuaries, the biochemical composition and isotopic signature of DOM changes across the salinity gradient with biomarkers and carbon isotopes indicating that a significant amount of DOM production and modification occurs within the estuary (Loh et al., 2006; Mannino and Harvey, 2000; Raymond and Bauer, 2001). In the Chesapeake Bay estuary, DOC exhibits a non-conservative distribution at certain times of the year, suggesting that seasonal autochthonous DOM production can be significant (Fisher et al., 1998; Rochelle-Newall and Fisher, 2002). Fisher et. al. (1998) estimated that this DOC accumulation was greater than atmospheric or terrestrial organic carbon inputs and was equivalent to ~ 10 % of estuarine primary production. Dissolved organic nitrogen (DON) has also been suggested to accumulate seasonally in estuaries as well (Bronk, 2002; Bronk et al., 1998; Lomas et al., 2002). Radiocarbon measurements of estuarine, continental shelf, and slope DOM have suggested that >10 kDa DOM is relatively young and has a residence time of 1 - 30 days, whereas the smaller fraction of DOM (1 – 10 kDa) is between 380 – 4,500 years old (Santschi et al., 1995). These observations suggest that a portion of both allochthonous and autochthonous DOM cycle rapidly within estuaries, with components of both persisting in the ocean for hundreds or thousands of years. An understanding of the degree of cycling that these components undergo is critical for constraining local carbon and nitrogen budgets and for evaluating the role of estuaries in the global carbon cycle.

In the euphotic zone of the Chesapeake Bay estuary, the site of this study, several sources and processes control DOM cycling. The major allochthonous source of DOM is the Susquehanna river (Fisher et al., 1998). Smaller rivers (sub-estuaries), atmospheric

deposition (Seitzinger and Sanders, 1999), wetland discharge (Tzortziou et al., 2008), and terrestrial runoff and leaching (Berman and Bronk, 2003) also add significant amounts of DOM to the estuary. Internal sources of DOM include benthic fluxes (Burdige and Zheng, 1998), extracellular release by phytoplankton, grazer-mediated release and excretion, release via cell lysis (both viral and bacterial), solubilization of particles, and bacterial transformation and release (Carlson, 2002). Free-living heterotrophic bacterioplankton are the dominant consumers of DOM (Nagata, 2000). Some phytoplankton also have the ability to take up DOM to supplement their metabolic needs (Mulholland et al., 2003). Photochemical processes, through UV excitation, directly and indirectly remove and transform DOM (Mopper and Kieber, 2002). DOM can also potentially form gels that may aggregate to form particulate organic matter (POC) (Verdugo et al., 2004) which may sink out of surface waters. As in other temperate systems, the rate and magnitude of these sources and sinks varies on a seasonal basis as changes in light, temperature, and freshwater flow affect the environment (Apple et al., 2006; Bronk et al., 1998; Jonas and Tuttle, 1990; Lomas et al., 2002; Malone et al., 1991; Mulholland et al., 2003; Shiah and Ducklow, 1994b; Wommack et al., 1992).

Quantifying the role of these sources and sinks in Chesapeake Bay DOM cycling has proven difficult. Most of the research has focused on characterizing the composition of DOM and understanding the individual role of different functional groups (i.e. primary producers, secondary consumers, predators, etc.) and species in DOM cycling. Few studies have quantified the amounts of C or N that flux into, and out, of the DOM pool relative to the other major C and N pools. Those that have provide an incomplete picture of DOM cycling as they often cannot distinguish between the individual sources and

sinks of DOM. Additionally, as far as we are aware, there are no long-term time series measurements of the C and N flux through the DOM pool that adequately describe the annual DOM cycle.

Models can be a powerful tool for integrating data and running long term simulations. They are also valuable for determining the magnitude and importance of processes that are difficult to measure and observe in the field. In this paper we describe a modeling study of the DOM cycle in the surface waters of Chesapeake Bay. Our objective is to elucidate the general seasonal cycles of DOC and DON in an area of high biological activity in the upper bay. We specifically focus on the roles that phytoplankton extra-cellular release, non-grazing mortality, bacterial and phytoplankton viral lysis, and grazer-mediated sloppy feeding, egestion, and excretion play in the production of DOM. In addition, we explore how seasonal variability affects the physical, chemical, and biological processes that drive DOM cycling. Observations are used to evaluate the model performance. Through comparisons with observations we show that the model is capable of reproducing the seasonal patterns in plankton biomass and productivity. This then allows us to examine how biologically mediated DOM production, transformation, and consumption change in response to the seasonal forcing. These comparisons also highlight the importance of some poorly constrained processes that require additional research or more complex numerical approaches.

Model Description

The model of Anderson and Williams (1998) provided the basic structure for our biogeochemical model. However, we modified their model in several significant ways: DOM is divided into labile, semi-labile, and refractory pools (following Anderson and

Williams (1999) model of DOC cycling), zooplankton and phytoplankton have two size classes, sediment is not included, and two virus compartments have been added along with a dissolved inorganic carbon (DIC) pool. A complete list of the model equations can be found in Appendix B. Tables 2.1 and 2.2 give lists of parameters and variables used in the model. Figure 2.1 is a schematic diagram that shows the flow of nitrogen and in some instances carbon between the model compartments.

The model includes 18 state variables that span the herbivorous and microbial food webs, with compartments for large phytoplankton (P_L), small phytoplankton (P_S), large zooplankton (Z_L), small zooplankton (Z_S), bacteria (B), phytoplankton viruses (V_P), bacteriophages (V_B), ammonium (A), nitrate (N_n), detritus (D_N and D_C), dissolved inorganic carbon (DIC), and labile (L_C and L_N), semi-labile (S_C and S_N), and refractory (R_C and R_N) DOC and DON. Nitrogen is the basic unit for simulation and mass balance. However, carbon has been accounted for by allowing the state variables to have fixed or varying C:N ratios. Close attention has been paid to the formulation of the interactions between these two elements. Thus, both the carbon and nitrogen cycles have been constrained. Phytoplankton and zooplankton were divided into two size classes to reflect the physiological differences between larger and smaller plankton species (i.e. copepods versus protists).

Station location and data availability

The model was formulated to simulate the mean seasonal cycling of dissolved organic matter in the surface layer at the Chesapeake Bay Program's (CBP) station CB3.3C (38.9960 °N, 76.3597 °W) which is located in the main channel of the upper Chesapeake Bay near the bay bridge (Figure 2.2). Station CB3.2 (39.1637 °N, 76.3063

°W) located to the north of station CB3.3C provided boundary condition data for our model runs.

Chemical, physical, and biological data from stations CB3.3C and CB3.2 was downloaded from the Chesapeake Bay Program website (CBP, online database) for forcing and model comparison. At each station, ammonium, nitrate, chlorophyll, primary production, total suspended solids (TSS), vertical light attenuation, DON, DOC, particulate carbon and nitrogen, temperature, salinity, surface layer depth, and biological (phytoplankton and zooplankton species and abundance) data was measured once or twice every month. We calculated mean seasonal values for these parameters by averaging the surface layer data on a monthly or bi-monthly basis from 1997 to 2007, except for DOC data, which was only available from 1987 to 1997. Biological data on phytoplankton and zooplankton species and numerical abundance was also only available up to 2002. The chlorophyll *a* data that we used is based on the maximum chlorophyll *a* concentration in the water column and not just surface layer data. We did this because in the spring dinoflagellates, which migrate to surface during the day and to the just above the pycnocline at night, are often present and represented most of the chlorophyll in the water column (Adolf et al., 2006; Keller, personal observation in 2007 and 2008). As CBP sampling at this station often occurred early in the morning when the dinoflagellates were just starting to migrate from above the pycnocline, surface measurements underestimate the amount of chlorophyll that will be present in upper water column throughout most of the day (i.e. the chlorophyll *a* maximum is just above the pycnocline early in the morning and moves up toward the surface as the day progresses). Photosynthetically available radiation (PAR) data used in the model was the monthly

seasonal average from a 17-yr time series taken near the Chesapeake Bay (38.6 °N, 78.2 °W) (Fisher et al., 2003). Monthly virus and bacterial abundance and production data from 2002 to 2007 was provided by the Microbial Observatory for Virioplankton Ecology research group (MOVE). Whenever possible we calculated means for MOVE data. However, samples were not taken for all months every year resulting in an incomplete data set (data availability: Feb.: 2005, 2007; Mar.: 2004-2006; Apr.: 2003-2005; May: 2004, 2005; June: 2003, 2004; July: 2004-2006; Aug.: 2003-2005; Sept.: 2002; Oct.: 2003-2005; Nov.: 2006). Daily mean Susquehanna river flow data (1997 to 2007) from a station at Conowingo, MD was downloaded from the U.S. Geological Survey website (U.S.G.S.) and averaged to calculate monthly mean flow.

Physical parameterization

Model circulation

A simple chemostat-like formulation was used to simulate circulation in the upper layer at station CB3.3C. We used this formulation because circulation in the main channel of the Chesapeake Bay is usually two-layered with a fresher layer flowing seaward at the surface and a saltier layer flowing landward at the bottom (Schubel and Pritchard, 1986). Strong stratification exists between these layers at this station throughout most of the year and limits the exchange of nutrients and plankton. Therefore, we felt that a simple chemostat formulation would allow us to simulate the inflow and outflow of nutrients, plankton, detritus, and DOM caused by this circulation pattern without invoking a complex hydrodynamic model. Additions and losses to state variables caused by other processes such as sinking, vertical migration, higher trophic level predation, advection, and diffusion have been accounted for by having additional

loss terms (see section below) or by adjusting the inflowing state variable mass. The inflow and outflow (μM N or C s^{-1}) of state variables is calculated as:

inflow = $h\ i^o$

outflow = $h\ i$

where h is the rate (s^{-1}) of flow, i^o is the upstream state variable mass (interpolated from station CB3.2 data), and i is the model state variable mass. The rate of flow, h, is based on Susquehanna river flow and the volume (analogous to chemostat vessel volume) of the surface layer in a selected area around station CB3.3C:

$$h = F_{river} / Z\ C_{area}$$

where F_{river} ($m^3\ s^{-1}$) is interpolated from Susquehanna river flow data, Z is interpolated surface layer depth (m), and C_{area} is a 3 nautical mile (width of the bay) by 5 km area (27,780,000 m^2) around station CB3.3C. Susquehanna river flow data was used because the Susquehanna river contributes approximately 87% of all freshwater that enters the upper bay and thus controls the circulation pattern in the main body of the upper bay (Schubel and Pritchard, 1986). C_{area} was chosen so that the flow of water was constrained by the width of the bay at station CB3.3C. This formulation gave us a seaward surface flow past station CB3.3C that ranged from 1.2 – 10.2 cm s^{-1} which is similar in magnitude to a 27-day record taken in the spring from nearby Thomas Point light that measured a mean surface flow of 8 cm s^{-1} (Beardsley and Boicourt, 1981).

Light attenuation

To calculate the underwater light field we used a simple model to derive the average irradiance of the surface layer:

$$I = (I_{surface} / Z)\ (-1 / K_d)\ \exp\ (-K_d\ Z\ -1)$$

where $I_{surface}$ is the interpolated PAR just below the surface of the water (95% of PAR at the surface, 5% reflectance loss), Z is interpolated surface layer depth, and K_d is the diffuse attenuation coefficient. K_d was calculated using a simple empirical optical model that was derived specifically for the Chesapeake Bay (Xu et al., 2005). In this model the specific attenuation coefficients for chlorophyll, total suspended solids (TSS), and salinity (used as a proxy for colored dissolved organic matter (CDOM)) are used to determine K_d as follows:

$K_d = 1.80 - 0.0044\ Chl + 0.0673\ TSS - 0.096\ S$

Salinity (S) was interpolated into the model from station CB3.3C data. The chlorophyll values (Chl) that we used in these calculations were obtained by converting the modeled biomass of phytoplankton (μM N) to chlorophyll a (μg l^{-1}) (described below). TSS was calculated by adding the modeled biomass of plankton and detritus (both carbon and nitrogen values converted to mg l^{-1}) to interpolated minimum TSS concentrations that were measured at station CB3.3C. Using data output from the biological model to calculate chlorophyll and TSS thus allowed us to provide a feedback mechanism between the optical model and the biological model (i.e. high concentrations of phytoplankton or biologically derived TSS can decrease light penetration).

Biological parameterization

Phytoplankton

The light- and nitrogen-dependant growth rate of phytoplankton is described by an exponential saturation function with photoinhibition for light dependence (Platt et al., 1980) and a non-dimensional Michaelis-Menten hyperbolic saturation function is used to describe nitrogen (ammonium, nitrate, and labile DON) dependence. This formulation

allows phytoplankton cells to take up ammonium and labile DON preferentially, with nitrate uptake inhibited in the presence of significant concentrations of ammonium (Christian et al., 2002; Harrison et al., 1996) and labile DON. DON uptake by phytoplankton was included in this model because recent research has shown that DON can be a significant nitrogen source (up to 50%) for phytoplankton (Fan et al., 2003; Mulholland et al., 2002; Mulholland et al., 2003). The maximum attainable daily growth rate of large phytoplankton, μ_P, was calculated using an exponential temperature function (Bissinger et al., 2008; Eppley, 1972) where: $\mu_P = 0.81 \exp(0.0631\, T)$ with temperature (T) interpolated into the model from station CB3.3C data. Based on allometric theory (Raven and Kübler, 2002) the maximum growth rate of small phytoplankton was set to be 30% higher than that of large phytoplankton. The half saturation constants for the uptake of ammonium and nitrate by phytoplankton were used to tune (optimize) the model. Thus they were set at values, which fall within the ranges reported for the uptake of ammonium and nitrate by phytoplankton at high nutrient concentrations (Collos et al., 2005; Eppley et al., 1969), reflecting the high nitrate and ammonium concentrations found at station CB3.3C throughout much of the year. The half saturation constants were also set so that the growth affinity for ammonium of small phytoplankton is better than that of large phytoplankton (Stolte et al., 1994). The uptake of DON by phytoplankton is poorly understood (Mulholland et al., 2003) so we set the half saturation constant for uptake by phytoplankton at 20 μM, which allows phytoplankton to take up some DON but restricts it from being their dominant nitrogen source. Phytoplankton use DIC in combination with nutrients at a fixed C:N ratio for production (Anderson and Pondaven, 2003). A constant fraction of phytoplankton

production is exuded as DOM, and "extra" DOC is also excreted in proportion to production (Anderson and Williams, 1998). The amount of DOC excreted can range between 5 and 70% of total primary production (Connolly et al., 1992). The factors that control this excretion are not fully understood (Flynn et al., 2008) so we chose to follow the simple parameterization of Anderson and Williams (1998) where extra DOC excretion, ϖ, is set at a mid-range value of 0.26 (dimensionless).

The addition of phytoplankton to the system is based on upstream chlorophyll *a* data which does not differentiate between large and small phytoplankton. Therefore, we split (Table 2.3) inflowing chlorophyll between large and small phytoplankton based on research which shows that larger phytoplankton (mostly diatoms and large dinoflagellates) dominate both biomass and productivity in the winter, early spring, and late fall and that smaller phytoplankton (cyanobacteria, cryptophytes, flagellates and small diatoms) dominate production, but not necessarily biomass, in the summer (Adolf et al., 2006; Malone, 1980; Malone et al., 1996). The phytoplankton chlorophyll to carbon ratio is modeled as a function of temperature, light, and nutrient availability (Cloern et al., 1995): Chl:C = 0.003 + 0.0154 exp (0.050 T) exp (-0.0591 I) Q_P.

Zooplankton

Use of food by zooplankton for growth is based on a stoichiometric model (Anderson and Hessen, 1995) that operates on the basis of a food-threshold elemental ratio, below which C limits growth and above which N limits growth. This formulation accounts for the respiration of DIC, the egestion of feces to detritus, and the excretion of ammonium and DOM. The maximum grazing rate, $C_{Z_{L \text{ or } S}}$, was set at 2.0 d^{-1} for small zooplankton and 1.0 d^{-1} for large zooplankton, reflecting the ability of nano- and micro-

zooplankton to grow faster than mesozooplankton (i.e. copepods vs. protists) (Tillmann, 2004). The carbon production efficiencies, $ge_{Z_{L \text{ or } S}}$, were set at 0.75 for large zooplankton and 0.40 for small zooplankton reflecting measured production efficiencies for *Acartia tonsa* (Kiørboe et al., 1985), a copepod common at this station, and general protozoan growth efficiencies (Caron et al., 1990). The model also allows for the assignment of "preferences" for different forms of organic nitrogen (i.e. prey) (Hood et al., 2001). Large zooplankton were assigned preferences (see Table 2.1) that describe the diverse diet they have been shown to have (Kleppel, 1993). Note that the preference assigned to them for grazing on bacteria was assigned to account for inadvertently ingesting particle-attached bacteria rather than actual selective grazing on bacteria. Small zooplankton grazing preferences (see table 2.1) were assigned to reflect known preferences for small phytoplankton, other small zooplankton, and bacteria (Boenigk and Arndt, 2002; Calbet and Landry, 2004; Tillmann, 2004).

The production of DOM and detritus as a result of large zooplankton sloppy feeding is based on a predator-to-prey size ratio that determines the amount of DOM and detritus produced. The following equation from Møller (2005) describes this relationship, $Q = 0.714 - 0.013*(ESD_{copepod}/ESD_{prey})$, where Q is the fraction of prey carbon removed from suspension and lost as DOC during feeding and ESD is the equivalent spherical diameter. This equation was only used for predator-to-prey ratios of < 55; sloppy feeding was assumed not to occur at higher ratios. Therefore, we estimated the average ESD of large zooplankton to be 484 μM and the average ESD of large phytoplankton to be 13.8 μM based on work by Møller (2005), which gives a Q value of 0.26 (ω_{P_L}) for large zooplankton feeding on large phytoplankton. For large zooplankton

feeding on other large zooplankton, an ESD of 484 μM was estimated for the predator and an ESD of 304 μM was used for the prey, simulating an average copepod feeding on an average copepodite, which gives a Q value of 0.69 (ω_{Z_L}). For large zooplankton feeding on detritus the predator-to-prey ratio was assumed to be 18:1, the optimal copepod predator-to- prey size ratio (Hansen et al., 1994), which gives a Q value of 0.48. However, as detritus is non-living it likely contains less DOM that can be released when sloppy feeding occurs, so we assume that DOM production from large zooplankton feeding on detritus is less and set the Q value to equal 0.24 (ω_D). We could not find any data that reported how much detritus is produced as a result of sloppy feeding, so we assumed that the amount of detritus produced is 25% of the Q value calculated above.

Zooplankton excretion of ammonium and DON was set so that 68% (κ_Z) of the nitrogen excreted is in the form of ammonium with the remaining 32% in the form of DON (Steinberg et al., 2002). Excretion of DOC by zooplankton was set so that 31% (1-σ_Z) of the carbon released (including respiration) was in the form of DOC (Steinberg et al., 2000).

The addition of zooplankton to the system was based on mean monthly abundance of mesozooplankton and microzooplankton at station CB3.3C (zooplankton data for station CB3.2 was unavailable). Large zooplankton inflow was based on the abundance of the copepods *Acartia tonsa* and *Eurytemora affinis* because these species dominate the Chesapeake Bay mesozooplankton community (Kimmel and Roman, 2004). We used a conversion factor of 2.5 μg carbon per copepod (Huntley and Lopez, 1992) to convert the number of adult copepods and copepodites to carbon biomass. Then, we increased the calculated carbon biomass by 10% to account for the presence of other mesozooplankton

and higher up-bay copepod abundances (Zhang et al., 2006). Small zooplankton biomass inflow was calculated by first estimating nano/microflagellate abundances from CBP microzooplankton data which only reported microzooplankton abundances for cells larger than 44 μm (mostly copepod nauplii, rotifers, and large ciliates). The nano/microflagellate to ciliate ratio of 500 that we used was based on a study of seasonal abundances of ciliates and microflagellates in Chesapeake Bay (Dolan and Coats, 1990). The abundances of nano/microzooplankton were then converted to carbon using conversion factors of 0.22 pg C times cell volume (μm^3) for nano/microflagellates (Børsheim and Bratbak, 1987) and 0.154 pg C times cell volume (μm^3) for ciliates (Müller and Geller, 1993). In these calculations we assumed an average cell volume of 200 μm^3 for nano/microflagellates and 100,000 μm^3 for ciliates and other microzooplankton.

Bacteria

The cycling of C and N by bacteria is described and parameterized following Anderson and Williams' stoichiometric model (Anderson and Williams, 1998). This formulation describes the adaptive capability of bacteria and assumes that labile DOC and DON are the primary growth substrates, with ammonium supplementing DOM only when the C:N of DOM is high. Thus, bacteria act as either remineralizers or consumers of ammonium, depending on the relationship between their fixed C:N ratio and that of the DOM they consume. Bacterial growth efficiency was set at 0.30 to reflect measured estuarine growth efficiencies (del Giorgio and Cole, 1998).

The addition of bacteria to the system was based on monthly mean MOVE data from station CB3.3C as data from a more northern station, which showed similar

abundance trends, was only partially available for one year. This data set was not as complete as the CBP data sets used for other state variables but provides us with information that we would otherwise be without. In addition, we are confident that this data set reflects the general pattern of bacterioplankton seasonal abundance as it shows a trend similar to mid-bay seasonal bacterioplankton measurements made in 1990 and 1991 (Shiah and Ducklow, 1994a). A conversion factor of 30.2 fg of C per cell (Fukuda et al., 1998) was used to convert bacterioplankton abundance to biomass.

Viruses

Viruses that infect phytoplankton and bacteria are considered to be a component of DOM even though they were treated as separate state variables for the purpose of this model. In our model viral infection and subsequently lysis of the host produced new viruses, detritus, and DOM. The infection of phytoplankton and bacteria by viruses was modeled so that 40% of bacteria, 7% of small phytoplankton, and 3% of large phytoplankton were lysed per day. These infection rates are within the wide range of reported infection rates that are based on calculations of the abundance of viruses and how many need to be produced daily to sustain that abundance given calculated decay rates (Fuhrman, 1999; MOVE; Weinbauer, 2004; Wommack and Colwell, 2000). To calculate the production of new viruses from lysis we used averaged burst size data which shows that the number of viruses produced per lysis event averages 24 phages per cell lysed for bacteria and up to 400 to 500 viruses per lysed cell for large phytoplankton like *Emiliania huxleyi* (Wommack and Colwell, 2000). Based on these burst sizes and our calculations of viral biomass (see below), 50% of the mass of a lysed cell was new viruses (ε_V) with the remaining cellular contents entering the detritus (37.5%) and DOM

pools (12.5%). Viral decay or loss was formulated using a power function (Fischer et al., 2004), to prevent viral biomass from oscillating uncontrollably, with destroyed viral material returning to the DOM pool. Because viral decay rates are poorly constrained and a large range is reported in the literature (Weinbauer, 2004) we used the decay rate to tune the model.

Because virus data is typically reported in terms of abundance we needed to convert viral abundance to biomass. In order to do this we assumed that roughly half of a virus's mass was DNA and half protein (Szybalski, 1974). Since virus data often includes the genome size (kb) we were able to calculate the amount of nitrogen and carbon for different sized viruses based on the amount of carbon and nitrogen in DNA (assuming viral DNA is 35% guanine and cytosine and 65% adenine and thymine). The amount of nitrogen and carbon in our viral protein was based on the amount of nitrogen and carbon in a 15,484 Da T4 bacteriophage capsid protein which contained 176 nitrogen atoms and 682 carbon atoms (Mazzone, 1998). So, according to our calculations the virus C:N ratio is 3.26 and a 40 kb virus (bacteriophage) has 3.11×10^{-11} μmol C, a 175 kb virus (small phytoplankton virus) has 1.36×10^{-10} μmol C, and a 225 kb virus (large phytoplankton virus) has 1.75×10^{-10} μmol C.

The addition of viruses to the system was based on monthly mean MOVE abundance data from station CB3.3C as data from a more northern station, which showed similar abundance trends, was only partially available for one year. This data set was not as complete as the CBP data sets used for other state variables but provides us with information that we would otherwise be without. Because the data set does not differentiate between different types of viruses we estimated that 80% are bacteriophages

(assuming an average size of 40 kb), 9% are small phytoplankton viruses (assuming an average size of 175 kb), and 9% are large phytoplankton viruses (assuming an average size of 225 kb) based on data that supports the hypothesis that most aquatic viruses are bacteriophages (Wommack and Colwell, 2000).

Mortality

Mortality terms (Table 2.3) were used to tune the model and account for biomass losses and export due to natural mortality, sinking, advection, diffusion, and higher trophic level predation. Our formulation allows some of the biomass from mortality, determined by m, to stay in the system (up to 2% for all plankton except large zooplankton who have an in system loss of up to 1%) and become detritus and DOM. Any biomass loss in excess of 2% (1% from large zooplankton) is exported from the model. The formulation used to determine m was:

$m = S_i - (S_i - 0.02 \text{ or } 0.01)$

where S_i is the mortality rate for state variable i. If S_i was less than 0.02 or 0.01 no export occurred. In addition, zooplankton mortality was calculated using a power function to provide additional closure and stabilize the model (Steele and Henderson, 1992). In order to reproduce the seasonal patterns observed in plankton biomass at this station it was necessary to vary the mortality terms (S_i) seasonally and occasionally set them at high values. Although these adjustments may seem somewhat arbitrary, they can be justified for a number of reasons. Mortality rates for phytoplankton were increased in the spring and fall to account for sinking and sedimentation following the spring bloom (Malone et al., 1996; Malone et al., 1988) and mixing of the water column associated with the fall overturn (Boicourt, 1992). Mortality rates for zooplankton were increased

during the summer and early fall to reflect high seasonal predation by ctenophores (Stoecker et al., 1987) and the jellyfish *Chrysaora quinquecirrah* (Baird and Ulanowicz, 1989; Purcell, 1992). Atlantic menhaden, bay anchovies, other filter-feeding fish, and larval fish may also exert predation pressure on both phytoplankton (mostly menhaden predation) and zooplankton at different times of the year (Baird and Ulanowicz, 1989; Hartman et al., 2004; Lewis and Peters, 1994). Plankton may also experience predation by benthic or attached predators as the surface waters from the channel are swept onto the shoals or past the bay bridge (which provides a structure for benthic predators to grow on) due to tidal circulation. This hypothesis is supported by a previous coupled physical-biological model (Xu and Hood, 2006) which demonstrated that bivalve filtration in shallow waters on the flanks had a significant effect on chlorophyll concentrations in the main stem of the bay.

Dissolved organic matter

Dissolved organic matter has separate state variables for C and N which are divided into labile, semi-labile, and refractory pools (Anderson and Williams, 1999). Dissolved organic matter is produced by phytoplankton excretion and leakage, zooplankton sloppy feeding, zooplankton excretion, viral lysis of phytoplankton and bacteria, plankton mortality, and detritus decay. Labile DOM is consumed directly by bacteria and phytoplankton. Semi-labile DOM requires ectoenzyme hydrolysis by bacteria to become available (labile) for consumption. A Michaelis-Menten kinetic formulation (Anderson and Williams, 1999) describes bacterial hydrolysis of semi-labile DOM, with semi-labile DOM entering the labile and refractory DOM pools upon hydrolysis. Refractory DOM is considered unavailable for consumption by bacteria and

phytoplankton.

Photochemical processes are assumed to be the only means of turnover for refractory material. These processes are included because some research has shown that UV radiation tends to make terrestrially derived refractory material from coastal and estuarine environments more available for use by bacteria (Mopper and Kieber, 2002). Our formulation followed that of Anderson and Williams (1999) with this process occuring at a rate of 0.0015 d^{-1}. Photochemical processes are also responsible for the conversion of DOC to dissolved inorganic carbon, and the global average removal rate is estimated to be approximately 0.038 d^{-1}, if all DOC is considered to be photoreactive (Miller and Zepp, 1995). As not all DOC is photoreactive or subjected to direct photochemical reactions and the exact removal rate is unknown, we formulated this conversion to occur at a lower rate of 0.004 d^{-1}. Recent research (Koopmans and Bronk, 2002) has also shown that in humic-rich surface waters photochemical processes can release ammonium from more refractory DON. Unfortunately, the rate at which this reaction occurs is poorly understood so we allowed only small amounts of DON (0.0005 d^{-1}) to be photooxidized to produce ammonium.

The amount of dissolved organic matter production that enters the labile, semi-labile, and refractory pools is difficult to estimate because it is poorly understood. Further complicating this partitioning is the fact that production, involving the same processes such as phytoplankton exudation, may be different for different species (i.e. the amount and lability of exuded DOM will not be the same for a diatom and a dinoflagellate). Previous modeling studies of DOM cycling have typically adjusted these parameters in order to achieve acceptable fits to the data (Christian and Anderson, 2002).

We have had to take a similar approach after trying to use previous modeling partitioning parameters, which were for coastal and open ocean models, and finding poor fits with station CB3.3.C data. However, our partitioning was not completely arbitrary. Partitioning of DOM to the labile fraction was based on work by Wetz et al. (2008) who measured a 41% average degradation of phytoplankton derived DOC after three days in coastal waters. Partition of DOM to the semi-labile fraction was based on a number of studies which have shown that a large fraction of freshly formed DOM is semi-labile and degraded over a period of weeks (Aluwihare and Repeta, 1999; Chen and Wangersky, 1996; Gobler and Sañudo-Wilhelmy, 2003; Meon and Kirchman, 2001). In addition, Anderson and Williams (1998) modeling study also suggested that a large fraction of the DOC produced by primary producers was semi-labile in nature. Little is known about the production of refractory DOM, although it has been shown to be directly produced during blooms in mesocosm studies (Kragh and Søndergaard, 2009). Bacterially-mediated remineralization of DOM has also been shown to produce refractory DOC (Brophy and Carlson, 1989; Ogawa et al., 2001). However, only a small fraction of biologically produced DOM escapes remineralization (Benner, 2002) so we partitioned only a small amount to the refractory fraction. Thus, on this basis 40% of phytoplankton exudation and non-detrital zooplankton and phytoplankton mortality was partitioned to labile DOM, 59% to semi-labile DOM, and the remaining 1% to refractory DOM. We also partitioned 53% of DOM from sloppy feeding and bacterial mortality to labile DOM, 45% to semi-labile DOM, and the remaining 2% to refractory DOM. DOM from viral lysis was partitioned so that it was split evenly between the labile and semi-labile pools with only a small amount <1% entering the refractory pool. Extra DOC from viral lysis (to account

for C:N ratio differences) was partitioned so that 1% went to the labile pool, 89.6% went to the semi-labile pool, and the remaining amount went to the refractory pool. DOM from the decay of detritus was partitioned so that 50% went to labile DOM, 49% went to semi-labile DOM, and the remaining 1% went to refractory DOM.

The addition of DOM to the system was based on mean monthly DOC and DON concentrations from station CB3.2. As this data did not report on the bioavailability of the DOM we set the bioavailability during the tuning process. While this may seem somewhat arbitrary, there is very little data available on the biodegradability of DOM discharged by rivers into estuaries and the few studies that have reported on the bioavailability of this DOM have shown that it is highly variable (0 to 73%) and dependent on hydrological processes in the watershed (Cauwet, 2002). In addition, it also appears that the estuarine turbidity maximum, which is upstream of station CB3.3C, can be a source of DOM, especially during the summer (Fisher et al., 1998) and thus may provide this station with "new" DOM that may be readily degradable by the unique communities of bacteria that develop in the middle of estuaries (Crump et al., 2004). Setting the bioavailability of inflowing DOM during the tuning process also allowed us to better constrain these parameters using the model results (i.e. inflowing DOM bioavailability must be near these values for the model to achieve a reasonable solution). Therefore, on this basis inflowing DON was partitioned between the labile (20%), semi-labile (30%), and refractory (50%) pools and inflowing DOC was partitioned between the labile (19%), semi-labile (30%), and refractory pools (51%).

DIC, DIN, and Detritus

The production and uptake of DIC are discussed in the sections above. In order to

avoid the complications of modeling CO_2 air-sea interactions, and because this process was not a focus of our research, DIC inflow was set so that it balanced the uptake of DIC and kept the concentration of DIC at about 2100 μM. Except for nitrification, the biological production and consumption of ammoium and nitrate are discussed above. Light inhibited nitrification was formulated following Martin and Pondaven (2006):

$$\varpi_1 = 0.16\ (1 - I/I_{surface})$$

where 0.16 is the maximum nitrification rate (d^{-1}) which is based on rates reported by Horrigan et al. (1990) for the Chesapeake Bay. The addition of ammonium and nitrate to the system was based on monthly mean measurements from station CB3.2. In addition, we found during tuning that we had to add extra ammonium to the system in the summer (Table 2.3) to account for the nitrogen added to surface waters from below by wind induced mixing or tilting of the water column and phytoplankton migrating to or below the pycnocline to acquire nutrients. Vertical migration by phytoplankton is well documented (Beckmann and Hense, 2004; Ross and Sharples, 2008) and almost certainly occurs at this station in the summer because of the phytoplankton species present, high productivity, and high concentration of ammonium below the pycnocline (CBP data). It has also been hypothesized that wind-driven mixing and tilting of the pycnocline can increase the transport of ammonium from below the pycnocline to surface waters and stimulate high summer primary productivity (Yeager et al., 2005). The biological production and consumption of detritus is discussed in the sections above. In addition to these processes, detritus decayed to DOM following the formulation of Anderson and Pondaven (2003) with nitrogenous detritus breaking down slightly faster (0.055 d^{-1}) than carbon detritus (0.040 d^{-1}). The addition of detritus to the system was based on

particulate carbon and nitrogen (PC, PN) data from station CB3.2. In order to account for the presence of living biomass in the PC and PN data we subtracted the inflowing biomass of phytoplankton, zooplankton, and bacteria from it. We do not have specific loss terms to account for the loss of detritus due to sinking although we have partially accounted for some of this loss by directly exporting plankton biomass, that may have become detritus, out of the system using the mortality terms described above.

Results and Discussion

In this section we discuss our main run solution, carry out some selected parameter sensitivity studies, and assess the skill of the model. In doing so we point out and discuss the successes and deficiencies of our model. Wherever possible, we suggest potential reasons for deficiencies and possible means of correcting them. Comparisons made to station data are compared to mean monthly or bi-monthly (climatological) measurements from 1997 to 2007. The quantitative metrics that we used to assess the model skill (root mean squared error (RMSE), the correlation coefficient (r), reliability index (RI), average error bias (AE), average absolute error (AAE), and modeling efficiency (MEF)) are as described in Stow et al. (2009). The model was solved numerically using a fourth order Runge-Kutta method (Press et al., 1992). A thirty second time step was used because we found that numerical errors occurred with larger time steps due to the large size of the refractory DOM pool and the small fluxes that it is subject to.

Comparison with CBP station CB3.3C data

Figure 2.3 shows comparisons between CBP station CB3.3C data and the model output. Simulated and observed seasonal ammonium and nitrate concentrations are shown in Fig. 2.3 a. In general the model results compare well with the data, although the modeled concentration of nitrate tends to be slightly high in the winter, spring, and fall and slightly low in the summer. A quantitative comparison between the simulated and observed concentrations of nitrate and ammonia (Table 2.4) also shows that the model output compares well with the observations.

Simulated and observed seasonal chlorophyll *a* concentrations are shown in Fig. 2.3 b. Overall, the model reproduced the general peaks and patterns observed at this station. A quantitative comparison between the simulated and observed chlorophyll *a* concentrations (Table 2.4) also shows that the model output compares well with the observations. However, the model did not capture the timing of when the spring bloom begins. This may be due to a phenomenon unique to Chesapeake Bay where dinoflagellates are transported in the bottom layer from near the mouth of the bay to the general area around this station where they surface and often cause late winter or early spring "blooms" (Tyler and Seliger, 1978, 1981). As our model was not embedded in a hydrodynamic model of the whole bay we could not easily reproduce this phenomenon and were therefore more reliant on temperature and light to trigger a spring bloom. In addition, our model did not account for the ability of mixotrophic species, which can be present at this station in high concentrations during the spring (Adolf et al., 2006; Keller, personal observation in 2007 and 2008), to supplement their photosynthetic growth with grazing and thus grow better than strict phototrophs at low spring temperatures and light

levels. The exponential temperature function that we used to set the maximum attainable daily growth rate of phytoplankton may have also contributed to the delay in the beginning of the spring bloom as it has often led models to under underestimate primary production at lower temperatures (Brush et al., 2002; Cerco and Noel, 2004).

Figures 2.3 c and d compare the simulated DOC and DON concentrations with measured DOC and DON concentrations. The modeled and observed DOC concentrations are generally in good agreement although there was a tendency for the model to slightly underestimate the DOC concentration at certain times of the year. The modeled DON concentrations were within the range of DON observations and agreed reasonably well with the observations in the early summer and at a point in the fall. However, the model missed the timing of a peak in DON in the spring and produced this peak later when observed springtime DON had decreased. In addition, the model overestimated the concentration of DON in the late summer, producing a peak that then declined to below the observed DON concentration in the late fall and winter. Although, we should note that the mean DON observations at the end of the year are much higher than the mean DON observations at beginning of year, indicating that DON decreases rapidly at some point during the winter. The quantitative comparison between the simulated and observed DOM concentrations (Table 2.4) also shows that the model output compares fairly well with the observations for DOC but not as well for DON. Most of the variability in the modeled DOM concentrations was due to changes in the semi-labile pools of DOC and DON. While we do not have measurements of seasonal bioavailability at this station for comparison this result is consistent with observations from various systems around that world, including Chesapeake Bay, which show that

DOC, and sometimes DON, concentrations vary seasonally as a result of changes in the labile and/or semi-labile DOM pool (Bronk, 2002; Bronk et al., 1998; Carlson, 2002; Cauwet, 2002; Raymond and Bauer, 2001).

Figure 2.4 compares the modeled and observed diffuse attenuation coefficient (K_d) and shows the photosynthetically available radiation (PAR) used to force the model. The empirical model light model that we used was able to reproduce the observed pattern of K_d values reasonably well, although there was a tendency for the model to overestimate K_d in the spring. The quantitative comparison between the simulated and observed K_d concentrations (Table 2.4) shows that the model output compares well with the observations for some metrics, but does poorly for other metrics such as the correlation coefficient (r) and the modeling efficiency (MEF). In fig. 2.4 b, which shows PAR at the surface and the average PAR in the mixed layer, it is interesting to note that even though the PAR input used by the model changed seasonally along with modeled K_d, the calculation of average PAR in the surface layer showed little change throughout the year. This occurred because the mean depth of the surface layer changed throughout the year (CBP data not shown) and was at its deepest during the summer when surface PAR values were highest. Because our calculated PAR values accounted for the depth of the surface layer the average amount of light experienced by phytoplankton in the surface layer changed little throughout the year. Thus indicating that phytoplankton growth at this station may be more dependent on temperature than light, unless the species present are able to regulate their buoyancy and remain mostly at the surface where light levels are highest.

Biomass and detritus

Figure 2.5 a shows the modeled seasonal biomass of plankton. Phytoplankton biomass had two peaks, one in the spring composed mostly of large phytoplankton, and one in the summer/early fall which was composed of a mix of large and small phytoplankton (Fig. 2.5 c shows similar results in terms of chlorophyll). As our results closely match the chlorophyll a concentrations reported at station CB3.3C (see Fig. 2.3 b) and the general patterns in phytoplankton composition and biomass reported for the Chesapeake Bay (Adolf et al., 2006; Malone et al., 1996) we believe that the model did a relatively good job of capturing the phytoplankton biomass dynamics at this station. The biomass of large zooplankton peaked in the spring following the springtime phytoplankton bloom and then leveled off with low biomass during the summer and very little biomass in the winter. These results are of a similar magnitude and consistent with the long-term trends in mesozooplankton abundance reported for the upper Chesapeake Bay (Kimmel and Roman, 2004) and with CBP data for station CB3.3C. The biomass of small zooplankton remained low (compared to other plankton) throughout the year with the highest biomass (1.02 μM N) occurring in the summer. Our modeled maximum summer microzooplankton biomass was very similar to the maximum microzooplankton biomass reported at station CB3.3C in summer of 2000 by Johnson et al. (2003) who found that the heterotrophic and mixotrophic ciliate biomass was 4.16 μM C (0.75 μM N using a microzooplankton C:N ratio of 5.5) and the heterotrophic dinoflagellate biomass was 5.82 μM C (1.01 μM N using a microzooplankton C:N ratio of 5.5). A direct comparison with CBP station CB3.3C microzooplankton data was not performed because this data was collected with a 44 μm net, which may capture less than half of the total

microzooplankton biomass (Brownlee and Jacobs, 1987). However, the trend in abundance showed a similar pattern to our modeled data with the highest abundance of microzooplankton occurring in the summer. The biomass of bacteria was the highest in the summer and relatively constant throughout the spring, winter, and fall. Our results are consistent with a study of Chesapeake Bay bacterioplankton by Shiah and Ducklow (1994a) who found similar seasonal trends in abundance and biomass (range 0.49 to 9.86 μM N; annual average: upper bay 2.69 μM N, mid-bay 3.87 μM N). The biomass of viruses (Fig. 2.5 b) generally followed the seasonal abundance of their hosts (Fig. 2.5 a) and was therefore rather constant throughout the year for bacteriophages and showed two peaks, a small one in the spring and a larger one in the summer, for phytoplankton viruses. These results are within the range of virus abundance data (when converted to biomass) reported by Wommack et al. (1992) for the Chesapeake Bay (range 0.042 to 2.09 μM N; annual mean 0.40 μM N) and show the same seasonal trend with the highest viral abundance (biomass) in the late summer and fall. Our results are also consistent with the limited MOVE virus data for station CB3.3C (comparison not shown).

Figure 2.5 d shows the modeled seasonal concentration of detritus (both C and N). In this figure the concentration of detritus was highest in the late summer when plankton biomass was at its seasonal maximum. It is interesting to note that the spring phytoplankton bloom did not result in a significant increase in the amount of detritus. Possibly because large phytoplankton tend to sink when they die and because the flow of water in the surface layer is high at this time of year which would transport freshly produced detritus seaward much faster than in the summer. However, the signal of the

spring bloom was evident in the detritus C:N ratio which dropped from almost 9 to 4.5 as the bloom ended.

Production

Primary production (Fig. 2.6 a) was lowest in the winter and peaked in the spring and again in late summer. The contribution to total primary production by the different size classes of phytoplankton changed seasonally with large phytoplankton dominating production in the spring and small phytoplankton dominating production in the late summer, a result that is consistent with studies of this area of the bay (Adolf et al., 2006). In the spring and early summer primary production was fueled by the uptake of nitrate, which was abundant at this time of year (Fig. 2.3 a), while in the late summer peak primary production was fueled by the uptake of ammonium (Fig. 2.6 b). We were unable to directly compare our primary production rates with CBP data because of the methodology used by them to calculate primary production. However, we can compare trends which show that our results are similar to the mean CBP primary production observations at station CB3.3C, with low winter productivity and peaks of nearly equal magnitude in the spring and late summer (comparisons not shown). But, unlike the CBP data, our model did not produce a productivity peak in June that was a large as the peaks in the spring and late summer. Direct comparisons with other reports of Chesapeake Bay primary productivity were not conducted because this data is reported in terms of integrated primary production while our data was generated by a zero dimensional model that calculated phytoplankton growth and subsequent productivity using averaged surface layer irradiance. However, we can make comparisons between our data and the seasonal trends in production reported in studies of Chesapeake Bay primary production by

looking at chlorophyll based rates of production. Overall, it appears that the model underestimated productivity in the summer as our calculated optimal chl-based photosynthetic rates, P^B_{opt} (mg C mg Chl a^{-1} h^{-1}), ranged from 0.8 to 2.4 (2.4 being the summer maximum) which was low compared to long-term measurements from this area of the bay in the spring, summer, and fall which had a mean range of 2.0 to 6.5 (with 6.5 being the summer maximum) (Harding et al., 2002). Winter measurements of P^B_{opt} can be as low as 0.1 at this station (Malone et al., 1996). Underestimation of primary production in ecosystem models that use the Epply curve (Eppley, 1972) to describe phytoplankton growth is common (Brush et al., 2002; Cerco and Noel, 2004) and we had hoped that we would avoid this problem by using an updated version of the Epply curve (Bissinger et al., 2008). As our model still underestimated primary production it may be that the new growth function described by Bissinger et al. (2008) was too reliant on diatom data and thus does not describe growth for the sometimes dinoflagellate dominated phytoplankton community at this station (Adolf et al., 2006). Indeed, reports of primary production have indicated that dinoflagellate blooms in this area often have high primary production per unit Chl *a* (Adolf et al., 2006). Alternatively, we may have underestimated the amount of nitrogen and/or light that was available to phytoplankton in the summer when production is highest. As nitrogen is generally low in surface waters during the summer (Fig. 2.3 a) a significant amount of nitrogen must be supplied to fuel production through a combination of rapid nutrient recycling due to predation, bacterial remineralization, nitrogen pulses from below the pycnocline due to wind event mixing or tilting of the pycnocline, and vertical migration by phytoplankton to nitrogen rich waters below the pycnocline. Predation may be particularly important as Cerco and Noel (2004) found that

to achieve the correct level of primary production in their model of Chesapeake Bay it was necessary to have a predator population that accounted for both lower and higher trophic levels, including planktivorous fish (i.e. menhaden), that was closely coupled to algal biomass, and rapidly recycled nutrients. We did try to account for some of the nitrogen acquired by phytoplankton vertical migration and nutrient pulse events by adding additional ammonium during the summer (see table 2.5). However, we may have not fully accounted for the remineralization by algal predators, even though the amount of primary production consumed daily by grazers was much higher in our model than the 6 to 16% in Cerco and Noel's model (2004), because the mortality terms that we used to control plankton biomass and account for higher trophic level predation resulted in the export of a significant amount of potentially recyclable biomass. Modeled bacterial excretion of ammonium, which is often an important source of nitrogen for phytoplankton, was low at this time of year (data not shown) and even stopped during the period of highest primary production as bacteria became nitrogen limited and started taking up ammonium (discussed below), indicating that they may not be an important source of nitrogen at this time of year. Underestimation of light availability may have also lead to lower productivity if our calculation of the average light in the surface layer was incorrect. However, we should note that light is likely a limiting factor of phytoplankton growth at this station as studies of phytoplankton throughout the Chesapeake Bay have shown that the chlorophyll *a* maximum usually occurs to the south of this station where light penetration increases allowing phytoplankton to utilize the high concentrations of nutrients in the water (i.e. if there was sufficient light at this station nutrients would not be as high) (Harding et al., 2002; Malone et al., 1996). The model

did a reasonable job of calculating K_d (see Fig. 2.4 a) so our concern is not with this calculation but with the calculated amount of PAR that phytoplankton would have been exposed to. This calculation was designed to simulate the average amount of light that phytoplankton would be exposed to as they were mixed throughout the surface layer. As discussed above, this resulted in an average light level that was almost the same throughout the year (Fig. 2.4 b) because the depth of the surface layer, which is taken into account in the calculation, was deeper in the summer than in the winter due to the physical circulation at this station. If phytoplankton are evenly mixed throughout the surface layer this calculation should not cause a problem, but if phytoplankton at this station are able to remain near the surface by migrating vertically or regulating their buoyancy then the model will underestimate the amount of light that the phytoplankton community is exposed to.

Modeled bacterial production fluctuated throughout the year between 0.4 and 0.7 μmol C d^{-1} (average 0.53 μmol C d^{-1}) which compares well with the 0.5 μmol C d^{-1} bacterial production measurements made by Raymond and Bauer (2001) during DOC consumption experiments in the nearby York River estuary, a sub-estuary of the Chesapeake Bay. However, our highest simulated production occurred in the spring, which is in contrast to measurements made in this area of the bay by Shiah and Ducklow (1994b) who found that production was mostly temperature limited and therefore highest in the late summer when water temperatures were highest. Correctly modeling bacterial production can be difficult and other modeling studies such as the one by Thingstad et al. (2007) have also had a problem with getting bacterial production correct without adjusting other parameter or state variable values in a manner that seriously deteriorated

the model performance in other respects. Our failure to correctly simulate bacterial production may have partially occurred because the formulation that we used to model bacterial production did not take into account temperature. Simple Monod-type stoichiometric models of bacterial growth also do not adequately account for the variable energy content and oxidation state of seasonally changing DOM. While more complex models of bacterial growth such as the bioenergetics model put forth by Vallino et al. (1996) exist, they are presently to complex to easily incorporate into full biogeochemical ecosystem models. However, the main reason for our low modeled summer bacterial production was because bacteria became substrate (nitrogen) limited and were subjected to the highest seasonal grazing pressure by small zooplankton. Shiah and Ducklow (1994a) suggested, in agreement with our results, that when temperatures were high (> 20 C) either substrate limitation or mortality appear to slow bacterial growth. However, unlike our results they also found that productivity was highest at this time of year.

Additional model runs that we conducted to address the issue of low primary and bacterial productivity were not successful as we were unable to increase productivity without compromising the performance of the model in other respects. Indeed there seemed to be a link between biomass and productivity that was inherent in the model formulation as we were unable to raise or lower one without increasing or decreasing the other by a similar amount. Solving this fundamental problem is beyond the scope of this paper and will have to be addressed in the future. Fortunately, we believe that it does not seriously compromise our study of DOM cycling at this station even though it may slightly reduce the flow of nitrogen and carbon through the DOM pool.

Zooplankton grazing

The sources of nitrogen in the diet of large zooplankton (Fig. 2.7 a) varied throughout the year, indicating a diverse diet, and reflecting the seasonal abundances of different food sources. The sources of nitrogen in the diet of small zooplankton (Fig. 2.7 b) were less varied, indicating a more selective diet, consisting of mostly phytoplankton and bacteria. The percentage of primary production lost to zooplankton grazing (Fig. 2.7 c) shows that zooplankton had the largest impact on primary production in the spring with large zooplankton consuming almost half of daily primary production. Grazing also had a strong impact on primary production in the mid- and late summer with zooplankton consuming over 30 % of primary production daily. White and Roman (1992) found that the amount of daily phytoplankton production consumed by 64 to >200 μm zooplankton in the mesohaline portion of Chesapeake Bay (south of station CB3.3C) in 1988 varied between 15.3 and 112 % with consumption in March (112 %) > August (52 %) > October (24.4 %) > May (15.3 %). While this data represents just one year and was taken to the south of the station that we modeled in the area of the chlorophyll *a* maximum, which makes a direct comparison unfeasible, it does indicate that while we got the pattern of grazing correct we may have underestimated the amount of production that is consumed daily. This may be especially true for small zooplankton grazing, as an analysis by Calbet and Landry (2004) indicates that microzooplankton consume on average 59.7 % of daily primary production in estuaries. However, we may have also modeled a station that has some unique biological characteristics, like seasonal blooms of dinoflagellates that were transported in bottom waters from near the mouth of the Bay (Adolf et al., 2006; Tyler and Seliger, 1978, 1981), that result in less microzooplankton grazing.

Supporting this is a study of phytoplankton pigments and microzooplankton grazing by McManus and Ederington-Cantrell (1992) who found that when high concentrations of peridinin (a dinoflagellate pigment) were present in this area of the bay their calculated grazing rates were negative. However, they also found, in agreement with Calbet and Landry (2004), that most of the time more than half of the primary production was grazed daily by microzooplankton. Another report of microzooplankton grazing on dinoflagellates in the Chesapeake Bay area by Johnson et al. (Johnson et al., 2003) also found that grazing pressure on a Potomac River (a Chesapeake Bay tributary) dinoflagellate bloom, similar to the ones that occur at this station, was low even though the microzooplankton biomass was high. In addition, they found that potential microzooplankton grazing rates on *Prorocentrum minimum* and *Karlodinium micrum* in July and August at station CB3.3C were much lower than at adjacent stations to the north and south. Overall these reports lead us to conclude that while we have gotten the seasonal trends correct we may have underestimated the amount of primary production that is consumed daily at this station by zooplankton. However, we were reluctant to make any major modifications to the model to address this issue as we lack a complete set of seasonal observations of zooplankton grazing at this station and cannot definitively say that our grazing formulations are incorrect.

DOM cycling

The production of DOM (Fig. 2.8) peaked in the spring and the late summer, corresponding to the peaks in plankton biomass and productivity described in the sections above. It is interesting to note that peaks in DOC production (Fig. 2.8 a) were of roughly the same magnitude (1.88 and 2.08 μM C d^{-1}) while the springtime DON production (Fig.

2.8 b) peak (159.5 nM N d^{-1}) was much higher than the late summer peak (98.7 nM N d^{-1}). A more detailed examination of DOC production shows that phytoplankton exudation was the dominant source of DOC, averaging 63 % of total DOC production throughout the year, except for a brief period during the spring when the production of DOC from sloppy feeding was high. Viral lysis was also an important source of DOC (averaging 14 % of total DOC production throughout the year), especially during the late summer and early fall. Mortality, the decay of detritus, zooplankton excretion, and sloppy feeding all produced minor amounts of DOC throughout the year, except for the noted peak in the production of DOC by sloppy feeding in the spring. The contribution of different sources of DON to total DON production varied much more seasonally than for DOC. In the spring sloppy feeding was the most important source of DON (up to 75 % of total DON production). This result is consistent with a study by Bronk et al. (1998), which suggested that sloppy feeding contributed significantly to spring DON production. In the summer when DON production peaked again, the peak was due to increases in all DON sources with production from viral lysis (36 %) > phytoplankton exudation (26 %) > the decay of detritus (18 %) > mortality (9 %) > sloppy feeding (7 %) > zooplankton excretion (4 %). We should also note that the decay of viruses (Fig. 2.5 b) transferred significant amounts of organic matter (61.62 to 154.94 nM N d^{-1} and 0.20 to 0.51 μM C d^{-1}) from viruses to the modeled pools of DOM. We did not include this in our figures of DOM production because viruses are small enough that they are considered to be DOM. However, from a DOM bioavailability perspective infective viruses are unavailable for uptake by bacteria or phytoplankton and thus their decay represents the production of "new" potentially bioavailable DOM. The amount of DOM, especially DON, produced

by viral decay is high compared to other sources of DOM and is a source of DOM that has generally been overlooked by the scientific community. Even if we overestimated viral production or the decay rate and the amount of DOM produced by viral decay is half of what we calculated this would still represent a significant source of potentially bioavailable DOM.

A more detailed look at individual sources of DOM (Fig. 2.9) highlights the seasonal role that different groups of plankton play in DOM cycling. The release of DOM by phytoplankton (Fig. 2.9 a) in the spring came mostly from large phytoplankton while in the late summer most of the DOM was produced by smaller phytoplankton. This seasonal pattern of phytoplankton DOM production corresponds with the seasonal biomass and productivity patterns of phytoplankton that we discussed in the previous sections. While our formulation for the release of DOM by phytoplankton is relatively simple (i.e. a fixed rate), compared to Flynn et al.'s (2008) models of DOM release, and does not take important factors such as the nutritional status or growth rate of phytoplankton into account, we feel that our model provides a reasonable description of seasonal DOM production by phytoplankton (i.e. high phytoplankton biomass and productivity at certain times of the year should result in increases in DOM exudation by phytoplankton at those times of the year).

The production of DOM by sloppy feeding (Fig. 2.9 b) peaked in the spring when the biomass (Fig. 2.5 a) of large zooplankton was highest. Most of the DOM produced by this process came from large zooplankton feeding on other large zooplankton with lesser amounts coming from large zooplankton feeding on large phytoplankton and detritus. Because the release of DOM by sloppy feeding is a size dependent process that

occurs when large zooplankton (copepods) feed (Møller, 2005, 2007; Møller and Nielsen, 2001) it was not surprising that DOM production from sloppy feeding was highest in the spring when large zooplankton were the most abundant.

The production of DOM by viral lysis (Fig. 2.9 c) peaked slightly in the spring and then reached a maximum rate in the late summer. This result seems reasonable given that viruses tend to show a seasonal trend in abundance with peak abundance occurring in the late summer and early fall (Wommack et al., 1992) which indicates that virus production is also high at this time of year. And because viral production also produces DOM it is reasonable to assume that DOM production by viral lysis is high when viral production is high. Lysis of bacteria was the most important source of DOM throughout the year but the maximum amount of DOM produced by lysis was from the lysis of small phytoplankton in the late summer. Since most virioplankton are thought to be bacteriophages (Weinbauer, 2004; Wommack and Colwell, 2000) and because bacteria are very abundant and productive in Chesapeake Bay, it was not surprising that our results show that seasonally most of the DOM from viral lysis comes from the lysis of bacteria. The peaks in DOM production from viral lysis of phytoplankton were because more DOM is produced when a phytoplankton cell lyses (i.e. the larger the cell lysed the more DOM produced), not because more phytoplankton than bacteria underwent lysis.

The production of DOM from mortality (individual sources not shown) and the breakdown detritus (Fig. 2.8) were formulated so that a fixed percentage of the state variable mass enters the DOM pool on a daily basis. Consequently, the amount of DOM produced by mortality and the breakdown of detritus tracks the mass of that source as it changes seasonally (i.e. the peak in large zooplankton biomass corresponds to a peak in

DOM from the mortality of large zooplankton). These processes are not well understood and there is very little information in the literature to parameterize the rates at which they occur or to make comparisons with. Therefore, it is difficult to conclude that our model, or any other ecosystem model, adequately simulates the true magnitude of the production of DOM from mortality and the breakdown of detritus. However, it is logical to assume that when the mass and/or productivity of plankton and detritus are high the amount of DOM produced by their mortality or breakdown will be higher than when their mass and/or productivity is low. This gives us some confidence that our model at least captures the seasonal trends in DOM production from these sources.

The transformation, uptake, and C:N ratio of DOM is shown in figure 2.10. The rate of ectoenzyme hydrolysis of the semi-labile DOM pool (Fig. 2.10 a) peaked in the summer when the concentration of semi-labile DOM and bacterial biomass were at their seasonal maxima. Due to the model formulation most (90 %) of this semi-labile DOM was transformed into labile DOM pool with only a small fraction becoming more refractory. Photochemical processes (Fig. 2.10 b) converted DOC to DIC at a mean rate of 0.029 μM C d^{-1}, DON to ammonium at a mean rate of 0.299 nM N d^{-1}, refractory DOC to labile DOC at a mean rate of 0.006 μM C d^{-1}, and refractory DON to labile DON at a mean rate of 0.467 nM N d^{-1}. As expected, the primary consumers of DON were bacteria (Fig. 2.10 c) with phytoplankton taking up minor amounts of DON when their biomass and productivity was highest. Our results show that the maximum uptake of DON by bacteria occurred in the spring. High rates of DON uptake by bacteria did not occur in the summer because the C:N ratio of labile DON (Fig. 2.10 d) was high at this time of year causing them to become nitrogen limited and start taking up ammonium. The

degree to which this actually occurs is unknown as DOM uptake by bacteria has not been measured seasonally at this station. However, previous studies (Apple et al., 2006; Shiah and Ducklow, 1994a, b) in the Bay have suggested that bacteria become substrate limited in the summer when the temperature exceeds 20° C.

Sensitivity analysis

Model sensitivity to selected parameters (see Figure 2.11) was assessed by varying each in turn ± 50 % of their default value. The affect of the parameter variations was then determined by comparing the adjusted model output to the main model run at times of the year when biomass and productivity were high, in the spring (day 90) and the late summer (day 225). Light limitation of phytoplankton growth was not addressed in this sensitivity analysis because the amount of light that phytoplankton received in the normal model run (Fig. 2.4 b) was similar throughout the year and always somewhat limiting (i.e. phytoplankton growth would always be sensitive to changes in light availability).

An examination of the sensitivity of modeled primary production indicates that in addition to light limitation, spring (Fig. 2.11 a) production was limited by the growth rate of phytoplankton, μ_P, and their growth efficiency (in this case, α, the amount of production not lost to DOM through leakage) with the availability of nitrogen not being an issue, as indicated by a lack of sensitivity to changes in the phytoplankton C:N ratio, λ_P. In the summer (Fig. 2.11 b) primary production was limited more by nitrogen (and light availability) than anything else (indicated by sensitivity to gge_B, which affects nitrogen remineralization by bacteria, and λ_P). These results are in agreement with an analysis by Malone et al. (1996), which suggest that Chesapeake Bay phytoplankton

growth in this region is nutrient saturated in the spring and nitrogen limited in the summer. Phytoplankton biomass was similarly sensitive (data not shown) to the parameters that affected production at different times of the year. However, unlike primary production sensitivity, phytoplankton biomass was also sensitive in the spring to variations in their C:N ratio, λ_P, because of the affect it had on zooplankton biomass and grazing mortality for phytoplankton (data not shown). Small phytoplankton biomass also showed a greater magnitude of sensitivity in the summer (2-fold change in biomass compared to spring). In addition, it was evident that competition was occurring between large and small phytoplankton, as their biomass and productivity was inversely sensitive to parameter variations that affected the other either negatively or positively.

Bacterial production in the spring (Fig. 2.11 c) was most sensitive to factors that affect growth (μ_B, gge_B, K_{L_C}), with only a slight indication of any nutrient (DOM) limitation (sensitivity to ζ and phytoplankton exudation parameters). In the summer, bacterial production was sensitive to parameter variations that increased the amount of available DOM (α, χ_{D_N}, ζ, λ_P, ϖ_2, KS) and their growth efficiency (Fig. 2.11 d). In addition, summer nutrient limitation was also indicated by bacterial production not being sensitive to variations in their growth rate, μ_B. Bacterial biomass was sensitive (data not shown) to the same parameter variations as production (Fig. 2.11 c, d) with the only difference being a greater magnitude of sensitivity in the summer (2-fold change in biomass compared to spring).

The biomass of large and small zooplankton was sensitive in both the spring and summer (data not shown) to parameter variations in their growth coefficients ($ge_{Z_{L\text{ or }S}}$) and the phytoplankton C:N ratio, λ_P. And except for small zooplankton biomass in the

spring, they were sensitive to variations in their mortality rates, mZ_L & mZ_S. Large zooplankton were also sensitive variations in the sloppy feeding parameters, ω_{Z_L}, ω_{P_L}, ω_D (which are essentially assimilation terms), and to variations that affected phytoplankton growth, with sensitivity to changes in the phytoplankton growth rate, μ_P, and efficiency, α.

Total DOC and DON concentrations were much more sensitive to parameter variations in the summer than they were in the spring (Fig. 2.12, note differences in the x-axis scales). Most of this sensitivity was in the semi-labile pools of DOM as the refractory pools were rather insensitive to parameter variations and the labile DOM pools actually exhibited the opposite behavior and were more sensitive in the spring than in the summer (data not shown). The labile DOM pools were for the most part sensitive only to parameter variations that affected bacterial growth and uptake of DOM. The semi-labile DOM pools were sensitive to parameters that controlled the production of DOM, with the semi-labile DOC pool being especially sensitive to phytoplankton DOC exudation, as well as the transformation of DOM (i.e. hydrolysis of semi-labile DOM). The model was also particularly sensitive to parameter variations that affected phytoplankton (i.e. C:N ratio, exudation, growth rate) which is not surprising since primary production ultimately provides the organic matter that is cycled through the various DOM pools.

A previous sensitivity analysis of this model at steady-state under high and low nutrient conditions examined in detail how sensitive the production, transformation, and uptake of DOM was to parameter variations (see Chapter 1). The results of this previous analysis are in agreement with the sensitivity analysis presented here and indicate that DOM cycling is intricately tied to the biomass and production of zooplankton,

phytoplankton, and bacteria with the relative magnitude of sources and sinks of DOM dependant on the relationships between these groups (i.e. high phytoplankton biomass and productivity results in increases in DOM exudation which then provides a substrate to fuel bacterial growth, resulting in more DOM release from bacterial viral lysis and so on).

Future Modeling Challenges

The development and implementation of this model has revealed important gaps in our general and local knowledge of DOM cycling that need to be addressed in future research efforts. Obtaining more data to force and validate certain aspects of the model is particularly important as we lacked seasonal measurements of some key variables and processes in this study despite choosing a location in a well-studied estuary. Improving equations that simulate a number of ecosystem processes is also important as our research indicates that some formulations do not adequately describe certain biological or chemical processes. Here we specifically highlight areas for future research that play in an important role in DOM cycling and need to be better understood. First, there was no adequate data on the biodegradability of DOM inputs from upstream sources. Second, data to fully constrain interactions with the benthos and adjacent terrestrial environments, such as tidal marshes, was unavailable. Third, some of the model parameters, especially those related to mortality and viral infection and decay, had to be estimated using assumptions that may not be valid. Fourth some processes, such as photochemical effects and the decay of detritus are modeled using simple linear equations that may not adequately describe these processes. Fifth, physical processes such as sorption/desorption and flocculation that may alter the concentration and chemical

structure of DOM and influence its bioavailability as it is transported through the estuary are also poorly understood, especially in estuaries with steep salinity gradients, and we did not include them in the model. Sixth, parameters describing the partitioning of freshly produced DOM to labile, semi-labile, and refractory pools were poorly constrained. Finally, the equations describing the growth and productivity of phytoplankton and bacteria were also a problem, as we could not uncouple productivity from biomass. Hopefully, our study increases awareness of these issues and can be used to guide future research on DOM cycling.

Summary and Conclusions

In this paper we describe a new model formulation that is designed to simulate and investigate DOM cycling in pelagic marine systems. This model includes a representation of DOM in terms of refractory, semi-labile and labile constituents for both DON and DOC. In addition, sources and sinks for DOM from multiple phytoplankton and zooplankton size classes and bacteria are included in the model, along with an explicit representation of the impacts of viruses and viral infection. The effects of light on DOM lability are also included. As such, the level of detail in the DOM pools and cycling in this model are unprecedented.

The model was tuned, parameterized, and physically forced with the explicit goal of describing the general seasonal cycle of DOM in the surface layer at station CB3.3C in Chesapeake Bay. Because many of the processes involved in DOM cycling are poorly constrained it was important to reproduce the observed patterns in biomass, productivity, nutrients, and DOM at this station before we could be confident that our model could simulate the interactions between plankton, nutrients, detritus, and DOM. Our results

show that we successfully reproduced the mean seasonal peaks in zooplankton, phytoplankton, bacteria, and viral biomass that have been observed at this station. The model also did a reasonable job of reproducing the observed seasonal concentrations of nitrate, ammonium, DOC, and DON. However, it appears that the model underestimated primary and bacterial productivity, either by incorrectly calculating their realized growth rates or by underestimating the availability of light and nitrogen. It is also unclear, given a lack of data for this station, as to whether or not the model underestimated the amount of primary production consumed daily by zooplankton. However, despite these discrepancies our results indicate that the model did a reasonable job of simulating the plankton dynamics at this station.

According to our model, DOM cycling was strongly influenced by seasonal changes in the planktonic community. The degree to which different groups of plankton influenced DOM cycling was strongly related to their biomass and productivity in relation to that of the other groups of plankton. Thus, in the spring DOM cycling was mostly controlled by interactions between large phytoplankton, large zooplankton, and bacteria. While in the summer, DOM cycling was mostly controlled by interactions between small phytoplankton, small zooplankton, viruses, and bacteria. The production of DOM peaked twice, in the spring and late summer, in correspondence with the peak productivity of the spring and summer plankton communities. Table 2.5 summarizes the most important processes involved in peak DOM production. Our results also indicate that viral decay may represent an important, and often overlooked, source of "new" potentially bioavailable DOM from within the DOM pool. Bacteria were the most important consumers of DOM throughout the year with phytoplankton consuming small

but significant amount of DOM in the spring and late summer. Furthermore, bacteria played an important role in hydrolyzing the semi-labile DOM that accumulated as a result of spring and summer productivity. Photochemical, chemical, and physical processes such as the decay of detritus and the transformation of refractory DOM to labile DOM also played an important role in DOM cycling at this station, and were especially important in turning over the refractory pools of DOM.

In general, our simulations of DOM cycling appear to agree with the current scientific understanding of DOM biogeochemistry. However, we cannot validate some of the model results because we lack the data to do so. Thus, many of our model-generated results about certain aspects of DOM cycling are predictions that need to be tested. These predictions can help guide future research. Moreover, this modeling effort has synthesized a large body of recent DOM literature and provided a means to look at the simultaneous flow of carbon and nitrogen throughout the whole ecosystem and compare the importance of various processes over a long time scale, something that is technically and economically unfeasible to do experimentally. Finally, the development of this model has highlighted important gaps in our knowledge of key processes that influence DOM cycling in marine waters.

Tables

Table 2.1. Model parameters

Description	Symbol	Value	Units
Phytoplankton light saturation parameter	I_P	40	W m^{-2}
Phytoplankton photoinhibition parameter	I_β	400	W m^{-2}
Partitioning of phytoplankton production	α	0.95	dimensionless
Phytoplankton excretion parameter	ϖ_2	0.26	dimensionless
Phytoplankton C:N ratio	λ_P	7.5	mol mol^{-1}
Half-sat. const. for N_n uptake by P_L	$K_{P_L N_n}$	20	μM
Half-sat. const. for A uptake by P_L	$K_{P_L A}$	15	μM
Half-sat. const. for N_n uptake by P_S	$K_{P_S N_n}$	20	μM
Half-sat. const for A uptake by P_S	$K_{P_S A}$	10	μM
Half-sat. const for DON uptake by phytoplankton	$K_{P_{L\text{ or }S} L_N}$	20	μM
Large zooplankton maximum consumption rate	C_{Z_L}	1.0	d^{-1}
Small zooplankton maximum consumption rate	C_{Z_S}	2.0	d^{-1}
Zooplankton assimilation efficiency (N)	β_{N_Z}	0.77	dimensionless
Zooplankton assimilation efficiency (C)	β_{C_Z}	0.64	dimensionless
Large zooplankton growth coefficient	ge_{Z_L}	0.75	dimensionless
Small zooplankton growth coefficient	ge_{Z_S}	0.40	dimensionless
Half-sat. const. for zooplankton grazing	K_Z	0.75	μM
Large zooplankton preference for P_L	Φ_{P_L}	0.20	dimensionless

Large zooplankton preference for P_S	Φ_{P_S}	0.15	dimensionless
Large zooplankton preference for D	Φ_D	0.20	dimensionless
Large zooplankton preference for Z_L	Φ_{Z_L}	0.20	dimensionless
Large zooplankton preference for Z_S	Φ_{Z_S}	0.20	dimensionless
Large zooplankton preference for B	Φ_B	0.05	dimensionless
Small zooplankton preference for P_L	φ_{P_L}	0.15	dimensionless
Small zooplankton preference for P_S	φ_{P_S}	0.25	dimensionless
Small zooplankton preference for D	φ_D	0.20	dimensionless
Small zooplankton preference for Z_S	φ_{Z_S}	0.20	dimensionless
Small zooplankton preference for B	φ_B	0.20	dimensionless
Zooplankton C:N ratio	λ_Z	5.5	mol mol^{-1}
Bacterial gross growth efficiency	gge_B	0.30	dimensionless
Maximum bacterial growth rate	μ_B	13.3	d^{-1}
Half-sat. const. for ammonium uptake by bacteria	K_{BA}	0.50	μM
Half-sat. const. for labile DOC uptake by bacteria	K_{L_C}	25	μM
Bacteria C:N ratio	λ_B	5.1	mol mol^{-1}
Viral decay rate	υ	0.08	h^{-1}
Virus C:N ratio	λ_V	3.26	mol mol^{-1}
Production of new viruses from lysis	ε_V	0.50	dimensionless
Partitioning of sloppy feeding on lrg. zooplankton	ω_{Z_L}	0.69	dimensionless
Partitioning of sloppy feeding on detritus	ω_D	0.24	dimensionless
Partitioning of sloppy feeding on lrg. phytoplankton	ω_{P_L}	0.26	dimensionless
Partitioning of mortality to detritus and DOM	β_1	0.66	dimensionless

Partitioning of "extra C" from lysis to LC	β_2	0.025	dimensionless
Partitioning of "extra C" from lysis to SC	β_3	0.224	dimensionless
Partitioning of "extra C" from lysis to RC	β_4	0.001	dimensionless
Partitioning of "extra C" from lysis to detritus	β_5	0.75	dimensionless
Partitioning of sloppy feeding and B mort to detritus	ρ_D	0.25	dimensionless
Partitioning of sloppy feeding and B mort. to labile DOM	ρ_L	0.40	dimensionless
Partitioning of sloppy feeding and B mort. to semi-labile DOM	ρ_S	0.34	dimensionless
Partitioning of sloppy feeding and B mort. to refractory DOM	ρ_R	0.01	dimensionless
Labile fraction of DOM from detritus decay	δ_1	0.50	dimensionless
Semi-labile fraction of DOM from detritus decay	δ_2	0.49	dimensionless
Refractory fraction of DOM from detritus decay	δ_3	0.01	dimensionless
Maximum rate of semi-labile DOM hydrolysis	μ_S	4.0	d^{-1}
Half-sat. const. for DOM hydrolysis	K_S	417	μM C
Partitioning of phytoplankton DOM leakage and plankton mortality to labile DOM	o_L	0.40	dimensionless
Partitioning of phytoplankton DOM leakage and plankton mortality to semi-labile DOM	o_S	0.59	dimensionless
Partitioning of phytoplankton DOM leakage and plankton mortality to refractory DOM	o_R	0.01	dimensionless
Partitioning of lysis product to D	ε_D	0.375	dimensionless
Partitioning of lysis product to labile DOM	ε_L	0.062	dimensionless
Partitioning of lysis product to semi-labile DOM	ε_S	0.062	dimensionless
Partitioning of lysis product to refractory DOM	ε_R	0.001	dimensionless
Breakdown of N detritus to DOM	χ_{D_N}	0.055	d^{-1}
Breakdown of C detritus to DOM	χ_{D_C}	0.040	d^{-1}

Partitioning of viral decay to DOM	η	0.10	dimensionless
UV photooxidation of refractory DOM	ζ	0.0015	d^{-1}
Partitioning of zooplankton excretion to DON and ammonium	κ_Z	0.68	dimensionless
Partitioning of zooplankton DOM excretion to labile and semi-labile pools	o_Z	0.70	dimensionless
Partitioning of zooplankton metabolized carbon to DIC and DOC	σ_Z	0.69	dimensionless
Rate of DOC photooxidation to DIC	χ_{UV_C}	0.004	d^{-1}
Rate of DON photooxidaiton to ammonium	χ_{UV_N}	0.0005	d^{-1}

Table 2.2. List of model variables

Variable	Symbol	Units
Ammonium	A	µM
Bacteria	B	µM N
Bacteriophages	V_B	µM N
Detritus	D_N	µM N
Detritus	D_C	µM C
Dissolved inorganic carbon	DIC	µM
Labile DOC	L_C	µM C
Labile DON	L_N	µM N
Large phytoplankton	P_L	µM N
Large zooplankton	Z_L	µM N
Nitrate	N_n	µM
Phytoplankton viruses	V_P	µM N
Refractory DOC	R_C	µM C
Refractory DON	R_N	µM N
Semi-labile DOC	S_C	µM C
Semi-labile DON	S_N	µM N
Small phytoplankton	P_S	µM N
Small zooplankton	Z_S	µM N
Irradiance	I	W m^{-2}
Vertical light attenuation coefficient	K_d	none
Mortality of plankton ($i = B, P_L, P_S, Z_L,$ or Z_S)	S_i	d^{-1}
Biomass from mortality not exported	m	d^{-1}
Maximum phytoplankton growth rate	μ_P	d^{-1}

Light-limited phytoplankton growth	$J_{P_{L\text{ or }S}}$	d^{-1}
Nutrient limitation of phytoplankton	$Q_{P_{L\text{ or }S}}$	none
Ammonium limitation of phytoplankton	$Q^1_{P_{L\text{ or }S}}$	none
Labile DON limitation of phytoplankton	$Q^2_{P_{L\text{ or }S}}$	none
Nitrate limitation of phytoplankton	$Q^3_{P_{L\text{ or }S}}$	none
Extra photosynthetic carbon exudation	$E_{P_{L\text{ or }S}}$	$\mu M\ C\ d^{-1}$
Viral infection rate ($i = B,\ P_L,$ or P_S)	Ψ_i	$\mu M^{-1}\ N\ d^{-1}$
Zooplankton production	$F_{Z_{L\text{ or }S}}$	$\mu M\ N\ d^{-1}$
Zooplankton grazing on bacteria	$G_{Z_{L\text{ or S}}B}$	$\mu M\ N\ d^{-1}$
Zooplankton grazing on large phytoplankton	$G_{Z_{L\text{ or S}}P_L}$	$\mu M\ N\ d^{-1}$
Zooplankton grazing on small phytoplankton	$G_{Z_{L\text{ or S}}P_S}$	$\mu M\ N\ d^{-1}$
Zooplankton grazing on small zooplankton	$G_{Z_{L\text{ or S}}Z_S}$	$\mu M\ N\ d^{-1}$
Z_L grazing on other Z_L	$G_{Z_L Z_L}$	$\mu M\ N\ d^{-1}$
Zooplankton grazing on nitrogenous detritus	$G_{Z_{L\text{ or S}}D_N}$	$\mu M\ N\ d^{-1}$
Zooplankton grazing on carbon detritus	$G_{Z_{L\text{ or S}}D_C}$	$\mu M\ C\ d^{-1}$
Zooplankton respiration	$R_{Z_{L\text{ or }S}}$	$\mu M\ C\ d^{-1}$
Zooplankton excretion	$E_{Z_{L\text{ or }S}}$	$\mu M\ N\ d^{-1}$
Bacterial production	B_{growth}	$\mu M\ N\ d^{-1}$
Uptake of DOC by bacteria	U_C	$\mu M\ C\ d^{-1}$
Uptake of DON by bacteria	U_N	$\mu M\ N\ d^{-1}$
Potential uptake of A by bacteria	U^*_A	$\mu M\ N\ d^{-1}$
Realized uptake of A by bacteria	U_A	$\mu M\ N\ d^{-1}$
Bacterial respiration	R_B	$\mu M\ C\ d^{-1}$
Bacterial excretion	b_χ	$\mu M\ N\ d^{-1}$

Nitrification rate	ϖ_1	d^{-1}
Total Suspended Solids	TSS	mg l^{-1}
Temperature	T	degrees C
Chlorophyll *a*	Chl	µg l^{-1}
Salinity	S	none
Mixed layer depth	Z	m
Rate of chemostat flow	h	s^{-1}
Susquehanna river flow	F_{river}	m^3 s^{-1}
Chemostat equation area (i.e. vessel area)	C_{area}	m^2
Amount of state variable (*i*) entering the system	i^o	µM C or N

Table 2.3. Seasonally variable parameters

Day	Phytoplankton Chl *a* ratio (% small)	Extra ammonium addition	Mortality				
			P_L	P_S	Z_L	Z_S	B
0	0.10	0	0.04	0.04	0.01	0.10	0.15
15	0.10	0	0.02	0.04	0.01	0.08	0.15
45	0.20	0	0.02	0.04	0.01	0.08	0.15
74	0.23	0	0.02	0.04	0.02	0.08	0.15
97	0.25	0	0.02	0.04	0.02	0.08	0.15
115	0.25	0	0.02	0.04	0.02	0.08	0.15
127	0.25	0	0.50	0.50	0.02	0.08	0.15
145	0.25	0	0.50	0.50	0.30	0.80	0.15
166	0.30	0	0.50	0.50	0.20	0.80	0.08
188	0.40	0	0.10	0.08	0.20	0.80	0.08
206	0.50	31	0.02	0	0.30	0.80	0.08
219	0.50	67	0.02	0	0.30	0.80	0.08
237	0.50	8	0.02	0	0.30	0.80	0.08
258	0.40	0	0.10	0.01	0.30	0.80	0.15
288	0.25	0	0.25	0.35	0.25	0.80	0.15
319	0.10	0	0.15	0.10	0.15	0.80	0.15
349	0.10	0	0.10	0.06	0.01	0.10	0.15
365	0.10	0	0.04	0.04	0.01	0.10	0.15

Table 2.4. Model skill assessment quantitative metrics

	Nitrate	Ammonium	DON	DOC	Chlorophyll	K_d
RMSE	6.62	1.14	3.54	18.79	3.61	0.17
r	0.97	0.79	0.25	0.81	0.89	0.62
RI	1.51	1.40	1.09	1.04	1.09	1.06
AE	1.55	-0.14	0.50	-12.97	-0.34	0.11
AAE	5.83	0.93	2.95	15.31	2.40	0.18
MEF	0.88	0.59	-0.40	0.02	0.79	-0.26

Table 2.5. Seasonally important sources of DOM

Spring		Late Summer	
DOC	DON	DOC	DON
Phytoplankton exudation (Lrg. Phytoplankton)		Phytoplankton exudation (Sm. Phytoplankton)	Viral lysis
	Sloppy Feeding		Phytoplankton Exudation
Sloppy Feeding		Viral lysis	
			Decay of Detritus
Viral Decay ?			

Figures

Figure 2.1. A schematic diagram of the ecosystem model. Symbols as described in the text.

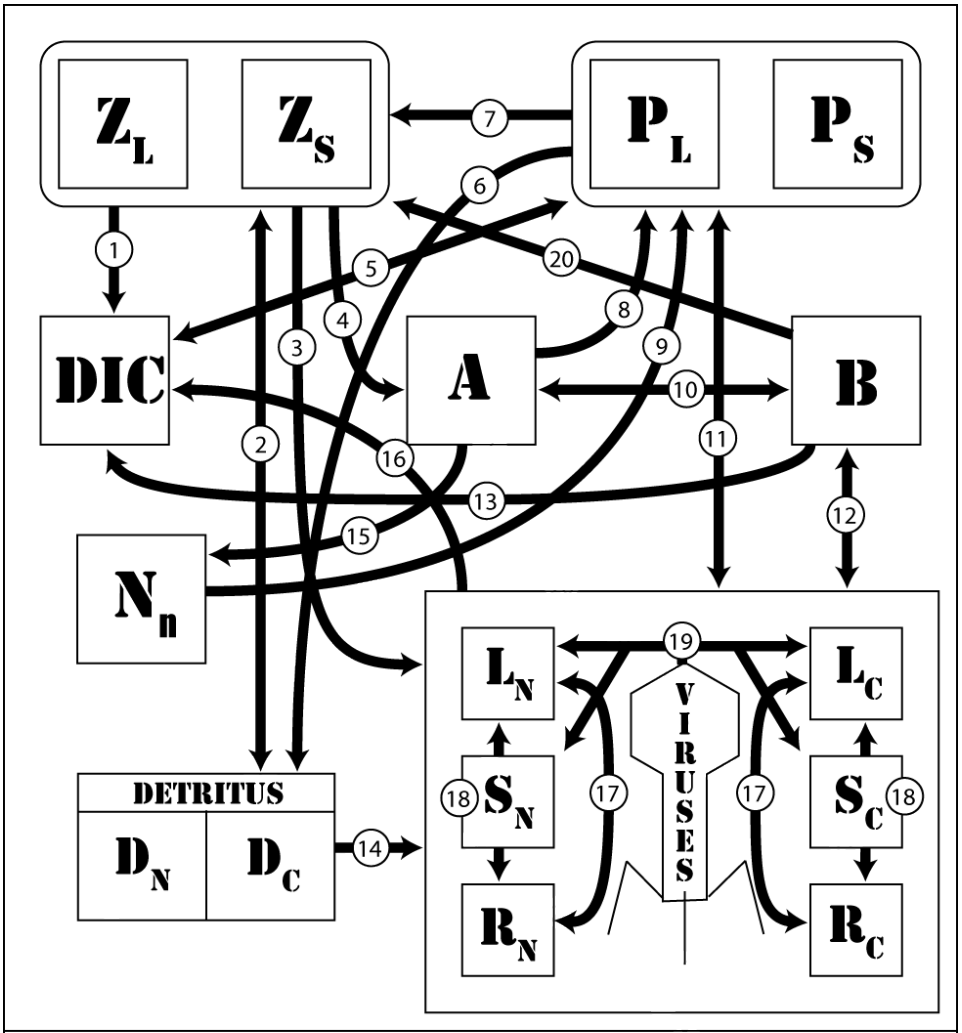

1. Zooplankton Respiration
2. Grazing, egestion, and mortality
3. Zooplankton excretion and mortality
4. Zooplankton excretion
5. Phytoplankton uptake and respiration
6. Phytoplankton mortality
7. Zooplankton grazing on phytoplankton
8. Phytoplankton ammonium uptake
9. Phytoplankton nitrate uptake
10. Uptake or excretion of ammonium
11. Uptake, exudation, mortality, and viral lysis
12. Uptake, mortality, and viral lysis
13. Bacterial respiration
14. Detritus decay
15. Nitrification
16. Photooxidation of DOC
17. Photooxidation of DOM
18. Hydrolysis of semi-labile DOM
19. Viral decay
20. Zooplankton grazing on bacteria

Figure 2.2. Chesapeake Bay Program monitoring station locations.

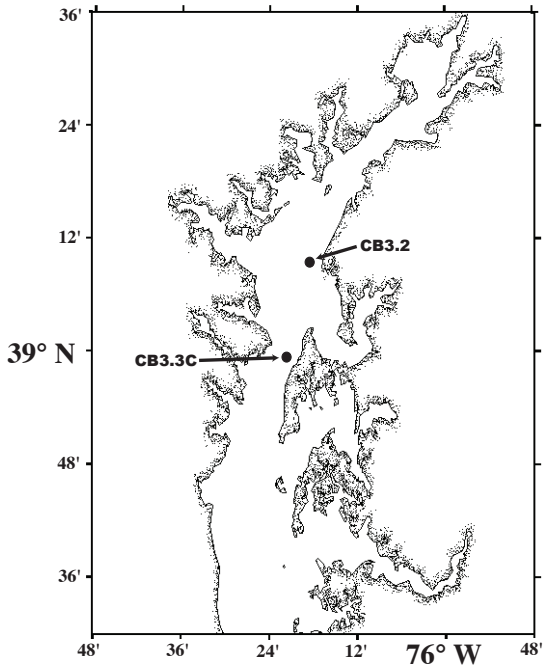

Figure 2.3. The modeled and mean observed concentrations of (a) ammonium and nitrate; (b) chlorophyll *a*; (c) DOC; (d) DON at station CB3.3C.

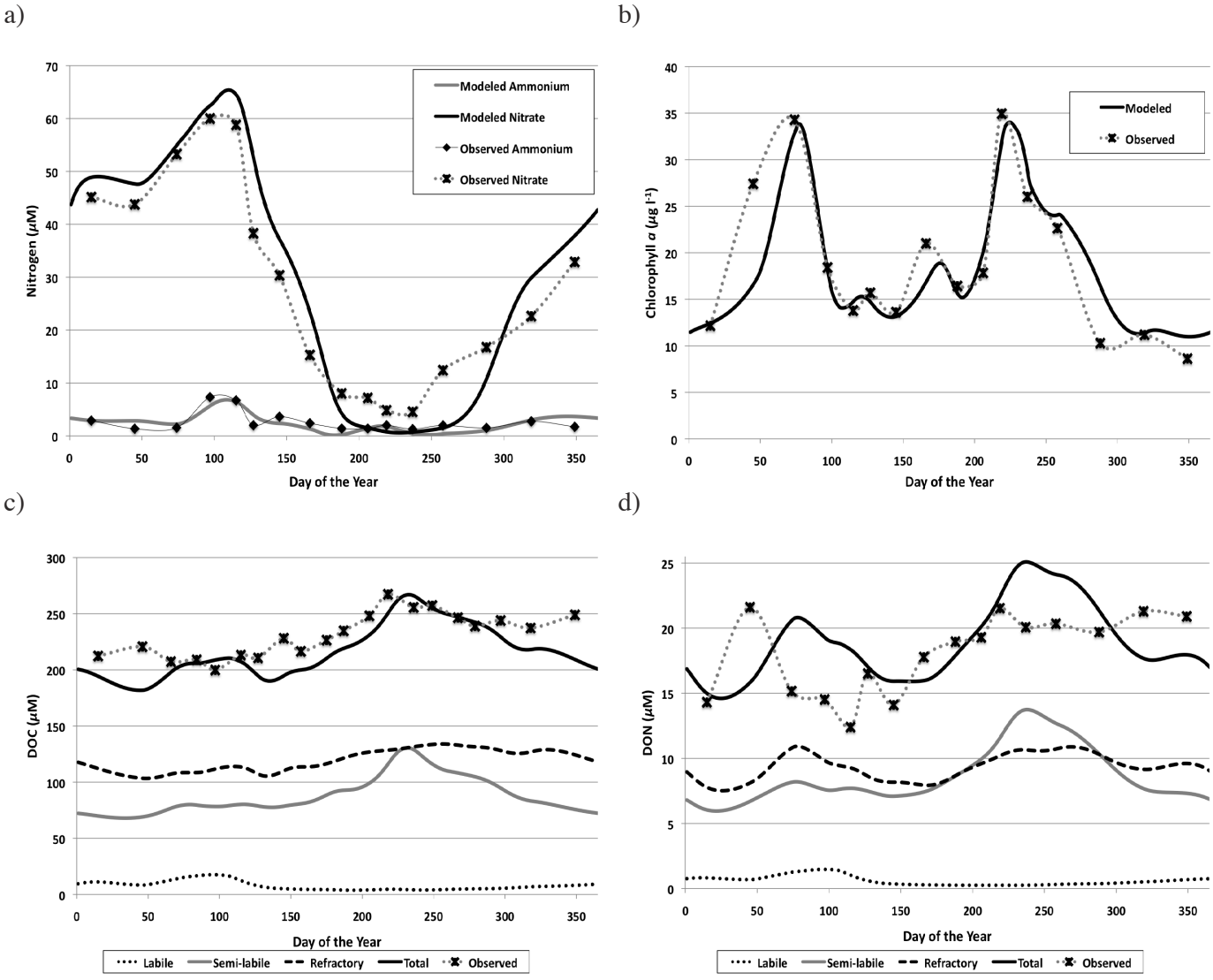

Figure 2.4. Comparisons between: (a) the modeled and mean observed vertical light attenuation coefficient (K_d)(m^{-1}); (b) modeled photosynthetically available radiation (PAR) and the amount of PAR just below the water surface (95 % of PAR at the surface, 5 % reflectance loss).

a)

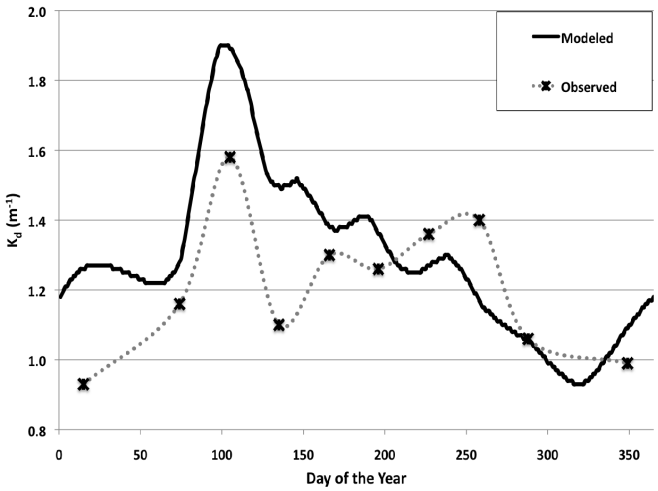

b)

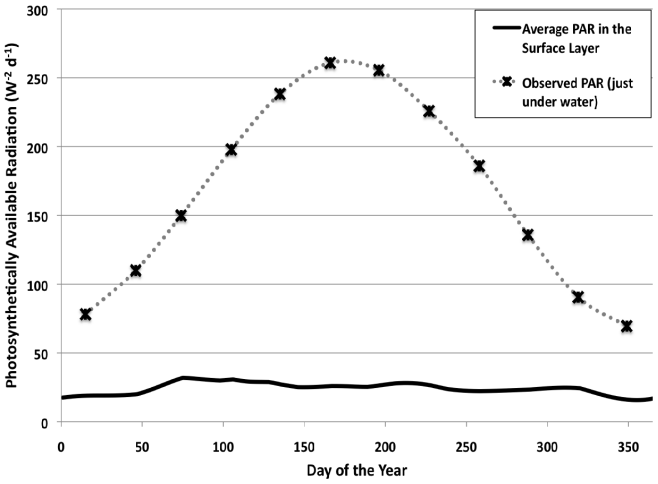

Figure 2.5. Model output: (a) plankton biomass; (b) phytoplankton [P] and bacterial [B] virus biomass, production, and decay; (c) large and small phytoplankton chlorophyll *a* concentration; (d) detritus mass and C:N ratio.

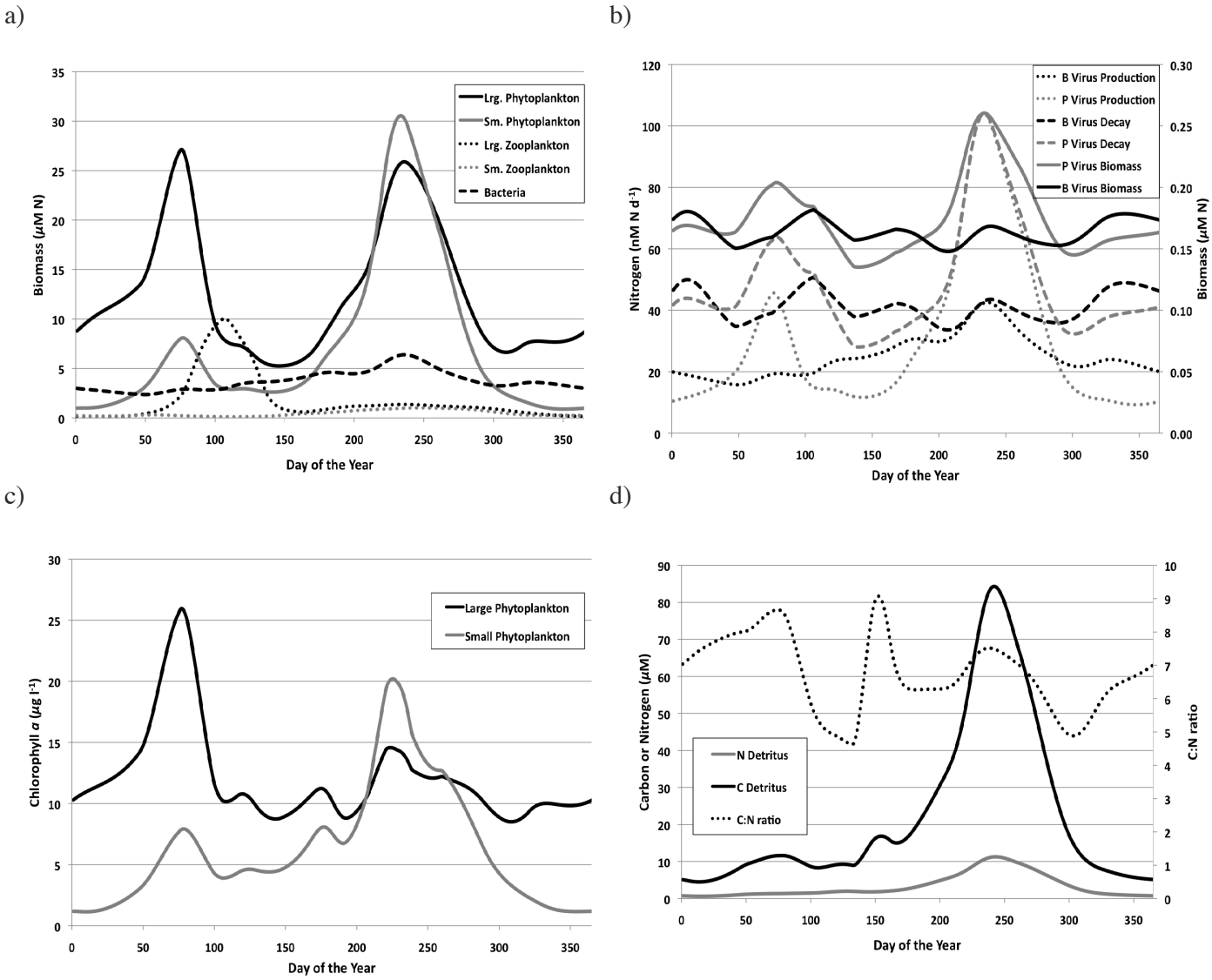

Figure 2.6. Model output: (a) primary production and (b) ammonium and nitrate uptake.

a)

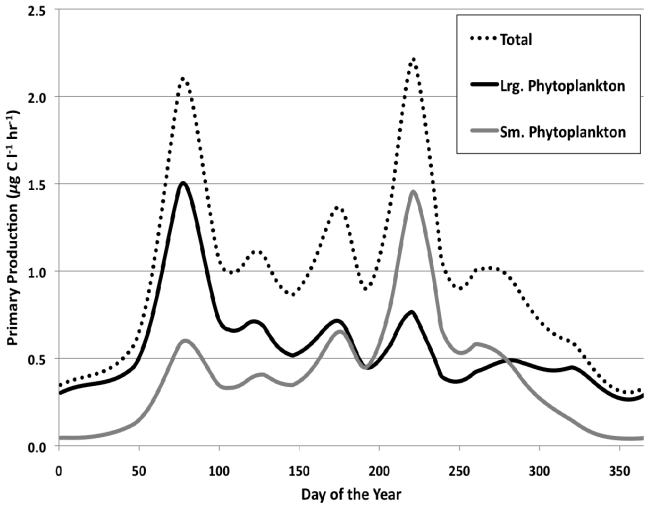

b)

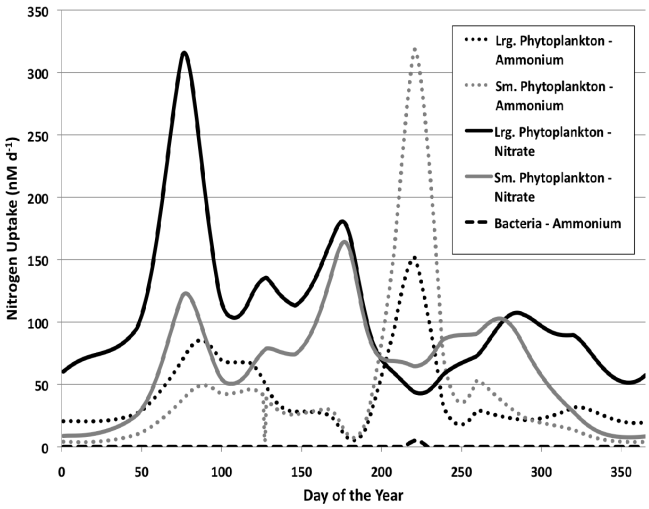

Figure 2.7. Model output: (a) contributions of P_L, P_S, Z_L, Z_S, D, and B to Z_L grazing; (b) contributions of P_L, P_S, Z_S, D, and B to Z_S grazing; (c) daily percentage of primary production lost to grazing.

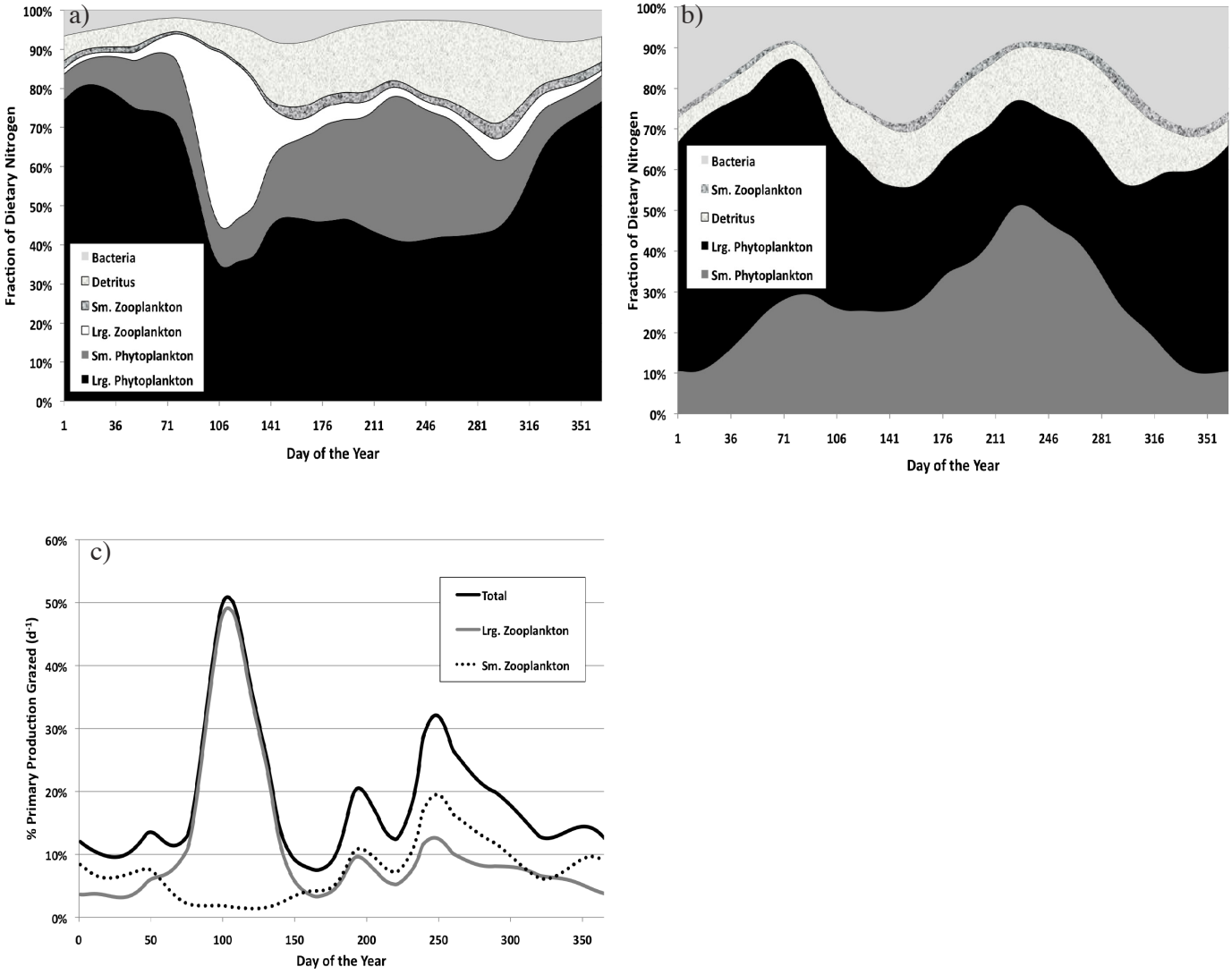

Figure 2.8. Modeled DOM production for (a) DOC and (b) DON.

a)

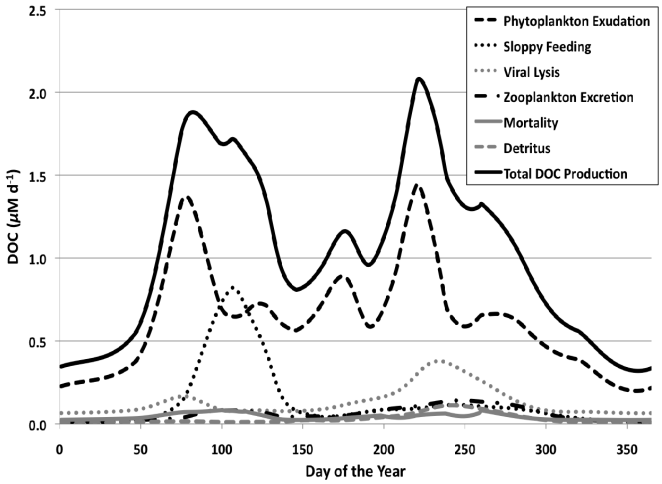

b)

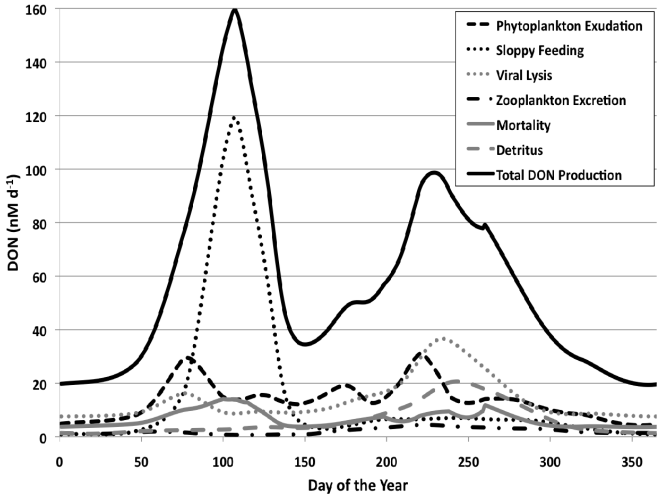

Figure 2.9. Modeled individual sources of DOM: (a) phytoplankton exudation; (b) sloppy feeding; (c) viral lysis.

a)

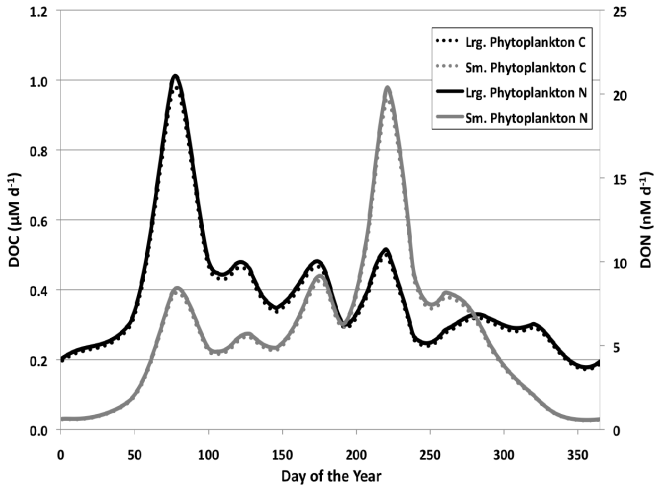

b)

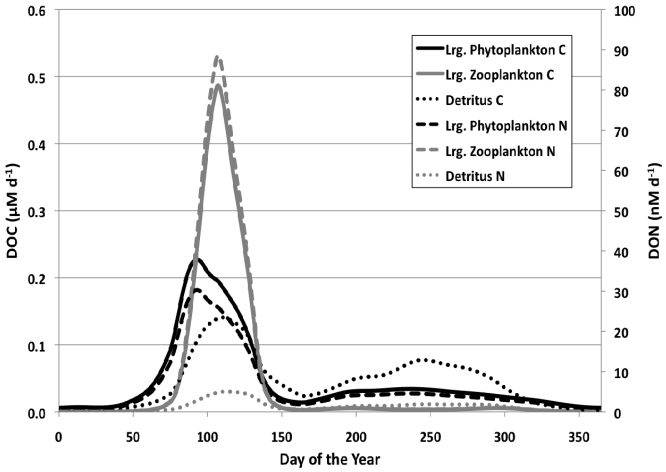

c)

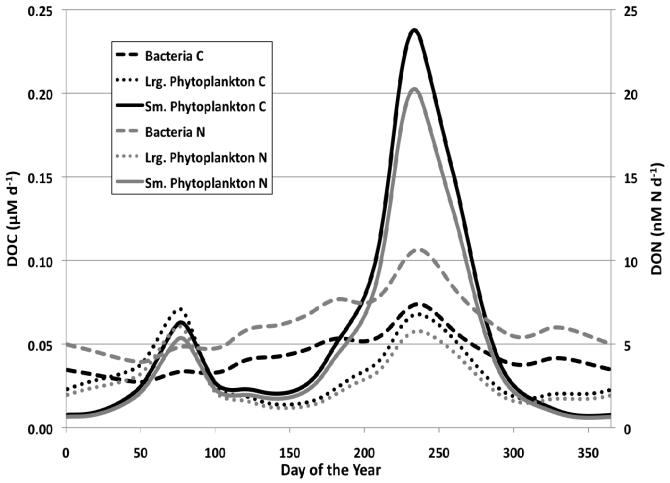

Figure 2.10. Model output: (a) rate of semi-labile DOM hydrolysis; (b) rate of photochemical DOM transformation; (c) DON uptake rate; (d) DOM C:N ratio.

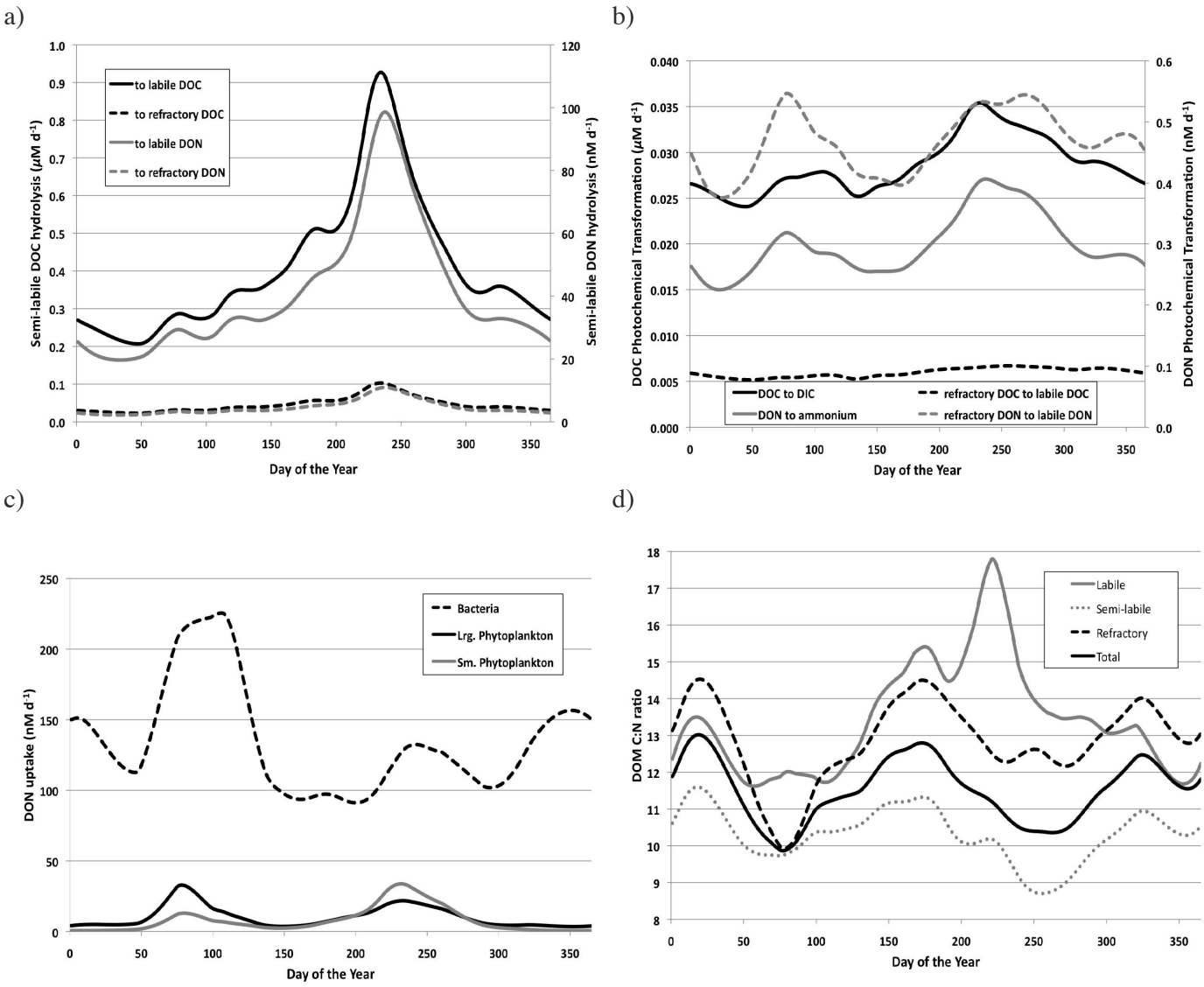

Figure 2.11. Results of a sensitivity analysis for parameter variations of ± 50 %. Day 90: (a) primary production; (c) bacterial production. Day 225: (b) primary production; (c) bacterial production. Parameter increases are in black (■) and parameter decreases are in white (□).

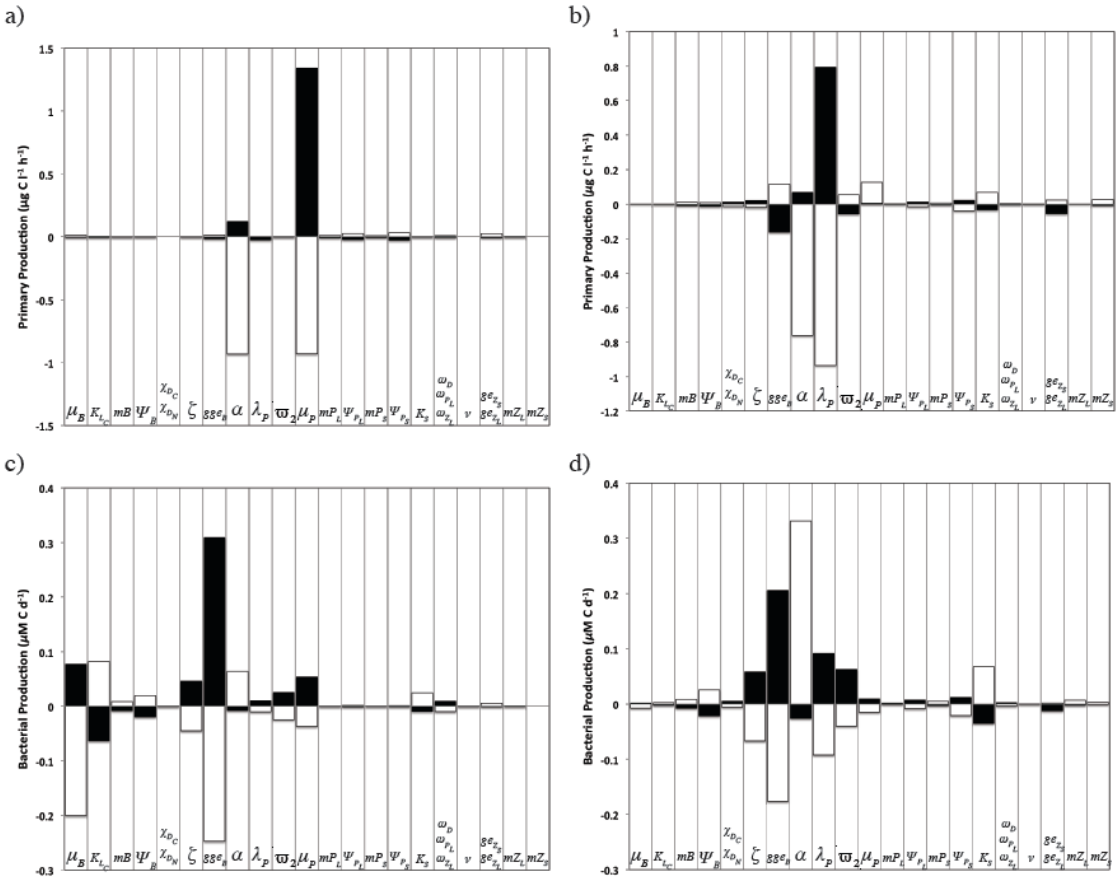

Figure 2.12. Results of a sensitivity analysis for parameter variations of ± 50 %. Day 90: (a) DOC; (c) DON. Day 225: (b) DOC; (d) DON. Parameter increases are in black (■) and parameter decreases are in white (□).

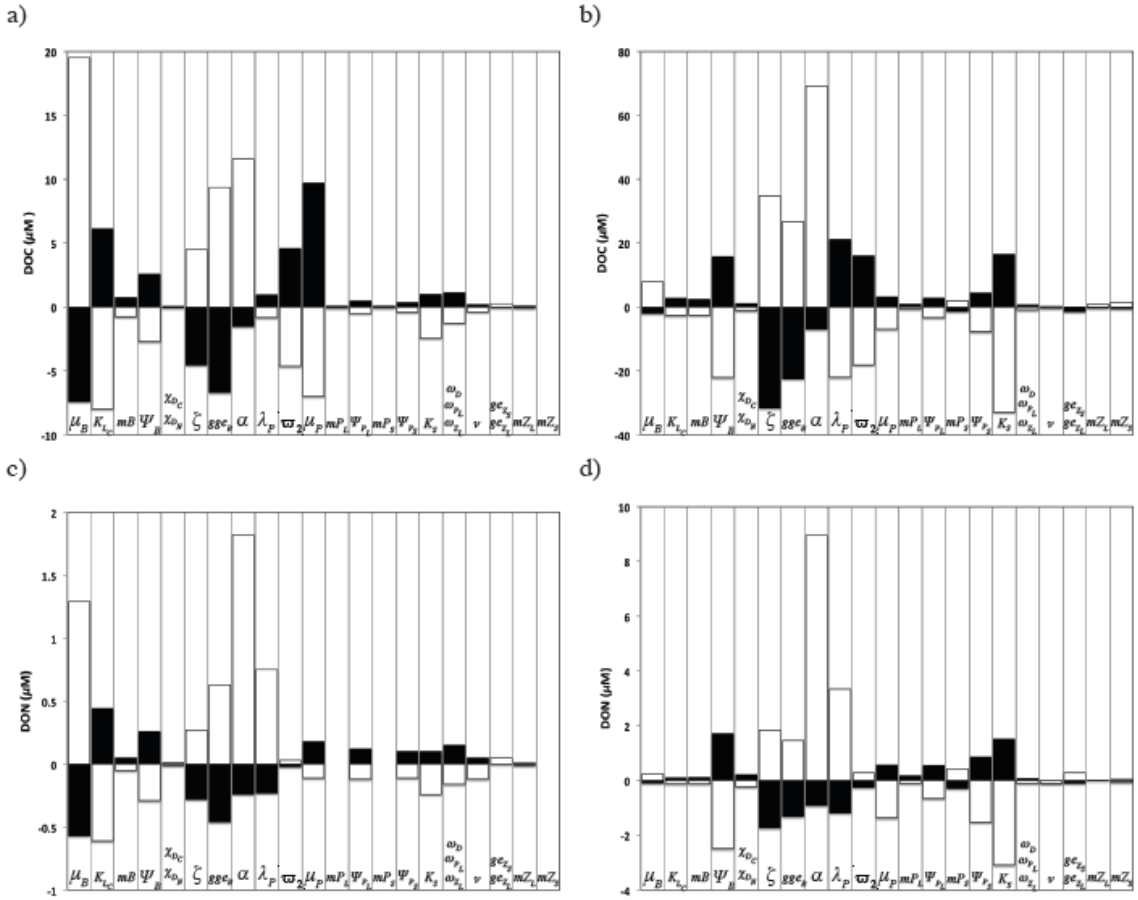

Chapter 3: Modeling the Food Web Dynamics and Biogeochemical Impact of Viruses and a Microzooplankton Grazer on Batch Cultures of the Prymnesiophyte *Phaeocystis globosa*

Abstract

Both viruses and microzooplankton grazers are known to play top-down (mortality) and bottom-up (nutrient regeneration) roles in marine food webs and to have the potential to significantly impact biogeochemical cycling. However, the importance of either of these roles and the processes involved, relative to other food web interactions and biogeochemical pathways, has been difficult to quantify. In this paper we use a numerical model that constrains both carbon and nitrogen cycling to examine the effects of viruses and a common microzooplankton grazer on the trophic dynamics and biogeochemistry of non-axenic batch cultures of the prymnesiophyte *Phaeocystis globosa*. Our results indicate that while both viruses and microzooplankton can exert substantial top-down control on *P. globosa*, the process of viral lysis tends to have a more rapid impact (i.e. higher initial mortality) upon the population even though microzooplankton grazing may ultimately cause more mortality. The bottom-up effects of viral lysis and microzooplankton grazing were also different. Viral lysis transferred material to dissolved organic matter pools before, or if, it was remineralized by heterotrophic bacteria while microzooplankton grazing provided a more direct route for the remineralization of organic matter through excretion. Microzooplankton grazing also had a greater potential to act as a direct link to higher trophic levels. These results have important implications for understanding both trophic interactions and biogeochemical cycling.

Introduction

Viruses and microzooplankton grazers can both have a top-down affect on marine planktonic communities by lysing or consuming various components of the food web (Sherr and Sherr, 2007; Wilhelm and Suttle, 1999). In addition, they can also have a bottom-up affect on the planktonic community when lysis or grazing processes release growth-limiting nutrients that stimulate primary production (Brussaard et al., 2008; Ferrier-Pages and Rassoulzadegan, 1994). Viral lysis and microzooplankton grazing also release dissolved organic matter (DOM) and can play an important role in DOM cycling (Nagata and Kirchman, 1991; Suttle, 2007). The interactions between these top-down and bottom-up processes are complex and depend on the composition of the food web, the relative availability of growth limiting substrates like nitrogen, and other environmental factors such as ambient light and temperature (Glibert, 1998). Unfortunately, simultaneously measuring these top-down and bottom-up controls of the planktonic food web and biogeochemical cycling is difficult, and sometimes impossible due to methodological constraints, and there is still little information on how the relationship between these processes affects nitrogen and carbon cycling in the marine environment.

Models may be one of the best methods for exploring the relationship between the top-down and bottom-up roles of viruses and microzooplankton. However, models of marine ecosystems and biogeochemical processes rarely include viruses as a state variable and often do not specifically or adequately describe the microzooplankton community. In order to better understand the roles of viruses and microzooplankton we have taken a biogeochemical ecosystem model (see Chapters 1 and 2) and configured it

to run as a batch culture experiment to examine the effects of viruses and microzooplankton on a phytoplankton based food web and DOM cycling.

The prymnesiophyte *Phaeocystis globosa* was chosen to represent the phytoplankton state variable in this modeling experiment because a number of studies have documented its growth (Peperzak et al., 2000) and interaction with nutrients and DOM in culture (Aluwihare and Repeta, 1999; Biddanda and Benner, 1997; Biersmith and Benner, 1998; Solomon et al., 2003). The infection of *P. globosa* by viruses has also been well documented (Baudoux and Brussaard, 2005; Brussaard et al., 2007), providing us with information to model the poorly constrained process of viral lysis. Furthermore, cultured *P. globosa* has been used to grow the fairly common heterotrophic dinoflagellate *Gyrodinium dominans* in culture (Tang et al., 2001; Tang and Simó, 2003), which provides us with some information on the interactions between *P. globosa* and a microzooplankton grazer. *P. globosa* was also selected because it, and other *Phaeocystis* species, play an important role in global biogeochemical cycling, climate regulation, food web dynamics, and fisheries yields (Schoemann et al., 2005; Verity et al., 2007).

Phaeocystis is a marine phytoplankton genus that is globally distributed and often dominates phytoplankton communities in temperate and polar regions (Lancelot et al., 1998). Members of this genus have a complex polymorphic life cycle and may be found as free-living cells and as colonies that consist of a gelatinous polysaccharidic matrix with thousands of cells embedded in it (Hamm, 2000). In the colonial phase of their life cycle some *Phaeocystis* species can form massive blooms which may constitute up to 90% of the total phytoplankton abundance and be responsible for up to 65% of the local annual primary production (Arrigo et al., 1999; Joiris et al., 1982; Lancelot and Mathot,

1987; Schoemann et al., 2005; Veldhuis et al., 1986). In addition to being a important primary producer, *Phaeocystis* plays a key role in biogeochemical cycling by producing large amounts of DOM and by sinking (often at the termination of a bloom) which can vertically transports large amounts of organic matter to deeper waters (Verity et al., 2007). *Phaeocystis* also has the ability to produce dimethylsulfoniopropionate (DMSP), a volatile sulfur compound that plays an important role in the atmospheric sulfur cycle and may deter grazing and microbial growth (Stefels et al., 2007; Verity et al., 2007). Combined, these physiological attributes have a significant impact on the food web structure and related biogeochemical cycles.

A number of models (see review in Verity et al. 2007) have been used to facilitate our understanding of the ecology, life cycle, and biogeochemical role of *Phaeocystis*. While some of them have focused, with varying levels of complexity, on trophic interactions and biogeochemical cycling, the role that microzooplankton and viruses play in *Phaeocystis* dominated communities and DOM cycling is not as well known. Although, there have been models such as the one by Ruardij et al. (2005) that do specifically include viruses and microzooplankton, they have generally not included a detailed description of the DOM cycle due a lack of data and the complex interactions between *Phaeocystis*, the food web, and different pools of DOM. In this study we have attempted to overcome some of these constraints by: 1) keeping the simulation as simple as possible and running the model as a batch culture; 2) simulating *P. globosa* growth alone (i.e. an experimental control); 3) simulating the impact of just viruses on *P. globosa*; 4) simulating the impact of just a microzooplankton grazer on *P. globosa*; and 5) simulating the combined impact of viruses and a microzooplankton grazer on *P.*

globosa. The model has been validated using published studies of cultured *P. globosa* biogeochemical cycling, as well as studies of interactions between *P. globosa* or similar phytoplankton species and viruses and microzooplankton.

Model Description

We used four models to investigate the impact of *P. globosa* viruses and a heterotrophic dinoflagellate grazer, *G. dominans*, on *P. globosa* cultures. These models describe the main chemical and biological processes in zero-dimensional batch cultures where the water is homogeneous and there is neither horizontal transport nor sedimentation. Nitrogen is the basic unit for simulation and mass balance. However, carbon has been accounted for by allowing the state variables to have fixed or varying C:N ratios. Close attention has been paid to the formulation of the interactions between these two elements. Thus, both the carbon and nitrogen cycles have been constrained. We have also chosen to only simulate the solitary form of *P. globsa* so that our results will be applicable to other non-colonial phytoplankton species. The first and most basic model configuration simulates a non-axenic batch culture of *P. globosa* (in exponential growth phase at time zero) without viruses or grazers. In the second model configuration a state variable representing *P. globosa* viruses is added to the *P. globosa* culture model. In the third model configuration a state variable representing *G. dominans* is added. In the final model configuration state variables representing both *P. globosa* viruses and *G. dominans* are added. Figure 3.1 shows the flow of nitrogen and carbon between state variables for all model configurations. Model variables, initial concentrations, and parameters are listed in tables 3.1 and 3.2. The batch cultures simulations were run for 60 days in order to provide an appropriate time scale to observe the slow rates at which

some of the DOM cycling occurs. The model was solved numerically with a fourth order Runge-Kutta method (Press et al., 1992) and run using an Intel™ Fortran compiler.

Basic culture model

The basic model has state variables representing *P. globosa*, heterotrophic bacteria, ammonium, nitrate, detritus, DIC, and labile, semi-labile, and refractory DOC and DON. This simulation was designed to provide a reference point (control) for understanding how phytoplankton host-virus and grazer interactions affect C and N cycling. Since the model structure follows the ecosystem model described in Chapters 1 and 2, we mainly focus on our modifications of this model in the following description. The first modification eliminates the two size classes of phytoplankton and replaces them with one phytoplankton compartment representing *P. globosa*. Only the solitary form of *P. globosa* is represented in the model as *P. globosa* does not tend to form colonies until the irradiance is at the saturating level (Peperzak, 1993), which is above the model irradiance of 89.68 W m^{-2}. Having *P. globosa* in the solitary form also avoids the complication of modeling the effect of a colonial structure on growth, grazing, DOM exudation, and viral infection. The maximum growth rate of *P. globosa* was set at 1.0 d^{-1} (Flynn et al., 2008) and the mortality rate was set at 0.07 d^{-1} (Peperzak et al., 2000). The C:N ratio of *P. globosa* cells was set at 5.0 mol mol^{-1} (Solomon et al., 2003). The half saturations constants for the uptake of ammonium (K_A) and nitrate (K_{Nn}) by *P. globosa* were set at 0.5 and 1.0 μmol N (Verity, 2000). The C:N ratio of polymers exuded by *P. globosa* in axenic cultures is approximately 8.0 mol mol^{-1} (Solomon et al., 2003). Therefore, the exudation of DOM by *P. globosa*, which is determined by α, was set so that DOC exudation is eight times that of DON. In the model described in Chapters 1

and 2 the state variables representing phytoplankton are capable of taking up small amounts of DON to supplement growth. However, there is no evidence that *P. globosa* has this capability so in this model they do not utilize DON. Aside from these modifications, the equations describing the flows of carbon and nitrogen between bacteria, ammonium, nitrate, detritus, DIC, and labile, semi-labile, and refractory DOC and DON are as described in Chapters 1 and 2 (see also Appendix B).

Virus addition model

In this model configuration a state variable representing *P. globosa* viruses is added to the basic culture model. This simulation is designed to examine how adding viruses to an exponentially growing culture of *P. globosa* affects C and N cycling. The initial biomass of viruses (table 3.1) was set so that there would be approximately 10 viruses per host at time zero. The rate of viral infection was set at 0.64125 μM^{-1} N d^{-1} during model calibration to achieve a realistic rate of viral induced *P. globosa* mortality. The equations describing viral infection, host lysis, viral decay, and the production of viruses are as described in Chapters 1 and 2 (see also Appendix B).

Grazer addition model

In this model configuration a state variable representing *G. domians* is added to the basic culture model. This simulation is designed to examine how adding a protozoan grazer to an exponentially growing culture of *P. globosa* affects C and N cycling. The growth rate and growth coefficient (% ingested prey converted to biomass) were set at 0.7 d^{-1} and 78%, based on measurements of *G. dominans* growing on *P. globosa* in non-axenic cultures (Tang et al., 2001). Grazing preferences (following the grazing equations

described in Keller and Hood (2010)) for *G. dominans* were set at 0.50 for grazing on *P. globosa*, 0.30 for grazing on detritus, and 0.20 for grazing on bacteria because observation of *G. dominans* grazing have shown that in addition to grazing on phytoplankton, *G. dominans* also graze heavily on bacterial flocs and amorphous phytoplankton aggregates populated by bacteria (Nakamura et al., 1995).

Virus and grazer addition model

In this model configuration state variables representing both *P. globosa* viruses and *G. domians* are added to the basic culture model. This simulation is designed to explore how adding both viruses and a microzooplankton grazer to a culture of *P. globosa* affect C and N cycling. The parameterization of these variables is as described above.

Results and discussion

Phaeocystis globosa biomass

The simulated population dynamics of *P. globosa* were strongly affected by the addition of viruses and grazers. In the control simulation *P. globosa* grew exponentially until day 12, reaching a peak biomass of 300 μM C (~ 3.87 X 10^8 cells l^{-1}), and then entered a stationary-senescent phase when nitrate was depleted, where the population slowly declined (Fig 3.2 a). These results are similar to measurements made by Biddanda and Benner (1997) of *P. globosa* growing in batch culture for 14 days. In contrast, *P. globosa* biomass increased for only three days after the addition of viruses, reaching a peak biomass of 116 μM C (~ 1.50 X 10^8 cells l^{-1})(Fig 3.2 b). The *P. globosa* population then declined and stabilized at level (28 μM C; 3.61 X 10^7 cells l^{-1}) below their biomass

at the time of viral introduction. Actual culture experiments have shown similar effects with *P. globosa* populations beginning to decline within 10 to 30 hours of viral introduction (Baudoux and Brussaard, 2005). Live/dead assays have also indicated that viral lysis rates in *Phaeocystis pouchetii* cultures can be as high as 0.8 d^{-1} (Brussaard et al., 2001) so it is not surprising that such a rapid decline in biomass can occur. Studies of other phytoplankton and cyanobacteria in culture have also shown similar rapid declines in the population size when infective viruses are introduced. Bratbak et al. (1998a, 1998b) found that exponentially growing cultures of *Phaeocystis pouchetii* were decimated within three days of viral introduction. Lennon and Martiny (2008) also found that *Synechococccus* (autotrophic cyanobacteria) in a chemostat culture began to decline almost immediately when *Synechococccus* viruses were introduced. In the simulation with *G. dominans* the biomass of *P. globosa* increased until day 16 when nitrate became depleted, reaching a peak biomass of 192 μM C (~2.48 X 10^8 cells l^{-1})(Fig 3.2 c). Then the population rapidly declined as it was consumed by *G. dominans,* with the *P. globosa* community going extinct by day 35. Culture studies have demonstrated that *G. dominans* grows well on a diet of *P. globosa* and can exert strong top down control on the community (Tang and Simó, 2003). When both viruses and *G. dominans* were added to the simulated culture, *P. globosa* biomass increased for only 2 days, reaching a peak biomass of 104 μM C (~ 1.34 X 10^8 cells l^{-1})(Fig. 3.2 d). The *P. globosa* community then declined and was extinct by day 23. The initial decrease in *P. globosa* was due to viral lysis with *G. dominans* exerting extra top-down pressure on the community and preventing it from reaching a stable biomass as in the virus only addition.

Bacterial, viral, and microzooplankton biomass

Heterotrophic bacterial biomass gradually increased in the control and virus addition simulations and remained low in the simulations with grazers (Fig. 3.2). At the end of the simulations (day 60) the biomass of heterotrophic bacteria was highest in the virus addition simulation (27 μM C). This same enhancement in bacterial production and biomass as a result of phytoplankton lysis releasing DOM has been observed in culture experiments with *P. pouchetii* (Bratbak et al., 1998a) and mesocosm experiments with *P. globosa* (Brussaard et al., 2005b). In the virus addition simulation the mass of *P. globosa* viruses peaked at 9 μM C, 2.5 days after the peak in *P. globosa* biomass, and then declined to leveled off around 3 μM C for the rest of the simulation (Fig. 3.2 b). In the grazer addition simulation the biomass of *G. dominans* rapidly increased, peaking at 306 μM C (~1.17 X 10^7cells l^{-1}) on day 34 (Fig. 3.2 c). Then the *G. dominans* population slowly decreased reaching a final biomass of 260 μM C (~ 9.92 X 10^6 cells l^{-1}) on day 60. In the simulation where both grazers and viruses were added (Fig. 3.2 d), the biomass of viruses peaked at 7.5 μM C on day five, three days after the peak in *P. globosa* biomass. Viral biomass then decreased and was at 0.2 μM C by day 60. The biomass of *G. dominans* slowly increased in this simulation to peak at 131 μM C (~5.0 X 10^6 cells l^{-1}) on day 19. Then, the *G. dominans* community slowly declined, reaching a final biomass of 101 μM C (~ 3.85 X 10^6 cells l^{-1}).

Dissolved inorganic nitrogen cycling

The simulated concentrations of ammonium and nitrate were strongly affected by the introduction of *P. golbosa* viruses and the dinoflagellate grazer, *G. dominans*. In the control simulation the concentration of nitrate decreased rapidly, from 50 μM N to less

than 0.01 μM N at day 13 (Fig. 3.2 e), as it was utilized by the *P. globosa* community. Biddanda and Benner (1997) observed a similarly rapid drawdown of nitrate in batch cultures of *P. globosa* which had been started at 100 μM of nitrate. The concentration of ammonium remained below 0.03 μM N for the duration of our control simulation even though bacteria began to excrete a significant amount of ammonium after day 20 (Fig. 3.3). In the grazer addition simulation the concentration of nitrate decreased from 50 μM N to less than 0.01 μM N by day 18. However, unlike in the control simulation, the concentration of ammonium increased around day 30, reaching and staying at a concentration of approximately 10 μM N. This increase was a result of a high rate of ammonium excretion by microzooplankton during their peak growth (Fig. 3.3). In the two simulations where viruses were added nitrate was never depleted (Fig. 3.2 f, h). The concentration of ammonium also increased in these simulations (Fig. 3.2 f, h) and was 2.35 and 4.45 μM N at day 60 in the plus viruses and plus viruses and grazers simulations. In the plus virus simulation the increase in ammonium was due bacterial excretion of regenerated DOM and occurred at higher rates toward the end of the simulation (Fig. 3.3). In the plus virus and grazer addition the increase in ammonium was mostly due to the excretion of ammonium by microzooplankton in the first 25 days of the simulation (Fig. 3.3). These results indicate that while both viruses and grazers can influence the food web in a bottom-up manner, grazing in particular has a stronger bottom-up effect. This likely occurs because grazing directly remineralizes the organic matter (i.e. phytoplankton biomass) as ammonium while viral lysis first releases the organic matter into the DOM pool where it must be remineralized by bacteria. Thus, grazing potentially provides a shorter pathway for recycling nitrogen.

Detritus

Particulate organic detritus (POD) increased in the control and virus addition simulations and initially increased but then decreased in the two simulations where grazers were added (Fig. 3.2 e-h). In the control simulation the concentration of POD gradually increased, due to *P. globosa* mortality, while the C:N ratio decreased. In the virus addition simulation the concentration of POD increased rapidly for the first 10 days, due to a high rate of viral lysis, and then gradually increased after that while the C:N ratio first decreased and then began to slightly increase again (Fig. 3.2 f). In the grazer addition simulation the concentration of POD initially increased as a result of *P. globosa* mortality and egestion by *G. dominans*. However, when the *P. globosa* population began to decline and *G. dominans* started to consume more bacterial flocs and detritus (preferred prey items (Nakamura et al., 1995)) the concentration of POD decreased and remained very low (Fig. 3.2 g). In the virus and grazer addition simulation the concentration of POD rapidly increased for the first few days as the *P. globosa* population was virally lysed at high rate. Then POD decreased and remained at a low concentration because of grazing by *G. dominans* (Fig. 3.2 h). In both of the simulations with grazers the C:N ratio of POD decreased throughout the simulation.

Dissolved organic matter cycling

The concentration of DOM was strongly affected by the introduction of viruses and/or the addition of a dinoflagellate grazer. In the control simulation both DOC and DON concentrations increased moderately during the simulation (Fig. 3.2 i, m). The most rapid increase in DOM occurred during the exponential growth of *P. globosa* (days 0-12), with DOC increasing by 87 μM and DON increasing by 4.5 μM. After day 12,

DOC and DON continued to increase until days 19 (160 μM DOC) and 25 (12 μM DON), when they began to decline. At day 30 the concentration of DON began to increase again. Changes in the concentration of DOM were mostly a result of changes in the labile and semi-labile pools, as refractory DOC and DON increased only slightly during the simulation. The labile pools of DOC and DON both increased during the first 16 to 22 days and then began to decrease as they were consumed by the increasing bacteria population. By day 30 the concentration of labile DOM was very low and remained so for the rest of the simulation. The semi-labile DON pool gradually increased throughout the simulation while the semi-labile DOC pool increased rapidly for the first 10 days, then gradually increased until day 31 when it began to decrease as the bacteria community gradually degraded it. In the virus addition simulation (Fig. 3.2 j, n), the concentration of DOM, especially DON, increased substantially when compared to the control. In 24 days DOC and DON increased by 107 μM C and 26 μM N, mostly as a result of DOM release by viral lysis of *P. globosa* cells (see below). Then, DOC and DON decreased, at first rapidly as labile DOM that had accumulated during the first 20 days was consumed by an increasing bacterial population, and then more gradually after the labile pools of DOC and DON were depleted. As in the control run the concentration of refractory DOM only increased slightly during the simulation. The semi-labile pools of DOM were responsible for much of the change in the total DOC and DON concentrations with semi-labile DOC and DON increasing rapidly in the first few days of the simulation and then only gradually decreasing after peaking around day 35. The DOM concentration in the grazer addition simulation (Fig. 3.2 k, o) increased throughout the 60 days except for a brief period when DOC declined slightly. Unlike in the control and virus addition simulations,

the concentrations of labile and semi-labile DOM were not consumed or degraded as much by bacteria because of the top-down pressure exerted on the bacterial community by *G. dominans*. This also had an effect on the refractory DOM pools, which actually decreased slightly as photochemical reactions removed refractory DOM slightly faster than it was being produced. In the simulation where both viruses and grazers were added the DOM concentration increased rapidly for the first ten days, as in the virus simulation, and then increased gradually after that as in the grazer addition simulation (Fig. 3.2 l p). As in the simulation with addition of grazers, the concentrations of labile and semi-labile DOM were not consumed or degraded as much by bacteria because of *G. dominans* grazing on bacteria. Refractory DOM also decreased slightly as well.

In all four simulation most of the DOM production occurred in first 10-20 days (Fig 3.4). In the control simulation most of the DON initially came from mortality or *P. globosa* exudation. However, as the simulation progressed the decay of detritus became increasingly important when *P. globosa* stopped exuding DON at a high rate as the community became nutrient limited. Most of the DOC that initially accumulated in the control simulation came from *P. globosa* exudation. However, after nitrate had been depleted and the *P. globosa* community stopped growing rapidly very little DOC was exuded for the rest of the simulation. The simulated rate of DOC exudation by *P. globosa* in the exponential growth phase is similar to measurements made by Biddanda and Benner (1997) who found that *P. globosa* exudation of DOC was fairly constant and reached a maximum of 13 μM DOC d^{-1} during the end of the exponential growth phase. The decay of detritus produced only minor amounts of DOC throughout the simulation. Mortality of *P. globosa* and bacteria also produced moderate amounts of DOC. In the

virus addition simulation viral lysis of *P. globosa* and viral decay produced large amounts of DON and DOC in the first ten days. After 20 days, when the rate of DOM production was lower, most of the DON was coming from viral decay and the breakdown of detritus while most of the DOC was being produced by *P. globosa* exudation, viral decay, and the breakdown of detritus. The production of DON in the grazer addition simulation was initially mostly from mortality and *P. globosa* exudation. However, as the simulation progressed excretion by *G. dominans* became more important and the rate of *P. globosa* exudation declined. Toward the end of the simulation when the *G. dominans* community was in decline, mortality became the dominant source of DON. The production of DOC in the grazer addition simulation was initially similar to the control, but as the simulation progressed the excretion of DOC by *G. dominans* became more important until the *G. dominans* community began to decline and mortality became the dominant source of DOC. In the simulation where both grazers and viruses were added viral lysis and decay were initially the dominant sources of DON. Then as the incidence of viral lysis decreased excretion of DON by *G. dominans* became the dominant source for about 10 days. Then very little DON was produced throughout the rest of the simulation except for some DON from mortality. The dominant sources of DOC in this simulation were initially *P. globosa* exudation, viral lysis and decay, and *G. dominans* excretion. However, after day 20 very little DOC was produced except through mortality.

The C:N ratio of dissolved and particulate organic matter changed in these simulations reflecting the influence of different components of the simulated ecosystem (Fig. 3.5). In the control simulation with only *P. globosa* and heterotrophic bacteria present the C:N ratio of DOM increased during the exponential grow phase of *P. globosa*

(days 0-12). Then it decreased throughout the rest of the simulation as bacteria began to consume and transform the DOM. These results are as we had expected because the C:N ratio of DOM released by *P. globosa* was set so that the release of DOC is eight times that of DON, which will result in an increase in the C:N ratio as long as the bacterial population is small enough that it does not take up large amounts of DOM. The C:N ratio of POM dropped slightly at the beginning of the simulation and then remained near 5.2, which is close to the C:N ratio of *P. globosa* and heterotrophic bacteria. A similar trend was also reported by Biddanda and Benner (1997) who found that the C:N ratio of POM in batch cultures of *P. globosa* varied little during growth. In contrast, in the virus addition simulation the C:N ratio of DOM dropped rapidly during the first 10 days as the *P. globosa* population was lysed (releasing DOM with the C:N ratio of *P. globosa*) by the introduced viruses. After the initially rapid decrease the C:N ratio then continued to gradually decrease throughout the simulation. While there is no comparable data available for *P. globosa*, Lennon and Martiny (2008) observed a similar rapid drop in the C:N ratio of DOM after the introduction of viruses to cultures of *Synechococcus*. The C:N ratio of POM increased in this simulation during the first 20 days and then remained near 6.6 for the rest of the simulation. In the dinoflagellate grazer addition simulation the C:N ratio of DOM increased slightly during the exponential growth phase of *P. globosa* and then declined throughout the rest of the simulation. The C:N ratio of POM in this simulation decreased initially but then increased and remained near 5.5 which is the C:N ratio of *G. dominans*. In the simulation with the addition both viruses and grazers the C:N ratio of DOM decreased, as in the virus addition simulation, but stayed slightly higher. However, the POM C:N ratio did not increase as it had in the virus addition

simulation, instead because of grazing it first decreased and then increased and remained around 5.5 as in the grazer addition simulation.

Summary

In agreement with other studies of phytoplankton viral lysis (Bratbak et al., 1998a; Bratbak et al., 1998b; Brussaard et al., 2007; Brussaard et al., 2005a), our simulations indicate that viruses act as a strong top-down control on *P. globosa.* Similarly, we show that microzooplankton grazers such as *G. dominans* also act as a strong top-down control on single cells of *P. globosa,* a trophic role that is fairly well established for microzooplankton (Landry and Calbet, 2004; Sherr and Sherr, 2002; Weisse and Scheffel-Möser, 1990). Our results also show that the bottom-up effects of viral lysis and microzooplankton were initially not as strong as the top-down effects in any of the simulations. However, this was to be expected because the phytoplankton were not initially nutrient limited and would thus not be stimulated by regenerated nutrients. When nutrients did eventually become limiting in some of the simulations, only phytoplankton in the virus addition simulation reached a point where mortality and growth, where the latter was stimulated by regenerated nitrogen, were nearly equal. In simulations with microzooplankton grazers a balance was never reached because top-down mortality was always greater than phytoplankton growth after nitrate became depleted. These results indicate that microzooplankton grazing by heterotrophic dinoflagellates like *G. dominans* may be a more important factor than viral lysis in controlling this stage (solitary cells) of the *P. globosa* life cycle.

The biogeochemical effects of viral lysis and microzooplankton grazing were different in our simulations and played an important role in the food web structure and

nutrient cycling. Viral lysis transferred large amounts of carbon, nitrogen, and other elements from a form (phytoplankton biomass) that could be easily be consumed by higher trophic levels (zooplankton, fish, etc.), to dissolved (carbohydrates, amino acids, etc.) and particulate (detritus) forms that were only partially available to other trophic levels (bacteria, some phytoplankton, detritivores). A portion of the phytoplankton biomass was also turned into viral biomass. In contrast, microzooplankton grazing transferred much less of it to these pools, respired some of it, and remineralized a significant portion of the nitrogen as ammonium. Microzooplankton grazing also retained a significant fraction of the organic matter in a form (microzooplankton biomass) that would be accessible to higher trophic levels. These differences affected the food web structure because viral lysis of phytoplankton stimulated bacterial growth, a result seen in our simulations and a number of experiments (Bratbak et al., 1998a; Brussaard et al., 2005b; Gobler et al., 1997). While microzooplankton grazing suppressed bacterial growth and retained a significant portion of the organic matter in the system at a higher trophic level as microzooplankton biomass. Nutrient cycling was primarily affected by the different ways in which nitrogen was regenerated. Viral lysis released the nitrogen from infected phytoplankton as viruses, PON, and DON, forms of nitrogen that are unavailable to most phytoplankton. Thus, the remineralization of nitrogen was dependant on the rate at which bacteria, who would have to be limited by something other than nitrogen in order to excrete it, consumed the organic matter. The decay rate of viruses was also a factor in the supply of potentially bioavailable nitrogen to the DON pool. In contrast, microzooplankton grazing directly regenerated some of the nitrogen as ammonium while also releasing minor amounts of DON. Microzooplankton also

suppressed the regeneration of nitrogen by bacteria by grazing on them. These results show how these two processes, which both have top-down and bottom-up effects on marine food webs, differ and can result in very different trophic interactions and elemental cycles.

Our results also indicate that the top-down and bottom-up effects of viral lysis and microzooplankton grazing on a phytoplankton community occur at different temporal scales. Lytic viruses multiply rapidly, especially when the host population is growing exponentially, and thus can quickly infect and cause high rates of mortality in a susceptible host population, a result seen in our simulations and a number of experiments (Baudoux and Brussaard, 2005; Bratbak et al., 1998a; Bratbak et al., 1998b; Brussaard et al., 2005a; Lennon and Martiny, 2008). Grazing by microzooplankton did not cause as high a rate of mortality as viruses (at our initial biomass concentrations) because the rate of grazing became limited by feeding clearance rates, growth rates, growth efficiencies, the nutritional value of the prey, and their mortality rate. Thus, from a top-down perspective viral lysis may have a more rapid effect than microzooplankton grazing if these processes are not restricted in any way. In contrast, the bottom-up effects of these processes will occur in reverse. Microzooplankton grazing can result in the release of ammonium shortly after digestion, while the bottom-up effect of viral lysis is dependant on the rate at which bacteria can recycle the POM and DOM released by lysis. Thus, microzooplankton grazing may have a more rapid bottom-up effect on a phytoplankton community than viral lysis.

When both viral lysis and microzooplankton grazing occur a significant amount of phytoplankton biomass is transferred to the DOM and detritus pools. Phytoplankton

biomass is also remineralized as DIN and respired as CO_2, either directly by microzooplankton or indirectly by bacteria growing on the released DOM. Some of the phytoplankton biomass ends up being incorporated into viral and microzooplankton biomass as well. The amount of carbon and nitrogen that flow through any of these pathways depends on many factors. Our simulation with both viruses and a microzooplankton grazer represent just one of the many possible interactions that could occur between phytoplankton, viruses, and grazers and we do not mean to imply that this is what occurs every time these organisms are part of the same aquatic ecosystem. Instead these results can be used to more quantitatively infer where carbon and nitrogen are going when it is not possible to measure all of the parameters necessary to truly trace their paths.

Future Research Challenges

Despite our progress there are still many unanswered questions concerning the role of viruses and microzooplankton in food webs and biogeochemical cycles. One of the major problems hampering this research is a lack of data. Due to their small size these organisms are extremely difficult to work with and consequently relatively little quantitative information has been published on their roles in biogeochemical cycling. There is also little information on the physiology and ecology of the many organisms that are commonly classified as microzooplankton. This makes it difficult to decide if we are properly modeling these organisms. Without more complete data sets to guide model creation and parameterization, as well for comparison, we cannot simulate these processes with a high quantitative confidence.

Another major problem lies in defining the bioavailability of DOM, as there is no standard that defines how readily DOM is consumed. In our model DOM bioavailability is based on measurements that have shown that a fraction of DOM from phytoplankton exudation and viral lysis is rapidly degraded (i.e. labile DOM) with the remaining DOM persisting in the environment for weeks, months (semi-labile DOM) or years (refractory DOM) (Aluwihare and Repeta, 1999; Gobler et al., 1997; Gobler and Sañudo-Wilhelmy, 2003; Meon and Kirchman, 2001; Wetz et al., 2008). While this method has allowed us to begin to understand the interactions between organisms and DOM, it is not an adequate description of these complex pools. Ideally, DOM should be characterized according to its chemical composition. Unfortunately, it is difficult to do this for a number of reasons. First, less than 25% of DOM has been identified as a specific biochemical coumpound (Hedges et al., 2000). Second, there is no standard in what constitutes the "dissolved" pool (Flynn et al., 2008). Finally, modeling the thousands of chemical compounds that comprise DOM, their interactions, and separate bioavailabilites would be impractical. Until these issues are resolved and a standard is set there will always be some uncertainty in any simulation of DOM cycling.

Conclusion

Marine food webs, and many models of them, are much more complicated than in our simple batch culture simulations. However, we feel that these simulations have provided insight into the roles that virus and microzooplankton may play in real and simulated ecosystems. Our results indicate that while both viruses and microzooplankton can exert substantial top-down control on *P. globosa*, the process of viral lysis tends to have a more rapid impact (i.e. higher initial mortality) upon the population even though

microzooplankton grazing may ultimately cause more mortality. The bottom-up effects of viral lysis and microzooplankton grazing were also different. Viral lysis transferred material to dissolved organic matter pools before, or if, it was remineralized by heterotrophic bacteria while microzooplankton grazing provided a more direct route for the remineralization of organic matter through excretion. Microzooplankton grazing also had a greater potential to act as a direct link to higher trophic levels because a large proportion of *P. globsa* biomass is converted into microzooplankton biomass which is more accessible to higher trophic levels than the DOM or detritus produced by viral lysis. These results have important implications for understanding both trophic interactions and biogeochemical cycling.

Our simulations are also important because the parameterization and modeling of both viruses and microzooplankton is poorly constrained in general. By parameterizing a model typically used to describe a whole community of microzooplankton and viruses with parameters measured in laboratory culture experiments, it was possible to gain a better understanding of how the model behaves and whether it could simulate these systems with any degree of accuracy. Our comparisons with published studies suggest that our model a reasonable job of simulating the effects of viruses and microzooplankton on cultures of *P. globosa,* which gives us more confidence in ability of the full model (See Chapters 1 and 2) to simulate their role in a whole ecosystem context.

Tables

Table 3.1. Model Variables and Initial Concentrations

Symbol	Description	Initial Concentration	Units
P	*P. globosa*	100	mmol C m^{-3}
Z	*G. dominans*	52.4	mmol C m^{-3}
B	bacteria	0.02	mmol C m^{-3}
V	*P. globosa* viruses	0.23	mmol C m^{-3}
A	ammonium	0	mmol N m^{-3}
N_n	nitrate	50	mmol N m^{-3}
DIC	dissolved inorganic carbon	2100	mmol C m^{-3}
D_c	C detritus	10	mmol C m^{-3}
D_n	N detritus	0.1	mmol N m^{-3}
Ln	labile DON	0.05	mmol N m^{-3}
Lc	labile DOC	4	mmol C m^{-3}
Sn	semi-labile DON	1.74	mmol N m^{-3}
Sc	semi-labile DOC	20.4	mmol C m^{-3}
Rn	refractory DON	3.71	mmol N m^{-3}
Rc	refractory DOC	43.25	mmol C m^{-3}

Table 3.2. Model Parameters

Description	Symbol	Value	Units
P. globosa maximum growth rate	μ_P	1.0	d^{-1}
Irradiance	I	89.68	W m^{-2}
P. globosa light saturation parameter	I_P	40	W m^{-2}
P. globosa photoinhibition parameter	I_β	400	W m^{-2}
Partitioning of *P. globosa* production	α	0.95	
P. globosa C:N ratio	λ_P	5.0	mol mol^{-1}
Half-sat. const. for N_n uptake by *P. globosa*	$K_{P_S N_n}$	1.0	μM N
Half-sat. const for *A* uptake by *P. globosa*	$K_{P_S A}$	0.5	μM N
P. globosa mortality rate	S_P	0.07	d^{-1}
G. dominans maximum consumption rate	C_{Z_S}	0.7	d^{-1}
G. dominans assimilation efficiency	β_{N_Z}	0.90	
G. dominans growth coefficient	ge_{Z_S}	0.78	
Half-sat. const. for zooplankton grazing	K_Z	0.75	μM
G. dominans preference for *P. globosa*	φ_{P_S}	0.50	
G. dominans preference for *D*	φ_D	0.30	
G. dominans preference for *B*	φ_B	0.20	
G. dominans C:N ratio	λ_Z	5.5	mol mol^{-1}
G. dominans mortality rate	S_Z	0.08	d^{-1}
Bacterial gross growth efficiency	gge_B	0.27	
Maximum bacterial growth rate	μ_B	13.3	d^{-1}
Half-sat. const. for ammonium uptake by bacteria	K_{BA}	0.50	μM
Half-sat. const. for labile DOC uptake by bacteria	K_{L_C}	25	μM
Bacteria C:N ratio	λ_B	5.1	mol mol^{-1}
Bacteria mortality	S_B	0.08	d^{-1}
Viral infection rate	Ψ_P	0.64125	μM^{-1} N d^{-1}
Viral decay rate	υ	0.08	h^{-1}
Virus C:N ratio	λ_V	3.26	mol mol^{-1}
Production of new viruses from lysis	ε_V	0.50	
Partitioning of mortality to detritus and DOM	β_1	0.66	
Partitioning of “extra C” from lysis to LC	β_2	0.025	
Partitioning of “extra C” from lysis to SC	β_3	0.224	
Partitioning of “extra C” from lysis to RC	β_4	0.001	
Partitioning of “extra C” from lysis to detritus	β_5	0.75	
Partitioning B mort to detritus	ρ_D	0.25	
Partitioning B mort. to labile DOM	ρ_L	0.40	
Partitioning B mort. to semi-labile DOM	ρ_S	0.34	
Partitioning B mort. to refractory DOM	ρ_R	0.01	
Labile fraction of DOM from detritus decay	δ_1	0.50	
Semi-labile fraction of DOM from detritus decay	δ_2	0.49	
Refractory fraction of DOM from detritus decay	δ_3	0.01	
Maximum rate of semi-labile DOM hydrolysis	μ_S	4.0	d^{-1}
Half-sat. const. for DOM hydrolysis	K_S	417	μM C

Partitioning of phytoplankton DOM leakage and plankton mortality to labile DOM	o_L	0.40	
Partitioning of phytoplankton DOM leakage and plankton mortality to semi-labile DOM	o_S	0.59	
Partitioning of phytoplankton DOM leakage and plankton mortality to refractory DOM	o_R	0.01	
Partitioning of lysis product to D	ε_D	0.375	
Partitioning of lysis product to labile DOM	ε_L	0.062	
Partitioning of lysis product to semi-labile DOM	ε_S	0.062	
Partitioning of lysis product to refractory DOM	ε_R	0.001	
Breakdown of N detritus to DOM	χ_{D_N}	0.055	d^{-1}
Breakdown of C detritus to DOM	χ_{D_C}	0.040	d^{-1}
Partitioning of viral decay to DOM	η	0.10	
Partitioning of zooplankton excretion to DON and ammonium	κ_Z	0.68	
Partitioning of zooplankton DOM excretion to labile and semi-labile pools	o_Z	0.70	
Partitioning of zooplankton metabolized carbon to DIC and DOC	σ_Z	0.69	

Figures

Figure 3.1. A schematic diagram of the batch culture model. Symbols as described in the text. Shading indicates the control batch culture (light shading), the virus addition (light shading plus the medium shaded area), and the grazer addition (light shading plus the dark shaded area).

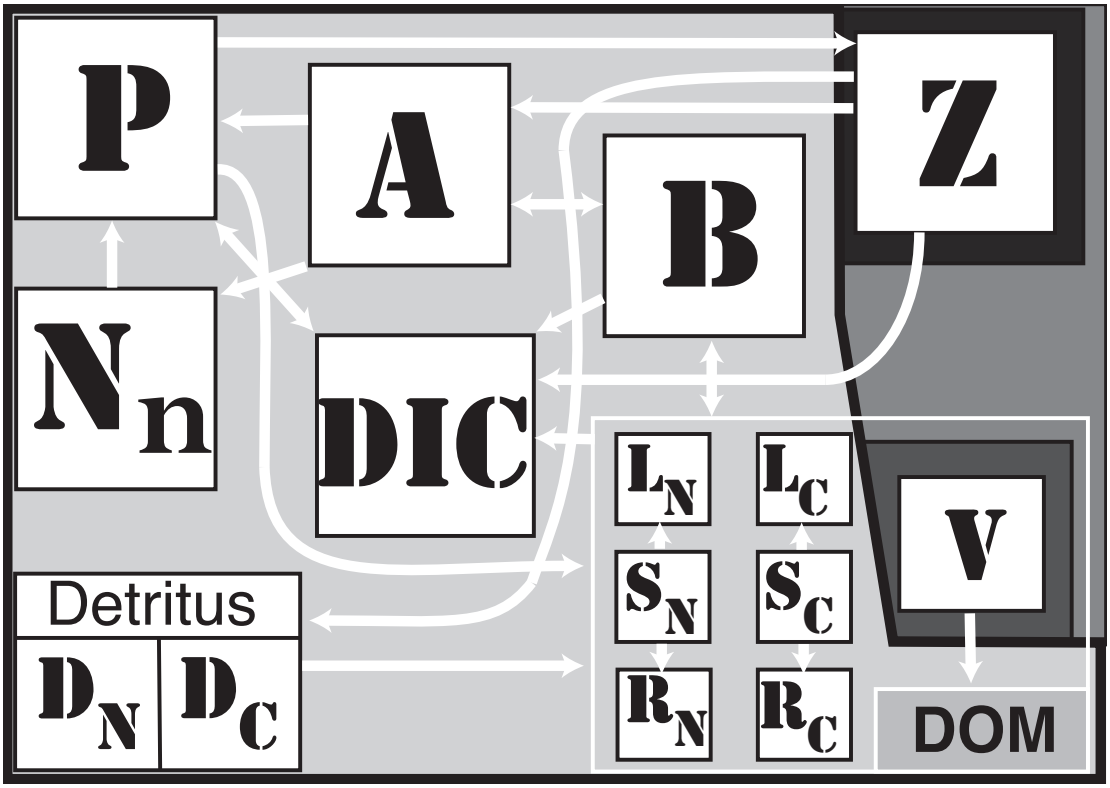

Figure 3.2 (next page). Model output for the control, plus viruses, plus grazers, and plus viruses and grazers simulations. (a-d) the biomass of *P. globosa* (solid line), bacteria (dashed line), viruses (dotted line), and *G. dominans* (dashed/dotted line); (e-h) the concentration of nitrate (solid line), ammonium (dashed/dotted line), C detritus (dotted line), and N detritus (dashed line); (i-l) the concentration of labile (dashed/dotted line), semi-labile (dotted line), and refractory (dashed line) DON, total DON is also indicated (solid line); (m-p) the concentration of labile (dashed/dotted line), semi-labile (dotted line), and refractory (dashed line) DOC, total DOC is also indicated (solid line).

Detritus (μM C)
Control
+ Viruses
+ Grazers
+ Viruses and Grazers
Biomass (μM C)
DIN and Detritus (μM N)
DON (μM N)
DOC (μM C)
a)
b)
c)
d)
e)
f)
g)
h)
i)
j)
k)
l)
m)
n)
o)
p)

Figure 3.3. The simulated rate of ammonium excretion by heterotrophic bacteria and microzooplankton in the control (solid line), plus viruses (dotted line), plus grazers (dashed line), and plus viruses and grazers (dashed/dotted line) simulations.

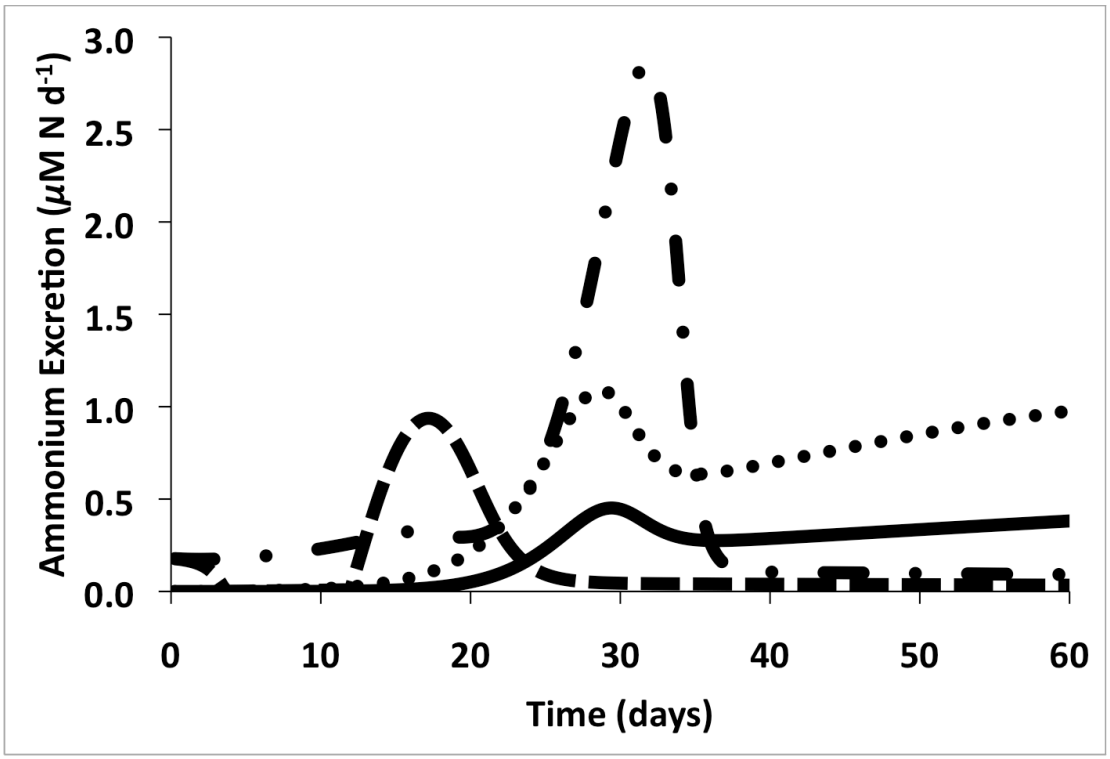

Figure 3.4. The simulated production of DON and DOC from phytoplankton release (solid line), mortality (short dashed line), the decay of detritus (dashed/dotted line), viral lysis (dotted line), viral decay (long dashed line), and *G. dominans* excretion (dashed/double dotted line).

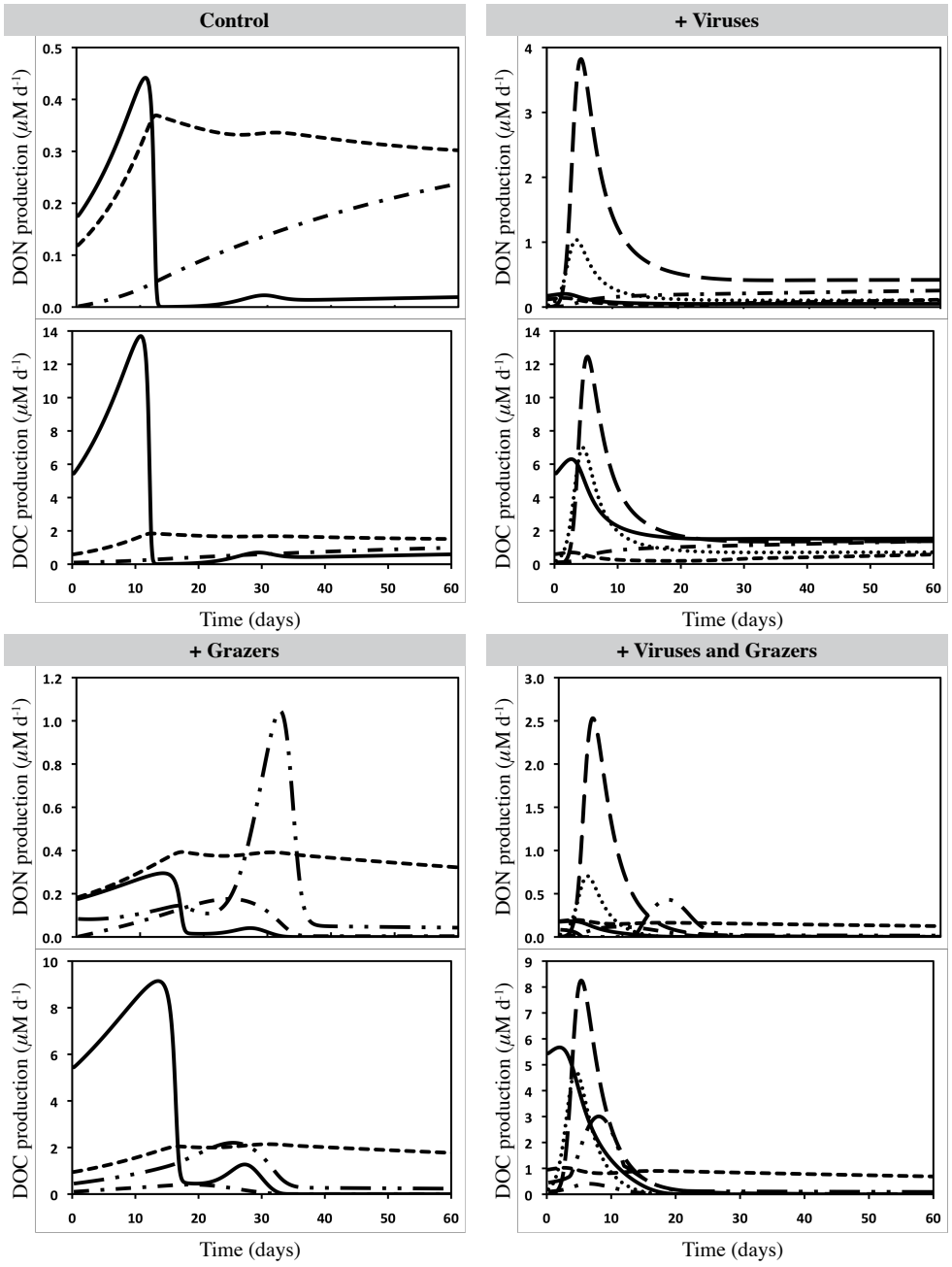

Figure 3.5. The C:N ratios for the control (solid line), plus viruses (dotted line), plus grazers (dashed line), and plus viruses and grazers (dashed/dotted line) simulations: (a) dissolved organic matter; (b) particulate organic matter.

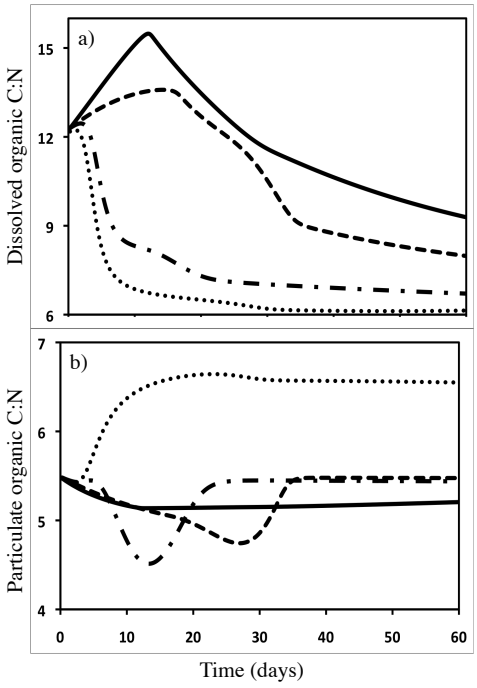

Chapter 4: Phytoplankton Biomass Distribution and Floral Composition in the Upper Chesapeake Bay in the Winter and Spring: Influences of Estuarine Physics and Turbidity Maximum Entrapment

Abstract

The objective of this study was to examine the biomass distribution and floral composition of the phytoplankton community in the upper Chesapeake Bay during the winter and spring to determine if phytoplankton could play an important role in the estuarine turbidity maximum (ETM) food web at this time of year. In late winter (January or February), April, and May of 2007 and 2008 a series of fluorometric and HPLC measurements were made along the main channel of the upper Bay and in the ETM. Water samples were also collected for microscopic analysis. The concentrations of chlorophyll *a* and marker pigments were contour plotted using a kriging gridding method. Chlorophyll *a* to pigement ratios were also calculated and phytoplankton in selected water samples were identified microscopically. The results of this analysis suggest that the general distribution of phytoplankton in the upper Bay appears to look somewhat like a classic estuarine "salt wedge" diagram with two distinct phytoplankton communities separated by a zone of increased mortality due to salinity stress and ETM entrapment. The northern most community in lower salinity waters was composed mostly of diatoms while the southern community in more saline waters was composed mostly of dinoflagellates who were often concentrated in a thin layer below the pycnocline. Cryptophytes were important members of both communities. High concentrations of phytoplankton pigment degradation products were often observed in the ETM suggesting that this is an area of high phytoplankton mortality and/or an area where phytoplankton derived particulate organic matter was being concentrated. Mechanisms of phytoplankton transport to the ETM are also proposed.

Introduction

Estuaries are an important transition zone between terrestrial and aquatic systems and thus have food webs with linkages to each system. The structure and dominant pathways of energy flow in an estuarine food web are strongly influenced by the amount of terrestrial organic matter that flows into the estuary and the physical process that occur when freshwater mixes with salty estuarine water. In some estuaries the food web appears to be primarily autotrophic with zooplankton grazing directly on riverine or estuarine phytoplankton (Winkler et al., 2003). However, in many estuaries, and the rivers that flow into them, turbidity limits light and consequently phytoplankton biomass and productivity are low (David et al., 2006; Thorp and Delong, 2002). Measurements often indicate that these regions are heterotrophic as well (Kemp et al., 1997a; Smith and Kemp, 1995; Thorp and Delong, 2002). Turbidity and hydrodynamic processes may play an especially important role in some estuarine food webs due to the formation of an estuarine turbidity maximum (ETM). ETMs are common physical features that are typically located at the heads of coastal plain estuaries near the freshwater/saltwater interface (Schubel, 1968). As the name implies they are characterized by high suspended sediment concentrations that result from a combination of the system's gravitational circulation, stratification, tidal asymmetry, topography, wind, waves, flocculation, and sediment characteristics (Sanford et al., 2001). The hydrodynamic processes that form ETMs also tend to trap particulate matter and may permanently bury much of the terrestrial material that enters the estuary (Schubel and Pritchard, 1986). Despite these conditions, these regions often have high secondary productivity (David et al., 2006). In many estuaries little is known about lower trophic levels and the food web that supports

this secondary production. In some of these systems the food web appears to mainly depend on the allochthonous input of organic matter to fuel a detritus based food chain (Heinle and Flemer, 1975; Hummel et al., 1988). In other systems the primary, annual energy source supporting higher trophic levels appears to be autochthonous primary production that enters food webs via algal-grazer and decomposer pathways with the decomposers being responsible for the system's heterotrophic state and secondary production being supported by the algal-grazer (Thorp and Delong 2002). Particle-attached, nutrient rich bacteria are also thought to act as an essential link in the transfer of energy through some of these food webs when they are eaten along with detritus by zooplankton (Hummel et al., 1988).

In the Chesapeake Bay the food web that supports secondary production in the ETM has not been elucidated. However, ETM copepods contribute substantially to Bay-wide production on a seasonal basis and dominate abundances during the spring when freshwater flow is high (Kimmel and Roman, 2004; Roman et al., 2001). In addition, ETM zooplankton appear to be a major source of food for fish larvae, such as white perch *Morone americana* (Shoji et al., 2005) and stripped bass *M. saxatilis,* which can be very abundant near the ETM in the spring(North and Houde, 2001; North and Houde, 2003). In order to sustain this high springtime secondary productivity there must be a continuous supply of nutritious organic matter.

Phytoplankton are one potentially important source of organic matter. The floral composition of the upper Chesapeake Bay is fairly well known (Marshall et al., 2005; Marshall et al., 2006). However, the winter and spring distribution of phytoplankton biomass, especially in the vicinity of the ETM, is not well characterized. Monitoring

programs (Maryland DNR stations) and single station studies that report on either the chl-*a* concentration or the composition of the phytoplankton community (Adolf et al., 2006; Harding, 1994; Marshall et al., 2005; Marshall et al., 2006) fail to provide data with enough spatial or temporal resolution to understand their role in the ETM food web. The studies (Fisher et al., 1988; Harding et al., 1986; Roman et al., 2001; Zhang et al., 2006) that have measured chl-*a* on transects through the ETM have generally shown that the chl-*a* concentration is much lower in and above the ETM when compared to the rest of the Bay. However, these studies have also noted years in which there were high concentrations of chl-*a* in and above the ETM. Unfortunately much of this research did not include an adequate description of the phytoplankton community floral composition. Knowledge of the floral composition is important for understanding the food web dynamics because some phytoplankton species are more nutritious than others (Danielsdottier et al., 2007) and some species are mixotrophic. In addition, zooplankton can be quite selective when feeding and may prefer one phytoplankton species over another (Kleppel, 1993; Sherr and Sherr, 2002). As far as we are aware there have also been no focused studies to determine if physical processes cause phytoplankton to become entrapped in the ETM where secondary productivity is high.

In this study we determined the biomass distribution and floral composition of phytoplankton in and around the ETM during the winter and spring using fluorometry, high performance liquid chromatography (HPLC), and microscopy. This methodology also allowed us to identify areas of high phytoplankton mortality via the presence of pigment degradation products and phytoplankton derived detritus. Our approach of mapping selected pigment distributions and relating them to hydrographic variables

shows common phytoplankton community patterns in the upper Bay and indicates that both riverine and estuarine phytoplankton may be an important source of organic matter for the ETM food web.

Methods

Over a period of two years six research cruises were conducted in the upper Chesapeake Bay (Fig. 1) on the R/V *Hugh R. Sharp*. Two cruises were in late winter (February 23-26, 2007 and January 23-26, 2008) and four cruises were in the spring (April 9-15 and May 8-14, 2007; April 17-23 and May 16-22, 2008). During each cruise two 6 to 8 h axial CTD surveys were conducted from south to north, except for the axial survey on February 26, 2007 which ran from north to south, beginning at 7 am (usually just after sunrise). Casts with a transmissometer and Wetlabs ECO fluorometer equipped Seabird CTD were made every 5 to 8 km up-estuary of 39°00'N to measure temperature, salinity, turbidity, and fluorescence at 11 stations (Fig. 4.1). Water samples were collected up-cast in 20 l Niskin bottles 1 m below the surface, in the pycnocline (determined during the initial downcast CTD cast), and 1 m above the bottom at 5 stations (Fig. 1) during each axial survey. In between the axial transects fixed stations at each end of the axis and within the ETM were also occupied for varying amounts of time (6-30 h). Hourly CTD casts were made at these fixed stations along with a limited number of water samples that were taken to measure specific features such as a sub-surface chlorophyll *a* maximum or the ETM during specific phases of the tide.

Samples for fluorometric and HPLC pigment analysis were collected by filtering water under low light conditions through 25mm GF/F filters. The filters for fluorometric analysis were frozen and stored at -20°C. The concentrations of chlorophyll *a* and

pheophytin *a* were then determined using EPA method 445.0 (Arar and Collins, 1997) which involves extracting the pigments in 90% acetone with the aid of a mechanical tissue grinder. Note that pheophorbides present in these samples were determined collectively as pheophytin *a*. The filters for HPLC pigment analysis were frozen and stored at -80°C using either liquid nitrogen or a low temperature freezer. Upon return to shore HPLC pigment analysis was performed by Horn Point Laboratory analytical services according to the methods of Van Heukelem and Thomas (2001).

All CTD data was processed by bin averaging over 0.25 m depth bins using Seasoft software (Seabird Electronics) while correcting raw depths for instrumental and atmospheric pressure offsets. The voltage output of the transmissometer was calibrated to NTUs using a well-mixed laboratory Formazin turbidity standard. CTD fluorometric measurements were converted to chlorophyll *a* equivalent concentrations by means of a calibration relationship derived for each cruise. The calibration relationship was derived by linear regression of water sample chlorophyll *a* values against the voltage values from the fluorometer on the CTD.

Salinity and the concentrations of chlorophyll *a*, several phytoplankton taxa specific accessory pigments, and chlorophyll degradation products were mapped with contour plots for each axial transect using EasyKrig V3.0 (Chu, 2004) and Matlab V7.4. The gridding method was kriging with an isotropic nonlinear semi-variogram model. Grid-line geometry was about half the average distance between measurements in the X (distance) and Y (depth) directions. In the contour plots the X axis was expressed in kilometers from the mouth of the Susquehanna River (Fig. 4.1).

Water samples for the microscopic identification of phytoplankton were transferred to 100 ml jars, preserved with cold glutaraldehyde (2% final concentration), and refrigerated. In the laboratory, 5-15 ml subsamples were filtered onto 25 mm polycarbonate filters with a 2 μm pore size and the filters were mounted with immersion oil under a cover slip on glass slides. Slides were stored frozen. Phytoplankton were enumerated at 200× on 2-4 transects (depending on phytoplankton density) using epifluorescence microscopy (Nikon filter set EF-4 B2-A; exciter filter 450-490 nm, dichromatic beam splitter 500 nm, barrier filter 515 nm) (Stoecker and Gustafson, 2002). Samples (100 ml) were also preserved with acid Lugol's solution (2 % final concentration) and stored in dark bottles. In the laboratory, 25 ml subsamples were settled in Utermohl chambers and enumerated on an inverted microscope at 200× magnification.

During a preliminary analysis of the HPLC data the CHEMTAX program (Mackey et al., 1996) was used to try to estimate the composition of the phytoplankton community as this program has been used with some success in other estuaries (Lewitus et al., 2005; Valdes-Weaver et al., 2006). However, the results of this analysis did not compare well with the taxa specific accessory pigment maps and the microscopic analysis. Therefore, we concluded that we did not have the necessary a priori knowledge (Irigoien et al., 2004) that is required to successfully use CHEMTAX methodology. So instead, depth integrated accessory pigment to chlorophyll *a* ratios were calculated to help determine the composition of the phytoplankton community.

A modified Owen settling tube was used to measure settling velocities of particles collected just above the bottom during the anchor stations. This tube is a modified 20 l

Niskin bottle which was deployed horizontally in the water column at the desired depth (usually 0.5 m above the bottom). After the tube was oriented into the flow a messenger was sent to close the ends of the tube, which was then raised back to the surface. On deck, the tube was placed vertically and wrapped in a thermal jacket to prevent convective cells from forming inside the tube. Water samples were then withdrawn from the bottom for analysis at specified, geometrically increasing time intervals. The sequence of bottom-withdraw water samples was analyzed using a spreadsheet implementation of the procedure described by Owen (1976). The product of this procedure is a settling velocity distribution of relatively undisturbed particles.

Particulate organic matter measurements (POC, PON, PO13C, PO15N) were made on suspended particles collected on pre-ashed 25mm diameter GF/F filters, which were stored at -20° C until processed. Filters were dried at (~56 degrees C) for 48 hours, fumed with concentrated HCl for 17 hours, dried again at ~56 degrees C for 24 hours, packaged in silver or tin capsules, and sent to the U. California Davis Stable Isotope Facility for analysis.

Results

Late Winter 2007

In February the upper Bay was not strongly stratified (see isohalines in Figs. 4.2 and 4.3), indicating that a substantial amount of mixing was occurring between inflowing river water and the more saline estuarine water. The water temperature was near 0° C throughout much of the upper Bay with only inflowing river water and the deepest waters at the southern end of the transects a few degrees above zero (data not shown). On the

first transect there was a strong ETM located between 30 and 40 km (max: 120 NTU at 36 km) from the head of the bay (Fig. 4.2). On the second transect there was a weak ETM located between 20 and 30 km (max: 44 NTU at 25 km) from the head of the bay (Fig. 4.3).

The cruise in February 2007 began during the end of a cold period that was sustained for long enough to freeze the surface waters of the upper Chesapeake bay for a period of approximately two weeks. At the start of the cruise the ice was just beginning to break up and on our initial transect over three quarters of the surface was covered by a layer of ice 1-24 inches thick. The ice continued to break up during the cruise, with the water becoming mostly ice-free by the end. Inspection of the ice at number of stations revealed what appeared to be algae growing on the underside. Unfortunately, we were not equipped to properly sample ice alga and were only able to qualitatively confirm the presence of chlorophyll *a* by scraping a small sample onto a filter for fluormetric analysis. However, from visual inspections there was obviously a large ice algal community that must have been growing at a relatively rapid rate to develop (in two weeks) to the point where it could be observed by the naked eye.

In the water column, the concentration of chlorophyll *a* along the axial transects was non-linearly correlated with salinity (Fig 4.4), especially on the first transect, with the highest chlorophyll *a* concentrations occurring at a salinities of 8-12. A plot of the chlorophyll *a* concentrations on the first transect reveals that chlorophyll *a* was highest south of the ETM (Fig. 4.5). In this area of high chlorophyll *a*, concentrations were patchy but there was an obvious subsurface maximum layer between 10 and 15 m deep where the concentration was as high as 39 μg l^{-1}. North of the ETM, in fresher water, the

chlorophyll *a* concentration was two to three times lower and homogenous, averaging only 10 μg l^{-1}. A plot of chlorophyll *a* concentrations along the second transect (Fig. 4.6) reveals a striking pattern where the maximum concentrations of chlorophyll *a* (up to 50 μg chl *a* l^{-1}) were found on the bottom between 36 and 55 km from the head of the bay. This area of high chlorophyll *a* was once again south of the ETM. The chlorophyll *a* concentrations north of the ETM were again much lower.

An examination of selected accessory pigment concentrations reveals that, as with chlorophyll *a*, there were non-linear correlations with salinity (Fig. 4.4). Alloxanthin and peridinin correlations with salinity had a similar pattern to that of chlorophyll *a*, while the fucoxanthin correlation with salinity had an inverse relationship when compared to the others. Maps of pigment concentrations along the transects (Figs. 4.5 and 4.6) reveal that the subsurface chlorophyll *a* maximum coincided with high concentrations of pigments specific to dinoflagellates (peridinin) and cryptophytes (alloxanthin). Interestingly, there was also a positive correlation between alloxanthin and peridinin on both transects (Fig. 4.7). The diatom pigment marker fucoxanthin was concentrated in the bottom waters at the southern most station and to the north of the ETM. Integrated accessory pigment to chlorophyll *a* ratios at stations along the transect (see Appendix C) also show an inverse relationship between peridinin and fucoxanthin indicating that dinoflagellates dominated the phytoplankton biomass in all but the deepest waters south of the ETM and that diatoms dominated waters north of the ETM. These plots also show that the proportion of cryptophytes in the phytoplankton community increased from north to south. The small cyanobacterial proportion of the phytoplankton

community (indicated by the cyanobacterial specific pigment zeaxanthin) had a distribution pattern similar to that of diatoms.

Microscopic examination of samples at the ends of the transect and in the ETM show that the dinoflagellate *Heterocapsa rotundatum* was the most abundant phytoplankter south of the ETM and likely (exact cell counts were unavailable) accounted for the majority of the peridinin and chlorophyll *a* (i.e. biomass) observed along these transects. Diatoms were by far the most abundant type of phytoplankon north of the ETM, with a chlorophytes (unidentified species) being the second most common group. Cryptophytes (not identified to species) were also fairly common in all of the water samples. Most of the biomass north of the ETM was also < 5 μm. The microscopic analysis also shows that while some groups of phytoplankton were concentrated in certain areas there were no completely distinct communities of phytoplankton as most of the species were present, although often a low abundance, in all of the samples along the transect. However, species that dominated the phytoplankton community at one end of the transect, such as *H. rotundatum,* often appeared to be visually unhealthy when they were present in samples at the other end of the transect.

Pigment degradation products were concentrated at the southern end of the transects (Figs. 4.2 and 4.3), with much of the material in bottom waters. High chlorophyllide *a* concentrations suggest that much of this material derived from senescent diatoms. Although the presence of pheophorbide *a*, does suggest that grazing was occurring as well.

Early Spring 2007

The upper Bay was more vertically stratified in April (see isohalines in Figs. 4.8 and 4.9) than in February with a noticeable pycnocline from approximately 30 km from the head of the Bay southward. The water was between 6 and 9° C (data not shown) with a temperature gradient corresponding to the stratification of the system (i.e. warmer, fresher water at the surface and colder more saline water at depth). On both transects a strong ETM was located between 35 and 48 km (max: 107 and 150 NTUs, respectively, at 42 km) from the head of the Bay (Figs. 4.8 and 4.9).

As in the February, the concentrations of chlorophyll *a* along the transects were non-linearly correlated with salinity (Fig. 4.10). However, these relationships were not as strong as in February. A map of the chlorophyll *a* concentration along the first transect reveals (Fig. 4.11) that chlorophyll *a* was highest far to the south of the ETM. The majority of the chlorophyll *a* was located in a tight layer between 5 and 10 m deep that extended from the southern most station northward to around 60 km from the head of the bay. In this tongue of high chlorophyll *a* the concentration reached up to 62 μg l^{-1}. Away from this feature, the chlorophyll *a* concentration was much lower and only averaged 4 μg l^{-1} in waters north of the ETM. A map of the second axial transect (Fig. 4.12) reveals the same subsurface chlorophyll *a* maximum (up to 32 μg l^{-1}) and an additional zone of high chlorophyll *a* at the surface slightly to the north. On this transect the chlorophyll *a* concentration was again low near and to the north of the ETM.

An examination of the selected accessory pigment concentrations versus salinity shows that as with chlorophyll *a* they are non-linearly correlated (Fig. 4.10). However, these relationships were not as strong as in February. Maps of pigment concentrations

along the transects (Figs. 4.11 and 4.12) reveal that as in February the subsurface chlorophyll *a* maximum coincided with high concentrations of pigments specific to dinoflagellates and cryptophytes. As in February, there was also a strong correlation between alloxanthin and peridinin (Fig. 4.7) on these transects. The diatom pigment marker fucoxanthin was concentrated in the bottom waters at the southern most station and in the surface around 60 km from the head of the Bay. Observations of fucoxanthin also suggest that we may have witnessed the beginning of a diatom bloom at the surface around 60 km from the head of the Bay as the chlorophyll *a* and fucoxanthin concentrations more than doubled in the time between transects. As in February, the integrated accessory pigment to chlorophyll *a* ratios (see Appendix C) show an inverse relationship between peridinin and fucoxanthin indicating that dinoflagellates dominate the phytoplankton community biomass in waters south of the ETM and diatoms dominate it in waters north of the ETM. These plots also show that the proportion of cryptophytes in the phytoplankton community was unevenly distributed along the transects with the highest proportion occuring in the ETM region. The small cyanobacterial proportion of the phytoplankton community was highest just north of the ETM and lowest at the two southern stations.

Microscopic examination of samples from the ends of the transects and in the ETM region show that as in February the most common and numerically abundant (1000's of cells ml^{-1}) phytoplankton in the subsurface chlorophyll *a* maximum was the dinoflagellate *H. rotundatum*. In areas where diatoms were abundant the majority of them belonged to the genus *Cyclotella* with 1000's of cells per ml^{-1}. Other common (100's of cells ml^{-1}) phytoplankton south of the ETM region include unidentified

cryptophytes, dinoflagellates such as *Prorocentrum minimum*, and an assortment of diatoms (*Leptodylindrus minimus, Dactyliosolen fragilissimus,* and unidentified centric diatoms). In the ETM region there were less than 100 cells ml^{-1} (all diatoms) in the waters above the very turbid bottom 3 m of the water column. In the turbid bottom waters there was a higher abundance of phytoplankton than at the surface (100's of cryptophytes ml^{-1} and a few <10 μm unidentified centric diatoms). North of the ETM region there were very few phytoplankton (<700 cells ml^{-1}) with the community consisting mostly of diatoms (*Cyclotella*, *Skeletonema*, <10 μm unidentified centric diatoms) and a few (<100 cells ml^{-1}) unidentified cryptophytes.

Pigment degradation products were concentrated in the ETM and the bottom waters at the southern most station on both of the transects (Figs. 4.8 and 4.9). The presence of chlorophyllide *a* in the bottom waters at the southern most station suggests that this material derived from senescent diatoms. The presence of pheophorbide *a* in the ETM suggests that predation is occurring in this region which is not surprising considering that copepods were very abundant in these water samples (i.e. when filtering 50 ml of water it was not uncommon to end up with 4-6 copepods on the filter). In addition, during the microscopic examination of samples from the ETM region a large number of empty diatom frustules and partially degraded dinoflagellates were observed further suggesting that this region was a zone of high phytoplankton mortality.

Late Spring 2007

In May the upper Bay was even more vertically stratified (see isohalines in Figs. 4.13 and 4.14) than in April with a noticeable pycnocline from 20-30 km from the head of the Bay southward. The water was between 10 and 21° C (data not shown) with a

temperature gradient corresponding to the stratification of the system (i.e. warmer, fresher water at the surface and colder more saline water at depth). On the first transect a strong ETM was located between 30 and 42 km (max: 140 NTU at 36 km) from the head of the Bay (Fig. 4.13). On the second transect a more moderate ETM was located between 35 and 45 km (max: 80 NTU at 42 km) from the head of the Bay (Fig. 4.14).

As in the February and April, the concentrations of chlorophyll *a* along the transects were non-linearly correlated with salinity (Fig. 4.15). Maps of the chlorophyll *a* concentration along the transects (Fig. 4.16 and 4.17) again show a subsurface chlorophyll *a* maximum layer between 5 and 15 m deep to the south of the ETM region. The maximum chlorophyll *a* concentrations measured in this layer were 57 and 79 μg chl *a* l^{-1}. North of the ETM the chlorophyll *a* concentration was lower throughout the water column and averaged only about 10 μg l^{-1}.

An examination of the selected accessory pigment concentrations versus salinity shows that they were again non-linearly correlated (Fig. 4.15). However, unlike in February and April there was no correlation between alloxanthin and salinity. A map of the pigment concentrations on the first transect (Fig. 4.16) shows that the cryptophyte specific pigment, alloxanthin, was concentrated in an area at the northern, slightly shallower tip of the chlorophyll *a* maximum layer while the dinoflagellate specific pigment, peridinin, was concentrated in the deeper more southern part of the layer, just below the pycnocline. The diatom indicating pigment fucoxanthin was distributed largely along the salinity gradient with the highest concentration occurring in the deepest most saline water. A map of the second transect (Fig. 4.17) shows significant overlap between populations of diatoms and dinoflagellates in the area of the subsurface

chlorophyll *a* maximum. However, diatoms were more abundant at the surface while dinoflagellates were most abundant at a depth of 5 to 10 m. Cryptophytes were concentrated in the surface and bottom waters surrounding the ETM. Unlike earlier in the year there was no correlation between peridinin and alloxanthin. Integrated accessory pigment to chlorophyll *a* ratios along the transect (see Appendix C) show that as in February and April there was an inverse relationship between fucoxanthin and peridinin with dinoflagellates dominating the phytoplankton community biomass in waters south of the ETM and diatoms dominating it in waters north of the ETM. These plots also show that the proportion of cryptophytes and cyanobacteria in the phytoplankton community decreased from north to south along the transects.

Microscopic examination of water samples from the ends of the transects and in the ETM region reveal a more diverse and numerically abundant phytoplankton community than earlier in the year with the dinoflagellate *Prorocentrum minimum* and small (< 10 μm) centric diatoms being the most common and numerically abundant (1000's of cells ml^{-1}) phytoplankton in the subsurface chlorophyll *a* maximum. Cryptophytes and small (<10 μm) centric diatoms were also fairly common in all of the water samples with 100-1000 cells ml^{-1}. Other common (100's of cells ml^{-1}) phytoplankton include dinoflagellates such as *H. rotundatum* and *Karlodinium micrum* and diatoms such as *Cyclotella*, *Skeletonema, Aulocosira, Nitzschia*, unidentified pennates, and unidentified larger (>10 μm) centric species. The microscopic analysis also shows that while some groups of phytoplankton were concentrated in certain areas there were no completely distinct communities of phytoplankton, as in April, as most of the species were present, although often a low abundance, in all of the samples along the

transect. However as in February, species that dominated the phytoplankton community at one end of the transect, such as *P. minimum,* often appeared to be visually unhealthy when they were present in samples at the other end of the transect.

Pigment degradation products on both axial transect were concentrated in the ETM and the more saline waters south of it (Figs. 4.13 and 4.14). Pheophytin *a* and pheophorbide *a* were concentrated mostly in the ETM and the bottom waters to the south of it while chlorophyllide *a* was concentrated in the surface waters south of the ETM region. On the second transect, this zone of high chlorophyllide *a* overlapped with the area where fucoxanthin concentrations were high. In addition, during the microscopic examination of samples from the ETM region a large number of empty diatom frustules and partially degraded dinoflagellates were observed further suggesting that this region was a zone of high phytoplankton mortality.

Winter 2008

In January there was strong vertical stratification (see isohalines in Figs. 4.18 and 4.19) throughout much of the upper Bay with a noticeable pycnocline from approximately 30 km from the head of the Bay southward. The water was between 0 and 6° C (data not shown) with a temperature gradient that reflected the stratification of the system, cold atmospheric temperatures, and mixing between cold river water and the slightly warmer estuarine water (i.e. it was colder and fresher at the surface and warmer and saltier at the bottom in areas where there was a pycnoline). On the first transect a weak ETM was located between 10 and 30 km (max: 62 NTU at 25 km) from the head of the Bay (Fig. 4.18). On the second transect a weak ETM was located between 25 and 35 km (max: 67 NTU at 30 km) from the head of the Bay (Fig 4.19).

Like the winter of 2007, there was a strong non-linear correlation between salinity and the chlorophyll *a* concentration (Fig. 4.20). However, unlike in February of 2007, the highest chlorophyll *a* concentrations were associated with the highest salinities. Maps of the chlorophyll *a* concentration along the transects (Figs. 4.21 and 4.22) show high concentrations of chlorophyll *a* at the southern end of the transects with the highest concentrations occurring at the bottom and in a layer between 5 and 12 m deep. The maximum chlorophyll *a* concentrations observed on both of these transects were near 30 μg l^{-1}. Chlorophyll *a* concentrations were low in the region of the ETM and only averaged around 5 μg l^{-1} in this area and to the north of it.

An examination of the selected accessory pigment concentrations versus salinity shows that as with chlorophyll *a* there were correlations with salinity (Fig. 4.20). However, unlike in the previous year when these relationships were often highly non-linear, there was a strong linear correlation between alloxanthin and salinity on the second transect and some of the other relationships were close to being linear ones. Maps of the accessory pigment concentrations along the transects (Figs. 4.21 and 4.22) show pigment distribution patterns that were similar to the patterns observed on many of the transects in the late winter and spring of 2007. Higher concentrations of alloxanthin, the cryptophyte specific pigment, and peridinin, the dinoflagellate specific pigment, were associated with the mid-depth subsurface chlorophyll *a* maximum and the moderate amounts of chlorophyll *a* at the surface at the southern end of the transect. High concentrations of fucoxanthin, the diatom specific pigment, were associated with areas of high chlorophyll *a* in the deepest, saltiest waters at the southern end of the transects. As in February and April of 2007, there was also a strong correlation between alloxanthin

and peridinin (Fig. 4.7). Integrated accessory pigment to chlorophyll *a* ratios (see Appendix C) show that the proportion of the phytoplankton community biomass that was diatoms and cryptophytes was similar at all stations with the phytoplankton community comprised mostly of diatoms. Dinoflagellates made up a large proportion of the phytoplankton community only at the more southern stations. In addition, these plots show that most cyanobacteria, which were a small portion of the phytoplankton community at all stations, were most abundant north of the ETM.

Microscopic examination of samples from the ends of the transects and in the ETM region, as well as samples from select regions of high chlorophyll *a,* show that the most common and numerically abundant phytoplankton in the subsurface chlorophyll *a* maximum were the dinoflagellate *H. rotundatum* (1000's of cells ml^{-1}) and *Skeletonema* diatoms (>15,000 cells ml^{-1}). Cryptophytes and small (<10 μm) centric diatoms were also fairly common in all of the water samples with 100-1000 cells ml^{-1}. A few other species of phytoplankton were present in many of the samples but their abundances were very low (<100 cells ml^{-1}).

Pigment degradation products on both transects (Figs. 4.18 and 4.19) were concentrated in the deepest, most saline waters. Although, there were some differences between the two transects. On the first one some pigment degradation products were also observed at the northern most station, while on the second one bottom waters along the whole transect had a higher concentration when compared to the surface.

Early Spring 2008

In April much of the upper Bay was vertically stratified (see isohalines in Figs. 4.23 and 4.24), with a noticeable pycnocline from 30-40 km from the head of the Bay

southward. The water was between 9 and 17° C (data not shown) with a temperature gradient that corresponded to the stratification of the system (i.e. warmer, fresher water at the surface and colder more saline water at depth). On the first transect a moderately strong ETM was located between 20 and 30 km (max: 85 NTU at 25 km) from the head of the Bay (Fig. 4.23). On the second transect a slightly stronger ETM was located between 20 and 35 km (max: 105 NTU at 30 km) from the head of the Bay (Fig. 4.24).

In April of 2008 there were no significant correlations between salinity and chlorophyll *a* concentrations (data not shown) as there had been earlier in the year and in the winter/spring of 2007. Maps of chlorophyll *a* concentrations along the transects (Figs. 4.25 and 4.26) show that, unlike in 2007, there were higher concentrations of chlorophyll *a* at the northern most station near the head of the Bay. In addition, a subsurface chlorophyll *a* maximum, which was discernable on the first transect, was not the sole dominant feature as there were areas of high chlorophyll *a* near the surface as well. The maximum chlorophyll *a* concentrations observed on these transects were 14 and 20 μg l^{-1} which is much lower than the 30 to 60 μg chl *a* l^{-1} that were observed in 2007. Chlorophyll *a* concentrations were lowest in the region of the ETM with a range of only 2-4 μg chl *a* l^{-1}.

As with chlorophyll *a*, there were no significant correlations between salinity and the accessory pigments. However, peridinin and alloxanthin concentrations did tend to be higher in more saline waters. Maps of the accessory pigment concentrations along the transects (Figs. 4.25 and 4.26) show that high concentrations of the cryptophyte indicating pigment, alloxanthin, were associated with an area of high chlorophyll *a* at the southernmost station on the first transect and an area of high chlorophyll *a* towards the

south on the second transect. High concentrations of the dinoflagellate indicating pigment, peridinin, were found at the southern most station on both transects. However, on the first transect peridinin was concentrated in the bottom most saline waters while on the second transect it was concentrated just a few meters below the surface. There was also a positive correlation between alloxanthin and peridinin (Fig. 4.7), but it was not as strong as in January. Concentrations of fucoxanthin, the diatom indicating pigment, were highest at the northern most station and in the surface waters 45 to 70 km from the head of the Bay. Integrated accessory pigment to chlorophyll *a* ratios along the transect (see Appendix C) show that a large proportion of the phytoplankton community was comprised of diatoms, with the proportion increasing northward along the transect. Dinoflagellates were only present at the southern end of the transect. Cryptophytes were present at all stations but tended to be less abundant at the more northern ones. Cyanobacteria, which were a small portion of the phytoplankton community at all stations, were most abundant in the ETM region.

Microscopic examination of samples from the ends of the transects and in the ETM region, as well as samples from select regions of high chlorophyll *a,* show that the most common and numerically abundant phytoplankton associated with areas of high chlorophyll *a* were cryptophytes and small (<10 μm) centric diatoms (not identified to species) with 100s to 1000s of cells ml^{-1}. The dinoflagellates *H. rotundatum* and *P. minimum* were present throughout the water column in the southern half of the transect with 100s of cells ml^{-1} at a ratio of approximately 2 *H. rotundatum* to 1 *P. minimum*. Interestingly, there were also ~ 300 *P. minimum* cells ml^{-1} in the bottom water at the northern most station. In the deepest waters at the southern end of the transect

Skeletonema diatoms were common (100s of cells ml^{-1}) as well. A few other species of phytoplankton were present in many of the samples but their abundance was very low (<100 cells ml^{-1}).

Pigment degradation products exhibited interesting patterns on both transects (Figs. 4.23 and 4.24) with specific ones often overlapping areas of high chlorophyll *a* and other pigments. On the first transect fluorometric measurements of pheophytin *a* (and other degradation products) were fairly uniform throughout most of the water column with lower concentrations observed only at the northern most station. Plotted pigment data also indicates that the highest concentrations of chlorophyllide *a* and pheophytin *a* were associated with areas of high chlorophyll *a*. Pheophorbide *a* concentrations were only high in the deepest, most saline waters at the southern end of the transect. On the second transect fluorometric measurements of pheophytin *a* indicated that it was more concentrated in the bottom waters along the whole transect. High chlorophyllide *a* concentrations were associated with areas of high alloxanthin and peridinin, although there was also an area of elevated chlorophyllide *a* at the northern end of the transect. High pheophytin *a* concentrations were associated with areas of high chlorophyll *a* and fuxoxanthin at the northern most station. Pheophorbide *a* was concentrated in the bottom more saline waters and appeared to form a gradient based on the stratification of the system.

Late Spring 2008

In May the lower portion of the upper Bay was vertically stratified (see isohalines in Figs. 4.27 and 4.28) with a noticeable pycnocline from 35-40 km from the head of the Bay southward. The water was between 13 and 18° C (data not shown) with a

temperature gradient that generally corresponded to the stratification of the system (i.e. warmer, fresher water at the surface and colder more saline water at depth). However, temperature measurements indicate that the inflowing river water cooled somewhat in the time between transects as water at the northernmost station on the second transect was cooler than the water just to the south of it. On the first transect a very weak ETM was located between 15 to 45 km (max: 45 NTU at 35 km) from the head of the bay (Fig 4.27). On the second transect a moderately strong ETM was located between 25 and 48 km (max: 125 NTU at 42 km) from the head of the Bay (Fig. 4.28).

As in April there were no strong correlations between chlorophyll *a* concentrations and salinity along the transects (data not shown). However, there were some very distinct areas of high chlorophyll *a* along these transects (Figs. 4.29 and 4.30). On both transects there were subsurface chlorophyll *a* maximum layers south of the ETM. On the first transect there was also an area of high chlorophyll *a* just below the surface to the south of the ETM. The maximum chlorophyll *a* concentrations observed on these transects occurred in the subsurface layers of high chlorophyll *a* and were 42 and 66 μg l^{-1}, respectively. Chlorophyll *a* concentrations on both transects were lowest in the ETM region (averaging around 4 μg l^{-1}) and only slightly higher at the northern most station (~8 μg l^{-1}).

As with chlorophyll *a*, there were no significant correlations between salinity and the accessory pigments. Maps of the accessory pigment concentrations along the transects (Figs. 4.29 and 4.30) show that high concentrations of the cryptophyte indicating pigment, alloxanthin, were associated with the subsurface chlorophyll *a* maximum layers and areas of low salinity at the northern end of the transect. High

concentrations of the diatom indicating pigment, fucoxanthin, were associated with the northern most station and surface waters south of the ETM region on both transects. High concentrations of the dinoflagellate indicating pigment, peridinin, were associated with areas of high chlorophyll *a* at the southern end of the first transect and the subsurface chlorophyll *a* maximum layer on the second transect. Integrated accessory pigment to chlorophyll *a* ratios (see Appendix C) show that, as on many of the previous cruises, there was an inverse relationship between fucoxanthin and peridinin with dinoflagellates dominating the phytoplankton community biomass in waters south of the ETM and diatoms dominating it in waters north of the ETM. The small proportion of the phytoplankton community that was cryptophytes and cyanobacteria was highest in the ETM region.

Microscopic examination of samples from the ends of the transects and in the ETM region, as well as samples from select regions of high chlorophyll *a,* show that the most common and numerically abundant phytoplankton specie associated with areas of high chlorophyll *a* was the dinoflagellate *P. minimum* (1000s of cells ml^{-1}). Cryptophytes and small (<10 μm) centric diatoms (not identified to species) were also fairly common in all of the water samples with 100-1000 cells ml^{-1}. Chlorophytes and *Skeletonema* diatoms were also occasionally abundant (100's of cells ml^{-1}) in some of the samples, although their distribution was patchy. A number of other phytoplankton species were present in many of the samples but their abundance was always very low (<100 cells ml^{-1}).

Pigment degradation products exhibited interesting patterns on both transects (Figs. 4.27 and 4.28) with specific ones often overlapping areas of high chlorophyll *a* and

other pigments. Fluorometric measurements of pigment degradation products were not available on the first transect. However, HPLC measurements show that high concentrations of chlorophyllide *a* were associated with areas of high chlorophyll *a* and fucoxanthin in surface waters to the south of the ETM region. Pheophytin *a* concentrations were highest in the deepest, saltiest waters at the southern end of the transect and in fresher water at the northern end of the transect. On the second transect fluorometric measurements show that the highest concentrations of pheophytin *a* were in fresher waters at the northern end of the transect and in the surface waters at the southern most station. On this transect high concentrations of chlorophyllide *a* and pheophytin *a* were associated with the subsurface chlorophyll *a* maximum. Pheophytin *a* and pheophorbide *a* were also concentrated in the ETM region. In addition, during the microscopic examination of samples from the ETM region a large number of empty diatom frustules and partially degraded dinoflagellates were observed further suggesting that this region was a zone of high phytoplankton mortality.

Settling Tube Measurements

Measurements of water samples collected from the settling tube show that there was a correlation between pheophytin *a* and particulate organic carbon and nitrogen during all of the cruises (Fig. 4.31), regardless of when the sample was withdrawn. This suggest that much of POM in these samples, the majority of which were collected in the ETM, derived from phytoplankton. In addition, the percentage of both chlorophyll *a* and pheophytin *a* that settled out of water column was higher in the ETM region than at either end of the transect (Fig. 4.32). Figure 4.32 also shows that the percentage of chlorophyll

a that settled out was much lower than the fraction of pheophytin *a* that settled out at all stations.

Discussion

Our measurements in the upper Bay indicate that there were some common patterns in the biomass distribution and floral composition of the winter and spring phytoplankton communities. Foremost, cryptophytes and small centric diatoms were almost always present throughout the upper estuary even though they were not always the dominant species. The biomass of phytoplankton generally tended to increase from north to south and there were often non-linear relationships between biomass and salinity. Phytoplankton biomass (as indicated by chl *a*) was always highest to the south of the ETM region with one or two dinoflagellate species often accounting for the majority of the biomass. However, these dinoflagellates tended to form distinct layers just below the pycnocline and thus there were vertical gradients in the distribution of phytoplankton in this region. For example on some occasions, diatoms would be the dominant phytoplankton group at the surface or the bottom with dinoflagellates dominating the phytoplankton community at mid-depth. Although in general if there was a distinct sub-surface chlorophyll *a* maximum then dinoflagellates would account for most of the phytoplankton biomass at all depths. In this region there were also interesting relationships between diatoms and dinoflagellates and cryptophytes and dinoflagellates with an inverse relationship between diatom and dinoflagellate biomass and a positive correlation between cryptophyte and dinoflagellate biomass. To the north of the ETM region phytoplankton biomass was usually low and the community was almost always composed mostly of diatom species. However, there were occasions when phytoplankton

biomass was moderately high at the very northern station (although never as high as to the south of the ETM). Cryptophytes were also occasionally abundant in the very upper portion of the Bay in the late spring. In the ETM region phytoplankton biomass was always low and the community was often composed of a mix of species from either end of the transects. The ETM also appeared to be an area of high phytoplankton mortality and/or an area where phytoplankton derived particulate organic matter was being concentrated.

The Influence of Estuarine Physics

In the upper reaches of the Neuse River Estuary (North Carolina) hydrological processes are the predominant factor that regulate the phytoplankton dynamics (Arhonditsis et al., 2007). Our results suggest that hydrodynamic processes are similarly important in the upper Chesapeake Bay. Previous studies on a Bay-wide scale have shown that the development of latitudinal gradients in light and nutrients in response to seasonal changes in Susquehanna River flow, play an important role in determining the floral composition, distribution, and growth of phytoplankton (Adolf et al., 2006; Harding, 1994; Malone et al., 1988). While our results do not dispute these findings, our observations suggest that on this smaller spatial and temporal scale gravitational circulation, which is still controlled by Susquehanna River flow, and the subsequent transport of phytoplankton source communities, is more important in determining the composition and distribution of phytoplankton than the development of latitudinal gradients in light and nutrients. However, we should note that the development of these gradients still plays an important role in determining the floral composition, distribution, and growth of the source communities and thus, is still very important. Changes in

salinity due to the mixing of river and estuarine water that inevitably occurs in the upper Bay, plus physical entrapment processes, and possibly grazing, in the ETM also appear to be very important factors affecting the distribution and composition of phytoplankton.

Our results suggest that freshwater phytoplankton from the river or that develop on the Susquehanna flats just to the north of our study area are transported southward with inflowing river water as it enters the upper Bay. In the winter and spring the river flow is often strong enough to overcome tidal mixing and a classic "salt wedge" forms with two-layer gravitational circulation (Schubel and Pritchard, 1986). As the river water flows southward and gradually mixes with saltier estuarine water these freshwater phytoplankton may be subjected to osmotic stress that causes mortality and subsequent sinking. Live phytoplankton could also sink out of the surface layer under the right conditions and be subjected to osmotic stress when they pass through the halocline. Diatoms, which dominate this freshwater phytoplankton community, are well known for sinking when currents and turbulence decrease below a certain threshold (Sarthou et al., 2005) and it is possible that riverine diatoms sink when the Susquehanna flows into the more open estuary and the current velocity decreases due to the increased width or tidal forcing (i.e. flood tide reducing downstream flow and allowing sinking). Diatoms are also known to aggregate and sink in areas of high turbulence and turbidity (Thornton, 2002; Tyler and Seliger, 1989), conditions that are common in the ETM region. Phytoplankton that sink in the very upper Bay are likely to be transported to the ETM where, if not already dead, they may die due to predation or unfavorable environmental conditions (i.e. low light). Phytoplankton that do not sink will continue to be transported southward in the surface layer towards areas of higher salinity. Thus, a freshwater

phytoplankton community composed mostly of diatoms dominates the very upper Bay with the community biomass decreasing to the south as salinity increases and mortality and sinking occurs.

In the southern part of the upper Bay where salinities are higher, dinoflagellates often accounted for the majority of the phytoplankton community biomass. Their distribution, along with the other phytoplankton in this community, is also strongly affected by gravitational circulation. However, instead of just being transported southward these phytoplankton may be transported northward as well because the dinoflagellates that dominate this community are often found in more saline waters below the pycnocline and thus are subjected to northward transport due to gravitational circulation. Like freshwater phytoplankton, these estuarine phytoplankton may also be subjected to osmotic stress, although in the opposite manner, as the northward flowing bottom water mixes with or becomes entrained in the fresher surface layer. Phytoplankton that are transported northward in bottom water are also likely to become entrapped in the ETM and die due to predation or unfavorable environmental conditions. We should however note that the dinoflagellates in this community appear to be able to control their position in the water column (see discussion below) and may therefore be able to take advantage of the two-layer circulation to maintain their latitudinal position in the estuary. Although our observations suggest that gravitational circulation is often strong enough to transport some of these dinoflagellates northward. Overall, the general distribution of phytoplankton in the upper Bay appears to look somewhat like a classic estuarine "salt wedge" diagram with two distinct phytoplankton communities separated by a zone of increased mortality due to salinity stress and ETM entrapment (Fig. 4.33).

Since both the pycnocline and the ETM are physical features that can move in response to hydrodynamic changes the location of the boundary between these two phytoplankton communities is not fixed and may change, resulting in mixing and overlap between the communities at times.

A significant amount of research has examined how short and long term variations in physical process effect circulation and plankton in the Chesapeake Bay. However, we do not intend to review this large body of literature here or describe these effects in detail, instead we would like to highlight a few of the most important physical changes that must affect phytoplankton in this region. First, seasonal and annual variations in river flow must play an important role in determining the biomass distribution and floral composition of upper Bay phytoplankton because of their effect (Hansen and Rattray, 1965; Schubel and Pritchard, 1986) on the strength of gravitational circulation and salt intrusion. Second, seasonal changes and annual variations in temperature and light are known to play an important role in determining the phytoplankton floral composition and succession in the Chesapeake Bay as a whole (Adolf et al., 2006), and certainly play a role in the upper Bay as well. Third, winds and tides that affect gravitational circulation, and other circulatory process (see below), will also affect the distribution of phytoplankton in the upper Bay, although these effects are more likely to be short-term. Finally, the residence time of water in the upper Bay will also play a role in determining how long phytoplankton are in the area and whether or not they have a chance to grow or die. However, the residence time of water can vary considerably since it is dependant on many of the same physical factors (i.e. variations in river flow) that effect gravitational circulation. For example, numerical simulations have

calculated that in two different years with very different environmental forcing conditions (i.e. river flow, wind, etc.) it required approximately 210 and 80 days, respectively, for a water parcel to be transported at the surface from the headwater of the Bay to the mouth of the Patuxent River (Shen and Wang, 2007). Thus, the amount of time that phytoplankton spend in the upper Bay could be quite variable from year to year. However, based on the simulations of Shen and Wang (2007) it appears that phytoplankton spend enough time in the upper Bay for the communities that we have described to grow during transport if they do not become limited by light, nutrients, or mortality losses. In order to understand these relationships the productivity of phytoplankton was measured in conjunction with our sampling. However, this research and how it relates to our study will be presented in a separate article.

While gravitational circulation appears to be the most important physical process affecting the general distribution and floral composition of phytoplankton in the upper Bay it is not the only physical process that affect these phytoplankton. Tidal excursions, lateral transport, wind events, internal waves, seiching, and other mixing processes certainly transport phytoplankton and affect their distribution in the upper estuary on smaller spatial and temporal scales and may even result in "patchiness" (Tyler and Seliger, 1989) . Tidal excursions in the upper Bay will of course shift all phytoplankton north and south. However, asymetrical tidal circulation may enhance this shift and have a disproportionate effect on one of the phytoplankton communities as the circulation favors either southward or northward transport (see Fig. 11 in Sanford et al. (2001)). Lateral circulation due to either tidal or wind forcing may also result in changes in the circulation of water onto or off of the shoal regions (Chen et al., 2009). Winds can also

effect the stratification of an estuarine system (Chen and Sanford, 2009) and thus change the location of areas where salinity stress will affect phytoplankton. Under certain river flow or wind conditions, there may also be an exchange with Delaware Bay phytoplankton communities through the canal at the head of the estuary (Tyler and Seliger, 1989). In addition, some of the small upper Bay tributaries may be sources of phytoplankton to the main stem of the Bay (Tyler and Seliger, 1989). The strength of ETM particle trapping is also affected by changes in wind, tides, and river flow (Sanford et al., 2001). Interactions between bathymetry and physical processes can also modify circulation and may also play a role in the formation and location of the ETM (Sanford et al., 2001). Therefore, the magnitude of phytoplankton mortality in the ETM may change as these factors vary.

Another factor to consider in the distribution and transport of upper Bay phytoplankton is that the volume and transport velocity of the water that each community resides in may be different. This is because during the late winter and spring when river flow is seasonally high, the residual current velocity of the southward flowing surface layer is much higher than the velocity of the northward flowing bottom layer (Schubel and Pritchard, 1986). The surface layer also occupies a much greater volume of the upper estuary because the denser bottom layer is mostly confined to the depths of the main channel. Thus, the freshwater phytoplankton community, which resides mostly in the surface layer, has a greater potential to be delivered southward or into to the ETM than the estuarine phytoplankton community which may be concentrated (i.e. sub-surface dinoflagellates) in a smaller volume of water below the pycnocline in the main channel. However, in our study the biomass of the freshwater community was always much lower

than the biomass of the estuarine phytoplankton community. Therefore, the contribution of either community to the total biomass of phytoplankton in the upper Bay, as well as the potential for phytoplankton of either community to become entrapped in the ETM, will depend on the circulation and the volume of water in each layer, the vertical distribution of the communities, and the other physical factors discussed in this section.

Diatoms

A number of analyses have shown that phytoplankton biomass in the Chesapeake Bay is dominated by diatoms (Adolf et al., 2006; Marshall, 1994; Marshall et al., 2006) so we were not surprised to find that they were abundant in the upper Bay. The composition of the spring diatom communities that we observed in the upper Bay were also very similar to those reported by Marshall et al. (2006). Interestingly there were not many pennate diatoms in our samples suggesting that the suspension of benthic diatoms, which are mostly pennate species, may not be important even in this area of high physical resuspension (i.e. the ETM) and tidal scouring.

Small centric diatoms (< 10 μm) were common throughout the upper Bay and there were almost always > 150 cells ml^{-1} in all samples taken for microscopic analysis. Since we did not identify these small centric diatoms to the species level or take samples for genetic analysis we were unable to determine if they were the same species of diatom at either end of the transect or if seasonal succession occurred. However, it seems unlikely that the exact same species were be present from season to season or throughout the upper Bay as the environmental conditions (i.e. light, temperature, salinity, etc.) changed substantially on both a temporal and spatial basis.

The presence of diatoms (both live and dead) in the bottom, most saline waters on some of the transects (see Fig. 9 for an example) is very likely due to northward bottom water transport from the mesohaline portion of the Bay. Phytoplankton, including diatoms, can be very abundant in this region (Adolf et al., 2006) and it is thought that much of the phytoplankton biomass sinks and provides a substrate for the planktonic and benthic respiration that is the mechanism behind seasonal anoxia throughout a large extent of the Chesapeake Bay (Kemp et al., 1997b; Malone et al., 1988). While most of the research on this subject has focused on the sinking of the spring phytoplankton bloom, our data suggests that fall and winter diatom communities in the mesohaline portion of the Bay may also sink and accumulate in bottom waters where they would be subjected to northward transport. Phytoplankton that sink during the fall and winter would not die or degrade as quickly as at other times of the year because low temperatures would help to preserve them by limiting microbial growth and consumption (Shiah and Ducklow, 1994a, b). Low temperature and light levels also slow the degradation of phytoplankton detritus and chlorophyll *a* (Mayer et al., 2009; Nelson, 1993; SooHoo and Kiefer, 1982a, b). Thus, these diatoms could accumulate all fall and winter and be subjected to northward gravitational circulation transport. However, it is difficult to determine if they play an important role in the upper Bay because their northward movement is likely restricted by distance and steep shoaling of the channel between the upper and middle Bay.

Dinoflagellates

Previous research has indicated that the southern portion of the upper Bay, where the depth of the main channel shoals, experiences dinoflagellate blooms in the spring

(Adolf et al., 2006). However, it was unclear from these studies if dinoflagellates played an important role in the upper Bay or the ETM food web. Our results suggest that these dinoflagellates are an important part of the phytoplankton community in the upper Bay during the winter and spring. Especially, since they exhibit some unique behavior such as vertical migration and mixotrophy.

Vertical migration is common among many dinoflagellate species (Ji and Franks, 2007) and appears to be important for the species found in this region of the Bay. The distribution of dinoflagellates in the water column is somewhat misleading in our plots because samples at this station were taken in the morning just after sunrise. At this time of the day all of the dinoflagellates tended to be concentrated in a layer just below the pycnocline. However, occasional sampling at these stations in the afternoon (data not shown) revealed that these dinoflagellates may migrate toward the surface during the day, as was evident by a more even distribution of chlorophyll *a* from the surface down to just below the pycnocline (although there was still often a noticeable subsurface chlorophyll *a* maximum). Unfortunately, we did not sample at a high enough frequency or over a 24 hr period to capture the full dynamics of this migration. Interestingly, when dinoflagellates were found at the most northern station in fresher water they were often concentration at either the surface or the bottom even though the area is shallow and the water appeared to be uniformly mixed. All of these results raise the question as to whether or not these dinoflagellates are be able to control their position in the estuary by migrating vertically and moving either southward with the surface layer or northward in the bottom layer. Unfortunately we again did not collect enough data to determine, the extent to which, or if, they use migration to maintain their position in the estuary. However, bi-layer

distribution of *P. minimum* with northward and southward moving populations have been observed in this region (Tyler and Seliger, 1978).

The physiological characteristics and behavior of dinoflagellates in combination with Bay-wide physical circulation is likely responsible for the presence of some of the dinoflagellates at the southern end of our transects. Tyler and Seliger (1978) first described the northward subsurface transport of the dinoflagellate now known as *P. minimum* from the southern portion of the Bay to a location that overlaps with the southern end of our transect. The mechanism proposed by Tyler and Seliger (Tyler and Seliger, 1978, 1981) begins in the winter at the mouth of the Bay where *P. minimum* populations are present year round in southern high-salinity tributaries and in the Chesapeake Bay plume itself. Positive phototaxis and convergent downwelling at plume frontal regions cause *P. minimum* to form subsurface biomass maxima. Increases in Susquehanna and Potomac River flow then provide the driving force to enhance stratification in the Bay and induce strong gravitational circulation. Once the Bay is stratified, repression of positive phototaxis at the salinity interface prevents *P. minimum* from crossing the halocline. Thus, resulting in northward transport with the bottom layer. When *P. minimum* nears the area at the southern end of our transects there is a sharp change in depth from over 30 m to 10 m. Upon encounter this sharp change in bathymetry the northward flowing bottom water is subjected to vertical advection that may enhance mixing and force *P. minimum* to the surface or reduce phototactic repression and allow vertical migration to occur. Thus, the presence of *P. minimum* in our spring samples is likely a result of these transport mechanisms. However, in the winter and early spring *H. rotundatum* was often by far the most abundant dinoflagellate

in our samples. Other studies have also identified this area as a location where blooms of dinoflagellates including both *P. minimum* and *H. rotundatum* frequently occur in the spring (Adolf et al., 2006; Marshall et al., 2006). Whether *H. rotundatum* is transported from farther down the Bay like *P. minimum* or originates from other potential sources such as tributaries like the Chester River or local cyst beds is unknown. However, in the Potomac, Patuxent, Patapsco, Magothy, and Severn Rivers, all tributaries of the Chesapeake Bay, winter blooms of *H. rotundatum* have been observed and are thought to be common (Cohen, 1985; Sellner et al., 1991; Tyler and Seliger, 1989). Tyler and Seliger (1989) also suggest that *H. rotundatum* can be swept out of these tributaries and into the bay proper during transient storm events. Thus, it is very likely that some of the dinoflagellates that we observed originated in upper Bay tributaries while others may have come from a resident Bay population.

Peridinin was often non-linearly correlated with salinity (Fig. 4.4, 4.10, 4.15, 4.20), suggesting that these dinoflagellate species preferred a certain range of salinity. This was especially evident in February of 2007 when the dinoflagellate community was composed almost entirely of *H. rotundatum*. These results are not surprising considering that many estuarine dinoflagellates prefer a certain range of salinity (Paerl et al., 2006). Interestingly, this non-linear correlation with salinity was the inverse of the relationship between diatoms and salinity. Thus, suggesting that environmental conditions may favor one group over another, that competition could be occurring between dinoflagellates and diatoms, and/or that they experience different levels mortality in this region depending on their location in the water column. However, further study would be needed to understand the reasons behind these correlations with salinity.

The dinoflagellate species (*H. rotundatum*, *P. minimum*, and *K. micrum*) that were abundant to the south of the ETM in 2007 and 2008 are all species that have been reported to be mixotrophic (Jeong et al., 2005; Li et al., 1999; Li et al., 1996). Furthermore, both *P.minimum* and *K. micrum* are known to prey on cryptophytes (Li et al., 1999; Li et al., 1996). Perhaps this was why there was a correlation between alloxanthin and peridinin (Fig. 4.7) in the winter and early spring (i.e. dinoflagellates were in the area to prey on cryptophytes). Although it is also possible that some other physical process or physiological requirement resulted in the overlap of these two phytoplankton groups. The abundance of these mixotrophic dinoflagellates in the upper Bay also has important implications for the food web as these species could occupy multiple trophic levels and contribute to both primary and secondary productivity in the region. Furthermore, mixotrophic dinoflagellates that become trapped in the ETM would also likely be able to survive longer without light than a true autotroph because they could acquire carbon heterotrophically.

Cryptophytes and Other Phytoplankton Groups

Previous analyses have shown that cryptophytes are common throughout the Bay as a characteristic component of the flora, and contribute substantially to Bay-wide phytoplankton biomass (Marshall et al., 2006). So we were not surprised to find that they were abundant in the upper Bay. Since we did not identify them to the species level or take samples for genetic analysis we were unable to determine if they were the same species all along the transect or if seasonal succession occurred. However, it seems unlikely that the exact same species were be present from season to season or throughout

the upper Bay as the environmental conditions changed substantially on both a temporal and spatial basis.

Other types of phytoplankton such as chlorophytes and cyanobacteria were occasionally present in the upper Bay. However, these groups almost never accounted for a very large portion of the phytoplankton community biomass. Therefore, they are probably only important members of the phytoplankton community in other seasons or during infrequent environmental perturbations that allow them to bloom or result in their transport into the region.

Pigment Degradation Products

The presence of high concentrations of phytoplankton pigment degradation products in the upper Bay indicates that substantial phytoplankton mortality occurs in this region. Pigment degradation products were often concentrated in the ETM, along the halocline, and in the bottom water at the southern end of the transects. They were also occasionally associated with areas of high chlorophyll *a* and other accessory pigments. The presence of degradation products in these areas was either the result of either local phytoplankton mortality (i.e. salinity stress, grazing, etc.) or due to the transport of deceased phytoplankton into the area (i.e. ETM entrapment, gravitational circulation, sinking). However, it is difficult to interpret some of the pigment degradation product patterns that we observed because these products are rapidly degraded when exposed to light or warm temperatures (Mayer et al., 2009; Nelson, 1993; SooHoo and Kiefer, 1982a, b) and thus often do not accumulate in surface waters. This makes it difficult to compare these patterns vertically or to infer the amount of phytoplankton mortality at the

surface. However, in areas where light or warm temperatures have not degraded these products, specific ones provide useful information about phytoplankton mortality.

Although caution must be taken when interpreting the presence of pheophorbide *a* and chlorophyllide *a* as indicators of predation and senescence (Louda et al., 1998), the elevated presence of these compounds in certain areas along the transects, and our knowledge of potential causes of mortality in this region of the Bay, does seem to suggest possible mechanisms of phytoplankton mortality. The presence of high concentrations of chlorophyllide *a* in the ETM, at the surface in salinities of 2-8, and in the deepest waters at the southern end of the transects suggests that senescent diatoms were abundant in these areas (Jeffrey, 1974, 1980; Jeffrey and Hallegraeff, 1986). A number of mechanisms could be responsible for diatom mortality in salinities between 2-8 and their presence in the ETM. As previously discussed, salinity stress is likely to be a major agent of mortality during transport for freshwater phytoplankton, which were mostly diatoms, from the Susquehanna River or the shallow "flats" region immediately to the north of our study area. Many studies have shown that as river water mixes with estuarine water at around salinities of 5-8 the biomass and diversity of plants and animals goes through a minimum (Muylaert and Sabbe, 1999). Deceased phytoplankton are more likely to sink than live ones (Smayda, 1970) and sinking phytoplankton in this region of the Bay are likely to become entrapped in the ETM. Live diatoms could also potentially sink and become entrapped in the ETM. As measurements of the amount of chlorophyll *a* that sinks out of the water column show (Fig. 4.32) there are differences between ETM, fresh, and saltwater samples, possibly because high turbidity enhances phytoplankton aggregation and promotes sinking (Thornton, 2002). The ETM is also an area of high

turbidity, which limits light penetration and it is possible that light limitation could cause mortality and subsequent sinking. Estimates of light availability and analyses of primary productivity during our cruises, which will be presented in a separate article, suggest that phytoplankton in this area were often light limited, but that there were also occasion when light did not appear to be limiting even though turbidity was high. The presence of chlorophyllide *a* in the deepest waters at the southern end of the transects was likely due to diatom senesce in the mesohaline portion of the Bay and subsequent transport northward in bottom waters due to gravitational circulation (see discussion above). The presence of high concentrations of pheophorbide *a* in Feb in the ETM suggests that predation was occurring (Shuman and Lorenzen, 1975) in this area. High levels of predation in the ETM would be possible if phytoplankton were being transported to, and trapped here, as this area often has high concentrations of zooplankton (>200 copepods l^{-1}) at these times of year (Roman et al., 2001).

Particles in the ETM region are suspended and settle out again with most tides (Sanford et al., 2001). Our results (settling tube measurements) suggest that both living and dead phytoplankton in this region also undergo some degree of resuspension and settling along with other ETM particles. Thus, they are exposed to very different environmental conditions on relatively short time scales. The effect of this frequent transport on living or dead phytoplankton is unknown. However, cold temperatures in winter and spring, along with low light levels, will slow the degradation of phytoplankton derived detritus (Mayer et al., 2009; Nelson, 1993; SooHoo and Kiefer, 1982a, b) and could be responsible for the accumulation of pigment degradation products in the ETM. How long particles persist in the ETM before sedimentation and permanent burial is

unknown. However, the residence time of particles in the ETM is finite (Sanford et al., 2001) so phytoplankton derived detritus that is not consumed or transported elsewhere will eventually be buried.

Conclusion

The presence of high concentrations of phytoplankton in certain areas, as well as the constant presence of small centric diatoms and cryptophytes throughout the upper Bay suggests the potential for phytoplankton to be an important component of the ETM food web. Furthermore, the presence of a variety of pigment degradation products suggests that live phytoplankton are being consumed by zooplankton in the ETM, that phytoplankton may be dying in the ETM, and that senescent phytoplankton are being transported into the ETM. Hydrodynamic processes appear to control much of these phytoplankton dynamics and result in the formation of the two main phytoplankton communities in the upper Bay. Hydrodynamic processes also appear to play an important role in the mortality of these two communities through salinity stress and ETM entrapment. The amount of phytoplankton derived organic matter that reaches the ETM will depend on the relationship between estuarine circulation, the strength of ETM particle trapping, and phytoplankton community biomass distribution, productivity, and mortality. Since these factors can be highly variable, ETM phytoplankton entrapment will not always be strong. However, when conditions are favorable, phytoplankton entrapment in the ETM may be high. The role that these phytoplankton play in the ETM food web, which is known to support a substantial numbers of copepods (Kimmel and Roman, 2004; Roman et al., 2001), is unknown. However, phytoplankton are a major

component of macro- and microzooplankton diets in many food webs so it is likely that at least some of this phytoplankton derived organic matter is consumed.

The abundance of mixotrophic dinoflagellates in the upper Bay also has important implications for the transfer of energy through the food web as these organisms could contribute significantly to both primary and secondary regional productivity. Furthermore, the subsurface transport of *P. minimum,* and possibly other dinoflagellates, to the upper Bay is important because it results in the transfer of organic matter, in the form of phytoplankton biomass, from the southern portion of the Bay and it's tributaries to near the head of the bay, a distance of over 200 km. Thus, the population dynamics of dinoflagellates in the York River may ultimately influence zooplankton and larval fish growth in the ETM.

Figures

Figure 4.1. The upper Chesapeake Bay, USA. Axial CTD survey stations (all symbols) and water sampling stations (filled circle in a circle) in 2007 and 2008. Water sampling stations for April and May of 2007 are not indicated in this figure.

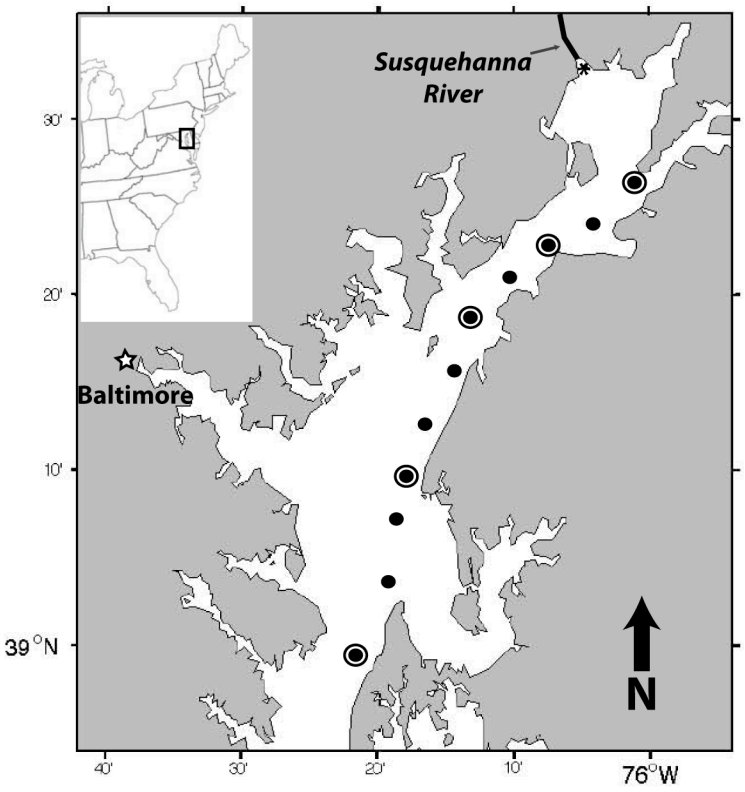

Figure 4.2. Contour plots of salinity (white dashed lines), turbidity, and the concentrations of chlorophyll degradation products along the main channel of the upper Chesapeake Bay on February 23, 2007. Sampling station locations are indicated by the open circles.

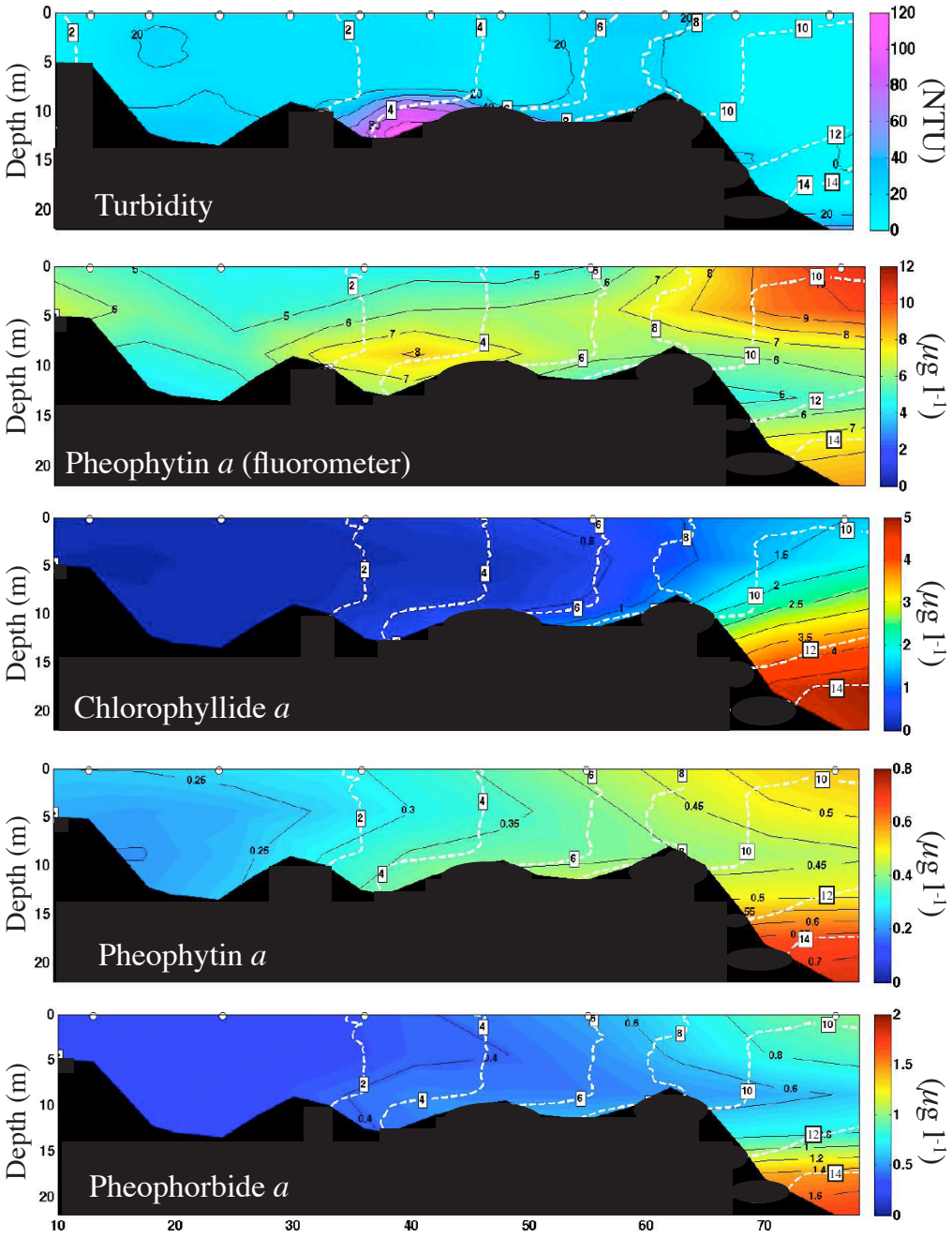

Figure 4.3. Contour plots of salinity (white dashed lines), turbidity, and the concentrations of chlorophyll degradation products along the main channel of the upper Chesapeake Bay on February 26, 2007. Sampling station locations are indicated by the open circles.

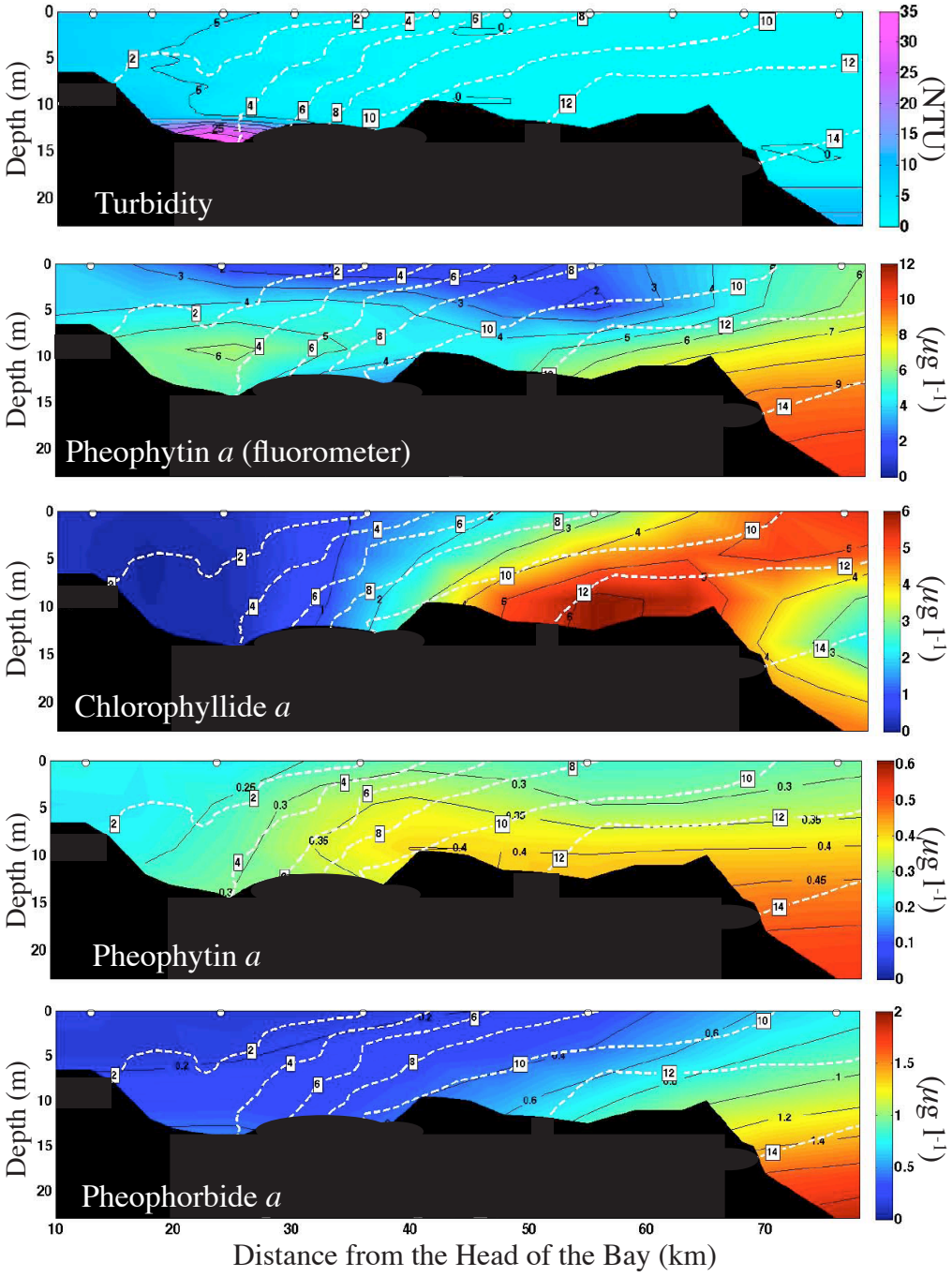

Figure 4.4. The concentrations of chlorophyll *a* and selected accessory pigments versus salinity in February 2007.

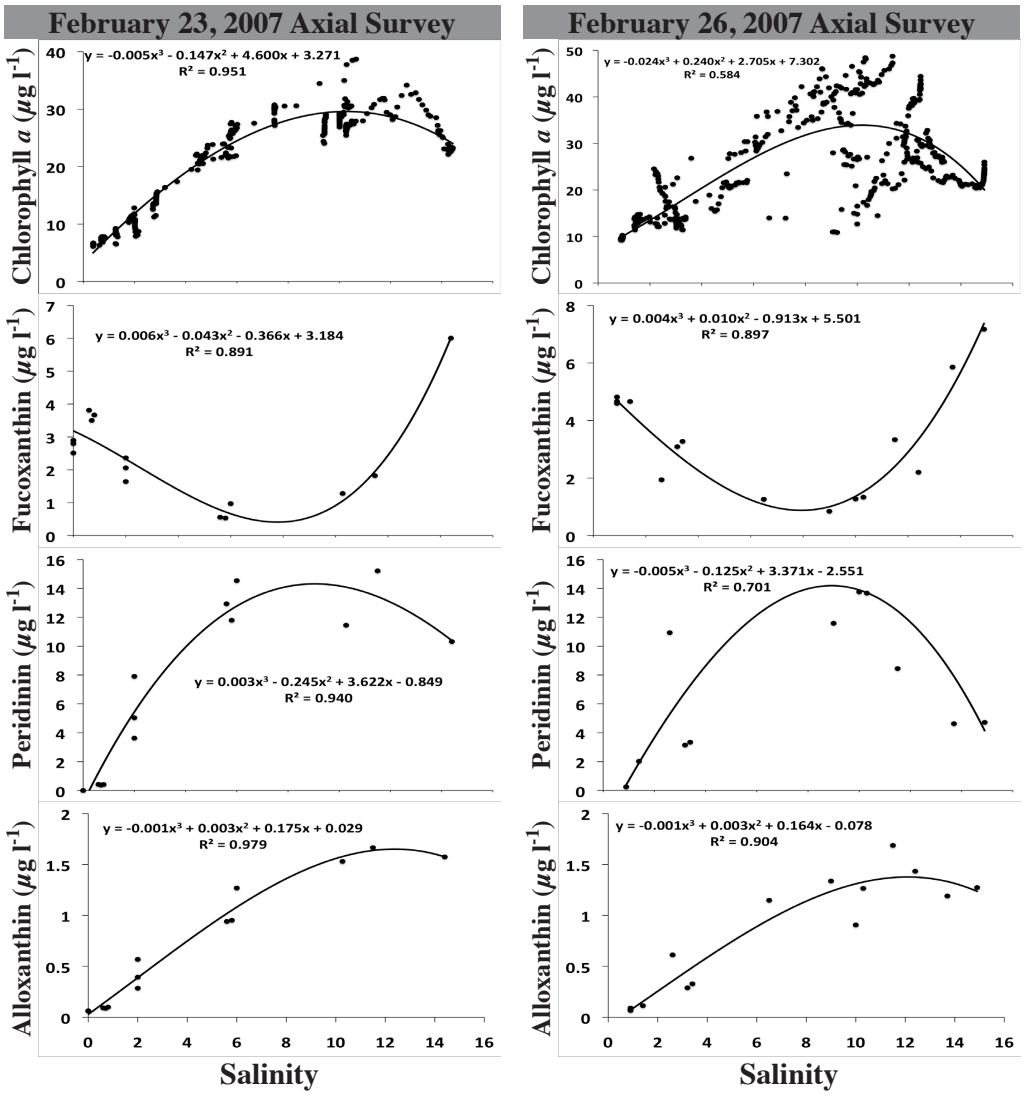

Figure 4.5. Contour plots of salinity (white dashed lines) and the concentrations of chlorophyll *a* and selected accessory pigments along the main channel of the upper Chesapeake Bay on February 23, 2007. CTD survey and water sampling station locations are indicated by the open circles.

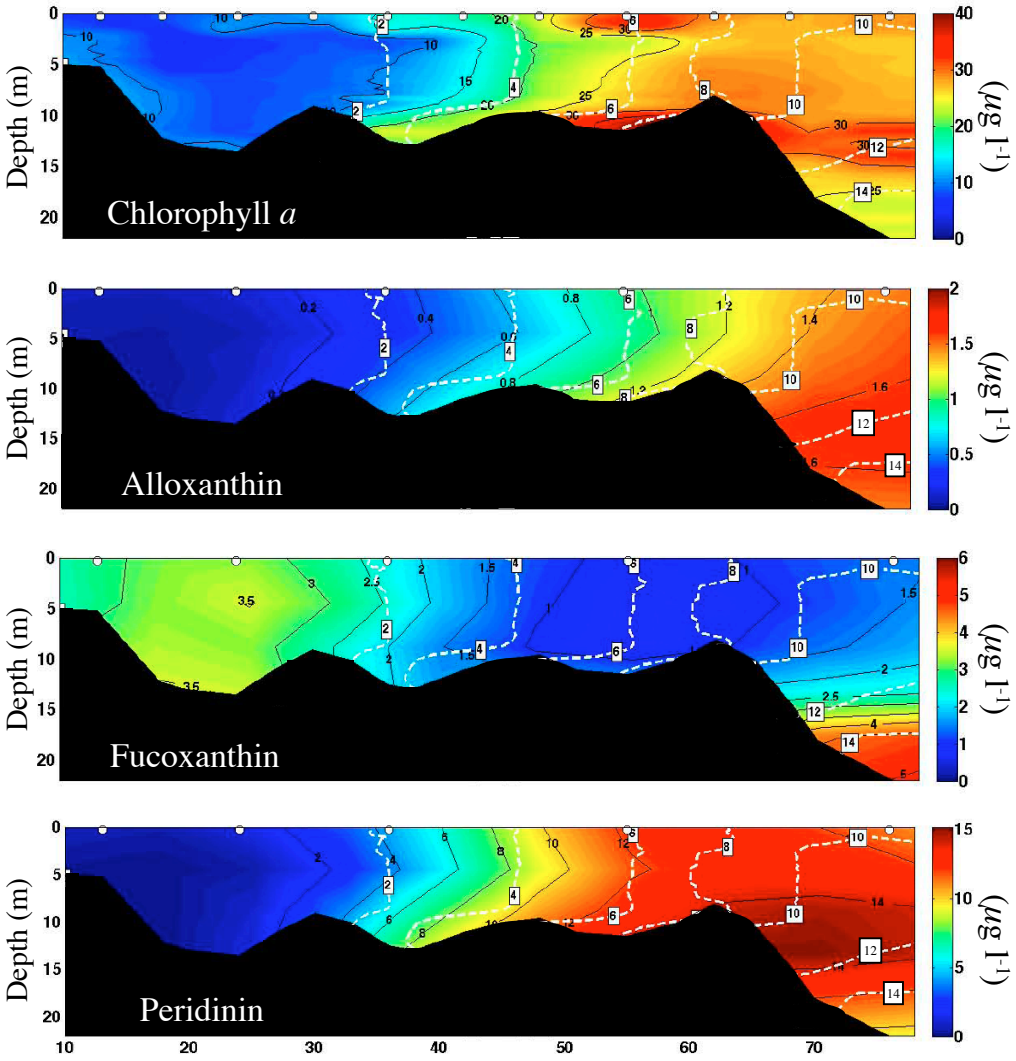

Figure 4.6. Contour plots of salinity (white dashed lines) and the concentrations of chlorophyll *a* and selected accessory pigments along the main channel of the upper Chesapeake Bay on February 26, 2007. CTD survey and water sampling station locations are indicated by the open circles.

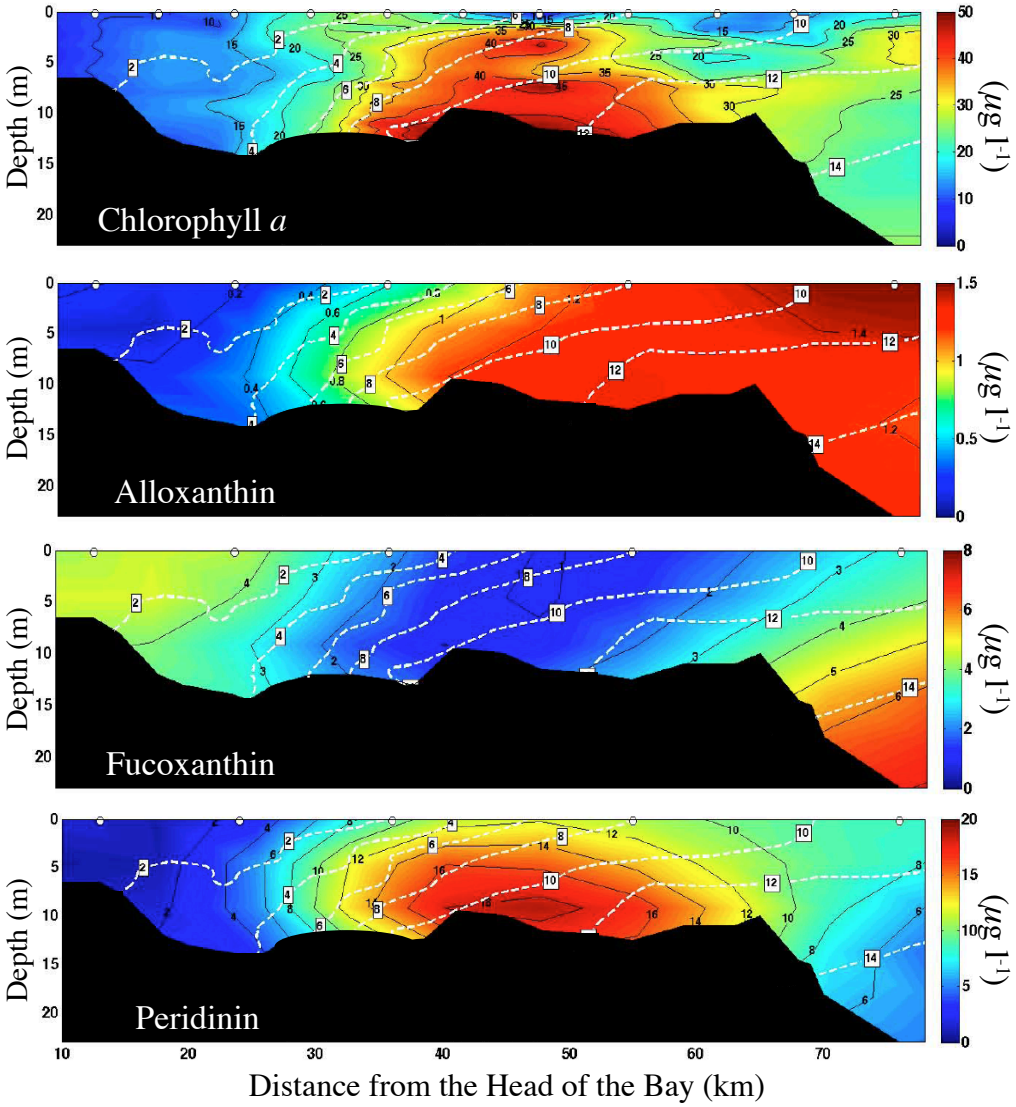

Figure 4.7. Alloxanthin versus peridinin pigment concentrations in the winter and early spring.

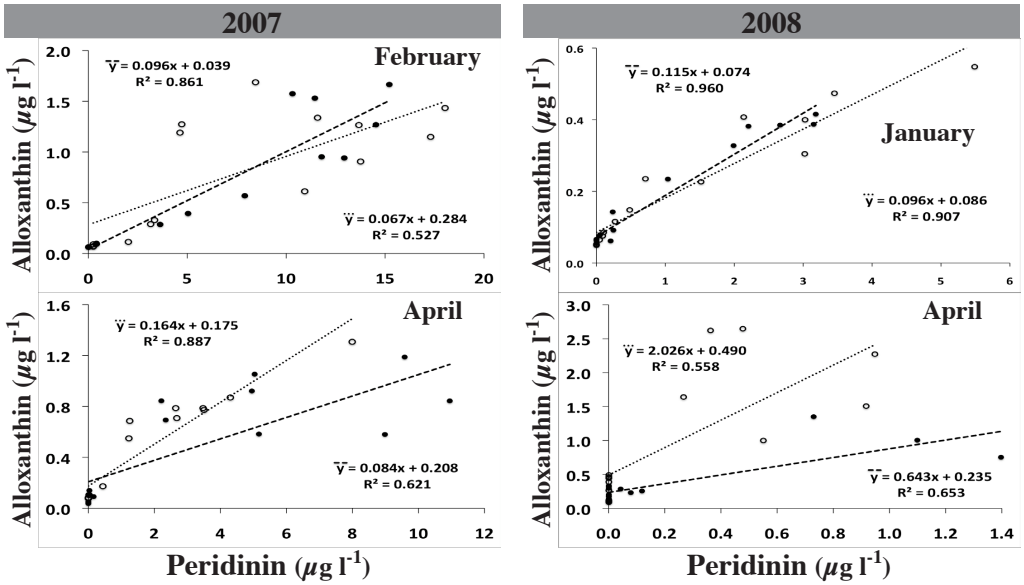

Figure 4.8. Contour plots of salinity (white dashed lines), turbidity, and the concentrations of chlorophyll degradation products along the main channel of the upper Chesapeake Bay on April 9, 2007. Sampling station locations are indicated by the open circles.

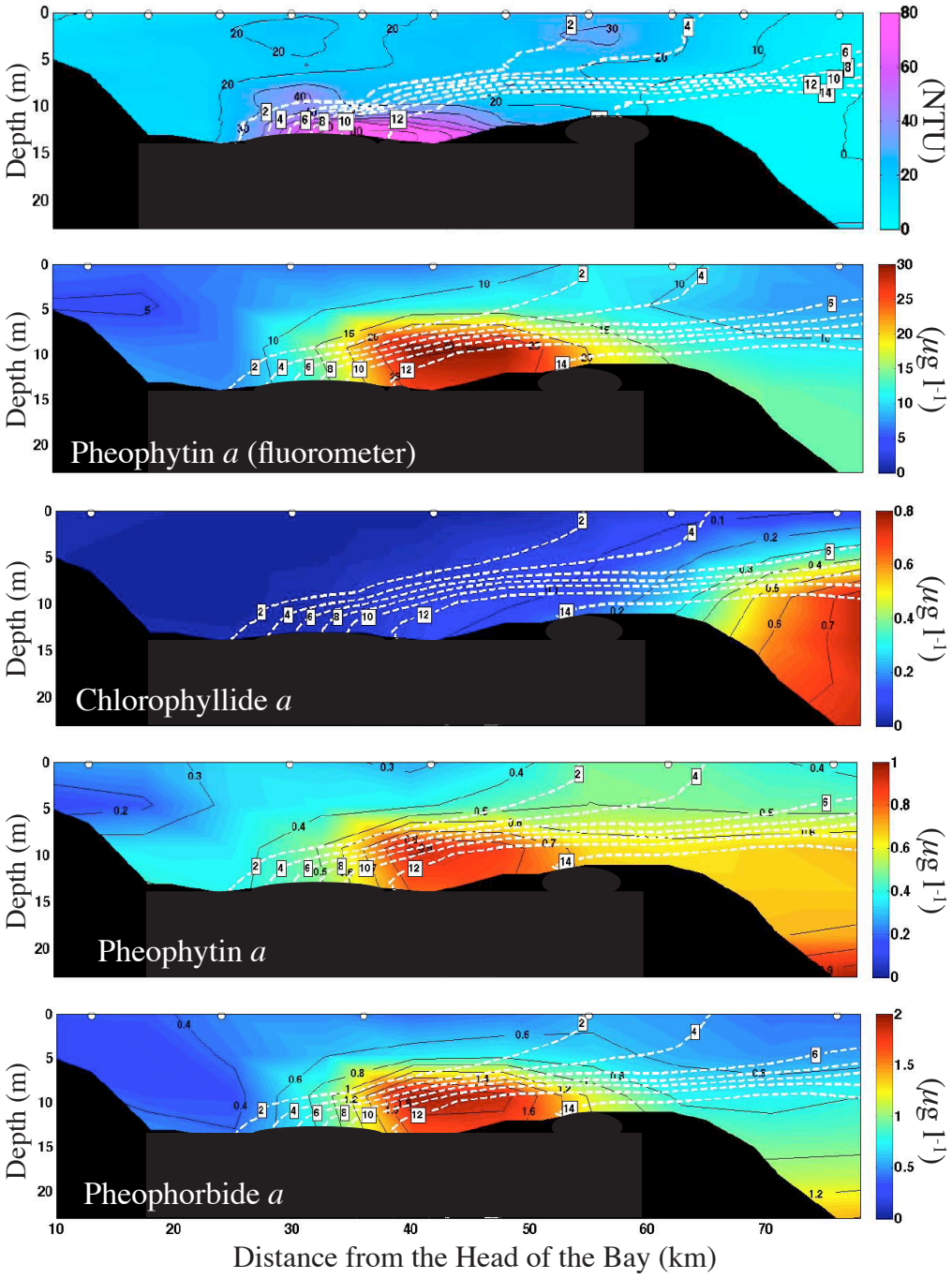

Figure 4.9. Contour plots of salinity (white dashed lines), turbidity, and the concentrations of chlorophyll degradation products along the main channel of the upper Chesapeake Bay on April 15, 2007. Sampling station locations are indicated by the open circles.

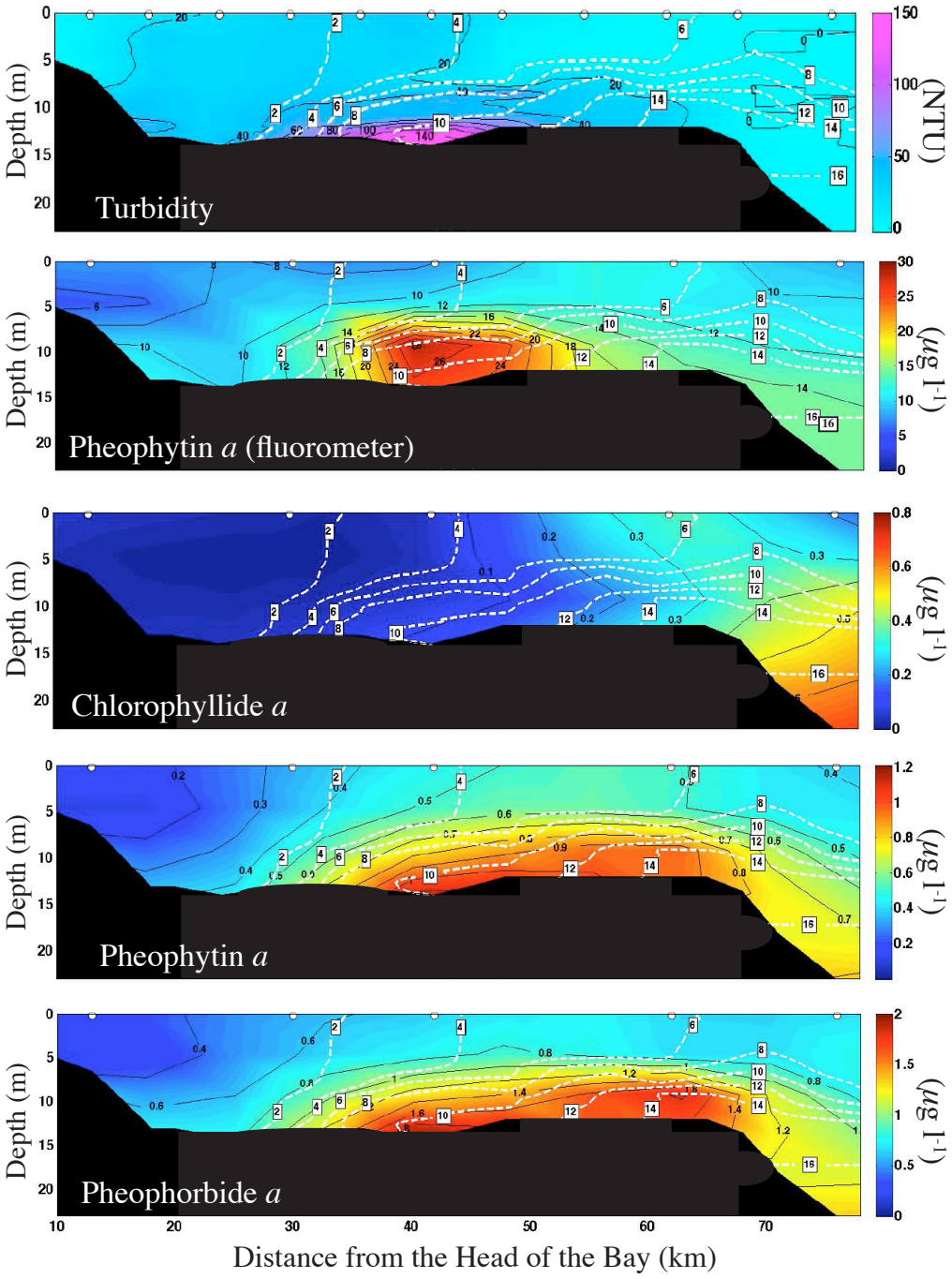

Figure 4.10. The concentrations of chlorophyll *a* and selected accessory pigments versus salinity in April 2007.

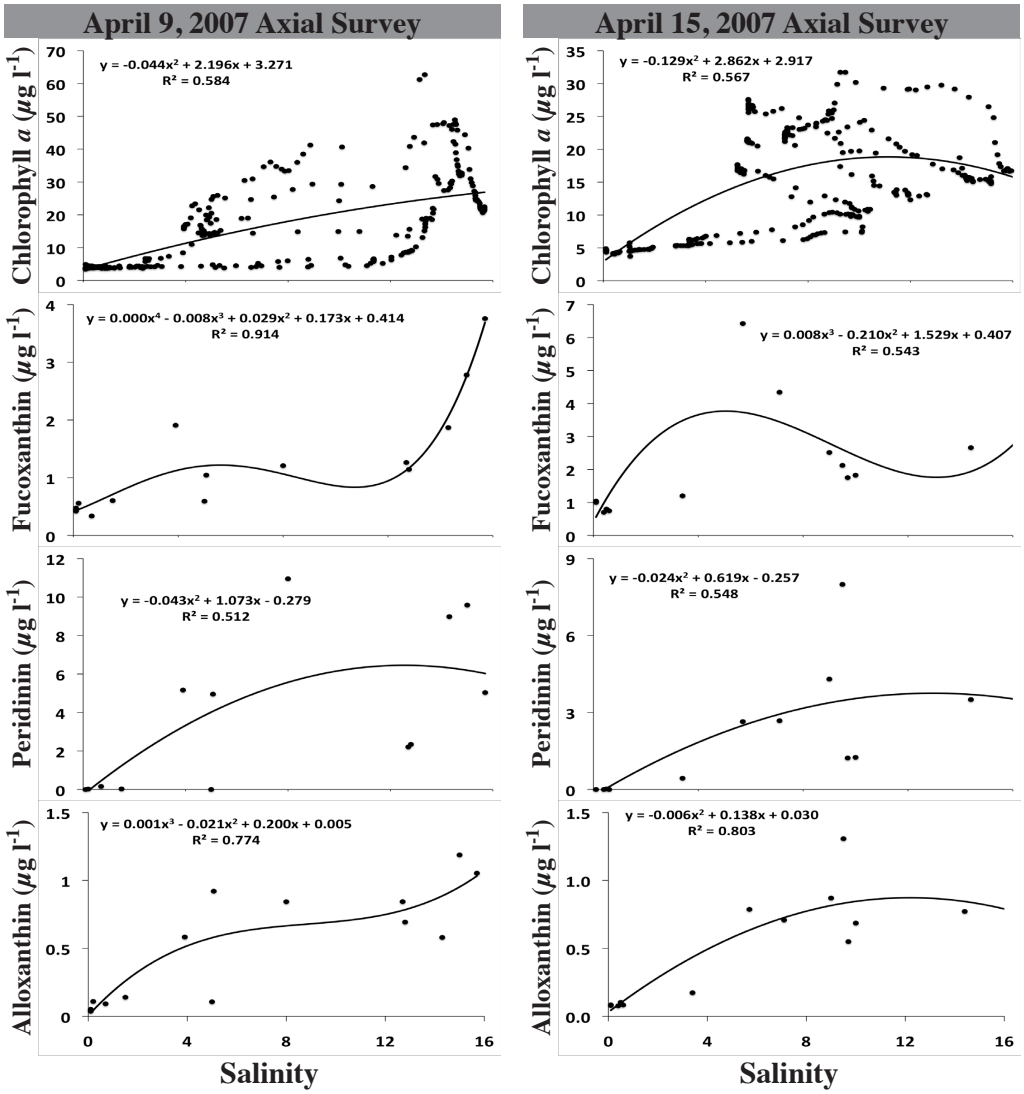

Figure 4.11. Contour plots of salinity (white dashed lines) and the concentrations of chlorophyll *a* and selected accessory pigments along the main channel of the upper Chesapeake Bay on April 9, 2007. CTD survey and water sampling station locations are indicated by the open circles.

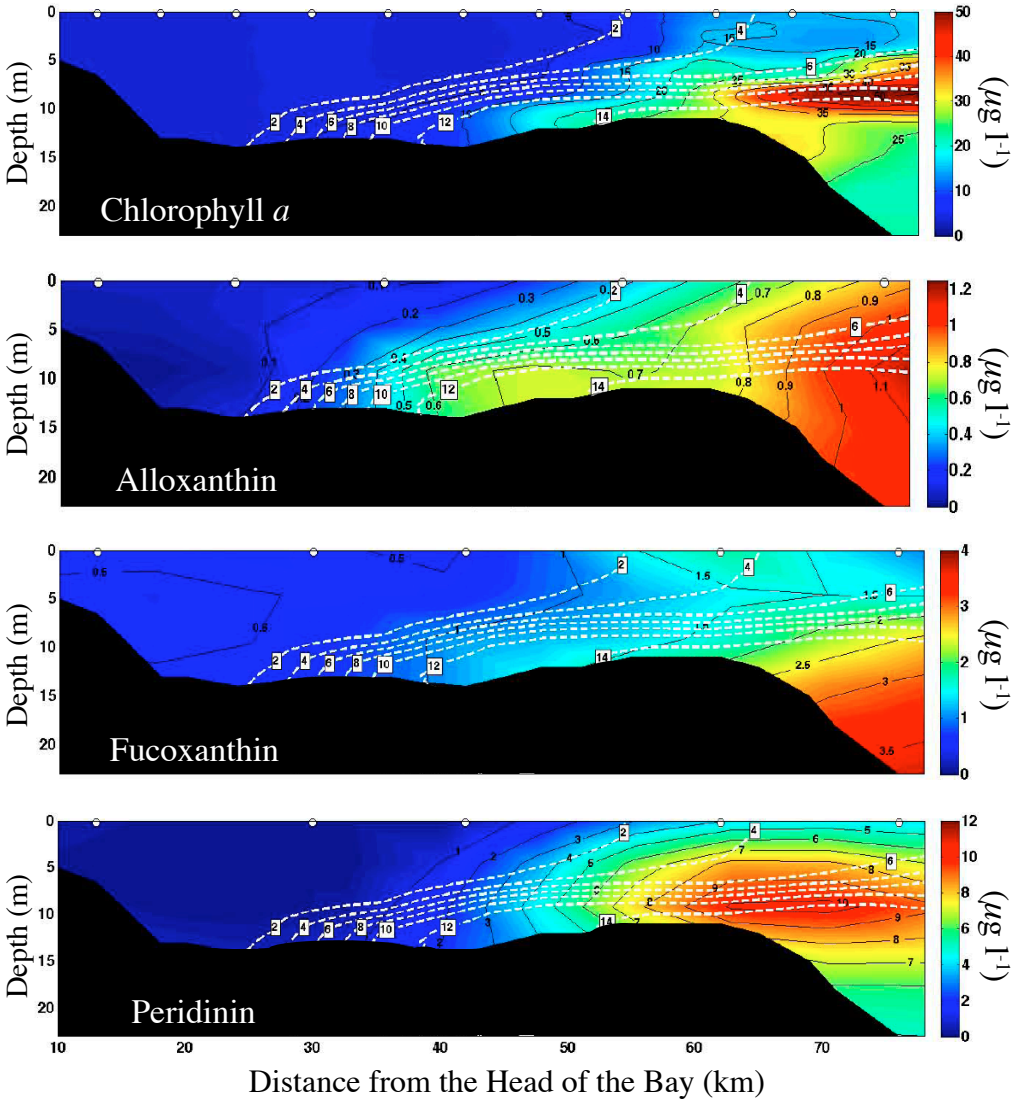

Figure 4.12. Contour plots of salinity (white dashed lines) and the concentrations of chlorophyll *a* and selected accessory pigments along the main channel of the upper Chesapeake Bay on April 15, 2007. CTD survey and water sampling station locations are indicated by the open circles.

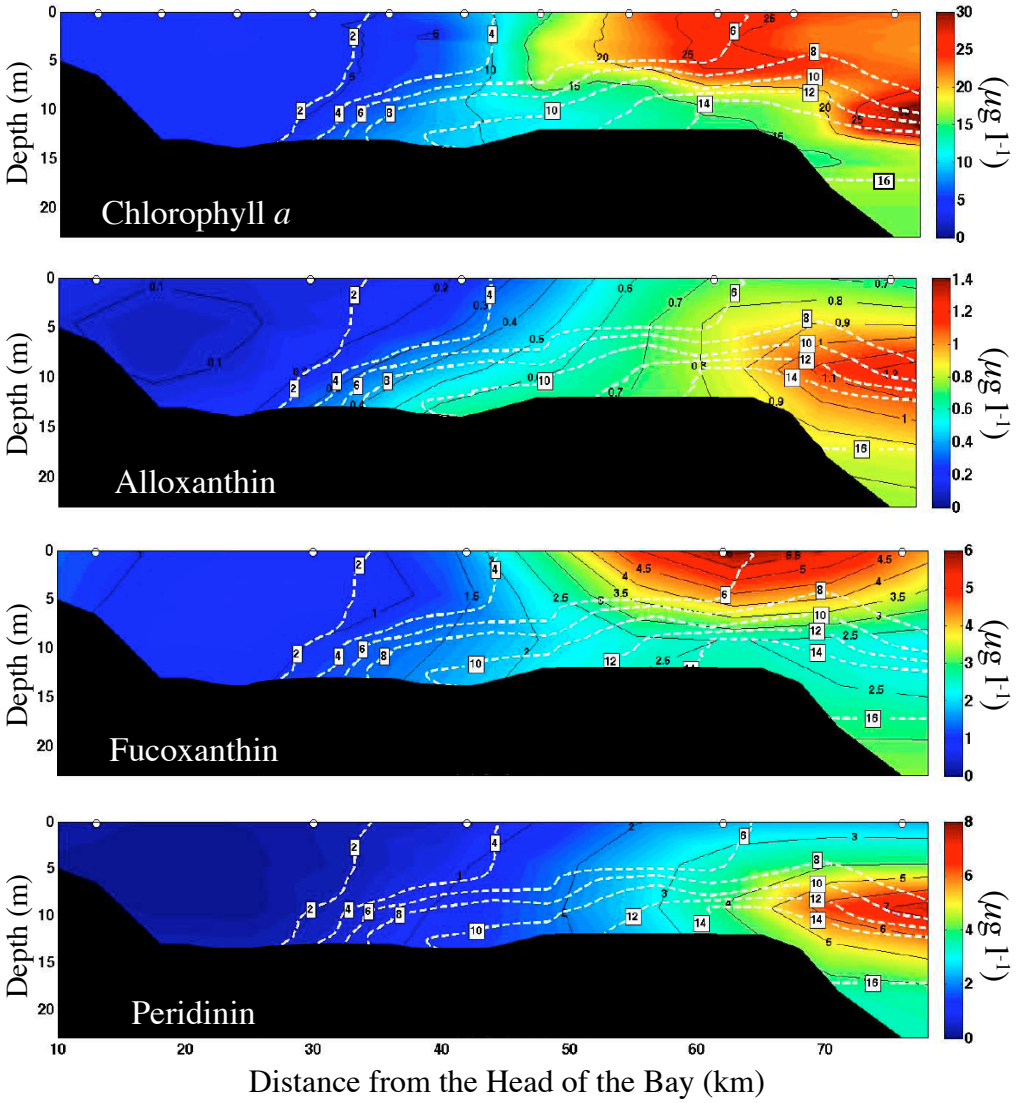

Figure 4.13. Contour plots of salinity (white dashed lines), turbidity, and the concentrations of chlorophyll degradation products along the main channel of the upper Chesapeake Bay on May 8, 2007. Sampling station locations are indicated by the open circles.

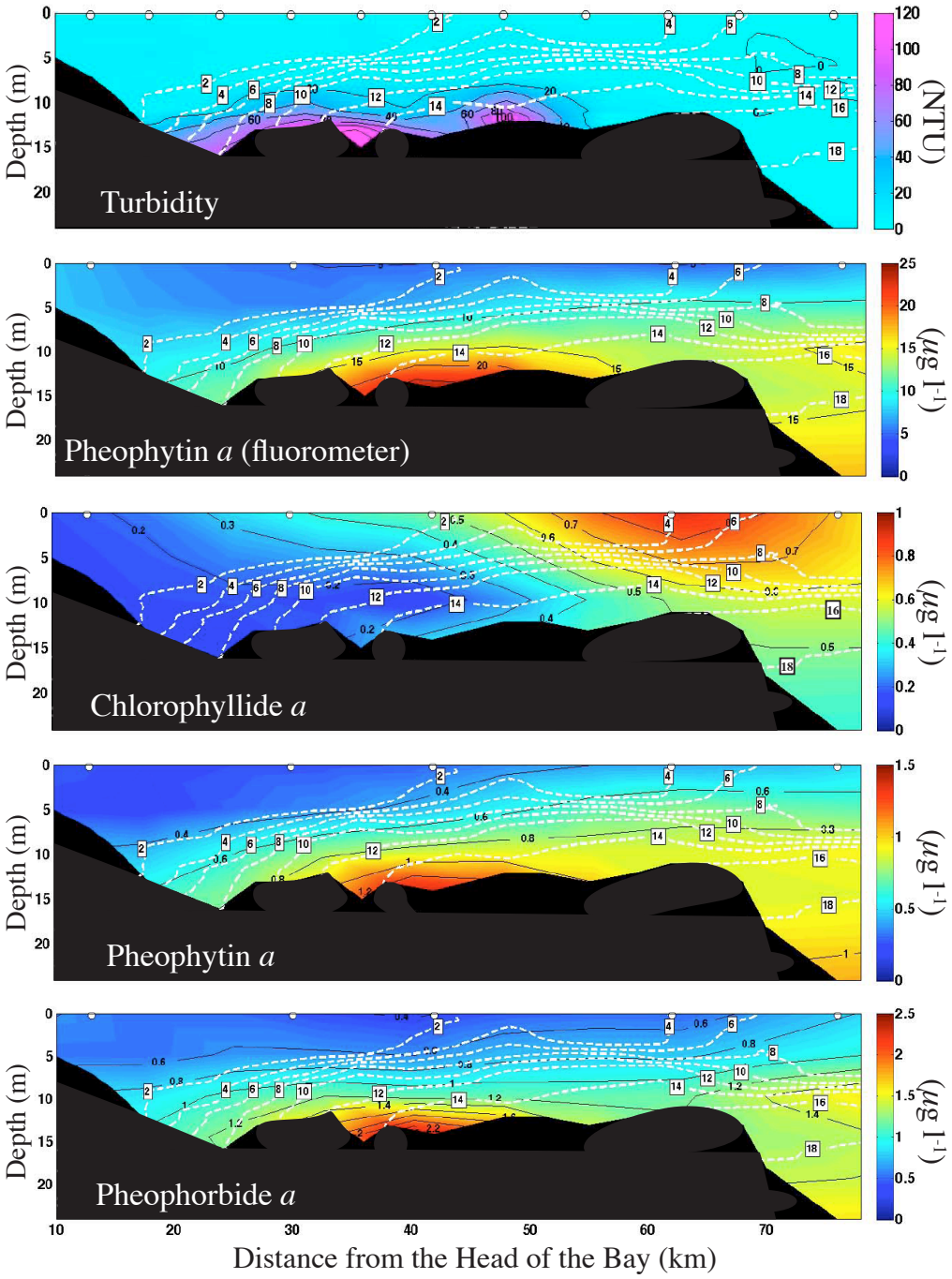

Figure 4.14. Contour plots of salinity (white dashed lines) and the concentration of chlorophyll degradation products along the main channel of the upper Chesapeake Bay on May 14, 2007. Sampling station locations are indicated by the open circles.

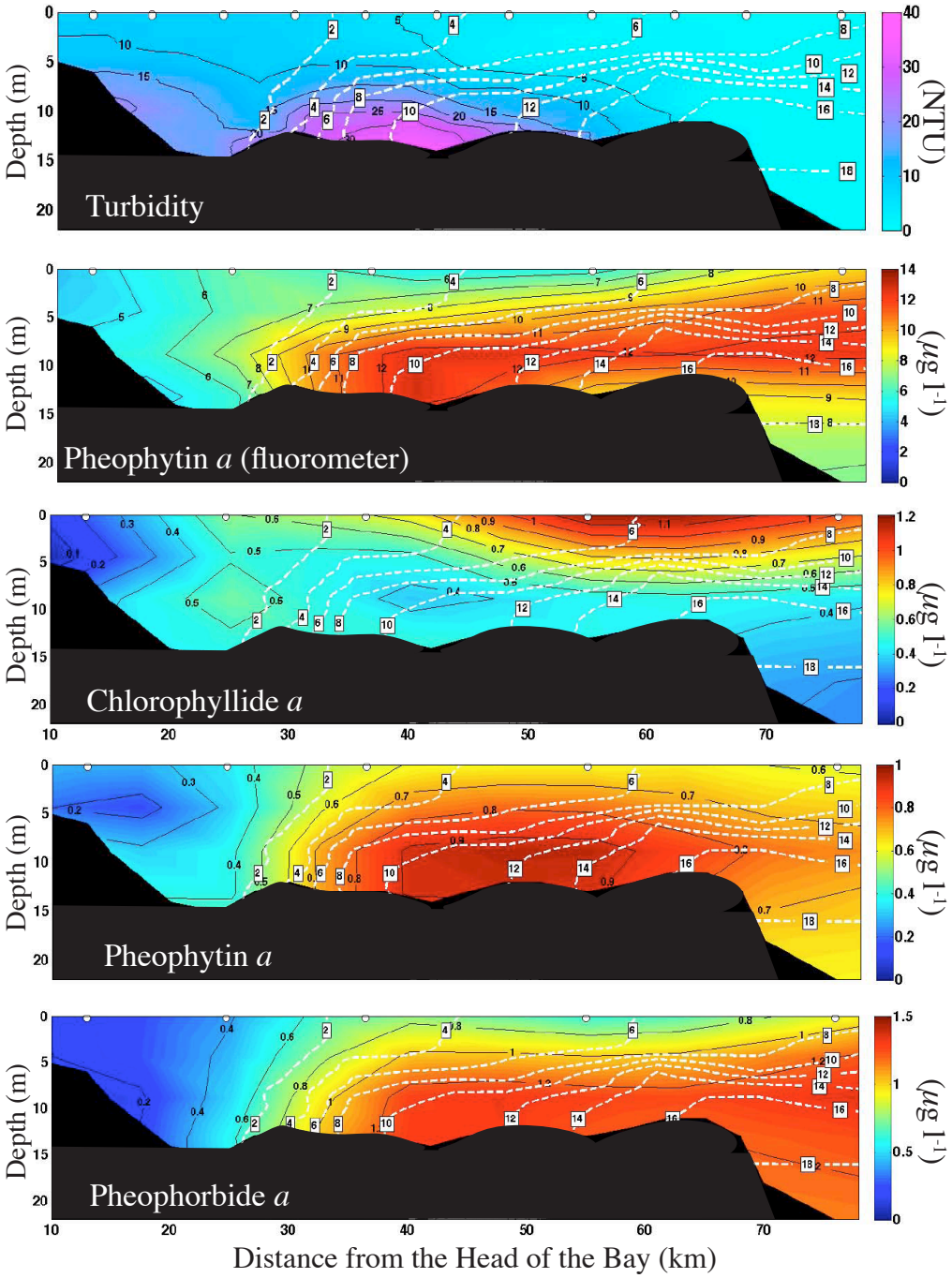

Figure 4.15. The concentrations of chlorophyll *a* and selected accessory pigments versus salinity in May 2007.

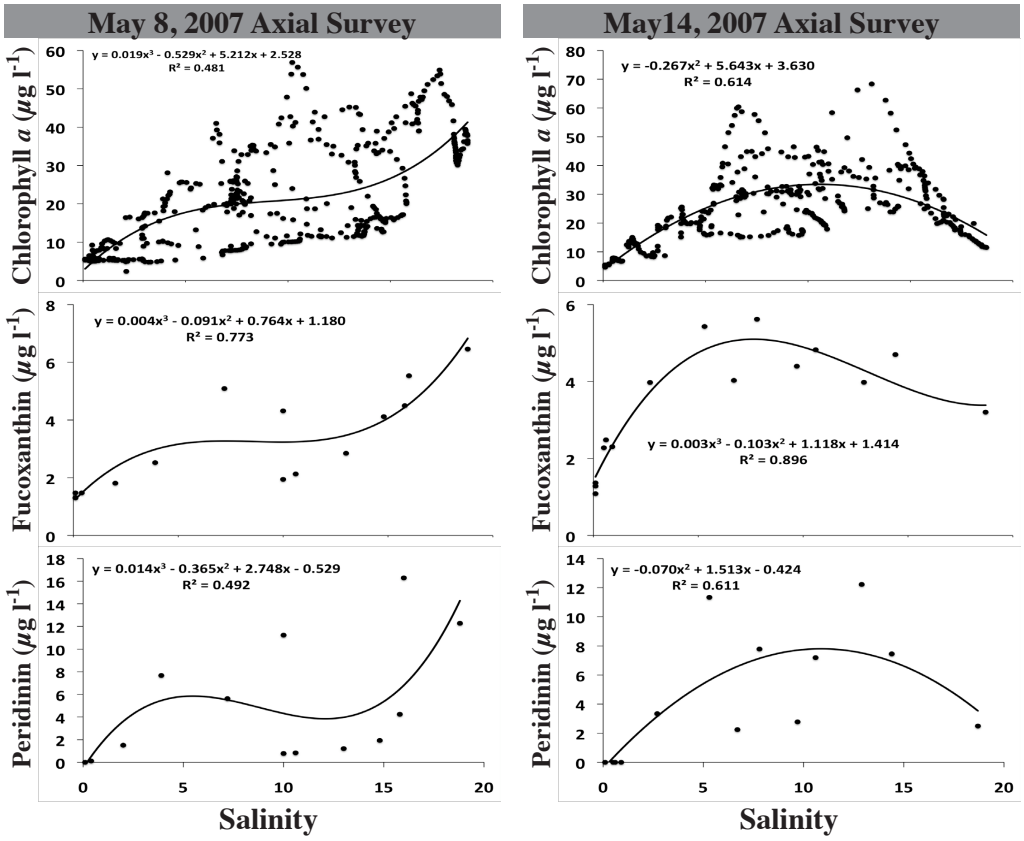

Figure 4.16. Contour plots of salinity (white dashed lines) and the concentrations of chlorophyll *a* and selected accessory pigments along the main channel of the upper Chesapeake Bay on May 8, 2007. CTD survey and water sampling station locations are indicated by the open circles.

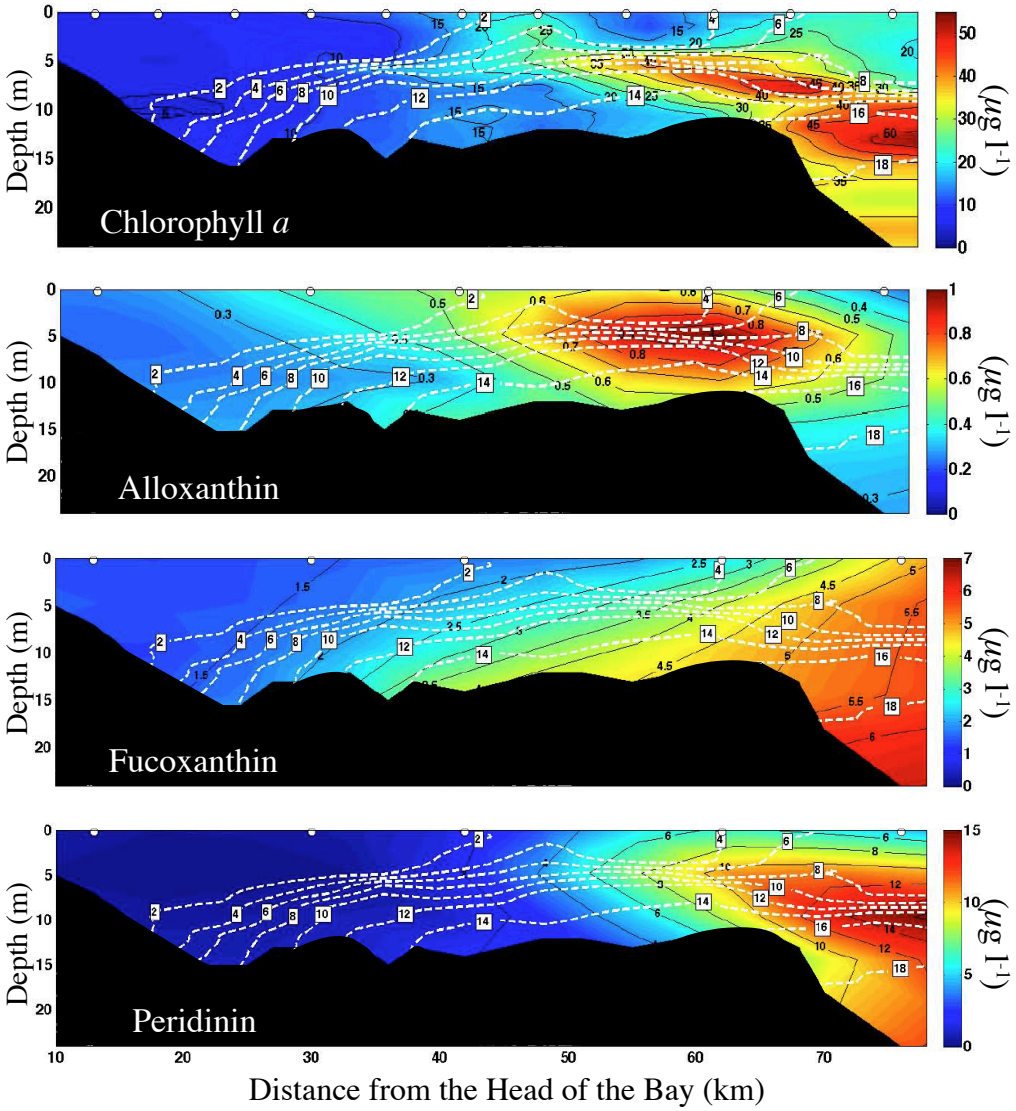

Figure 4.17. Contour plots of salinity (white dashed lines) and the concentrations of chlorophyll *a* and selected accessory pigments along the main channel of the upper Chesapeake Bay on May 14, 2007. CTD survey and water sampling station locations are indicated by the open circles.

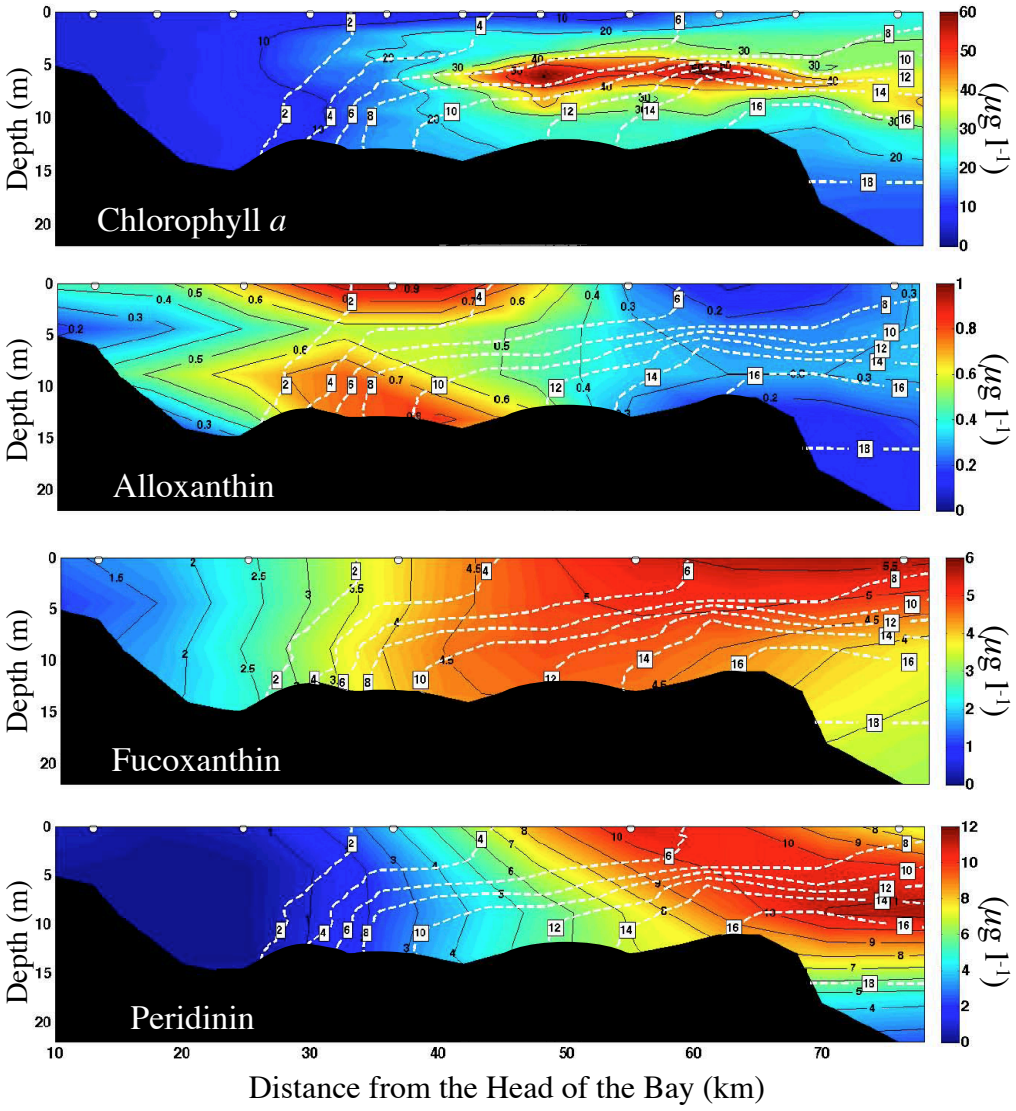

Figure 4.18. Contour plots of salinity (white dashed lines), turbidity, and the concentrations of chlorophyll degradation products along the main channel of the upper Chesapeake Bay on January 23, 2008. Sampling station locations are indicated by the open circles.

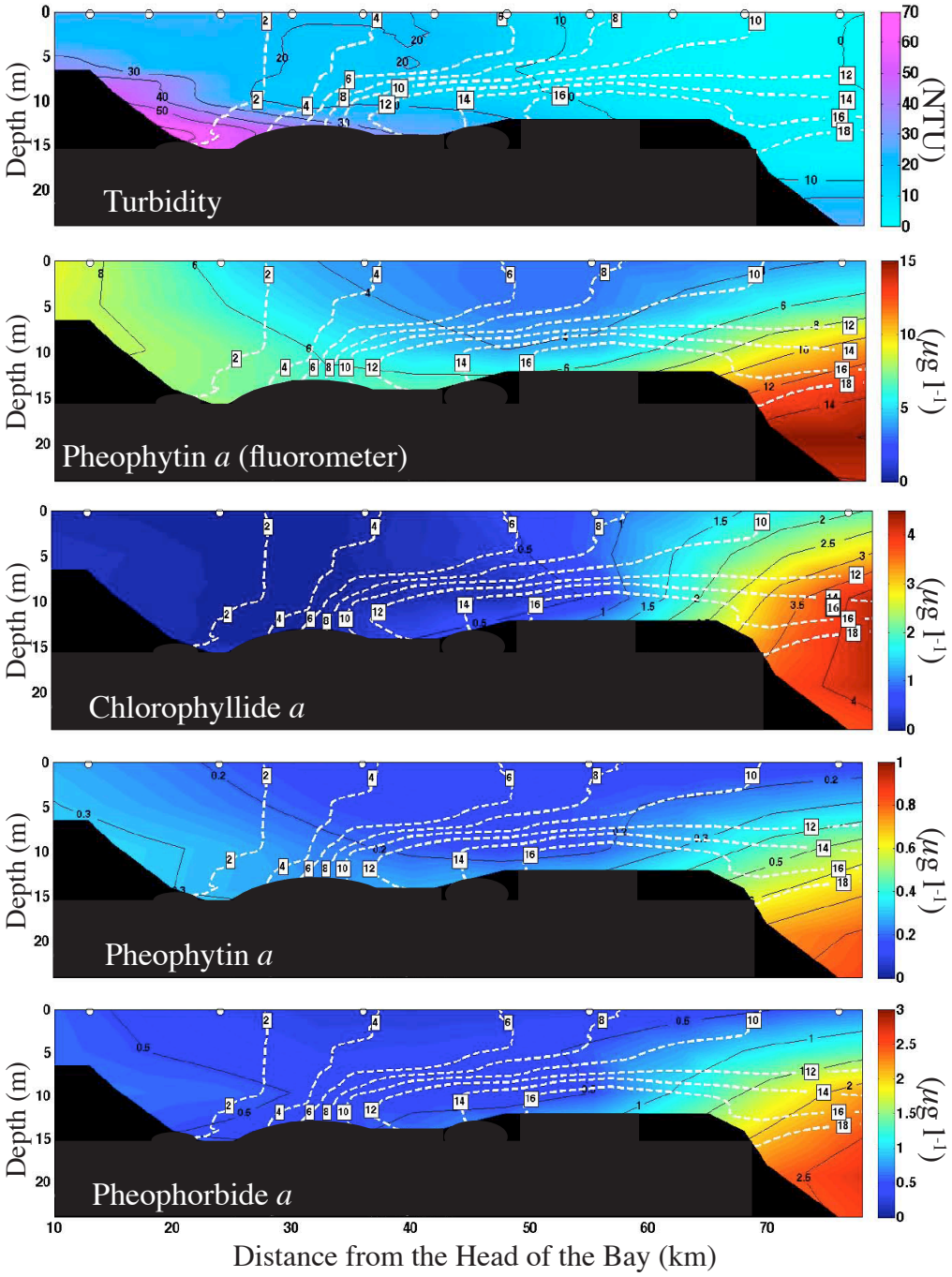

Figure 4.19. Contour plots of salinity (white dashed lines), turbidity, and the concentrations of chlorophyll degradation products along the main channel of the upper Chesapeake Bay on January 26, 2008. Sampling station locations are indicated by the open circles.

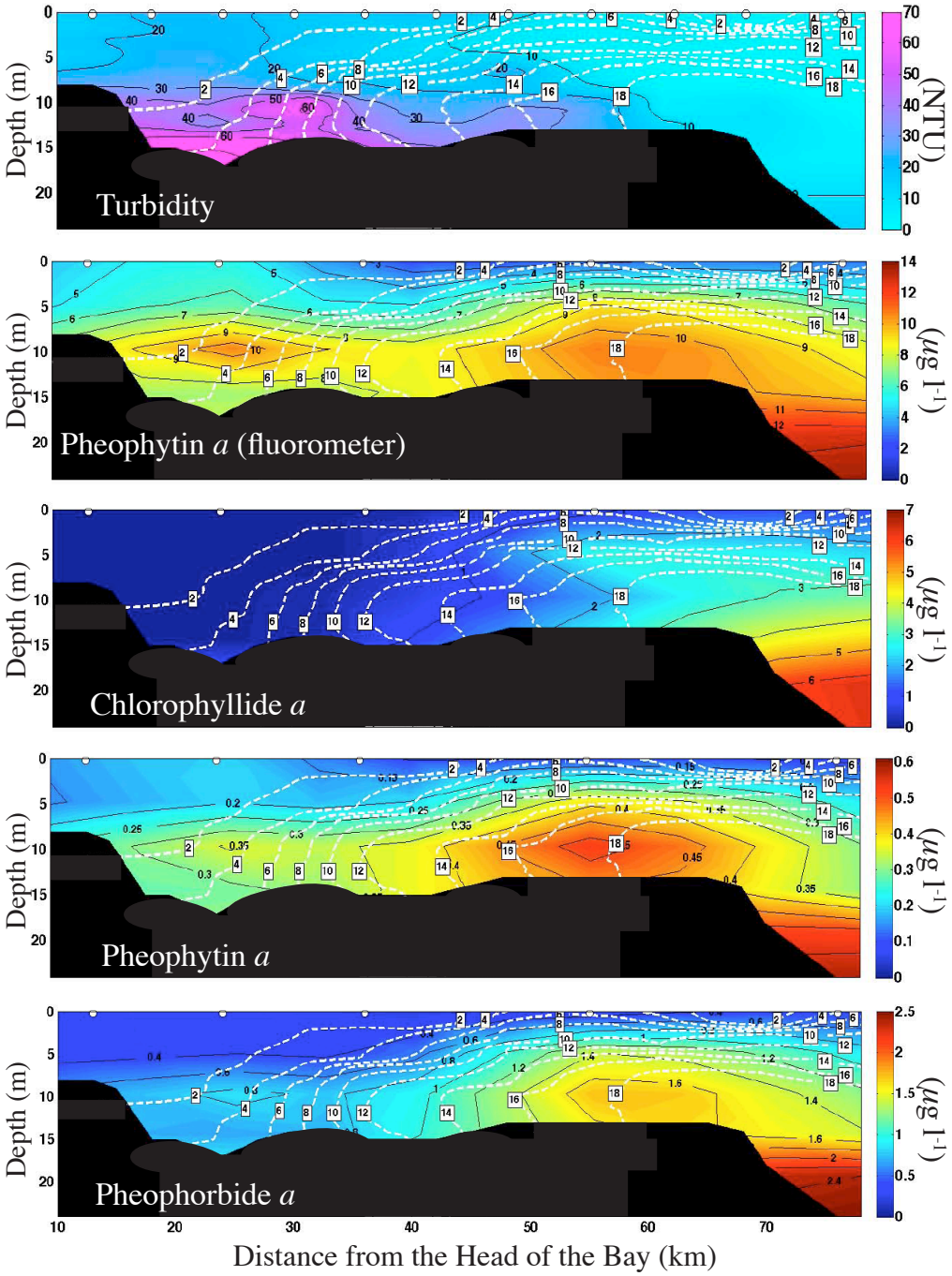

Figure 4.20. The concentrations of chlorophyll *a* and selected accessory pigments versus salinity in January 2008.

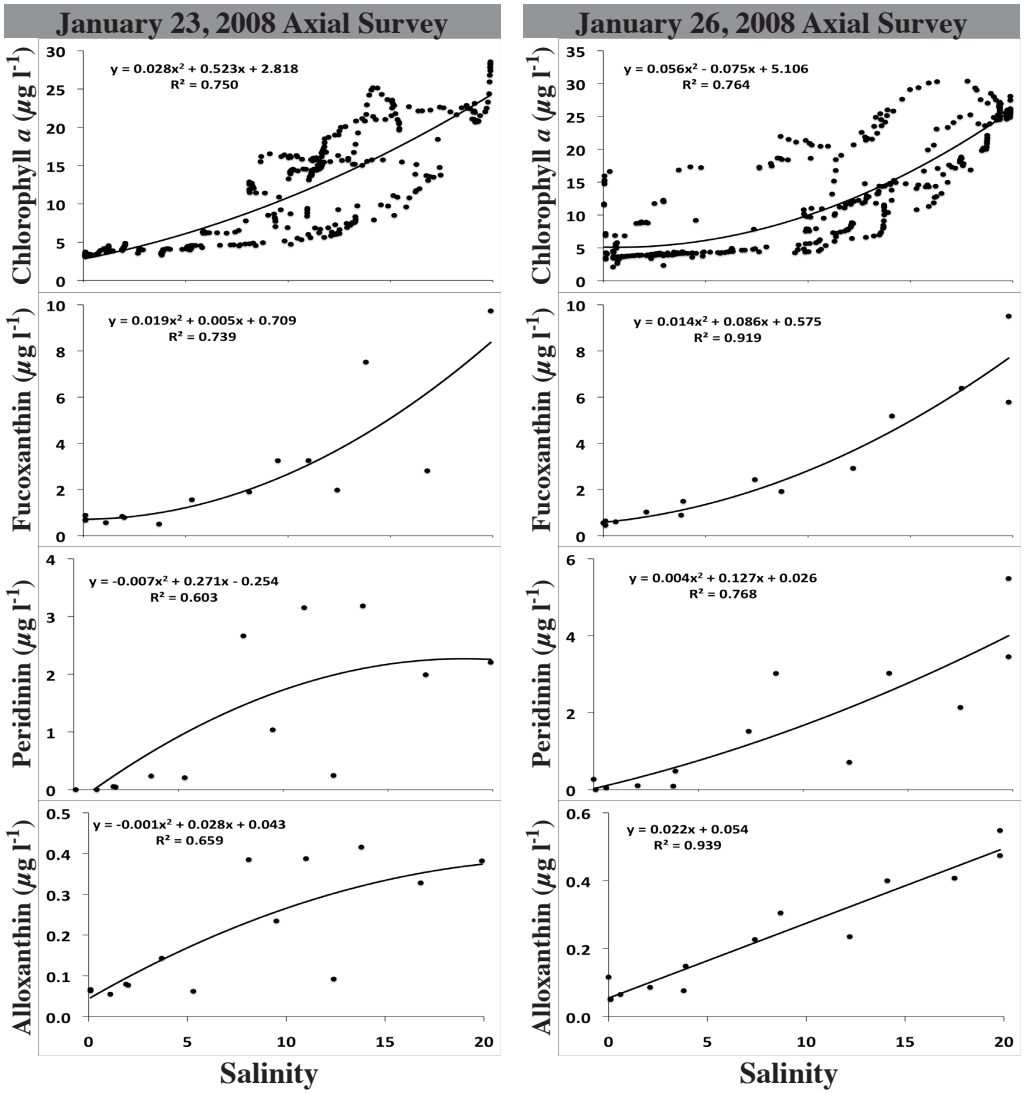

Figure 4.21. Contour plots of salinity (white dashed lines) and the concentrations of chlorophyll *a* and selected accessory pigments along the main channel of the upper Chesapeake Bay on January 23, 2008. CTD survey and water sampling station locations are indicated by the open circles.

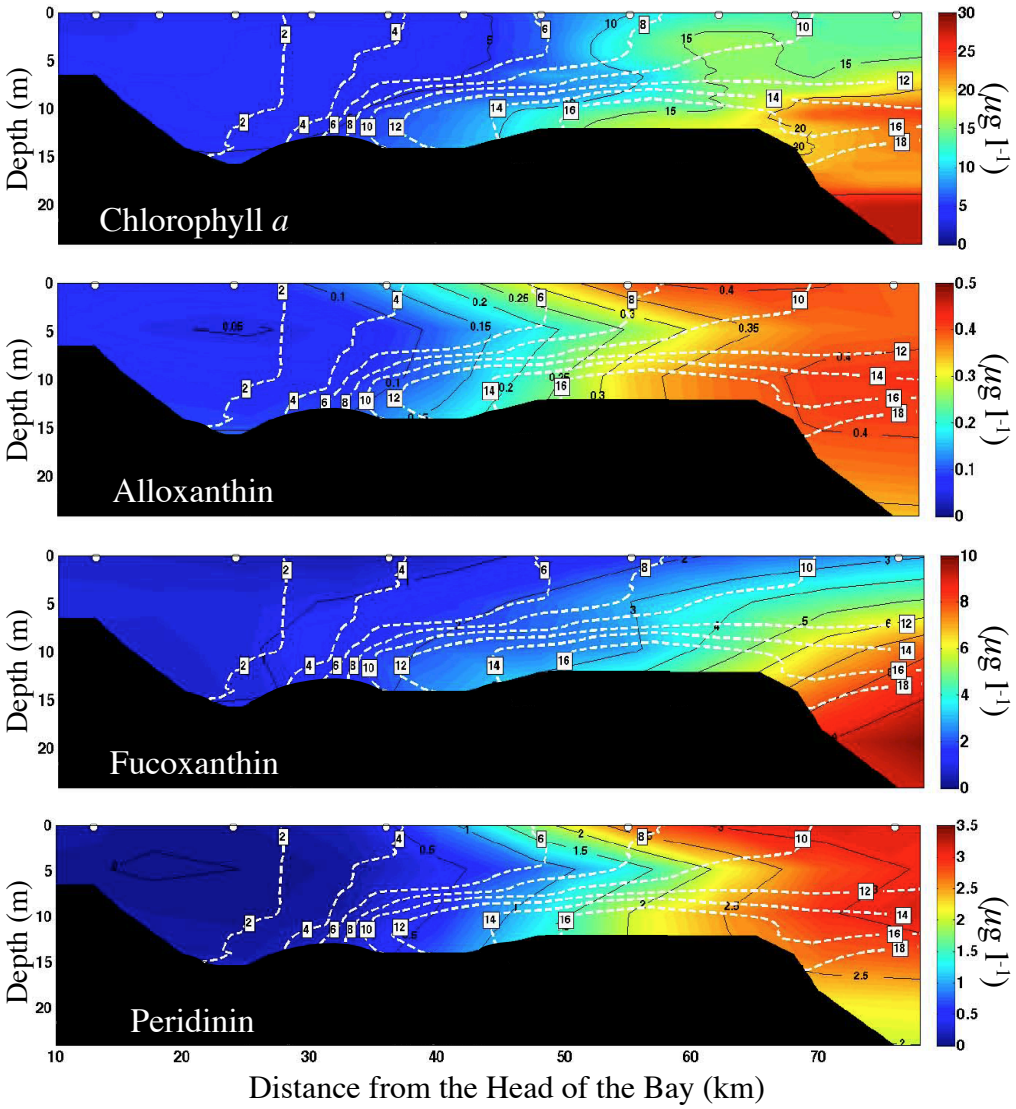

Figure 4.22. Contour plots of salinity (white dashed lines) and the concentrations of chlorophyll *a* and selected accessory pigments along the main channel of the upper Chesapeake Bay on January 26, 2008. CTD survey and water sampling station locations are indicated by the open circles.

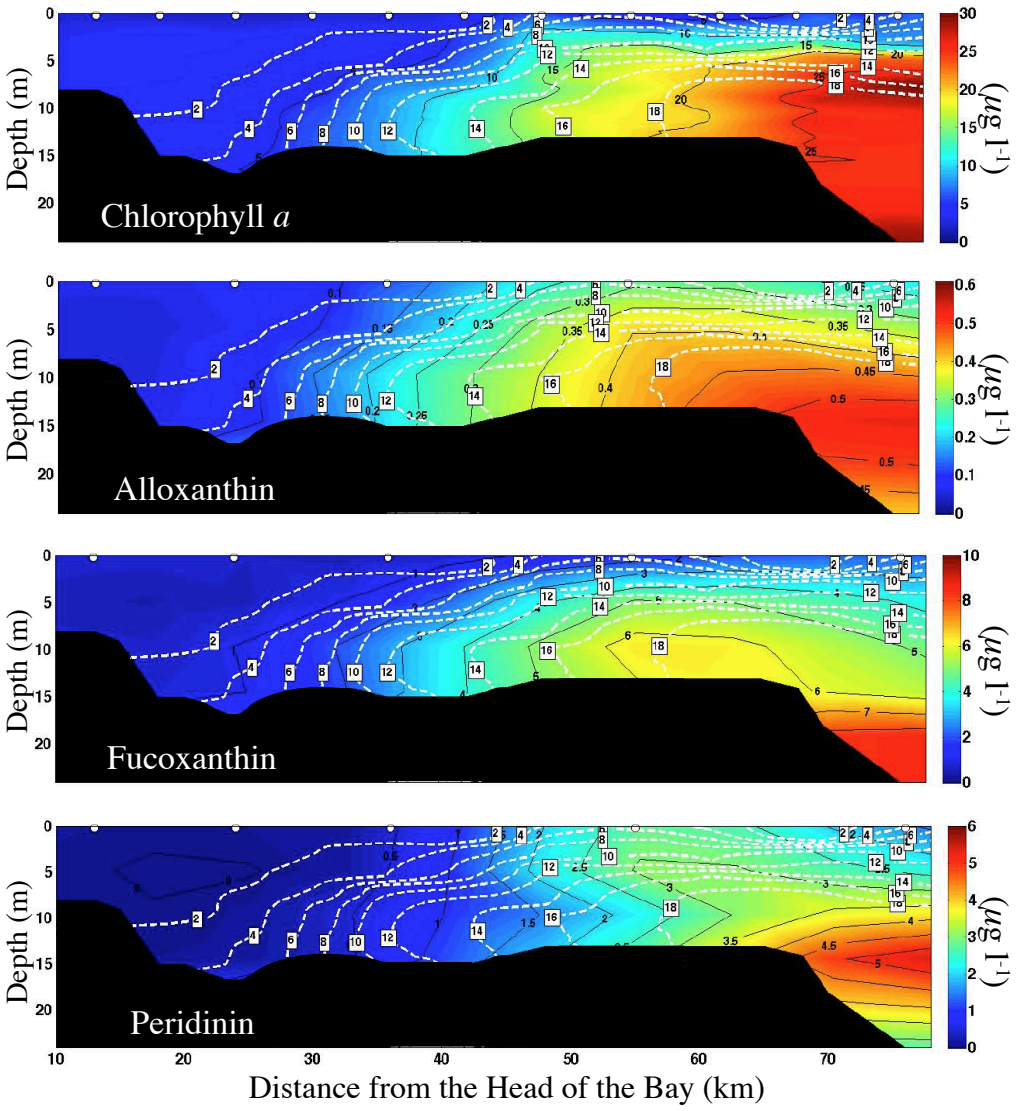

Figure 4.23. Contour plots of salinity (white dashed lines), turbidity, and the concentrations of chlorophyll degradation products along the main channel of the upper Chesapeake Bay on April 17, 2008. Sampling station locations are indicated by the open circles.

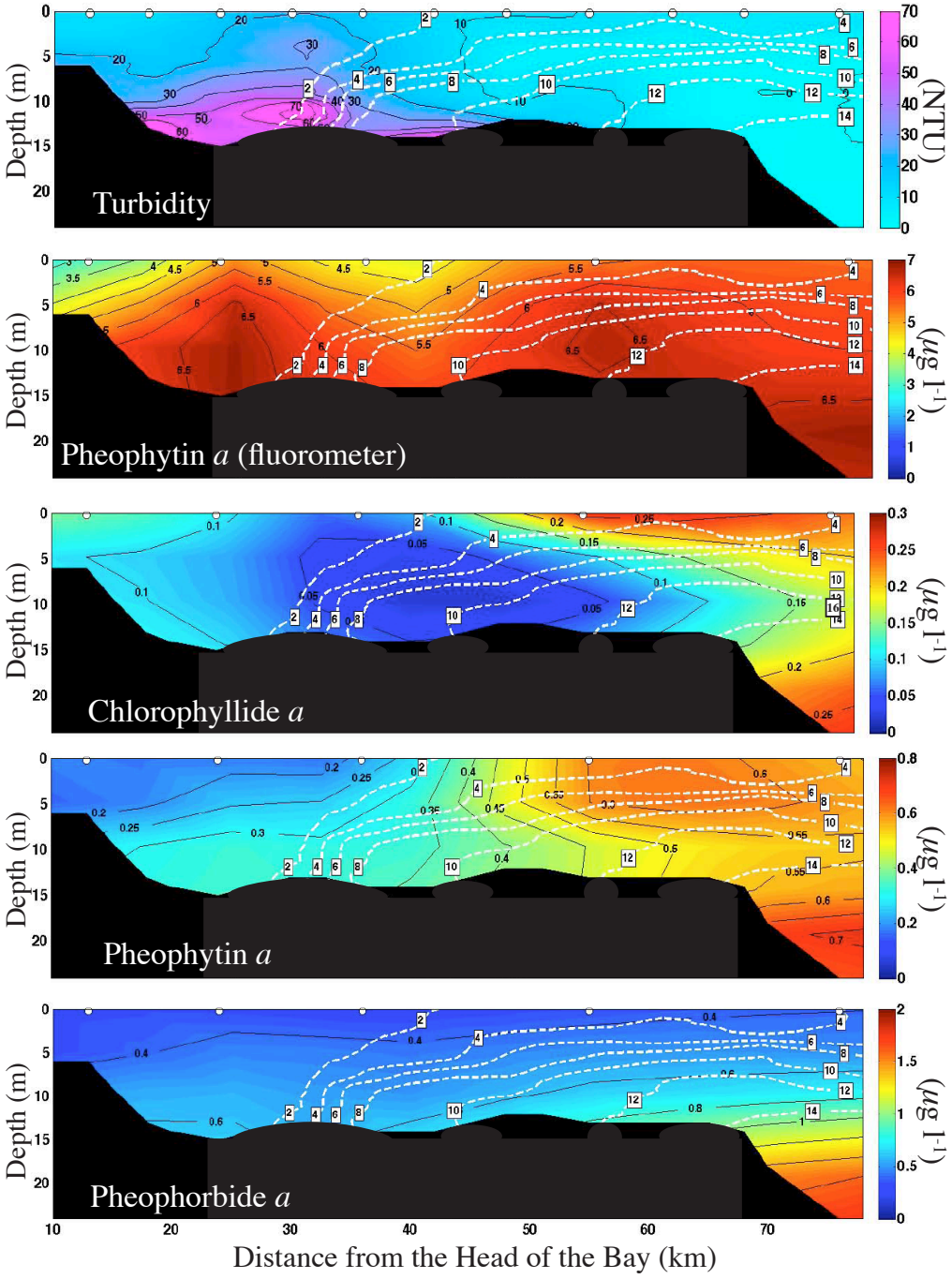

Figure 4.24. Contour plots of salinity (white dashed lines), turbidity, and the concentrations of chlorophyll degradation products along the main channel of the upper Chesapeake Bay on April 23, 2008. Sampling station locations are indicated by the open circles.

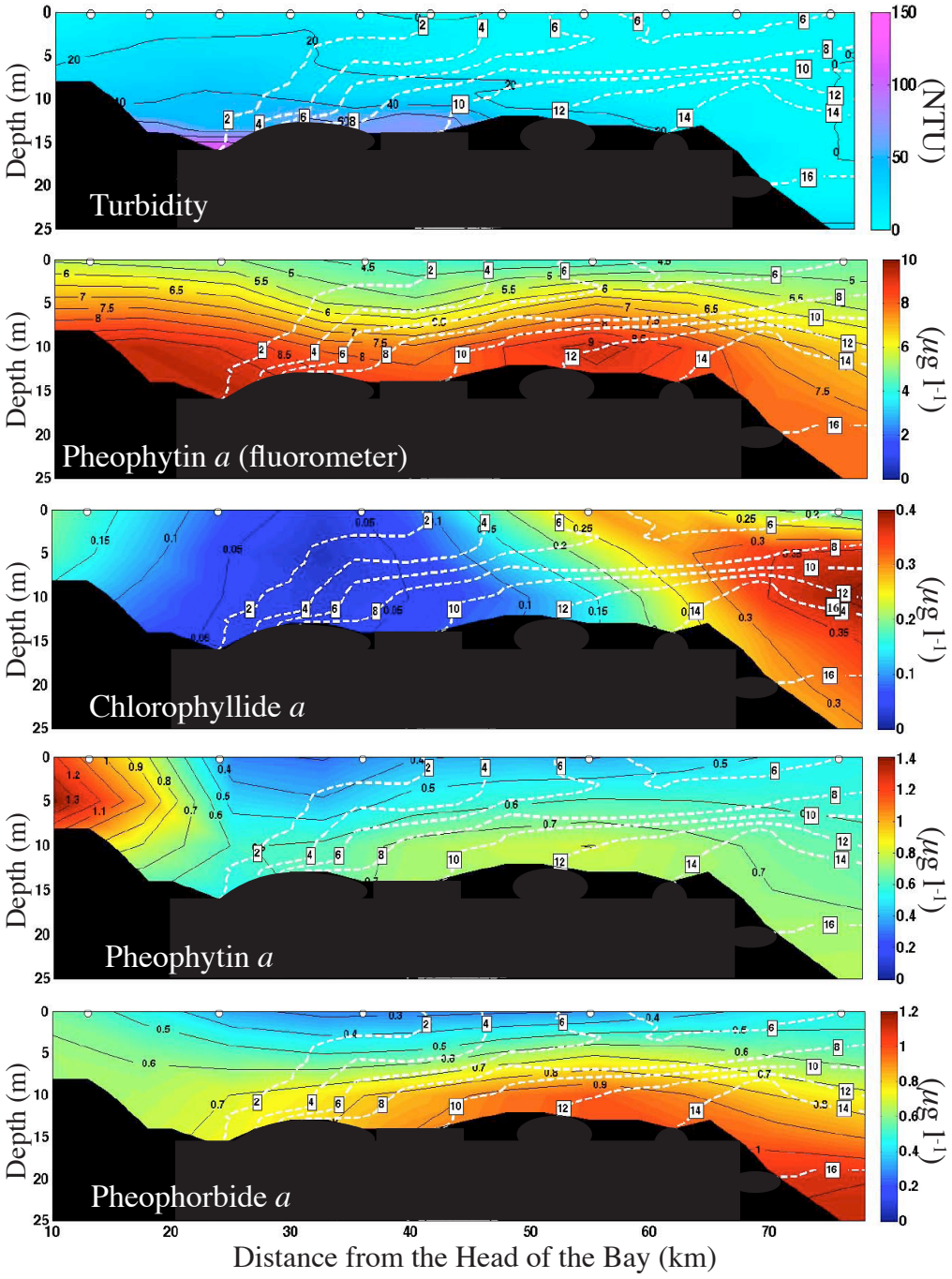

Figure 4.25. Contour plots of salinity (white dashed lines) and the concentrations of chlorophyll *a* and selected accessory pigments along the main channel of the upper Chesapeake Bay on April 17, 2008. CTD survey and water sampling station locations are indicated by the open circles.

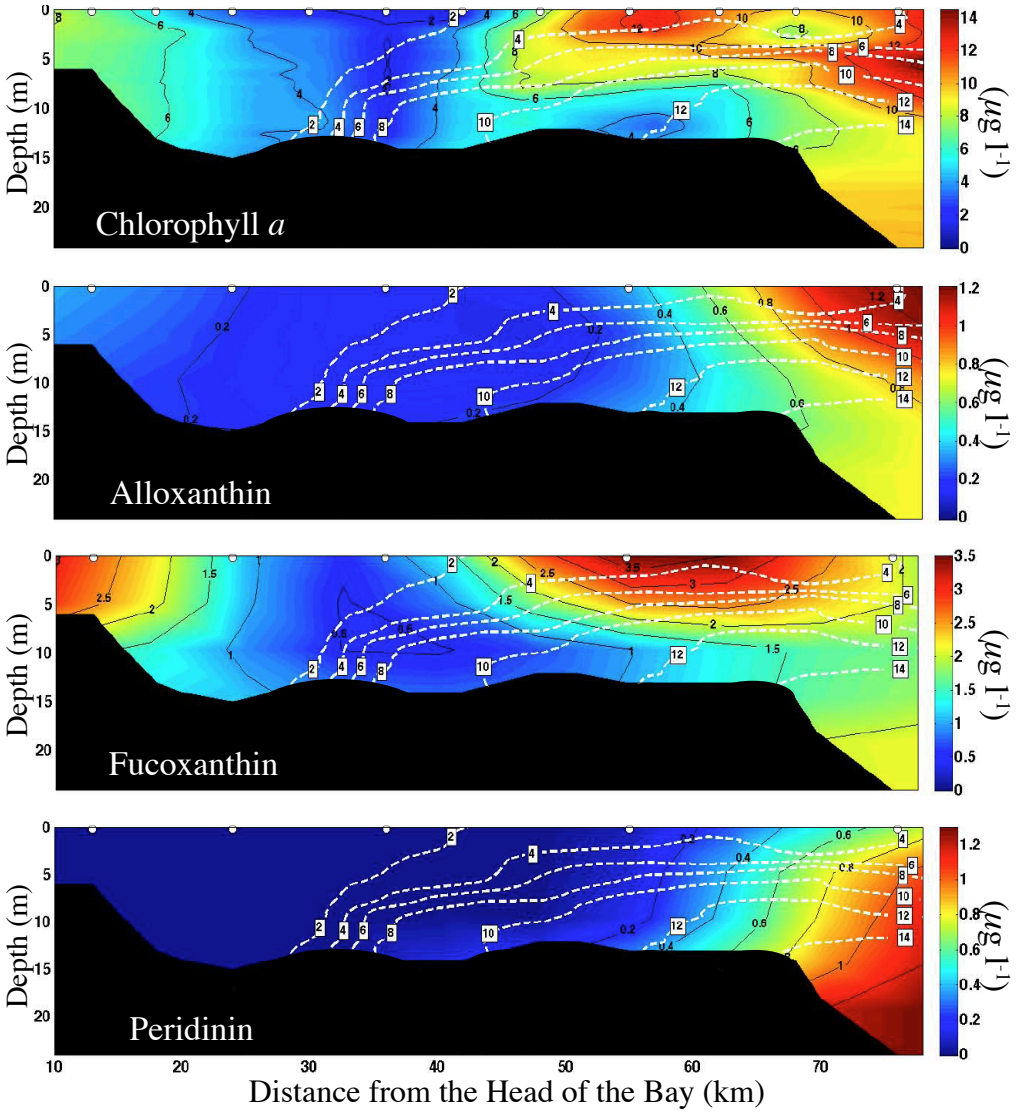

Figure 4.26. Contour plots of salinity (white dashed lines) and the concentrations of chlorophyll *a* and selected accessory pigments along the main channel of the upper Chesapeake Bay on April 23, 2008. CTD survey and water sampling station locations are indicated by the open circles.

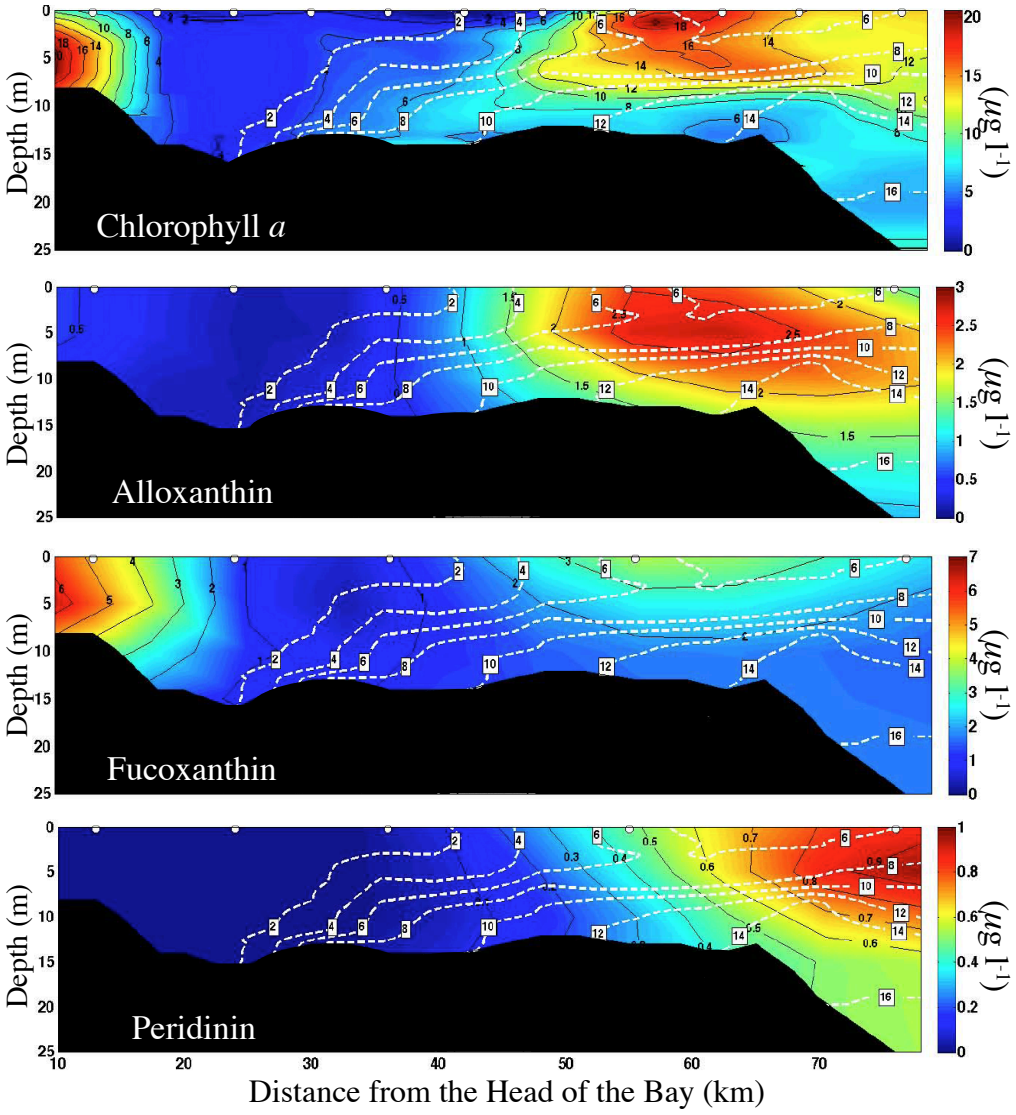

Figure 4.27. Contour plots of salinity (white dashed lines), turbidity, and the concentrations of chlorophyll degradation products along the main channel of the upper Chesapeake Bay on May 16, 2008. Sampling station locations are indicated by the open circles.

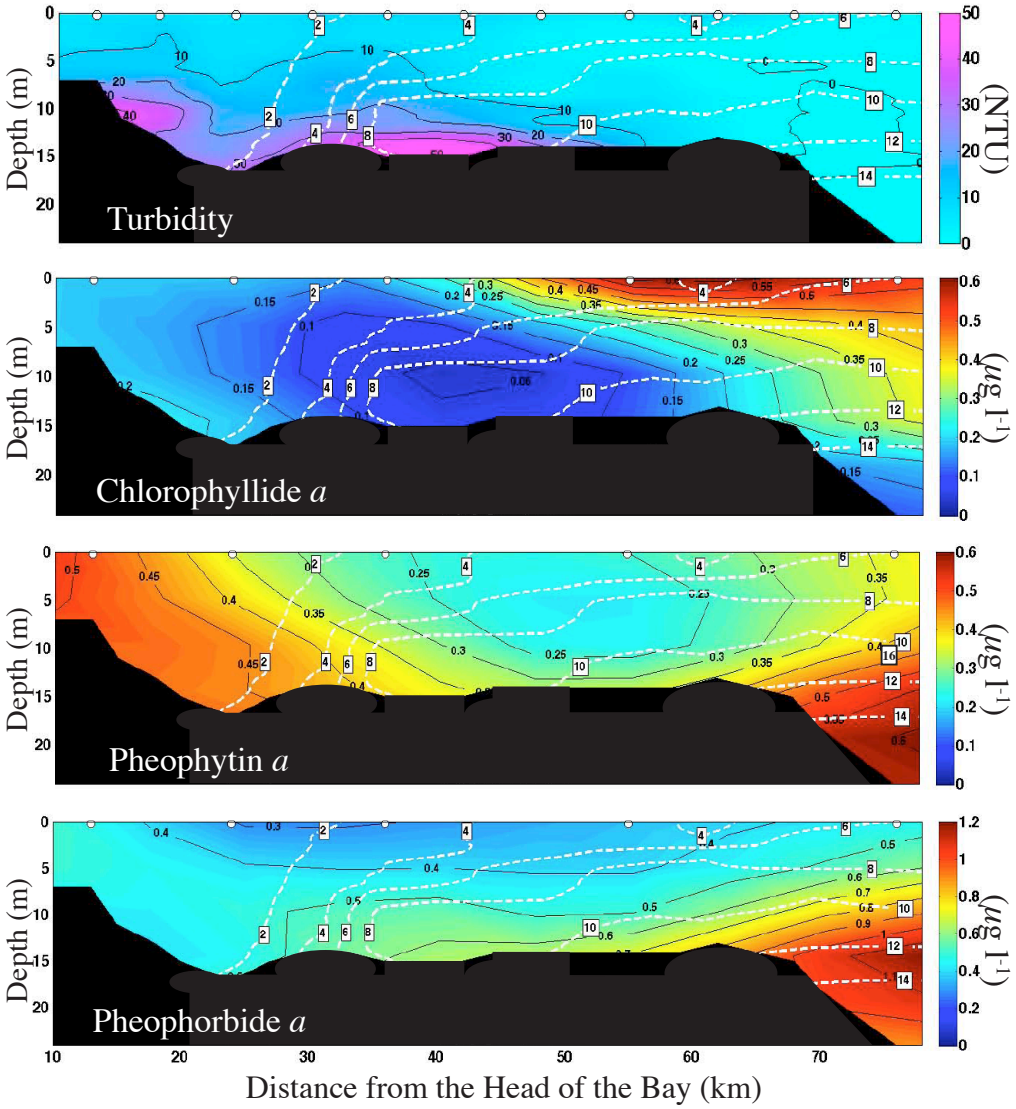

Figure 4.28. Contour plots of salinity (white dashed lines), turbidity, and the concentrations of chlorophyll degradation products along the main channel of the upper Chesapeake Bay on May 22, 2008. Sampling station locations are indicated by the open circles.

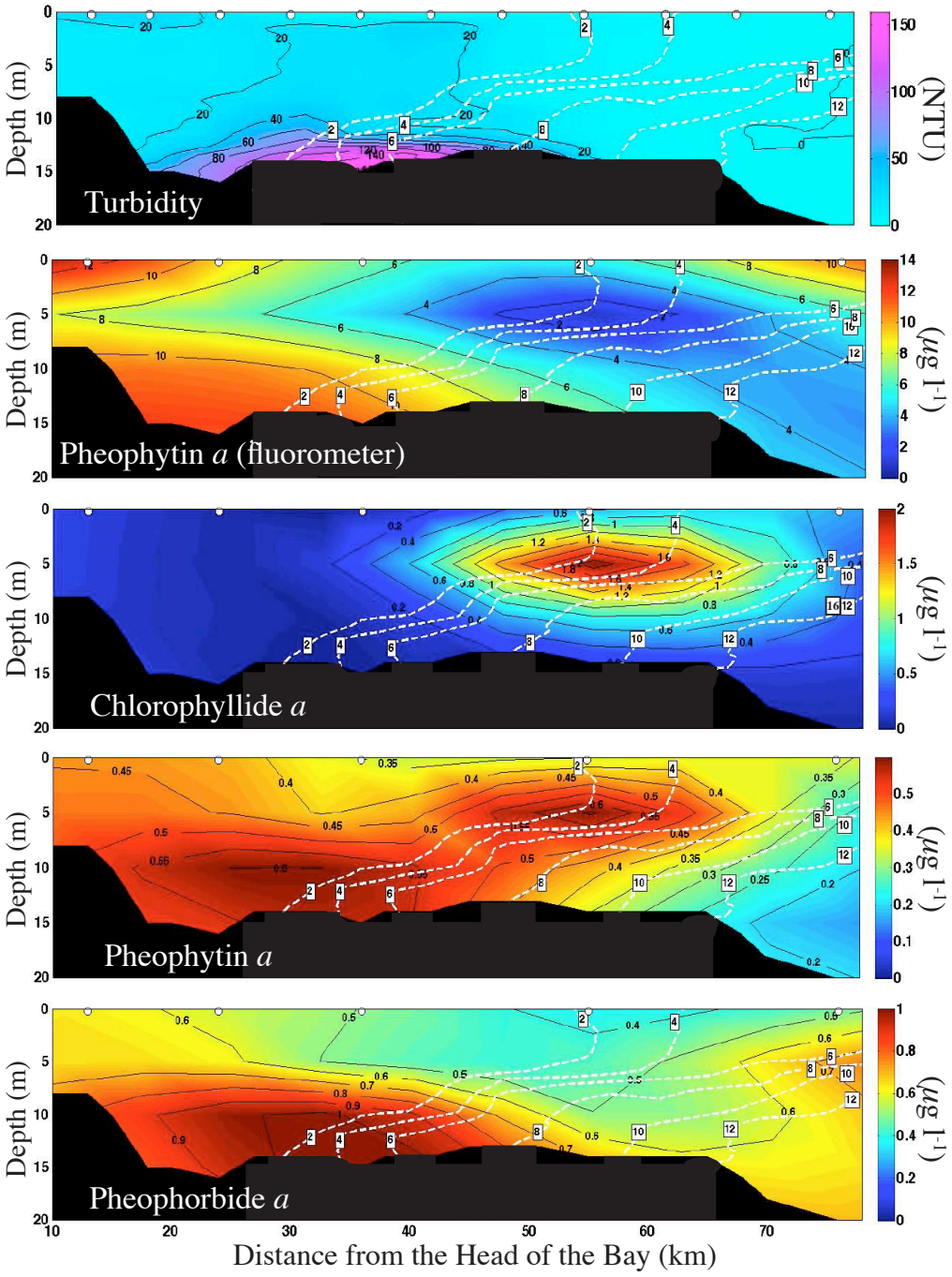

Figure 4.29. Contour plots of salinity (white dashed lines) and the concentrations of chlorophyll *a* and selected accessory pigments along the main channel of the upper Chesapeake Bay on May 16, 2008. CTD survey and water sampling station locations are indicated by the open circles.

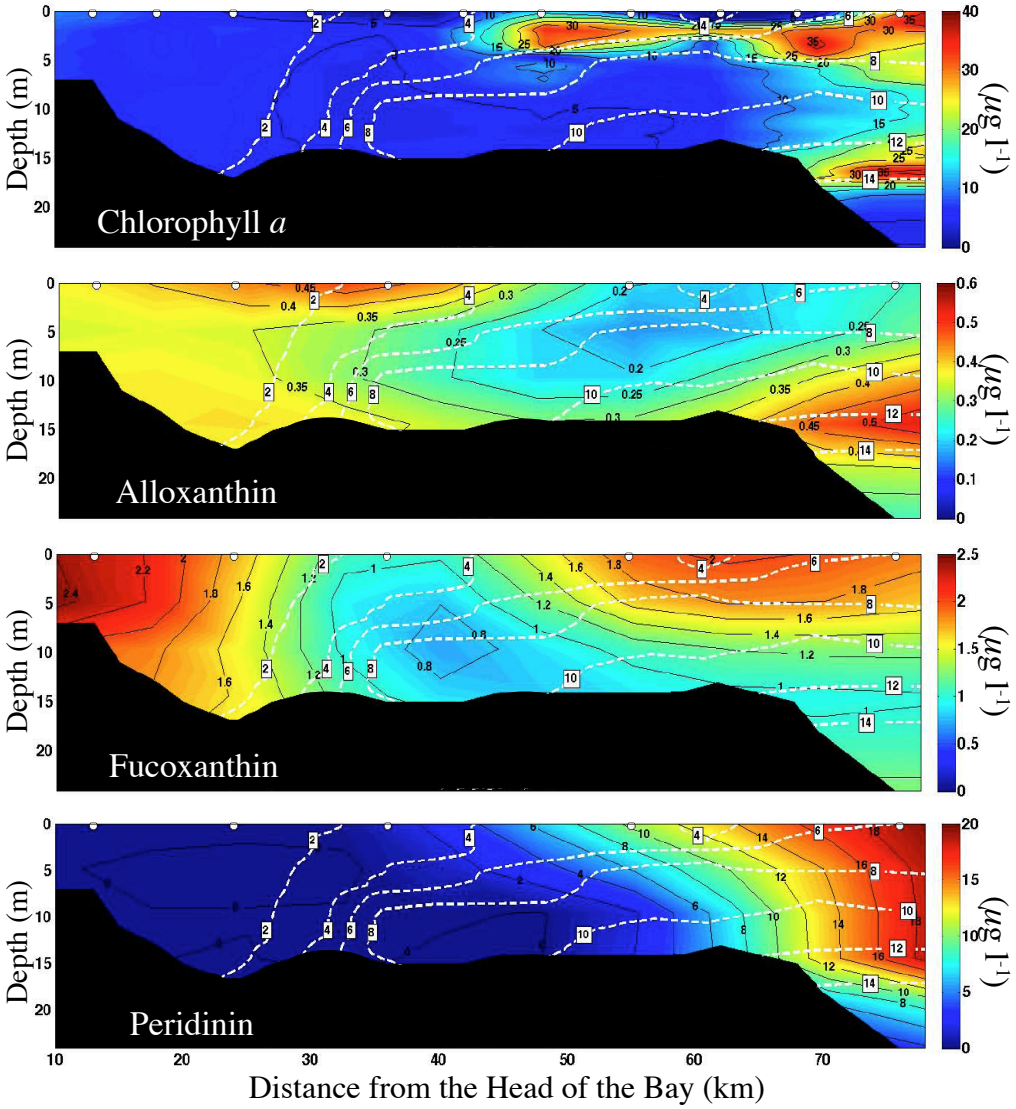

Figure 4.30. Contour plots of salinity (white dashed lines) and the concentrations of chlorophyll *a* and selected accessory pigments along the main channel of the upper Chesapeake Bay on May 22, 2008. CTD survey and water sampling station locations are indicated by the open circles.

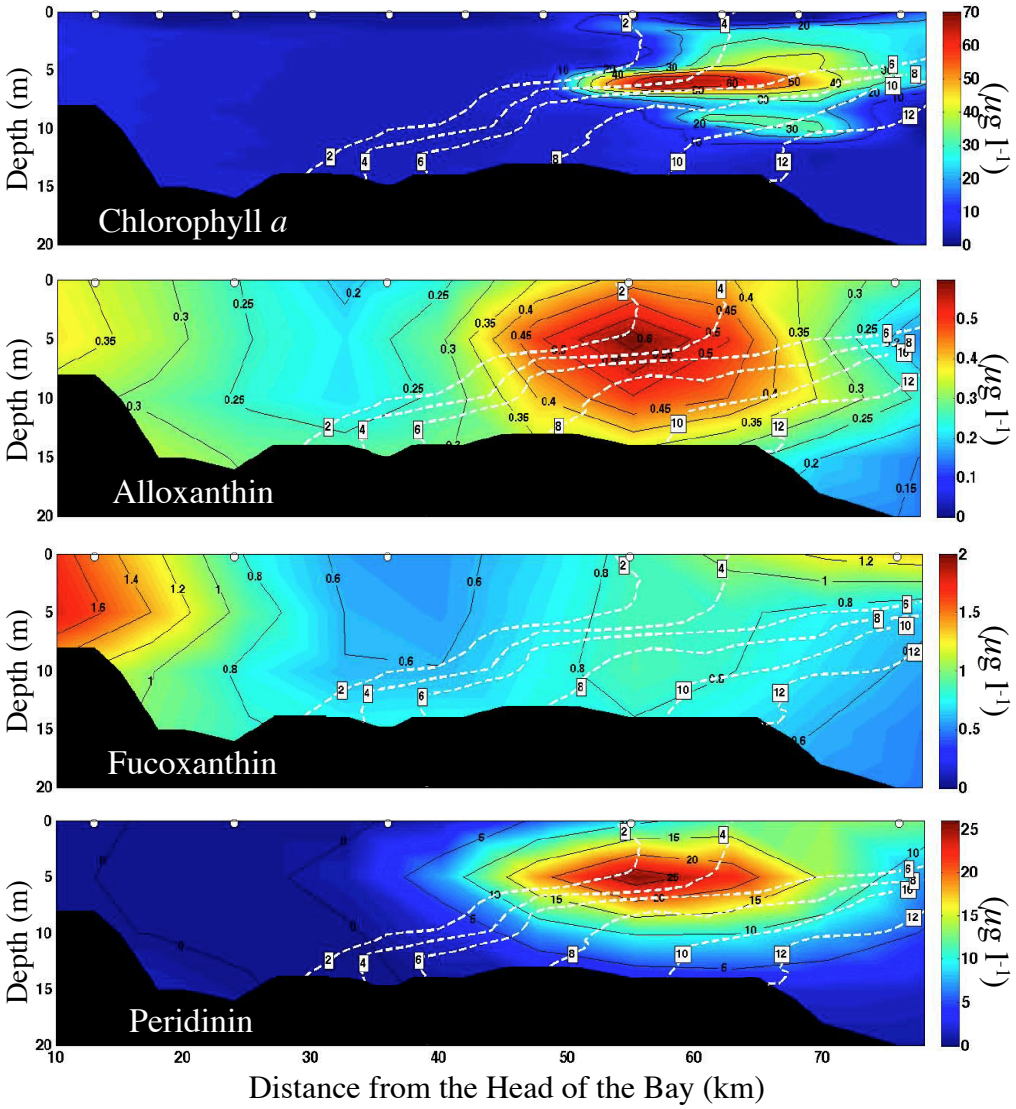

Figure 4.31. Pheophytin *a* (fluorometric measurements) versus particulate organic (a) carbon and (b) nitrogen concentrations in settling tube water samples.

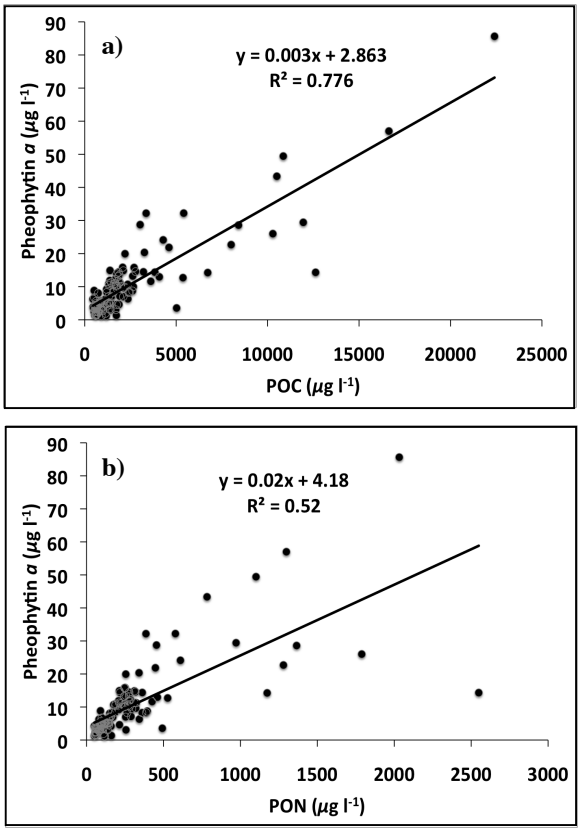

Figure 4.32. The mean percentage of chlorophyll *a* and pheophytin *a* (fluorometric measurements) that settled out of the water column on all cruises during settling tube sampling in the ETM and at the northern most station in freshwater and the southern most station in the most saline water.

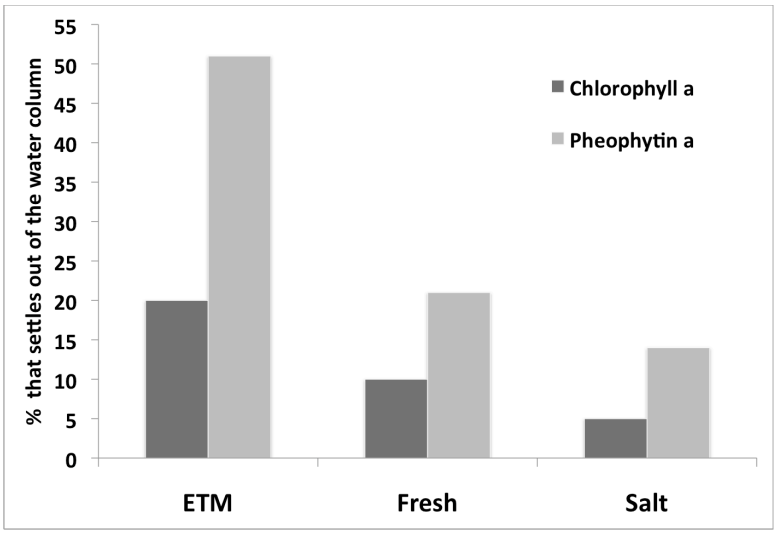

Figure 4.33. A conceptual diagram showing how gravitational circulation (black arrows), salinity, and ETM entrapment play a role in the distribution and floral composition of phytoplankton in the upper Chesapeake Bay.

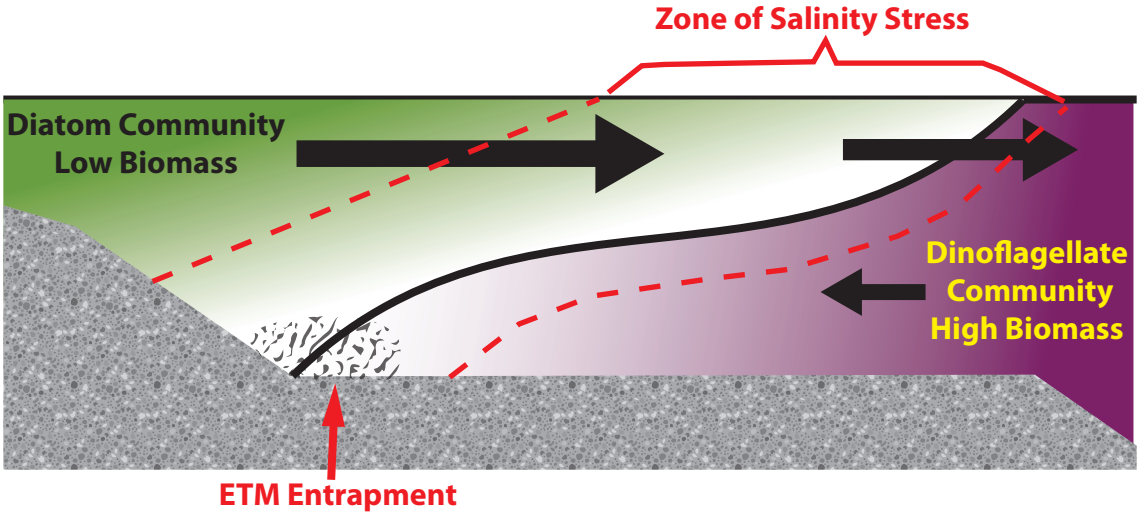

Summary

The research presented in this dissertation adds to decades of marine C and N cycling study and increases our understanding of how the flow of C and N through planktonic food webs and the environment *controls* and is *regulated* by the biology of different marine ecosystems. In Chapters 1, 2, and 3 a modeling approach was used to simulate certain aspects of C and N cycling, like the role of DOM, in different ecosystems. The results of this research have improved our conceptual knowledge and generated theoretical predictions about C and N cycling. In Chapter 4 an observational approach was used to describe the biomass distribution and floral composition of phytoplankton in the upper Chesapeake Bay estuary during the spring and winter. The results of this research suggest the importance of phytoplankton in the upper Bay food web and C and N cycling. A summary of the results from each of these sections is presented below.

Modeling Carbon and Nitrogen Cycling

Since a numerical modeling approach was used in Chapters 1, 2, and 3 a significant amount of the initial research was spent synthesizing the most recent published studies of food web interactions and DOM cycling to formulate and parameterize the new model. The model then provided a means to simulate the simultaneous flow of carbon and nitrogen throughout different ecosystems and compare the importance of various processes at steady-state or over long time scales, something that is technically and economically unfeasible to do experimentally. In addition to facilitating the model development, the synthesis of recent literature was a useful

endeavor that improves upon our conception of how C and N flow through marine ecosystems. The literature synthesis and development of the model has also highlighted important gaps in our knowledge of key processes that influence C and N cycling in marine waters.

Chapters 1 and 2 both describe the new model formulation, which includes a representation of DOM in terms of refractory, semi-labile and labile constituents for both DON and DOC. The sources and sinks for DOM from multiple phytoplankton and zooplankton size classes and bacteria are also included in the model, along with an explicit representation of the impacts of viruses and viral infection. The effects of light on DOM lability are also included in the model. As such, the level of detail in the DOM pools and C and N cycling in this model are unprecedented.

Model Validation

In general the model results compared reasonably well with the available (although somewhat limited) published research (i.e. biomass distributions, DOM and nutrient concentrations, etc.). In all three studies the model was able to reproduce planktonic biomass distributions, DOM concentrations, and nutrient concentrations that either compared directly to or were within the ranges reported for each simulated ecosystem. Furthermore, in Chapter 2 where more data was available for validation, the simulated concentrations of ammonium, nitrate, DOC, and chlorophyll *a* were determined by skill assessment metrics to closely match the observed concentrations. The simulated concentration of DON and the light attenuation coefficient did not as closely match the observations in the skill assessment, although the simulated values were well within the annual range of the observations. The modeled rates of many

processes (i.e. primary, bacterial, DOM production) were also within the ranges reported in the literature (note that for some processes there is very little published rate data). However, the model did have a tendency to underestimate primary and bacterial production in some cases (see Chapters 1 and 2 for further discussion). Overall, the model was able to reasonably simulate enough ecosystem properties for it to be useful as a tool to address the research objectives in each Chapter.

DOM Cycling in Idealized Oceanic, Coastal, and Estuarine Ecosystems

Differences in the forcing and parameterizations of the oceanic, coastal and estuarine steady-state simulations gave rise to significant differences in DOM cycling that were intricately tied to differences in the biomass concentration, distribution, and production of phytoplankton, zooplankton, and bacteria. Abiotic processes such as photooxidation, which differed from system to system, also played an important role in DOM cycling by altering the bioavailability of some DOM and acting as a turnover mechanism for different pools of DOM.

The model suggests that the relative importance of the different plankton groups in controlling DOM cycling is very different in oceanic, coastal and estuarine waters. In the oceanic simulations bacteria were particularly important for mediating DOM cycling because they were the primary agents that control nutrient recycling and supply. In contrast, in the estuarine runs zooplankton had the most influence on DOM production due to the impact of their grazing and excretion, with grazing processes being particularly important. In addition, DOM cycling was generally less dependant on interactions between phytoplankton, zooplankton, and bacteria in the estuarine case because there was more DOM loading to account for terrestrial sources. The coastal simulations were

somewhere in between, i.e., small zooplankton and bacteria both had a strong influence on DOM cycling because they were both important agents that controlled nutrient recycling and supply. Furthermore, in the oceanic and coastal cases the concentrations of labile, semi-labile and refractory DON and DOC varied little in response to parameter variations even though the relative importance of the different sources and sinks changed substantially. This result is consistent with the general observation that DOM concentrations in oceanic and coastal waters are relatively constant in time and space even though the composition of the plankton (and the sources and sinks) varies. In contrast, in the estuarine simulation the concentrations of labile, semi-labile and refractory DON and DOC concentrations were much more sensitive to changes in the parameter values.

Despite the differences between these systems there were a few general trends that were evident in the three simulations: 1) DOC production was always dominated by phytoplankton exudation; 2) viral lysis was always an important source of DOM; and 3) the sensitivity analyses suggest that the production of DOM from a particular source can vary in magnitude by a considerable amount in response to a perturbation that affects the planktonic community structure. The last result (3) has important implications for the cycling of DOM and even for the composition of the communities that utilize the DOM because the quality or bio-availability of DOM is likely different for each DOM source. The model also makes some specific predictions about 1) the role of bacteria and zooplankton in nutrient and DOM cycling; 2) the degree of competition between large and small phytoplankton species and their role in DOM production; 3) the effect of viruses on the plankton dynamics and DOM cycling; and 4) the inherent variability of

DOM concentrations in oceanic, coastal and estuarine waters. These predictions can be viewed as testable hypotheses that can be used to help guide future field studies.

The Seasonal Cycle and Autochthonous Production of DOM at station CB3.3C in the Chesapeake Bay

Seasonal differences in the forcing and parameterization of the station CB3.3C simulation gave rise to significant differences in biologically mediated DOM cycling that were intricately tied to changes in the planktonic community structure. As in the Chapter 1 steady-state simulations the degree to which different groups of plankton influenced DOM cycling was strongly related to their biomass and productivity in relation to that of the other groups of plankton. Thus, in the spring DOM production was mostly from large phytoplankton and large zooplankton. While in the summer, DOM production was mostly controlled by interactions between small phytoplankton, small zooplankton, viruses, and bacteria.

The production of DOM peaked twice, in the spring and late summer, in correspondence with the peak productivity of the spring and summer plankton communities. Table 2.5 summarizes the most important processes involved in peak DOM production. The results also indicate that viral decay may represent an important, and often overlooked, source of "new" potentially bioavailable DOM from within the DOM pool. Bacteria were the most important consumers of DOM throughout the year with phytoplankton consuming small but significant amount of DOM in the spring and late summer. Furthermore, bacteria played an important role in hydrolyzing the semi-labile DOM that accumulated as a result of spring and summer productivity. Photochemical, chemical, and physical processes such as the decay of detritus and the

transformation of refractory DOM to labile DOM also played an important role in DOM cycling, and were especially important in turning over the refractory pools of DOM.

The Simulated Roles of Viruses and Microzooplankton in Non-Axenic Batch Cultures of *Phaeocystis globosa*

The theoretical predictions of these simulated batch culture experiments indicate that while both viruses and microzooplankton can exert substantial top-down control on *P. globosa*, the process of viral lysis tends to have a more rapid impact (i.e. higher initial mortality) upon the population even though microzooplankton grazing may ultimately cause more mortality. The bottom-up effects of viral lysis and microzooplankton grazing were also different in these experiments. Viral lysis transferred material to dissolved organic matter pools before, or if, it was remineralized by heterotrophic bacteria while microzooplankton grazing provided a more direct route for the remineralization of organic matter through excretion. Microzooplankton grazing also had a greater potential to act as a direct link to higher trophic levels because a large proportion of *P. globosa* biomass was converted into microzooplankton biomass, which is then potentially more accessible to higher trophic levels than the DOM or detritus produced by viral lysis. These results have important implications for understanding both trophic interactions and biogeochemical cycling in other systems.

The Biomass Distribution and Floral Composition of Phytoplankton in the Upper Chesapeake Bay: The Influence of Hydrodynamic Processes and the Implications for the ETM Food Web

The biomass distribution and floral composition of the phytoplankton community in the upper Chesapeake Bay was studied during the winter and spring to determine if phytoplankton could play an important role in the ETM food web at this time of year. The presence of high concentrations of phytoplankton in certain areas, as well as the constant presence of small centric diatoms and cryptophytes throughout the upper Bay suggests the potential for phytoplankton to be an important component of the ETM food web. Furthermore, the presence of a variety of pigment degradation products suggests that live phytoplankton are being consumed by zooplankton in the ETM, that phytoplankton may be dying in the ETM, and that senescent phytoplankton are being transported into the ETM. Hydrodynamic processes appear to control much of these phytoplankton dynamics and result in the formation of two main phytoplankton communities in the upper Bay (see Fig. 4.33). Hydrodynamic processes also appear to play an important role in phytoplankton mortality through salinity stress and ETM entrapment. The amount of phytoplankton derived organic matter that reaches the ETM will depend on the relationship between estuarine circulation, the strength of ETM particle trapping, and phytoplankton community biomass distribution, productivity, and mortality. Since these factors can be highly variable, ETM phytoplankton entrapment will not always occur. However, when conditions are favorable, phytoplankton entrapment in the ETM may be high.

Conclusion

The research presented in this dissertation contributes to our understanding of marine C and N cycling in a number of ways. First, it demonstrates the importance of the planktonic community biomass distribution and productivity in C and N cycling, particularly as it relates to the flow of material through the food web and pools of DOC and DON. Second, it provides more insight into how C and N cycling changes seasonally in temperate eutrophic regions, especially as it relates to the autochthonous production of DOM. Third, it suggests how differences between the top-down and bottom-up roles of viral lysis and microzooplankton grazing can affect C and N cycling and the food web. Finally, this research suggests that phytoplankton have the potential to be an important component of the food web and C and N cycling in estuarine ETMs.

Appendix A: Chapter 1 Model Parameters

Light conditions used in the model, I = 89.68 W m^{-2} and 98.13 W m^{-2} from Stickney, et al. (2000) simulate the mid-summer average irradiance in the mixed layer of typical coastal/estuarine and oceanic waters. The phytoplankton light saturation parameter I_{P_i} was set at 40 W m^{-2}, and the photoinhibition parameter $I_{\beta P_i}$ was set at 400 W m^{-2} (Platt et al., 1980). A value of 3.22 d^{-1} was used for the maximum phytoplankton growth rate, μ_P. Scaling the growth rate of large phytoplankton to be 0.7 times that of small phytoplankton results in a maximum realized growth rate of 2.30 d^{-1} for small cells and 1.61 d^{-1} for large cells (Hood et al., 2001; Platt et al., 1980; Tian et al., 2000). The half saturation constants for phytoplankton ammonium and nitrate uptake were set at 0.5 μM and 1 μM for large cells and 0.2 μM and 1 μM for small cells (Tian et al., 2000). The half saturation constants for phytoplankton DOM uptake are poorly constrained and were set to zero for all model runs. However, we included the formulation to allow for phytoplankton DOM uptake in future model runs. Phytoplankton excretion of DOM through leakage and active release processes was formulated after Anderson and Williams (1998). This DOM was partitioned so that 40% (o_L = 0.40) is labile, 50% (o_S = 0.50) is semilabile, and 10% (o_R = 0.10) is refractory material. The phytoplankton C:N ratio (λ_P) was set at 7.5 mol mol^{-1} (Anderson and Pondaven, 2003). Phytoplankton non-grazing mortality (S_{PL} and S_{PS}) is poorly constrained and was used to tune the model biomass distributions. Consequently the mortality rates for large and small phytoplankton were 0 and 0.06 d^{-1} (oceanic run), 0.01 and 0.06 d^{-1} (coastal run), and 0.03

and 0.02 d^{-1} (estuarine run). The products of non-grazing mortality directly enter the detritus pool ($\beta_1 = 0.75$) and the DOM pool ($1\text{-}\beta_1 = 0.25$). Furthermore, DOM from non-grazing mortality was partitioned between labile ($\delta_1 = 0.10$), semi-labile ($\delta_2 = 0.80$), and refractory pools ($\delta_3 = 0.10$).

A maximum rate of 2.0 d^{-1} for small zooplankton C_{Z_S} and 1.0 d^{-1} for large zooplankton C_{Z_L} describes zooplankton grazing. The half saturation constant for zooplankton ingestion (ZK_S) was set at 0.75 mmol N m^{-3}, the zooplankton assimilation efficiencies for C (β_{C_Z}) and N (β_{N_Z}) were set at 0.64 and 0.77, and the zooplankton C:N ratio (λ_Z) was set at 5.5 mol mol^{-1} (Anderson and Pondaven, 2003). The zooplankton net C growth efficiency (ge_Z) (fraction assimilated C allocated to production, remainder respired) was used to tune the model biomass distributions and was 0.45 (oceanic run) and 0.65 (coastal and estuarine runs) for large zooplankton and 0.40 (oceanic run) and 0.50 (coastal and estuarine runs) for small zooplankton. Large zooplankton grazing preferences for large phytoplankton ($\Phi_{P_L} = 0.19$), other large zooplankton ($\Phi_{Z_L} = 0.19$), detritus ($\Phi_D = 0.19$), small zooplankton ($\Phi_{Z_S} = 0.19$), small phytoplankton ($\Phi_{P_S} = 0.19$), and bacteria ($\Phi_B = 0.05$) were assigned to reflect the known diversity of the large zooplankton diet (Kleppel, 1993). Note that we are assuming that large zooplankton do not graze selectively on bacteria but that they inadvertently ingest attached bacteria as a result of grazing on other items. Small zooplankton grazing preferences for large phytoplankton ($\Phi_{P_L} = 0$), detritus ($\Phi_D = 0.15$), small zooplankton ($\Phi_{Z_S} = 0.30$), small phytoplankton ($\Phi_{P_S} = 0.35$ and 0.40), and bacteria ($\Phi_B = 0.15$ and 0.20) were assigned to reflect known grazing preferences for small phytoplankton, other small zooplankton,

and bacteria (Boenigk and Arndt, 2002; Calbet and Landry, 2004). These grazing preferences were also used to help tune the model.

The amount of DOM produced from sloppy feeding by large zooplankton during grazing was calculated by adapting the sloppy feeding equation from Møller (2005), Q = 0.714 – 0.013*($ESD_{copepod}/ESD_{prey}$), where Q is the fraction of prey carbon removed from suspension and lost as DOC during feeding and ESD is the equivalent spherical diameter. This equation was only used for predator-to-prey ratios of < 55; sloppy feeding was assumed not to occur at higher ratios. Therefore, we estimated the average ESD of large zooplankton to be 484 μM and the average ESD of large phytoplankton to be 13.8 μM based on (Møller, 2005), which gives a Q value of 0.26 (ω_{P_L}) for large zooplankton feeding on large phytoplankton. For large zooplankton feeding on other large zooplankton, an ESD of 484 μM was estimated for the predator and an ESD of 304 μM was used for the prey, simulating an average copepod feeding on an average copepodite, which gives a Q value of 0.69 (ω_{Z_L}). For large zooplankton feeding on detritus the predator-to-prey ratio was assumed to be 18:1, the optimal copepod predator-to- prey size ratio (Hansen et al., 1994), which gives a Q value of 0.48. However, as detritus is non-living it likely contains less DOM that can be released when sloppy feeding occurs, so we assume that DOM production from large zooplankton feeding on detritus is less and set the Q value to equal 0.24 (ω_D). We could not find any data that reported how much detritus is produced as a result of sloppy feeding, so we assumed that the amount of detritus produced is 25% of the Q value calculated above.

Zooplankton excretion of ammonium and DON was set so that 68% (K_Z) of the nitrogen excreted is in the form of ammonium with the remaining 32% in the form of

DON (Steinberg et al., 2002). Excretion of DOC b y zooplankton was set so that 31% of the carbon released (including respiration) was in the form of DOC (Steinberg et al., 2000). Small zooplankton non-grazing mortality was used to tune the model, so the rate was 0.06 d^{-1} for the oceanic and coastal runs and 0.04 d^{-1} for the estuarine run.

Bacterial cycling of C and N was formulated so that their maximum growth rate was 13.3 d^{-1} and the half saturation constant for bacterial ammonium uptake was set at 0.50 mmol N m^{-3} (Anderson and Williams, 1998). The bacterial half saturation constant for semi-labile DOC hydrolysis was set at 417 mmol C m^{-3}, the maximum semi-labile DOC hydrolysis rate was set at 4.0 d^{-1}, and the bacteria C:N ratio was set at 5.1 mol mol^{-1} (Anderson and Pondaven, 2003). Bacterial mortality (S_B) is poorly constrained and was therefore used to tune the model, so the rate was 0 d^{-1} for the oceanic and estuarine runs and 0.02 d^{-1} for the coastal run. Due to their small size, the products of non-grazing bacterial mortality enter the labile (β_3), semi-labile (β_4), and refractory (β_5) DOM pools.

Viral infection of phytoplankton and bacteria was parameterized so that roughly 7% of phytoplankton and 30% of bacteria are lysed per day. These infection rates are from calculations based on the average abundance of viruses and how many need to be produced daily to sustain that abundance given calculated viral decay rates (Fuhrman, 1999; Weinbauer, 2004; Wommack and Colwell, 2000). We calculated the model infection rate by multiplying the percentage of hosts lysed per day by the inverse of the average host specific viral mass. The viral biomass in terms of carbon and nitrogen was calculated according to the number of carbon and nitrogen atoms in viral DNA and a piece of viral protein. We then estimated that roughly half of a virus's mass was DNA and half protein. So, according to our calculations the virus C:N ratio is 3.26 and a 40 kb

virus has 3.11 x 10^{-11} μmol C, a 175 kb virus has 1.36 x 10^{-10} μmol C, and a 225 kb virus has 1.75 x 10^{-10} μmol C. We set viral abundances at 1.0 x 10^{6} viruses ml^{-1} for the oceanic runs and 2.50 x 10^{7} viruses ml^{-1} for the coastal and estuarine runs, abundances that are well within the range of reported abundance for each type of environment (Wommack and Colwell, 2000; Wommack et al., 1992). We also estimated that 80% of the viruses are bacteriophages (assuming an average size of 40 kb), 9% are small phytoplankton viruses (assuming an average size of 175 kb), and 9% are large phytoplankton viruses (assuming an average size of 225 kb). For our oceanic model run, bacteria are infected at a rate of 3 μM^{-1} N d^{-1}, small phytoplankton at 4 μM^{-1} N d^{-1}, and large phytoplankton at 3 μM^{-1} N d^{-1}. For the coastal and estuarine model runs, bacteria were infected at a rate of 1 μM^{-1} N d^{-1}, small phytoplankton at 0.75 μM^{-1} N d^{-1}, and large phytoplankton at 0.58 μM^{-1} N d^{-1}. The number of viruses produced per lysis event averages 24 phages per cell lysed for bacteria and up to 400 to 500 viruses per lysed cell for large phytoplankton like *Emiliania huxleyi* (Wommack and Colwell, 2000). Therefore, based on these burst sizes and our calculations, 50% of the mass of a cell that is lysed are new viruses ($\varepsilon_V = 0.50$) that enter the virus pool. For phytoplankton the remaining cellular contents were partitioned between detritus ($\varepsilon_D = 0.375$) and labile, semi-labile, and refractory DOM ($\varepsilon_L = 0.08$, $\varepsilon_S = 0.03$, and $\varepsilon_R = 0.015$) based on an experiment by Gobler et al. (1997). For bacteria the remaining cellular contents enter the labile ($\varepsilon_{B1} = 0.35$), semi-labile ($\varepsilon_{B2} = 0.10$), and refractory ($\varepsilon_{B3} = 0.05$) DOM pools.

Viral decay rates are poorly constrained and a large range is reported in the literature (Weinbauer, 2004), therefore we set the coastal and estuarine decay rate at a

conservative 0.08 h^{-1}. We set the oceanic viral decay rate at 0.2 h^{-1} because we were unable to sustain a reasonable bacterial biomass with a lower decay rate.

The nitrification of ammonium (ϖ_1) was set a 0.03 d^{-1} (Anderson and Williams, 1998) and the detritus decay rates were set at 0.055 d^{-1} and 0.040 d^{-1} for N and C detritus (Anderson and Pondaven, 2003). In the coastal and estuarine model runs photochemical processes acted on DOM to convert refractory DON and DOC to labile DON and DOC at a rate of 0.0015 d^{-1} (Anderson and Pondaven, 2003). Photochemical processes are also responsible for converting DOC into DIC at a rate of 0.004 μM C d^{-1} for coastal and estuarine runs and 0.001 μM C d^{-1} for the oceanic run. Based on recent research (Koopmans and Bronk, 2002) we allowed photochemical processes to convert DON to ammonium in the estuarine run at a rate of 0.0005 d^{-1}.

The inflow of nutrients and DOM and outflow (μM N or C s^{-1}) of all state variables is calculated as:

inflow = $h\ i^o$

outflow = $h\ i$

where h is the rate (cm s^{-1}) of flow, i^o is the upstream ammonium, nitrate, or DOM concentration, and i is the model state variable mass.

Table A

Model Parameters

Description	Symbol	Value	Units
Phytoplankton			
Maximum phytoplankton growth rate	μ_P	3.22	d^{-1}
Phytoplankton light saturation parameter	I_P	40.00	W m^{-2}
Phytoplankton photoinhibition parameter	I_β	400.00	W m^{-2}
Phytoplankton light parameter	I	89.68, 98.13	W m^{-2}
Partitioning of phytoplankton production	α	0.70	Dimensionless
Phytoplankton excretion parameter	ϖ_2	0.26	Dimensionless
Phytoplankton C/N ratio	λ_P	7.5	mol mol^{-1}
Saturation const. for N_n uptake by P_L	$P_L K_{N_n}$	1.0	μM
Saturation const. for A uptake by P_L	$P_L K_A$	0.5	μM
Saturation const. for N_n uptake by P_S	$P_S K_{N_n}$	1.0	μM
Saturation const. for A uptake by P_S	$P_S K_A$	0.2	μM
Saturation const. for L_N uptake by phytoplankton	PK_{L_N}	0	μM
Large phytoplankton non-grazing mortality	S_{PL}	0, 0.01, 0.03	d^{-1}
Small zooplankton non-grazing mortality	S_{PS}	0.02, 0.06	d^{-1}
Zooplankton			
Z_S maximum consumption rate	C_{Z_S}	2.0	d^{-1}
Z_L maximum consumption rate	C_{Z_L}	1.0	d^{-1}
Zooplankton assimilation efficiency (N)	β_{N_Z}	0.77	Dimensionless
Zooplankton assimilation efficiency (C)	β_{C_Z}	0.64	Dimensionless
Large zooplankton growth coefficient (C)	ge_{Z_L}	0.45, 0.65	Dimensionless
Small zooplankton growth coefficient (C)	ge_{Z_S}	0.40, 0.50	Dimensionless
Saturation const. for zooplankton consumption	ZK_S	0.75	mmol N m^{-3}
Large zooplankton preference for P_L	Φ_{P_L}	0.19	Dimensionless
Large zooplankton preference for P_S	Φ_{P_S}	0.19	Dimensionless
Large zooplankton preference for D	Φ_D	0.19	Dimensionless

Large zooplankton preference for Z_L	Φ_{Z_L}	0.19	Dimensionless
Large zooplankton preference for Z_S	Φ_{Z_S}	0.19	Dimensionless
Large zooplankton preference for B	Φ_B	0.05	Dimensionless
Small zooplankton preference for P_L	φ_{P_L}	0	Dimensionless
Small zooplankton preference for P_S	φ_{P_S}	0.35, 0.40	Dimensionless
Small zooplankton preference for D	φ_D	0.15	Dimensionless
Small zooplankton preference for Z_S	φ_{Z_S}	0.30	Dimensionless
Small zooplankton preference for B	φ_B	0.15, 0.20	Dimensionless
Zooplankton C/N ratio	λ_Z	5.5	mol mol^{-1}
Large zooplankton non-grazing mortality	S_{ZL}	0	d^{-1}
Small zooplankton non-grazing mortality	S_{ZS}	0.04, 0.06	d^{-1}
Bacteria			
Bacterial gross growth efficiency	gge_B	0.20, 0.40, 0.60	Dimensionless
Maximum bacterial growth rate	μ_B	13.3	d^{-1}
Saturation const. for ammonium uptake by B	BK_A	0.50	mmol N m^{-3}
Bacterial non-grazing mortality	S_B	0, 0.02	d^{-1}
Bacteria C/N ratio	λ_B	5.1	mol mol^{-1}
Viruses			
P_L viral infection rate	Ψ_{P_L}	3.0, 0.58	μM^{-1} N d^{-1}
P_S viral infection rate	Ψ_{P_S}	4.0, 0.75	μM^{-1} N d^{-1}
Bacteria viral infection rate	Ψ_B	3.0, 1.0	μM^{-1} N d^{-1}
Production of new virus from lysis	ε_V	0.50	Dimensionless
Viral decay rate	υ	0.08, 0.2	h^{-1}
Virus C/N ratio	λ_V	3.26	mol mol^{-1}
DOM, detritus, and other parameters			
Partitioning of sloppy feeding on Z_L	ω_{Z_L}	0.69	Dimensionless
Partitioning of sloppy feeding on D	ω_D	0.24	Dimensionless
Partitioning of sloppy feeding on P_L	ω_{P_L}	0.26	Dimensionless
Partitioning of organic matter to D and DOM	β_1	0.75	Dimensionless
Partitioning of sloppy feeding products to D and DOM	β_2	0.25	Dimensionless

Labile fraction of DOM production	δ_1	0.10	Dimensionless
Semi-labile fraction of DOM production	δ_2	0.80	Dimensionless
Refractory fraction of DOM production	δ_3	0.10	Dimensionless
Maximum semi-labile DOM hydrolysis	μ_S	4.0	d^{-1}
Saturation const. for DOM hydrolysis	K_S	417	mmol C m^{-3}
Partitioning of phytoplankton exudation to labile DOM	o_L	0.40	Dimensionless
Partitioning of phytoplankton exudation to semi-labile DOM	o_S	0.50	Dimensionless
Partitioning of phytoplankton exudation of refractory DOM	o_R	0.10	Dimensionless
Nitrification rate	ϖ_1	0.03	d^{-1}
Partitioning of phytoplankton lysis product to D	ε_D	0.375	Dimensionless
Partitioning of phytoplankton lysis product to L_C and L_N	ε_L	0.08	Dimensionless
Partitioning of phytoplankton lysis product to S_C and S_N	ε_S	0.030	Dimensionless
Partitioning of phytoplankton lysis product to R_C and R_N	ε_R	0.015	Dimensionless
Partitioning of B lysis product to L_C and L_N	ε_{B1}	0.35	Dimensionless
Partitioning of B lysis product to S_C and S_N	ε_{B2}	0.10	Dimensionless
Partitioning of B lysis product to R_C and R_N	ε_{B3}	0.05	Dimensionless
Breakdown of N detritus to DOM	χ_{D_N}	0.055	d^{-1}
Breakdown of C detritus to DOM	χ_{D_C}	0.040	d^{-1}
Partitioning of viral decay L_C and L_N	η	0.70	Dimensionless
Labile fraction of DOM from refractory DOM hydrolysis	τ	0.9965	Dimensionless
UV photooxidation of refractory DOM	UV	0.0015	d^{-1}
Partitioning of zooplankton excretion to DON and NH_4^+	κ_Z	0.68	Dimensionless
Partioning of zooplankton DOM excretion to L and S	o_Z	0.80	Dimensionless
Partitioning of zooplankton metabolized C to DIC and DOC	σ_Z	0.31	Dimensionless
DOC photooxidation to DIC	χ_{UV_C}	0.001, 0.004	d^{-1}
Velocity of material entering and leaving the system	h	0.01	m h^{-1}
Concentration of ammonium entering the system	A^0	0.1, 2, 50	mmol N m^{-3}
Concentration of nitrate entering the system	N_n^0	0.2, 2, 85	mmol N m^{-3}
Concentration of DON entering the system	DON^0	10, 15, 100	mmol N m^{-3}
C:N ratio of detritus	λ_D	D_C / D_N	mol mol^{-1}
Redfield C:N ratio	$\lambda_{C:N}$	6.625	mol mol^{-1}
C:N of DOM entering the system	λ_{DOM}	14, 17, 10	Dimensionless

Appendix B: Model Equations

Phytoplankton

The equation for large phytoplankton is:

Equation 1

$$\frac{\partial P_L}{\partial t} = \alpha J_{P_L} \mathrm{Q}_{\mathrm{P_L}} P_L + hP_L^o - S_{P_L} P_L - \mathrm{G}_{\mathrm{Z_L} P_L} - \mathrm{G}_{\mathrm{Z_S} P_L} - \Psi_{P_L} V_P P_L - hP_L.$$

The equation for small phytoplankton is:

Equation 2

$$\frac{\partial P_S}{\partial t} = \alpha J_{P_S} Q_{P_S} P_S + hP_S^o - S_{P_S} P_S - \mathrm{G}_{\mathrm{Z_L} P_S} - \mathrm{G}_{\mathrm{Z_S} P_S} - \Psi_{P_S} V_P P_S - hP_S.$$

In (1): $J_{P_L} = \mu_P (1 - e^{-I/I_P})(e^{-I/I_\beta})$ and $Q_{P_L} = Q_{P_L}^1 + Q_{P_L}^2 + Q_{P_L}^3$.

In (2): $J_{P_S} = 1.3\ \mu_P (1 - e^{-I/I_P})(e^{-I/I_\beta})$ and $Q_{P_S} = Q_{P_S}^1 + Q_{P_S}^2 + Q_{P_S}^3$

The uptake of nitrogen by phytoplankton, $Q_{P_{L\,or\,S}}$, is designed so that the uptake of nitrate, $Q_{P_{L\,or\,S}}^3$, is inhibited if the nitrogen requirements are met by the uptake of ammonium, $Q_{P_{L\,or\,S}}^1$, and labile DON, $Q_{P_{L\,or\,S}}^2$. Where $Q_{P_{L\,or\,S}}^1 = \frac{A}{K_{P_{L\,or\,S}A} + A}$, $Q_{P_{L\,or\,S}}^2 = \frac{L_N}{K_{P_{L\,or\,S}L_N} + L_N}$, and if $Q_{P_{L\,or\,S}}^1 + Q_{P_{L\,or\,S}}^2$ is less than one then $Q_{P_{L\,or\,S}}^3 = \frac{N_n}{K_{P_{L\,or\,S}N_n} + N_n}(1 - (Q_{P_{L\,or\,S}}^1 + Q_{P_{L\,or\,S}}^2))$. Else $Q_{P_{L\,or\,S}}^3 = 0$.

Phytoplankton also exude "extra carbon" due to metabolic instabilities that are caused by shifts in environmental conditions (light, nutrients, salinity, etc.). This is modeled by transferring carbon from DIC to DOC in proportion, ϖ_2, to total phytoplankton growth: $E_{P_{L\,or\,S}} = \varpi_2 \lambda_P J_{P_{L\,or\,S}} Q_{P_{L\,or\,S}} P_{L\,or\,S}$.

Zooplankton

The equation for large zooplankton is:

Equation 3

$$\frac{\partial Z_L}{\partial t} = F_{Z_L} + hZ_L^o - G_{Z_L Z_L} - S_{Z_L} Z_L^2 - hZ_L$$

In (3) large zooplankton production, F_{Z_L} (mmoles N m^{-3} d^{-1}), is calculated according to the stoichiometric model of Anderson and Hessen (1995). This model operates on the basis of a food threshold elemental ratio, $\theta^*_{f_{Z_L}}$ (mol C mol^{-1} N), below which C limits growth and above which N limits growth. $\theta^*_{f_{Z_L}} = \frac{\beta_{N_Z} \lambda_Z}{\beta_{C_Z} ge_{Z_L}}$ where β_{N_Z} and β_{C_Z} are assimilation efficiencies for N and C, λ_Z is the zooplankton C/N ratio and ge_{Z_L} is C production efficiency (fraction assimilated C allocated to production, remainder respired). Intakes of N and C, $I_{N_{Z_L}}$, $\mathrm{I}_{C_{Z_L}}$ (mmol m^{-3} d^{-1}) are the sum of large zooplankton grazing on large and small phytoplankton, large and small zooplankton, bacteria, and detritus less "sloppy feeding" losses:

$$I_{N_{Z_L}} = (1-\omega_{P_L})\mathrm{G}_{\mathrm{Z_L}P_L} + \mathrm{G}_{\mathrm{Z_L}P_S} + (1-\omega_{D_N})\mathrm{G}_{\mathrm{Z_L}D_N} + \mathrm{G}_{\mathrm{Z_L}B} + (1-\omega_{Z_L})\mathrm{G}_{\mathrm{Z_L}Z_L} + \mathrm{G}_{\mathrm{Z_L}Z_S}$$

$$I_{C_{Z_L}} = (1-\omega_{P_L})\lambda_P \mathrm{G}_{\mathrm{Z_L}P_L} + \lambda_P \mathrm{G}_{\mathrm{Z_L}P_S} + (1-\omega_{D_C})\mathrm{G}_{\mathrm{Z_L}D_C} + \lambda_B \mathrm{G}_{\mathrm{Z_L}B} + (1-\omega_{Z_L})\lambda_Z \mathrm{G}_{\mathrm{Z_L}Z_L} + \lambda_Z \mathrm{G}_{\mathrm{Z_L}Z_S}$$

where the coefficient ($1-\omega_i$) represents prey that is ingested and not lost to sloppy feeding and $\mathrm{G}_{\mathrm{Z_L}P_L} = m_{P_L} Z_L C_{Z_L} P_L, \mathrm{G}_{\mathrm{Z_L}P_S} = m_{P_S} Z_L C_{Z_L} P_S, \mathrm{G}_{\mathrm{Z_L}D_N} = m_D Z_L C_{Z_L} D_N, \mathrm{G}_{\mathrm{Z_L}Z_L} = m_{Z_L} C_{Z_L} Z_L^2,$ $\mathrm{G}_{\mathrm{Z_L}B} = m_B Z_L C_{Z_L} B$, $\mathrm{G}_{\mathrm{Z_L}D_C} = m_D Z_L C_{Z_L} D_C$, and $\mathrm{G}_{\mathrm{Z_L}Z_S} = m_{Z_S} Z_L C_{Z_L} Z_S$. The coefficient C_{Z_L} is the maximum large zooplankton consumption rate and

$$m_{P_L} = \Phi_{P_L}/\Theta,\ m_{P_S} = \Phi_{P_S}/\Theta,\ m_D = \Phi_D/\Theta,\ m_{Z_L} = \Phi_{Z_L}/\Theta,\ m_B = \Phi_B/\Theta,\ m_{Z_S} = \Phi_{Z_L}/\Theta.$$

$$\Theta = \Phi_{P_L} P_L + \Phi_{\mathrm{P_S}} P_S + \Phi_D D_N + \Phi_{Z_L} Z_L + \Phi_B \mathrm{B} + \Phi_{Z_S} Z_S + K_Z.$$

This formulation allows assignment of "preferences" for the different forms of organic nitrogen (Fasham et al., 1990; McCreary et al., 1996). For simplicity, the half-saturation constant K_Z, is assumed to be the same for all substrates.

If the C/N ratio of ingested food ($\theta_{f_{Z_L}} = I_{C_{Z_L}} / I_{N_{Z_L}}$) is greater than $\theta^*_{f_{Z_L}}$ then N limits production, excretion of N (E_{Z_L}, mmol m^{-3} d^{-1}) is zero, and F_{Z_L} is (Anderson and Hessen, 1995): $F_{Z_L} = \beta_{N_Z} I_{N_{Z_L}}$ whereas if $\theta_{f_{Z_L}} < \theta^*_{f_{Z_L}}$ then C limits production and the equations for F_{Z_L} and E_{Z_L} are: $F_{Z_L} = \dfrac{\beta_C g e_{Z_L} I_{C_{Z_L}}}{\lambda_{Z_L}}$ and $E_{Z_L} = I_C \left(\dfrac{\beta_N}{\theta_{f_{Z_L}}} - \dfrac{\beta_C g e_{Z_L}}{\lambda_{Z_L}} \right)$.

Large zooplankton respiration, R_{Z_L} (mmol C m^{-3} d^{-1}), is $R_{Z_L} = \beta_{C_Z} I_{C_{Z_L}} - \lambda_Z F_{Z_L}$.

The equation for small zooplankton is:

Equation 4

$$\frac{\partial Z_S}{\partial t} = F_{Z_S} + hZ_S^o - G_{Z_L Z_S} - G_{Z_S Z_S} - S_{Z_S} Z_S^2 - hZ_S,$$

Small zooplankton production, F_{Z_S} (mmoles N m^{-3} d^{-1}), is calculated according to the stoichiometric model of Anderson and Hessen (1995) described above. However, there are notable differences between small and large zooplankton such as no grazing by small zooplankton on large zooplankton and no losses due to "sloppy feeding" during small zooplankton grazing. Thus, the equations for small zooplankton growth are the same as for large zooplankton (substituting the appropriate subscripts) except for the following:

$I_{N_{Z_S}} = \mathrm{G}_{\mathrm{Z_S}P_L} + \mathrm{G}_{\mathrm{Z_S}P_S} + \mathrm{G}_{\mathrm{Z_S}D_N} + \mathrm{G}_{\mathrm{Z_S}B} + \mathrm{G}_{\mathrm{Z_S}Z_S}$ and

$I_{C_{Z_S}} = \lambda_P \mathrm{G}_{\mathrm{Z_S}P_L} + \lambda_P \mathrm{G}_{\mathrm{Z_S}P_S} + \mathrm{G}_{\mathrm{Z_S}D_C} + \lambda_B \mathrm{G}_{\mathrm{Z_S}B} + \lambda_Z \mathrm{G}_{\mathrm{Z_S}Z_S}$ where $G_{Z_S P_L} = n_{P_L} Z_S C_{Z_S} P_L$,

$G_{Z_S P_S} = n_{P_S} Z_S C_{Z_S} P_S$, $G_{Z_S D_N} = n_D Z_S C_{Z_S} D_N$, $G_{Z_S Z_S} = n_{Z_S} C_{Z_S} Z_S^2$, $G_{Z_S B} = n_B Z_S C_{Z_S} B$, and

$$G_{Z_S D_C} = n_D Z_S C_{Z_S} D_C .$$

$n_{P_L} = \varphi_{P_L} / \sigma,\ n_{P_S} = \varphi_{P_S} / \sigma,\ n_D = \varphi_D / \sigma,\ n_{Z_S} = \varphi_{Z_S} / \sigma,\ n_B = \varphi_B / \sigma$, and
$\sigma = \varphi_{P_L} P_L + \varphi_{P_S} P_S + \varphi_D D_N + \varphi_{Z_S} Z_S + \varphi_B B + K_Z .$

Bacteria

The equation for bacteria is:

Equation 5

$$\frac{\partial B}{\partial t} = B_{growth} + hB^o - G_{Z_L B} - G_{Z_S B} - S_B B - \Psi_B\ V_B\ B - hB$$

Bacterial growth, excretion, and respiration (B_{growth}, b_χ, and R_B) are calculated from elemental stoichiometry. This formulation follows that of Anderson and Williams (1998) and assumes that labile DOC and DON are the primary growth substrates, with ammonium supplementing DOM when the C/N of DOM is high. Uptake rates of labile DOC and DON, U_C and U_N, and the potential (uptake only occurs if required) uptake of ammonium, U_A^*, is:

$$U_C = \lambda_B B \mu_B \left(\frac{L_C}{K_{L_C} + L_C} \right),\ U_N = \frac{U_C L_N}{L_C}, \text{ and } U_A^* = \frac{\mu_B B A}{K_{BA} + A} .$$

If potential ammonium and labile DON uptake is sufficient to ensure complete utilization of DOC, then bacterial growth, excretion, and respiration (B_{growth}, b_χ, and R_B) are:

$$B_{growth} = \frac{gge_B U_C}{\lambda_B},\ R_B = U_C (1 - gge_B), \text{ and } b_\chi = U_C \left(\frac{U_N}{U_C} - \frac{gge_B}{\lambda_B} \right) .$$

The realized uptake of ammonium, U_A, is then zero for $b_\chi > 0$, and $-b_\chi$ for $b_\chi < 0$. If labile DON and ammonium uptake cannot deliver enough nitrogen for bacteria to utilize all

available labile DOC, excess DOC is respired and the uptake of ammonium equals U_A^*.

In this case the equations for B_{growth}, b_χ, and R_B are:

$B_{growth} = U_N + U_A$, $R_B = \lambda_B B_{growth}(1/gge_B - 1)$, and $b_\chi = -U_A$.

Detritus

Changes in nitrogenous detritus (mmoles N m^{-3}) are modeled as:

Equation 6

$$\frac{dD_N}{dt} = (1-\beta_{N_Z})(I_{N_{Z_L}} + I_{N_{Z_S}}) + \rho_D(\omega_{P_L} G_{Z_L P_L} + \omega_D G_{Z_L D_N} + \omega_{Z_L} G_{Z_L Z_L} + mB)$$
$$+\beta_1(mP_L + mP_S + mZ_L^2 + mZ_S^2) + \varepsilon_D(\Psi_{P_L} V_P P_L + \Psi_{P_S} V_P P_S + \Psi_B V_B B)$$
$$-\chi_{D_N} D_N - G_{Z_L D_N} - G_{Z_S D_N} - hD_N + hD_N^o$$

Changes in carbon detritus (mmoles C m^{-3}) are modeled as:

Equation 7

$$\frac{dD_C}{dt} = (1-\beta_{C_Z})(I_{C_{Z_L}} + I_{C_{Z_S}}) + \rho_D(\omega_{P_L}\lambda_P G_{Z_L P_L} + \omega_D \lambda_D G_{Z_L D_C} + \omega_{Z_L}\lambda_Z G_{Z_L Z_L} + m\lambda_B B)$$
$$+\beta_1(m\lambda_P P_L + m\lambda_P P_S + m\lambda_Z Z_L^2 + m\lambda_Z Z_S^2) + \beta_5\varepsilon_V(\Psi_{P_L} V_P(\lambda_P - \lambda_{VP})P_L + \Psi_{P_S} V_P(\lambda_P - \lambda_{VP})P_S$$
$$+\Psi_B V_B(\lambda_B - \lambda_{VB})B) + \varepsilon_D(\Psi_{P_L} V_P \lambda_P P_L + \Psi_{P_S} V_P \lambda_P P_S + \Psi_B V_B \lambda_B B) - \chi_{D_C} D_C - G_{Z_L D_C} - G_{Z_S D_C}$$
$$-hD_C + hD_C^o$$

Dissolved inorganic carbon

Equation 8

$$\frac{dDIC}{dt} = -\mathrm{J}_{P_L} \mathrm{Q}_{\mathrm{P_L}} P_L \lambda_{\mathrm{P}} - J_{P_S} Q_{P_S} P_S \lambda_{\mathrm{P}} - E_{P_L} - E_{P_S} + \sigma_Z(R_{Z_L} + R_{Z_S})$$
$$+R_B + \chi_{UV_C}(L_C + S_C + R_C) + hDIC^o - hDIC$$

Nutrients

Equations for nitrate (N_n) and ammonium (A) are:

Equation 9

$$\frac{dN_n}{dt} = -J_{P_L} Q^3_{P_L} P_L - J_{P_S} Q^3_{P_S} P_S + \varpi_1 A + hN^0_n - hN_n$$

Equation 10

$$\frac{dA}{dt} = \kappa_Z (E_{Z_L} + E_{Z_S}) + b_\chi - J_{P_L} Q^1_{P_L} P_L - J_{P_S} Q^1_{P_S} P_S - U_A - \varpi_1 A + \chi_{UV_N} (S_N + R_N) + hA^0 - hA$$

Dissolved organic matter

Equations for labile (L_C and L_N), semi-labile (S_C and S_N), and refractory (R_C and R_N) DOM are:

Equation 11

$$\begin{aligned}\frac{dL_N}{dt} &= o_L(1-\alpha)(J_{P_L} Q_{P_L} P_L + J_{P_S} Q_{P_S} P_S) + (1-\beta_1)(mP_L + mP_S + mZ^2_L + mZ^2_S)) + o_Z((1-\kappa_Z)(E_{Z_L} \\ &+ E_{Z_S})) + \rho_L(\omega_{P_L} G_{Z_L P_L} + \omega_D G_{Z_L D_N} + \omega_{Z_L} G_{Z_L Z_L} + mB) + \delta_1 \chi_{D_N} D_N + \eta \upsilon (V^2_P + V^2_B) \\ &+ \varepsilon_L(\Psi_{P_L} V_P P_L + \Psi_{P_S} V_P P_S + \Psi_B V_B B) + \tau \frac{\mu_S S_N \lambda_B B}{K_S + S_C} - U_N - J_{P_L} Q^2_{P_L} P_L - J_{P_S} Q^2_{P_S} P_S \\ &+ \zeta R_N + hL^o_N - hL_N\end{aligned}$$

Equation 12

$$\begin{aligned}\frac{dL_C}{dt} &= o_L((1-\alpha)\lambda_P(J_{P_L} Q_{P_L} P_L + J_{P_S} Q_{P_S} P_S) + E_{P_L} + E_{P_S} + (1-\beta_1)(m\lambda_P P_L + m\lambda_P P_S + m\lambda_Z Z^2_L \\ &+ m\lambda_Z Z^2_S)) + \rho_L(\omega_{P_L} \lambda_P G_{Z_L P_L} + \omega_D G_{Z_L D_C} + \omega_{Z_L} \lambda_Z G_{Z_L Z_L} + m\lambda_B B) + \delta_1 \chi_{D_C} D_C \\ &+ \eta \upsilon \lambda_V (V^2_P + V^2_B) + \varepsilon_L(\Psi_{P_L} V_P \lambda_P P_L + \Psi_{P_S} V_P \lambda_P P_S + \Psi_B V_B \lambda_B B) + \beta_2 \varepsilon_V(\Psi_{P_L} V_P(\lambda_P - \lambda_V) P_L \\ &+ \Psi_{P_S} V_P(\lambda_P - \lambda_V) P_S + \Psi_B V_B(\lambda_B - \lambda_V) B) + \tau \frac{\mu_S S_C \lambda_B B}{K_S + S_C} - \lambda_B B_{growth} - R_B \\ &+ o_Z(1-\sigma_Z)(R_{Z_L} + R_{Z_S}) - \chi_{UV_C} L_C + \zeta R_C + hL^o_N - hL_N\end{aligned}$$

Equation 13

$$\frac{dS_N}{dt} = o_S((1-\alpha)(J_{P_L}Q_{P_L}P_L + J_{P_S}Q_{P_S}P_S) + (1-\beta_1)(mP_L + mP_S + mZ_L^2 + mZ_S^2))$$
$$+(1-o_Z)(1-\kappa_Z)(E_{Z_L} + E_{Z_S}) + \rho_S(\omega_{P_L}G_{Z_LP_L} + \omega_D G_{Z_LD_N} + \omega_{Z_L}G_{Z_LZ_L} + mB)$$
$$+\delta_2\chi_{D_N}D_N + \varepsilon_S(\Psi_{P_L}V_PP_L + \Psi_{P_S}V_PP_S + \Psi_BV_BB) + (1-\eta)\upsilon(V_P^2 + V_B^2) - \chi_{UV_N}S_N$$
$$-\frac{\mu_S S_N \lambda_B B}{K_S + S_C} + hS_N^o - hS_N$$

Equation 14

$$\frac{dS_C}{dt} = o_S((1-\alpha)\lambda_P(J_{P_L}Q_{P_L}P_L + J_{P_S}Q_{P_S}P_S) + E_{P_L} + E_{P_L} + (1-\beta_1)(m\lambda_P P_L + m\lambda_P P_S$$
$$+m\lambda_Z Z_L^2 + m\lambda_Z Z_S^2)) + (1-o_Z)(1-\sigma_Z)(R_{Z_L} + R_{Z_S}) + (1-\eta)\upsilon\lambda_V(V_P^2 + V_B^2)$$
$$+\rho_S(\omega_{P_L}\lambda_P G_{Z_LP_L} + \omega_D G_{Z_LD_C} + \omega_{Z_L}\lambda_Z G_{Z_LZ_L} + m\lambda_B B) + \varepsilon_S(\Psi_{P_L}V_P\lambda_P P_L + \Psi_{P_S}V_P\lambda_P P_S$$
$$+\Psi_BV_B\lambda_B B) + \beta_3\varepsilon_V(\Psi_{P_L}V_P(\lambda_P - \lambda_V)P_L + \Psi_{P_S}V_P(\lambda_P - \lambda_V)P_S) + \Psi_BV_B(\lambda_B - \lambda_V)B)$$
$$+\delta_2\chi_{D_C}D_C - \frac{\mu_S S_C \lambda_B B}{K_S + S_C} - \chi_{UV_C}S_C + hS_N^o - hS_N$$

Equation 15

$$\frac{dR_N}{dt} = o_R((1-\alpha)(J_{P_L}Q_{P_L}P_L + J_{P_S}Q_{P_S}P_S) + (1-\beta_1)(mP_L + mP_S + mZ_L^2 + mZ_S^2))$$
$$+\rho_R(\omega_{P_L}G_{Z_LP_L} + \omega_D G_{Z_LD_N} + \omega_{Z_L}G_{Z_LZ_L} + mB) + \delta_3\chi_{D_N}D_N - \xi R_N$$
$$+\varepsilon_R(\Psi_{P_L}V_PP_L + \Psi_{P_S}V_PP_S + \Psi_BV_BB) + (1-\tau)\left(\frac{\mu_S S_N \lambda_B B}{K_S + S_C}\right) - \chi_{UV_N}R_N$$
$$+hR_N^o - hR_N$$

Figure 16

$$\frac{dR_C}{dt} = o_R((1-\alpha)\lambda_P(J_{P_L}Q_{P_L}P_L + J_{P_S}Q_{P_S}P_S) + E_{P_L} + E_{P_S} + (1-\beta_1)(m\lambda_P P_L + m\lambda_P P_S$$
$$+m\lambda_Z Z_L^2 + m\lambda_Z Z_S^2)) + \rho_R(\omega_{P_L}\lambda_P G_{Z_L P_L} + \omega_D G_{Z_L D_C} + \omega_{Z_L}\lambda_Z G_{Z_L Z_L} + m\lambda_B B)$$
$$+\beta_4\varepsilon_V(\Psi_{P_L}V_P(\lambda_P - \lambda_{VP})P_L + \Psi_{P_S}V_P(\lambda_P - \lambda_{VP})P_S + \Psi_B V_B(\lambda_B - \lambda_{VB})B)$$
$$+\delta_3\chi_{D_C}D_C + \varepsilon_R(\Psi_{P_L}V_P\lambda_P P_L + \Psi_{P_S}V_P\lambda_P P_S + \Psi_B V_B\lambda_B B) - \xi R_C$$
$$+(1-\tau)\left(\frac{\mu_S S_C \lambda_B B}{K_S + S_C}\right) - \chi_{UV_C}R_C + hR_C^o - hR_C$$

Viruses

The equation for bacteria viruses is:

Equation 16

$$\frac{\partial V_B}{\partial t} = \varepsilon_V\ \Psi_B\ V_B\ B\ -\ \upsilon\ V_B^{\ 2} + hV_B^o - hV_B.$$

The equation for phytoplankton viruses is:

Equation 17

$$\frac{\partial V_P}{\partial t} = \varepsilon_V(\Psi_{P_L}V_P P_L + \Psi_{P_S}V_P P_S) - \upsilon V_P^2 + hV_P^o - hV_P.$$

The infection rates for Chapter 2 are calculated as follows:

$$\Psi_B = \frac{0.40}{V_B}$$

$$\Psi_{P_S} = \frac{0.07}{0.44V_P}$$

$$\Psi_{P_L} = \frac{0.03}{0.56V_P}$$

Appendix C: Integrated Phytoplankton Accessory Pigment to Chlorophyll a Ratio Figures

Figure C.1. The depth integrated ratio of selected phytoplankton accessory pigments to chlorophyll *a* at five stations along a transect in the upper Chesapeake Bay on February 23, 2007.

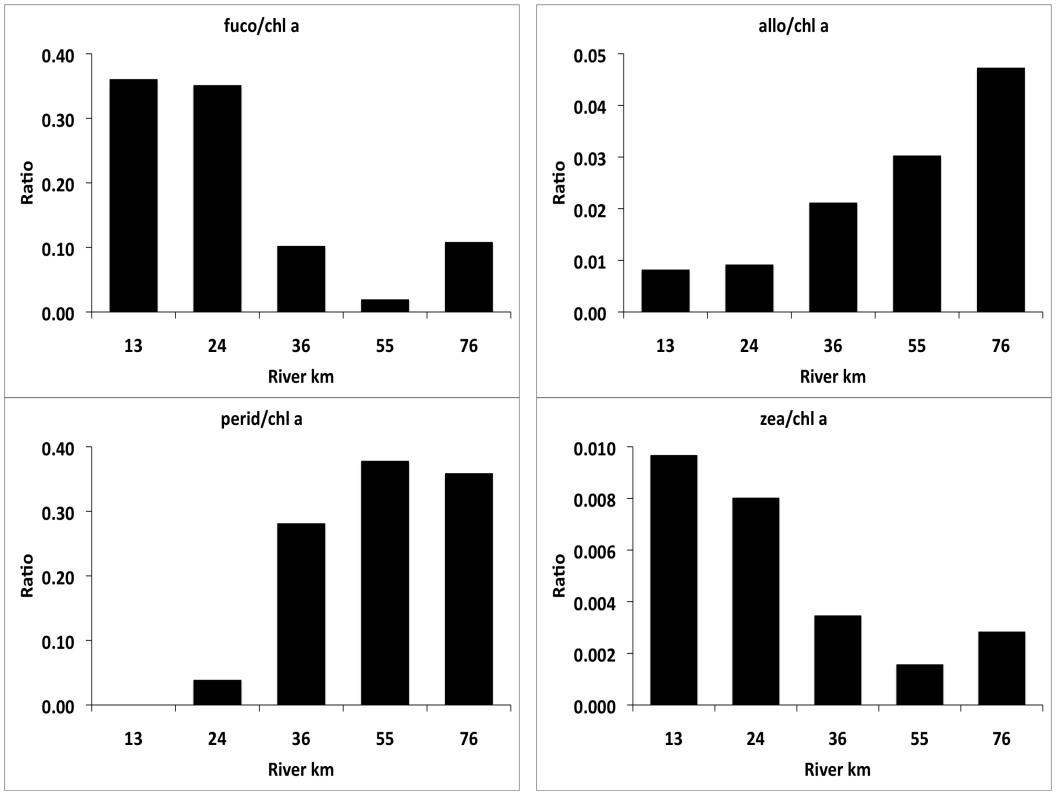

Figure C.2. The depth integrated ratio of selected phytoplankton accessory pigments to chlorophyll *a* at five stations along a transect in the upper Chesapeake Bay on February 26, 2007.

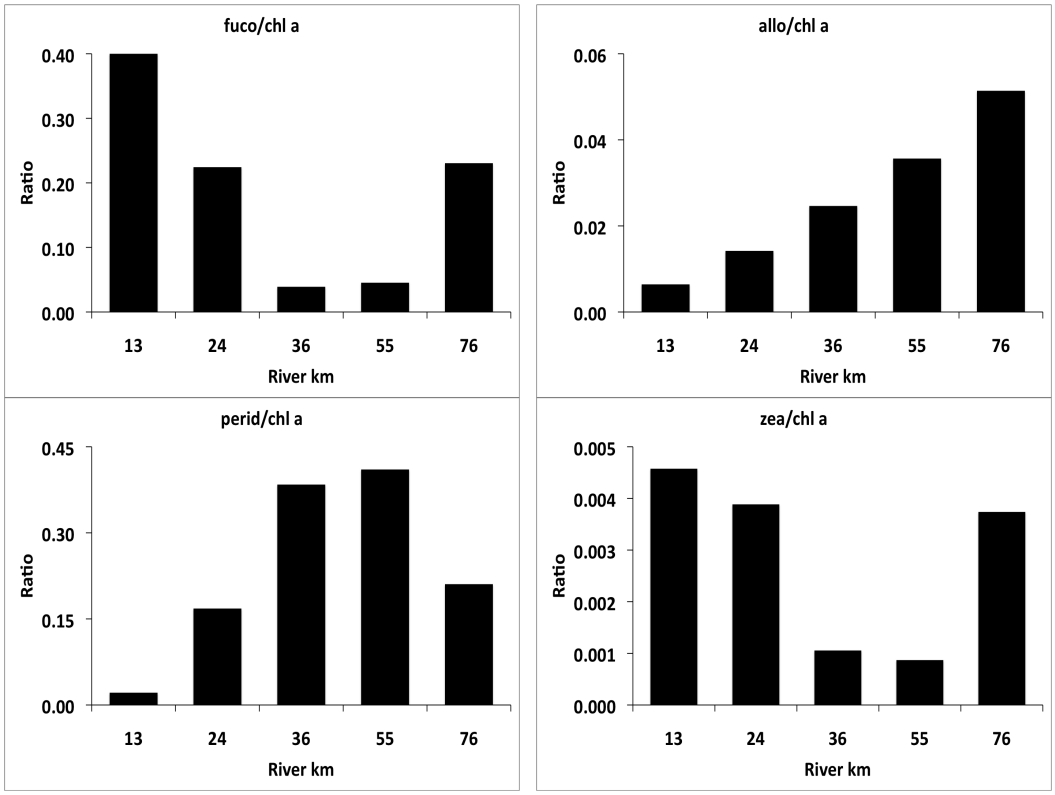

Figure C.3. The depth integrated ratio of selected phytoplankton accessory pigments to chlorophyll *a* at five stations along a transect in the upper Chesapeake Bay on April 9, 2007.

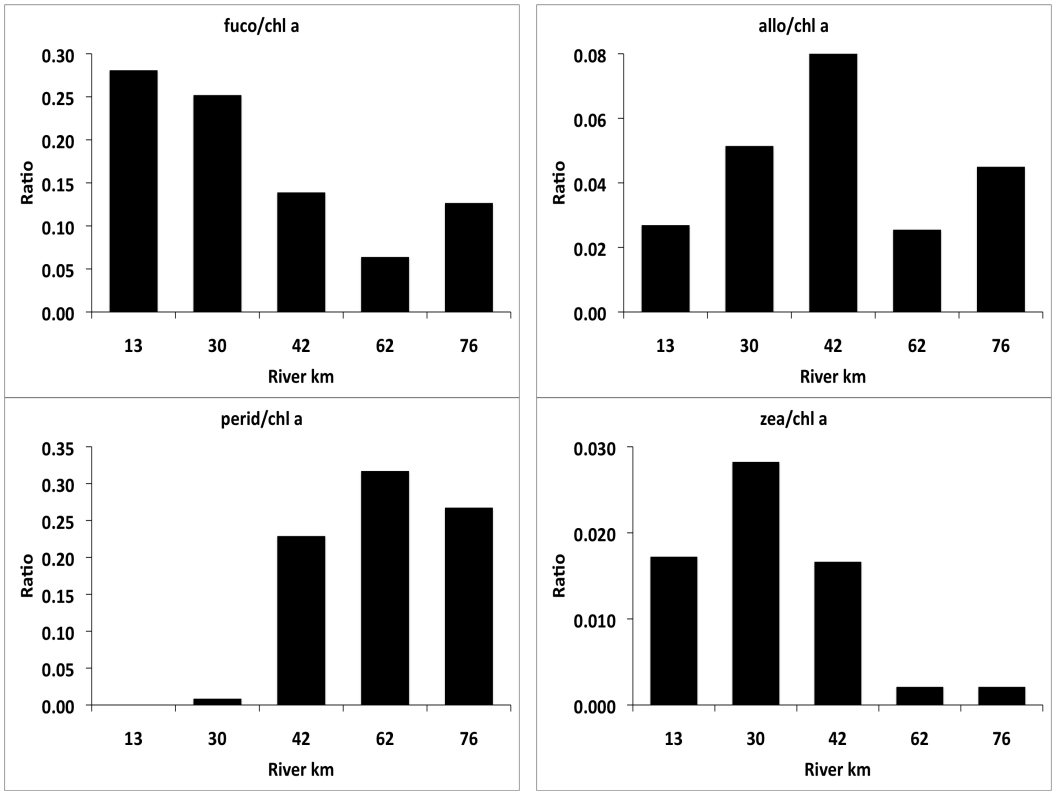

Figure C.4. The depth integrated ratio of selected phytoplankton accessory pigments to chlorophyll *a* at five stations along a transect in the upper Chesapeake Bay on April 15, 2007.

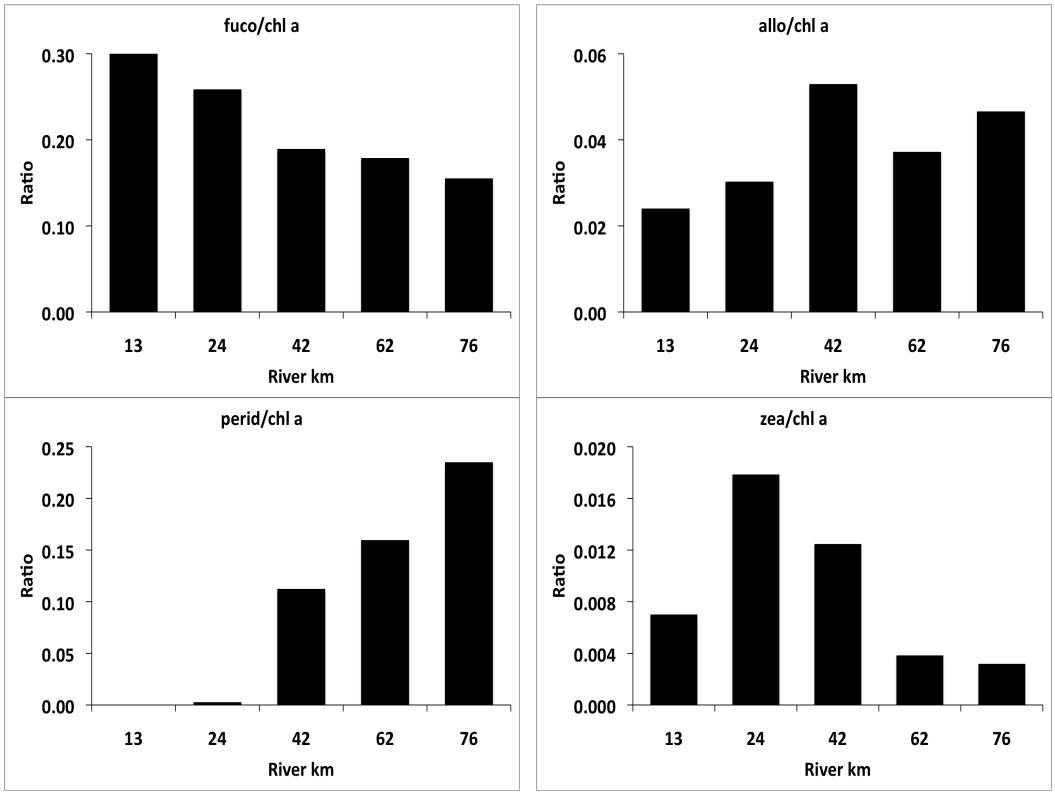

Figure C.5. The depth integrated ratio of selected phytoplankton accessory pigments to chlorophyll *a* at five stations along a transect in the upper Chesapeake Bay on May 8, 2007.

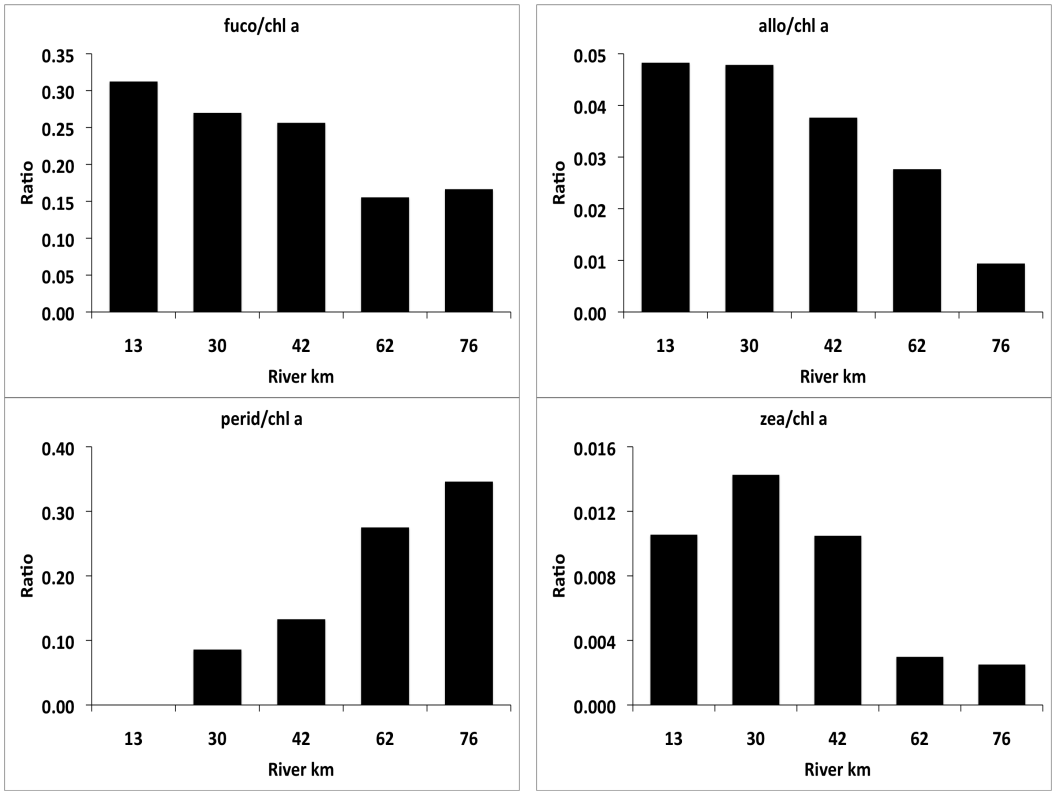

Figure C.6. The depth integrated ratio of selected phytoplankton accessory pigments to chlorophyll *a* at five stations along a transect in the upper Chesapeake Bay on May 14, 2007.

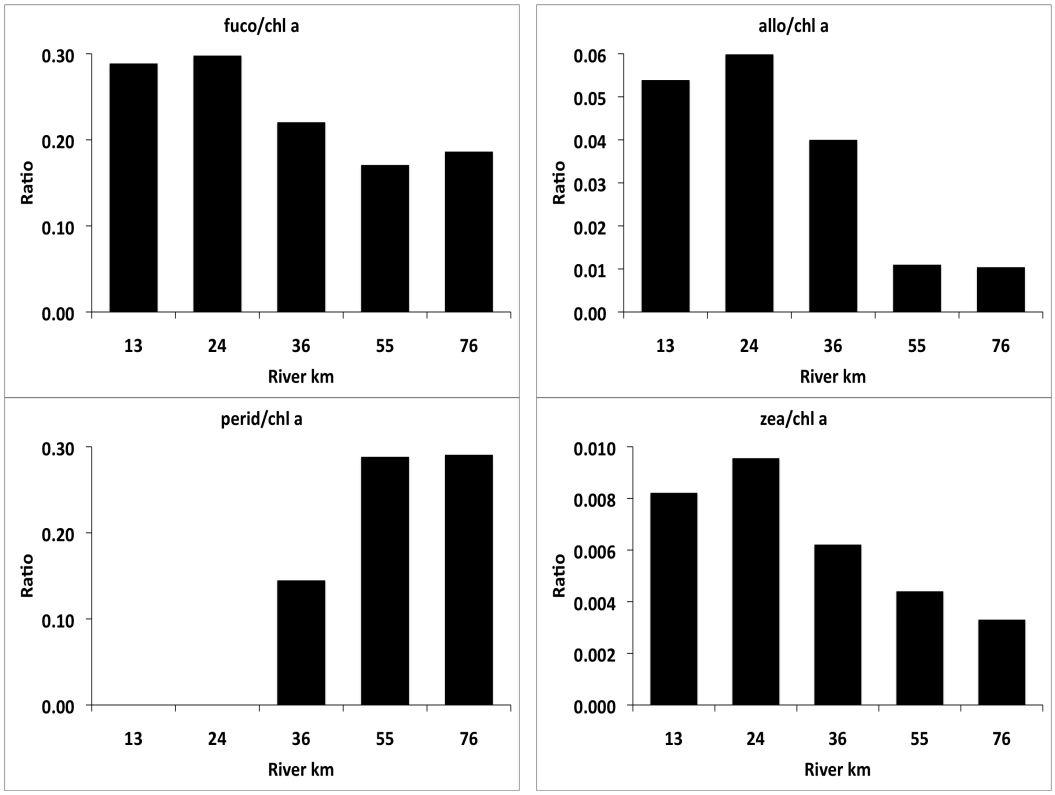

Figure C.7. The depth integrated ratio of selected phytoplankton accessory pigments to chlorophyll *a* at five stations along a transect in the upper Chesapeake Bay on January 23, 2008.

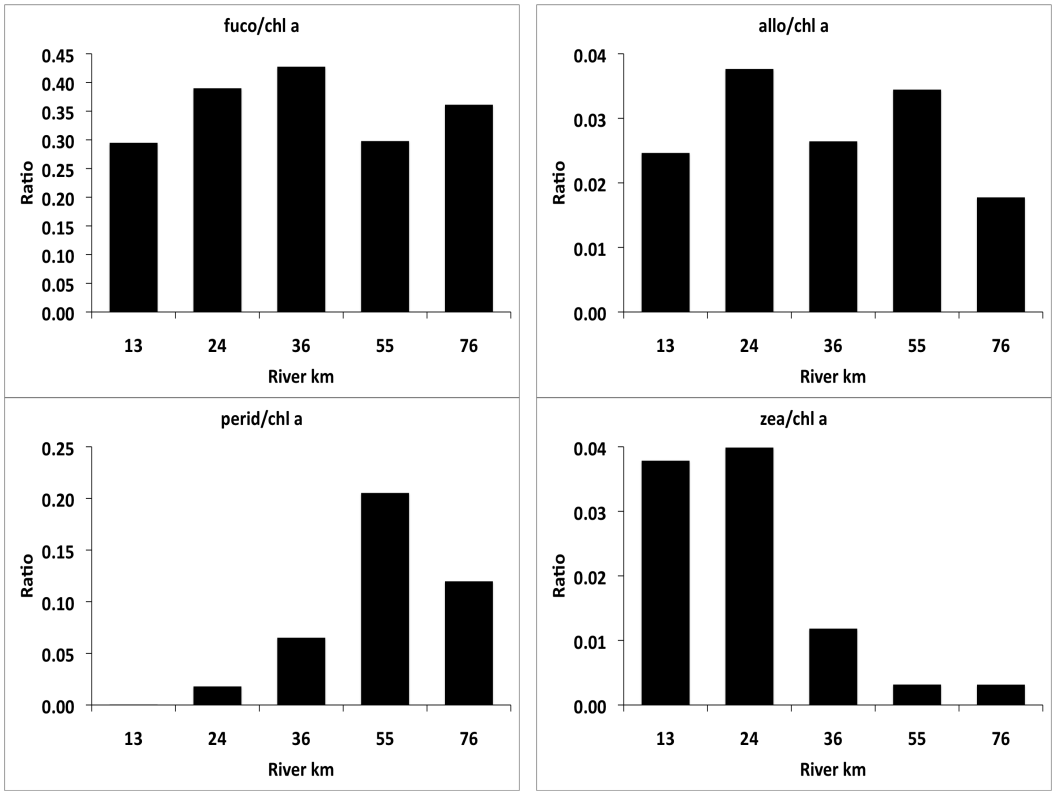

Figure C.8. The depth integrated ratio of selected phytoplankton accessory pigments to chlorophyll *a* at five stations along a transect in the upper Chesapeake Bay on January 26, 2008.

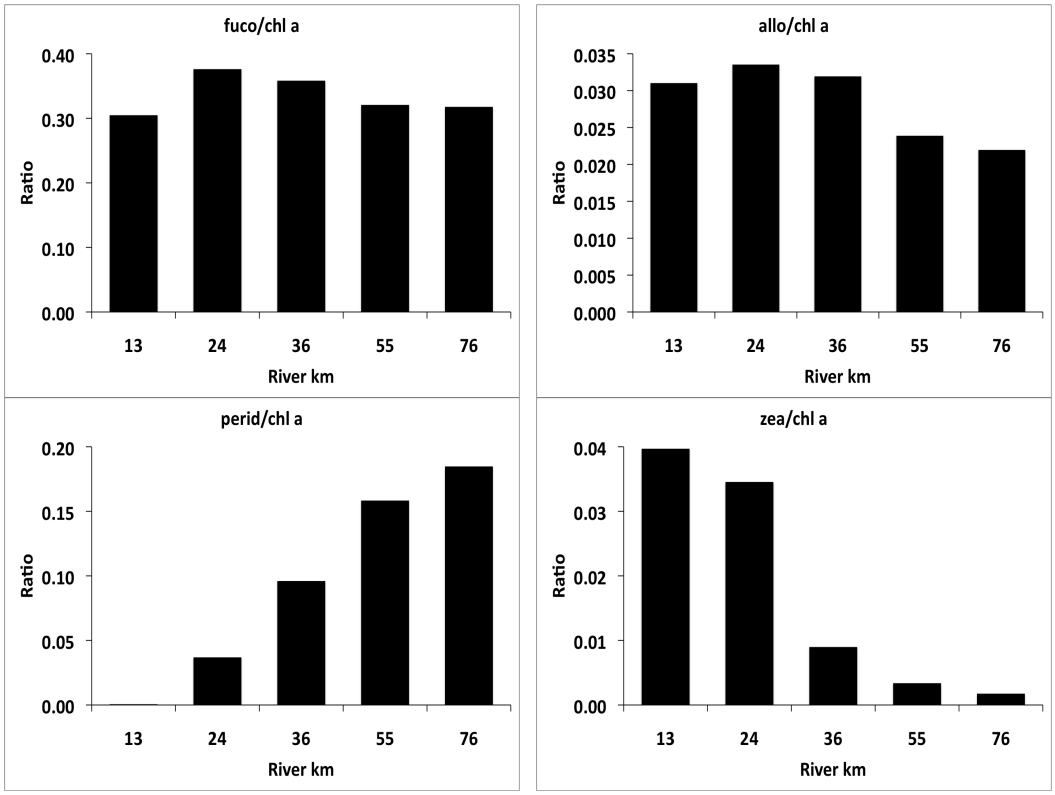

Figure C.9. The depth integrated ratio of selected phytoplankton accessory pigments to chlorophyll *a* at five stations along a transect in the upper Chesapeake Bay on April 17, 2008.

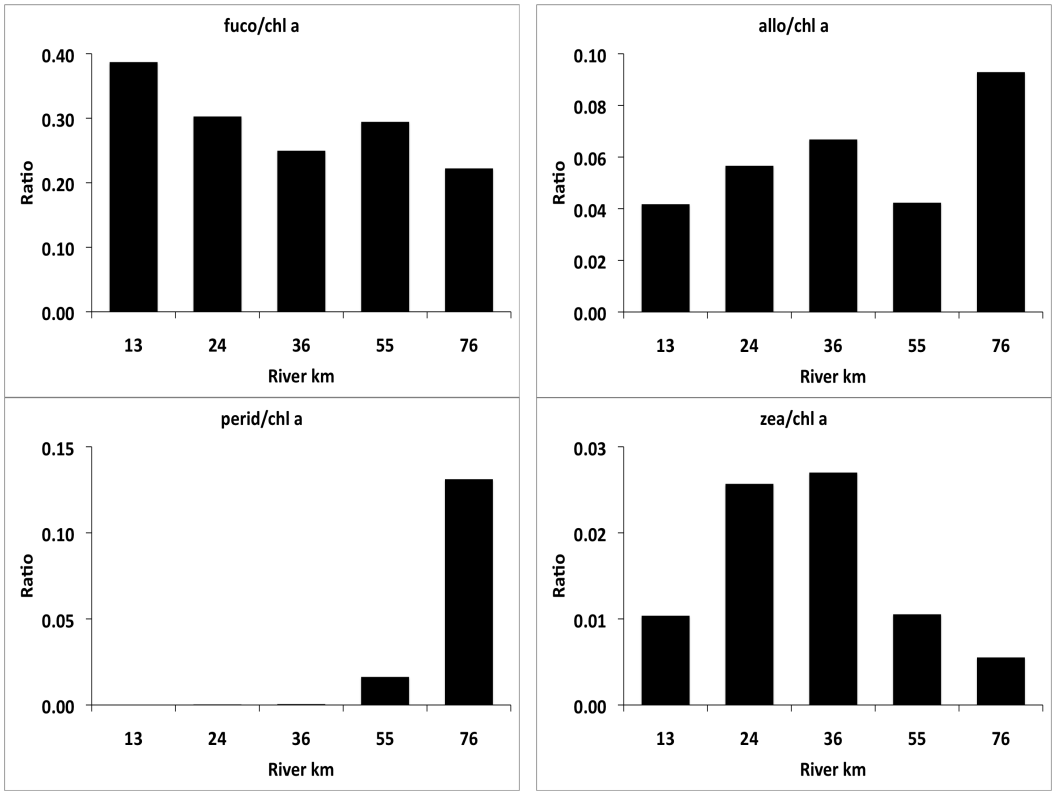

Figure C.10. The depth integrated ratio of selected phytoplankton accessory pigments to chlorophyll *a* at five stations along a transect in the upper Chesapeake Bay on April 23, 2008.

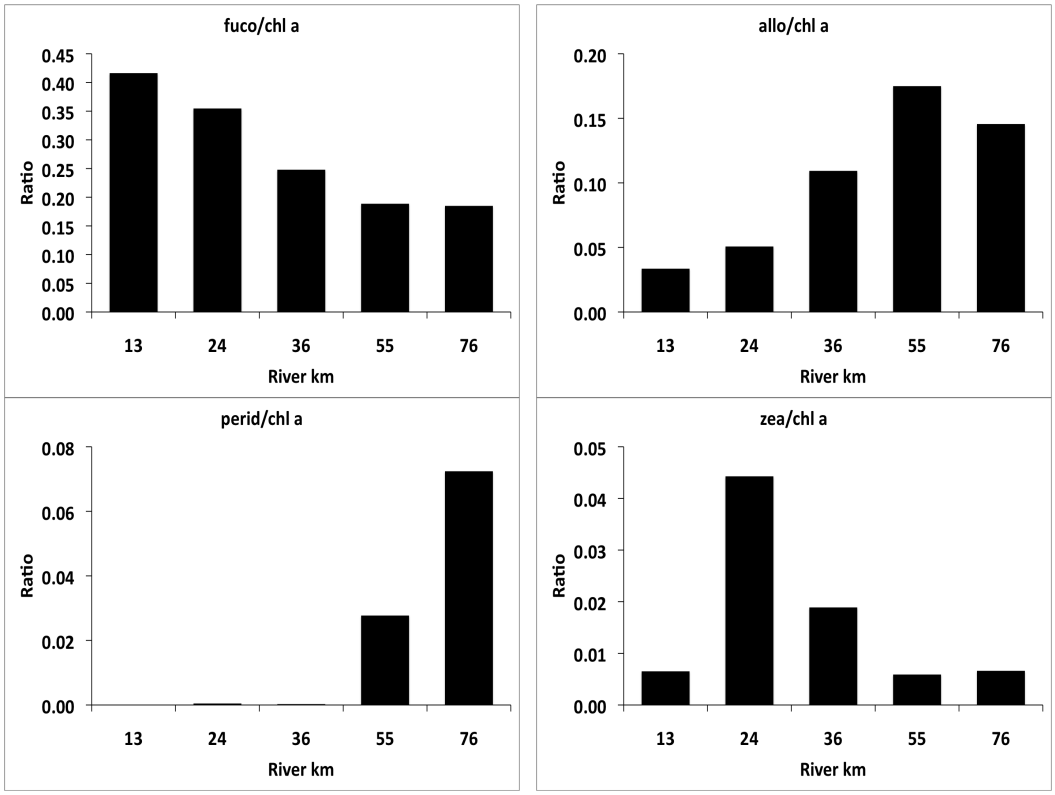

Figure C.11. The depth integrated ratio of selected phytoplankton accessory pigments to chlorophyll *a* at five stations along a transect in the upper Chesapeake Bay on May 16, 2008.

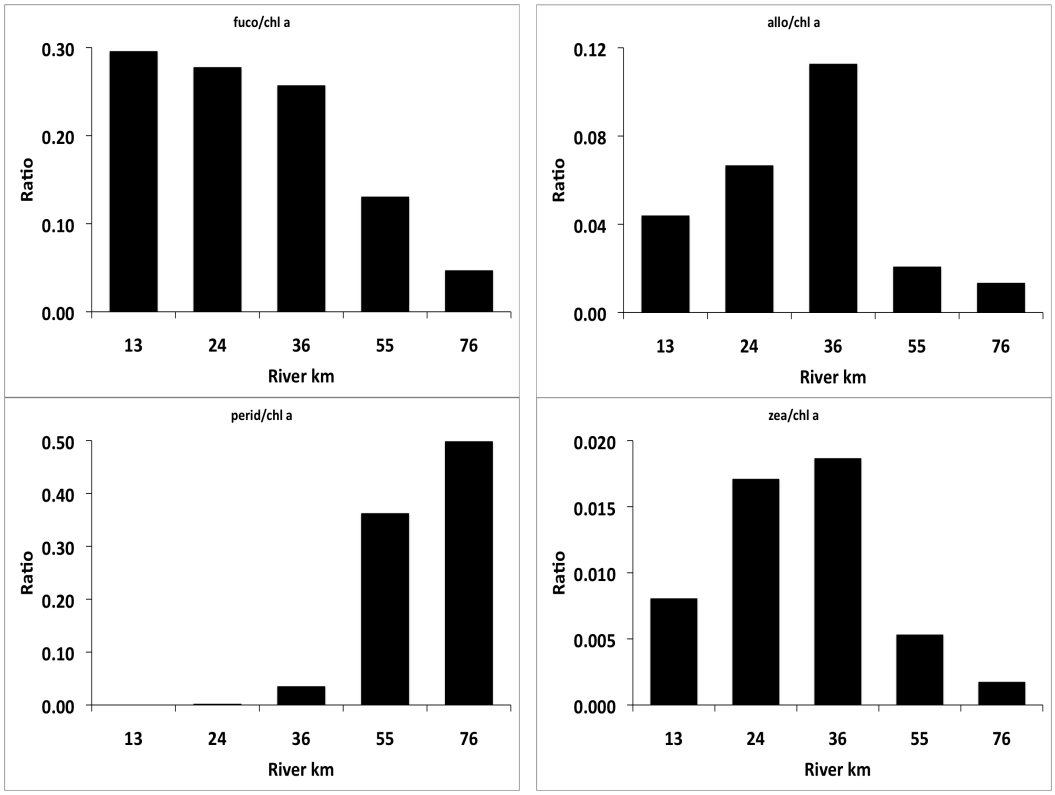

Figure C.12. The depth integrated ratio of selected phytoplankton accessory pigments to chlorophyll *a* at five stations along a transect in the upper Chesapeake Bay on May 22, 2008.

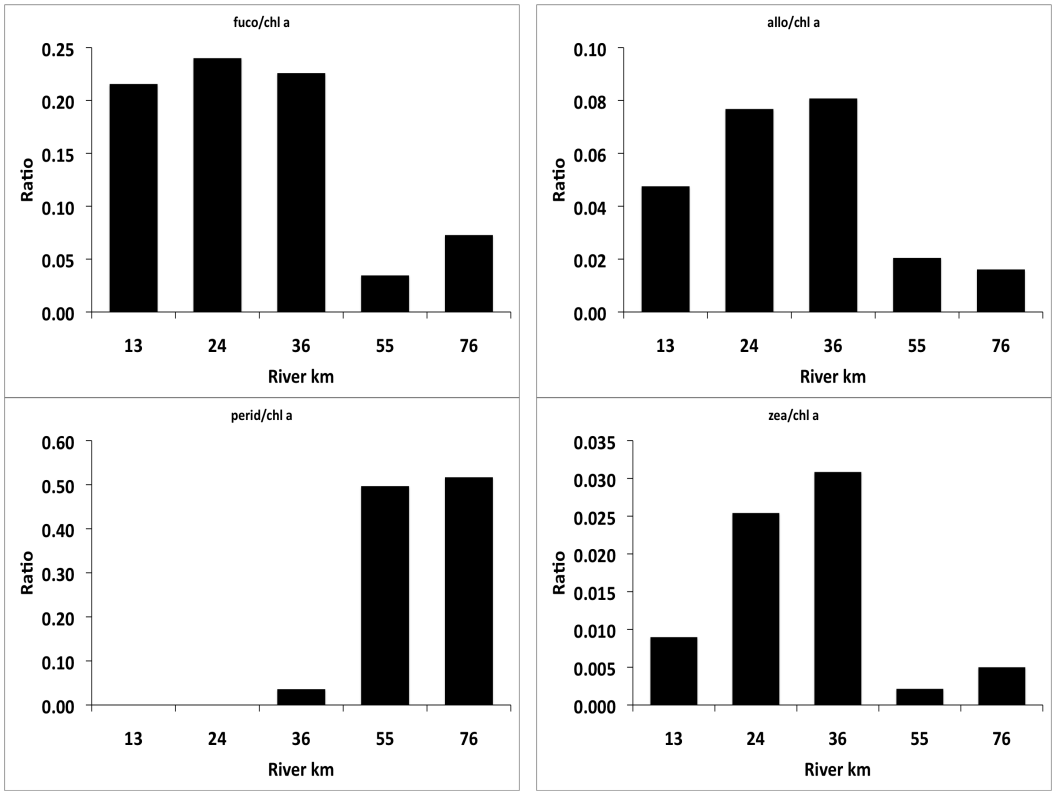

Glossary

If needed.

Bibliography

Adolf, J.E., Yeager, C.L.J., Miller, W.D., Mallonee, M.E., and Harding, L.W. (2006). Environmental forcing of phytoplankton floral composition, biomass, and primary productivity in Chesapeake Bay, USA. Estuarine, Coastal and Shelf Science *67*, 108-122.

Aluwihare, L.I., and Repeta, D.J. (1999). A comparison of the chemical characteristics of oceanic DOM and extracellular DOM produced by marine algae. Marine Ecology Progress Series *186*, 105-117.

Amon, R.M.W., and Benner, R. (1996). Bacterial Utilization of Different Size Classes of Dissolved Organic Matter. Limnology and Oceanography *41*, 41-51.

Anderson, T.R., and Hessen, D.O. (1995). Carbon or nitrogen limitation of marine copepods? Journal of Plankton Research *17*, 317-331.

Anderson, T.R., and Pondaven, P. (2003). Non-redfield carbon and nitrogen cycling in the Sargasso Sea: pelagic imbalances and export flux. Deep-Sea Research I *50*, 573-591.

Anderson, T.R., and Williams, P.J.l.B. (1998). Modelling the Seasonal Cycle of Dissolved Organic Carbon at Station E1 in the English Channel. Estuarine, Coastal and Shelf Science *46*, 93-109.

Anderson, T.R., and Williams, P.J.l.B. (1999). A one-dimensional model of dissolved organic carbon cycling in the water column incorporating combined biological-photochemical decomposition. Global Biogeochemical Cycles *13*, 337-349.

Apple, J.K., del Giorgio, P.A., and Kemp, M. (2006). Temperature regulation of bacterial production, respiration, and growth efficiency in a temperate salt-marsh estuary. Aquatic Microbial Ecology *43*, 243-254.

Arar, E.J., and Collins, G.B. (1997). *In Vitro* Determination of Chlorophyll *a* and Pheophytin *a* in Marine and Freshwater Algae by Fluorescence (U.S. Environmental Protection Agency method 445.0).

Arhonditsis, G.B., Stow, C.A., Paerl, H.W., Valdes-Weaver, L.M., Steinberg, L.J., and Reckhow, K.H. (2007). Delineation of the role of nutrient dynamics and hydrologic forcing on phytoplankton patterns along a freshwater-marine continuum. Ecological Modelling *208*, 230-246.

Arrigo, K.R., Robinson, D.H., Worthen, D.L., Dunbar, R.B., DiTullio, G.R., VanWoert, M., and Lizotte, M.P. (1999). Phytoplankton community structure and the drawdown of nutrients and CO2 in the Southern Ocean. Science *283*, 365-367.

Azam, F., Fenchel, T., Field, J.G., Gray, J.S., Meyer-Reil, L.A., and Thingstad, T.F. (1983). The ecological role of water-column microbes in the sea. Marine Ecology Progress Series *10*, 257-263.

Baines, S.B., and Pace, M.L. (1991). The Production of Dissolved Organic Matter by Phytoplankton and its Importance to Bacteria: Patterns Across Marine and Freshwater Systems. Limnology and Oceanography *36*, 1078-1090.

Baird, D., and Ulanowicz, R. (1989). The Seasonal Dynamics of The Chesapeake Bay Ecosystem. Ecological Monographs *59*, 329-364.

Baudoux, A.-C., and Brussaard, C.P.D. (2005). Characterization of different viruses infecting the marine harmful algal bloom species *Phaeocystis globosa*. Virology *341*, 80-90.

Bauer, J.E., Williams, P.M., and Druffel, E.R.M. (2002). ^{14}C activity of dissolved organic carbon fractions in the north-central Pacific and Sargasso Sea. Nature *357*, 667-670.

Beardsley, R.C., and Boicourt, W.C. (1981). On estuarine and continental shelf circulation in the Middle Atlantic Bight. In Evolution of Physical Oceanography, B.A. Warren, and C. Wunsch, eds. (Cambridge, MA, The MIT Press), pp. 198-233.

Beckmann, A., and Hense, I. (2004). Torn between extremes: the ups and downs of phytoplankton. Ocean Dynamics *54*, 581-592.

Behrenfeld, M., and Falkowski, P.G. (1997). Photosynthetic rates derived from satellite-based chlorophyll concentrations. Limnology and Oceanography *42*, 1-20.

Behrenfeld, M., Falkowski, P.G., Babin, M., Karl, D.M., Barber, R., Siegel, D., Morel, A., O'Reilly, J., and Balch, W. (2006a). Ocean Primary Productivity Working Group (OPPWG) Data (Rutgers University).

Behrenfeld, M.J., O'Malley, R.T., Siegel, D.A., McClain, C.R., Sarmiento, J.L., Feldman, G.C., Milligan, A.J., Falkowski, P.G., Letelier, R.M., and Boss, E.S. (2006b). Climate-driven trends in contemporary ocean productivity. Nature *444*, 752-755.

Benner, R. (2002). Chemical Composition and Reactivity. In Biogeochemistry of Marine Dissolved Organic Matter, D.A. Hansell, and C.A. Carlson, eds. (Elsevier Science (USA)), pp. 59-90.

Benner, R., and Biddanda, B. (1998). Photochemical Transformations of Surface and Deep Marine Dissolved Organic Matter: Effects on Bacterial Growth. Limnology and Oceanography *43*, 1373-1378.

Berman, T., and Bronk, D.A. (2003). Dissolved organic nitrogen: a dynamic participant in aquatic ecosystems. Aquatic Microbial Ecology *31*, 279-305.

Berman, T., and Chava, S. (1999). Algal growth on organic compounds as nitrogen sources. Journal of Plankton Research *21*, 1423-1437.

Biddanda, B., and Benner, R. (1997). Carbon, nitrogen, and carbohydrate fluxes during the production of particulate and dissolved organic matter by marine phytoplankton. Limnology and Oceanography *42*, 506-518.

Biersmith, A., and Benner, R. (1998). Carbohydrates in phytoplankton and freshly produced dissolved organic matter. Marine Chemistry *63*, 131-144.

Bissinger, J.E., Montagnes, D.J.S., Sharples, J., and Atkinson, D. (2008). Predicting marine phytoplankton maximum growth rates from temperature: Improving on the Eppley curve using quantile regression. Limnology and Oceanography *53*, 487-493.

Boenigk, J., and Arndt, H. (2002). Bacterivory by heterotrophic flagellates: community structure and feeding strategies. Antonie van Leeuwenhoek *81*, 465-480.

Boicourt, W.C. (1992). Influence of circulation processes on dissolved oxygen in the Chesapeake Bay. In Oxygen Dynamics in Chesapeake Bay: A Synthesis of Research, D. Smith, M. Leffler, and G. Mackiernan, eds. (University of Maryland Sea Grant), pp. 7-53.

Børsheim, K.Y., and Bratbak, G. (1987). Cell volume to cell carbon conversion factors for a bacterivorous *Monas* sp. enriched from seawater. Marine Ecology Progress Series *36*, 171-175.

Bratbak, G., Jacobsen, A., and Heldal, M. (1998a). Viral lysis of *Phaeocystis pouchetii* and bacterial secondary production. Aquatic Microbial Ecology *16*, 11-16.

Bratbak, G., Jacobsen, A., Heldal, M., Nagasaki, K., and Thingstad, F. (1998b). Virus production in *Phaeocystis pouchetii* and its relation to host cell growth and nutrition. Aquatic Microbial Ecology *16*, 1-9.

Bronk, D.A. (2002). Dynamics of DON. In Biogeochemistry of Marine Dissolved Organic Matter, D.A. Hansell, and C.A. Carlson, eds. (Elsevier Science (USA)), pp. 153-247.

Bronk, D.A., Glibert, P.M., Malone, T.C., Banahan, S., and Sahlsten, E. (1998). Inorganic and organic nitrogen cycling in Chesapeake Bay: autotrophic versus heterotrophic processes and relationships to carbon flux. Aquatic Microbial Ecology *15*, 177-189.

Brophy, J.E., and Carlson, D.J. (1989). Production of biologically refractory dissolved organic carbon by natural seawater microbial populations. Deep-Sea Research A *36*, 497-507.

Brownlee, D., and Jacobs, F. (1987). Mesozooplankton and microzooplankton in the Chesapeake Bay. In Contaminant problems and management of living Chesapeake Bay

resources, S. Majumdar, L. Hall, and H. Austin, eds. (Philadelphia, PA, Pennsylvania Academy of Science), pp. 217-269.

Brush, M.J., Brawley, J.W., Nixon, S.W., and Kremer, J.N. (2002). Modeling phytoplankton production: problems with the Epply curve and an emperical alternative. Marine Ecology Progress Series *238*, 31-45.

Brussaard, C.P.D., Bratbak, G., Baudoux, A.-C., and Ruardij, P. (2007). *Phaeocystis* and its interaction with viruses. Biogeochemistry *83*, 201-215.

Brussaard, C.P.D., Kuipers, B., and Veldhuis, M.J.W. (2005a). A mesocosm study of *Phaeocystis globosa* population dynamics I. Regulatory role of viruses in bloom control. Harmful Algae *4*, 859-874.

Brussaard, C.P.D., Mari, X., Van Bleijswijk, J.D.L., and Veldhuis, M.J.W. (2005b). A mesocosm study of *Phaeocystis globosa* (Prymnesiophyceae) population dynamics II. Significance for the microbial community. Harmful Algae *4*, 875-893.

Brussaard, C.P.D., Marie, D., Thyrhaug, R., and Bratbak, G. (2001). Flow cytometric analysis of phytoplankton viability following viral infection. Aquatic Microbial Ecology *26*, 157-166.

Brussaard, C.P.D., Timmermans, K.R., Uitz, J., and Veldhuis, M.J.W. (2008). Virioplankton dynamics and virally induced phytoplankton lysis versus microzooplankton grazing southeast of the Kerguelen (Southern Ocean). Deep-Sea Research Part II-Topical Studies in Oceanography *55*, 752-765.

Burdige, D.J., and Zheng, S. (1998). The Biogeochemical Cycling of Dissolved Organic Nitrogen in Estuarine Sediments. Limnology and Oceanography *43*, 1796-1813.

Calbet, A., and Landry, M.R. (2004). Phytoplankton growth, microzooplankton grazing, and carbon cycling in marine systems. Limnology and Oceanography *49*, 51-57.

Carlson, C.A. (2002). Production and Removal Processes. In Biogeochemistry of Marine Dissolved Organic Matter, D.A. Hansell, and C.A. Carlson, eds. (Elsevier Science (USA)), pp. 91-151.

Carlson, C.A., and Ducklow, H.W. (1995). Dissolved organic carbon in the upper ocean of the central equatorial Pacific Ocean, 1992: Daily and finescale vertical variations. Deep-Sea Research II *42*, 639-656.

Caron, D.A., Goldman, J.C., and Fenchel, T. (1990). Protozoan respiration and metabolism. In Ecology of marine protozoa, G.M. Capriulo, ed. (Oxford University Press), pp. 307-322.

Carr, M.E., Friedrichs, M.A.M., Schmeltz, M., Aita, M.N., Antoine, D., Arrigo, K.R., Asanuma, I., Aumont, O., Barber, R., Behrenfeld, M.*, et al.* (2006). A comparison of

global estimates of marine primary production from ocean color. Deep-Sea Research Part Ii-Topical Studies In Oceanography *53*, 741-770.

Cauwet, G. (2002). DOM in the Coastal Zone. In Biogeochemistry of Marine Dissolved Organic Matter, D.A. Hansell, and C.A. Carlson, eds. (Elsevier Science (USA)), pp. 579-609.

CBP (online database) (www.chesapeakebay.net/data/index.htm).

Cerco, C.F., and Noel, M.R. (2004). Process-based primary production modeling in Chesapeake Bay. Marine Ecology Progress Series *282*, 45-58.

Chen, S.-N., and Sanford, L.P. (2009). Axial Wind Effects on Stratification and Longitudinal Salt Transport in an Idealized Partially Mixed Estuary. Journal of Physical Oceanography *39*, 1905-1920.

Chen, S.-N., Sanford, L.P., and Ralston, D.K. (2009). Lateral circulation and sediment transport driven by axial winds in an idealized, partially mixed estuary. Journal of Geophysical Research *114*.

Chen, W., and Wangersky, P.J. (1996). Rates of microbial degradation of dissolved organic carbon from phytoplankton cultures. Journal of Plankton Research *18*, 1521-1533.

Cherrier, J., and Bauer, J.E. (2004). Bacterial utilization of transient plankton-derived dissolved organic carbon and nitrogen inputs in surface ocean waters. Aquatic Microbial Ecology *35*, 229-241.

Christian, J.R., and Anderson, T.R. (2002). Modeling DOM Biogeochemistry. In Biogeochemistry of Marine Dissolved Organic Matter, D.A. Hansell, and C.A. Carlson, eds. (Elsevier Science (USA)), pp. 717-755.

Christian, J.R., Verschell, M.A., Murtugudde, R., Busalacchi, A.J., and McClain, C.R. (2002). Biogeochemical modelling of the tropical Pacific Ocean. I. Seasonal and interannual variability. Deep-Sea Research II *49*, 509-543.

Chu, D. (2004). EasyKrig3.0.

Cloern, J.E., Grenz, C., and Lucas, L.V. (1995). An empirical model of the phytoplankton chlorophyll : carbon ratio - the conversion factor between productivity and growth rate. Limnology and Oceanography *40*, 1313-1321.

Cohen, R.R.H. (1985). Physical processes and the ecology of a winter dinoflagellate bloom of *Katodinium rotundatum*. Marine Ecology Progress Series *26*, 135-144.

Cole, J.J., and Caraco, N.F. (2001). Carbon in catchments: connecting terrestrial carbon losses with aquatic metabolism. Marine and Freshwater Research *52*, 101-110.

Collos, Y., Vaquer, A., and Souchu, P. (2005). Acclimation of nitrate uptake by phytoplankton to high substrate levels. Journal of Phycology *41*, 466-478.

Connolly, J.P., Coffin, R.B., and Landeck, R.E. (1992). Modeling carbon utilization by bacteria in natural water systems. In Modeling the Metabolic and Physiologic Activities of Micro-organisms, C.J. Hurst, ed. (New York, John Wiley), pp. 249-276.

Crump, B.C., Hopkinson, C.S., Sogin, M.L., and Hobbie, J.E. (2004). Microbial biogeography along an estuarine salinity gradient: the combined influences of bacterial growth and residence time. Applied Environmental Microbiology *70*, 1494-1505.

Danielsdottier, M.G., Brett, M.T., and Arhonditsis, G.B. (2007). Phytoplankton food quality control of plankton food web processes. Hydrobiologia *589*, 29-41.

David, V., Sautour, B., Galois, R., and Chardy, P. (2006). The paradox high zooplankton biomass-low vegetal particulate organic matter in high turbidity zones: What way for energy transfer? Journal of Experimental Marine Biology and Ecology *333*, 202-218.

del Giorgio, P.A., and Cole, J.J. (1998). Bacterial Growth Efficiency in Natural Aquatic Systems. Annual Review of Ecology and Systematics *29*, 503-541.

Del Giorgio, P.A., and Williams, P.J.l.B. (2005). Respiration in Aquatic Ecosystems (Oxford University Press).

Dolan, J.R., and Coats, D.W. (1990). Seasonal Abundances of Planktonic Ciliates and Microflagellages in Mesohaline Chesapeake Bay Waters. Estuarine Coastal And Shelf Science *31*, 157-175.

Druffel, E.M.R., Bauer, J.E., Williams, P.M., Griffin, S., and Wolgast, D.M. (1996). Seasonal variability of particulate organic radiocarbon in the northeast Pacific Ocean. Journal of Geophysical Research *101*, 543-552.

Ducklow, H.W. (1999). The bacterial component of the oceanic euphotic zone. FEMS Microbiology Ecology *30*, 1-10.

Ducklow, H.W. (2001). Bacterioplankton. In Encyclopedia of Ocean Sciences, J.H. Steele, S.A. Thorpe, and K.K. Turekian, eds. (Academic Press), pp. 217-223.

Ducklow, H.W., and Carlson, C.A. (1992). Oceanic Bacterial Production. In Advances in Microbial Ecology, K.C. Marshall, ed. (New York, Plenum Press), pp. 113-181.

Elser, J.J., Bracken, M.E.S., Cleland, E.E., Gruner, D.S., Harpole, W.S., Hillebrand, H., Ngai, J.T., Seabloom, E.W., Shurin, J.B., and Smith, J.E. (2007). Global analysis of nitrogen and phosphorus limitation of primary producers in freshwater, marine and terrestrial ecosystems. Ecology Letters *10*, 1135-1142.

Eppley, R.W. (1972). Temperature and phytoplankton growth in the sea. Fisheries Bulletin *70*, 1063-1085.

Eppley, R.W., Rogers, J.N., and McCarthy, J.J. (1969). Half-saturation constants for uptake of nitrate and ammonium by marine phytoplankton. Limnology and Oceanography *14*, 912-920.

Fan, C., Glibert, P.M., Alexander, J., and Lomas, M.W. (2003). Characterization of urease activity in three marine phytoplankton species, *Aureococcus anophagefferens, Protocentrum minimum,* and *Thalassiosira weissflogii*. Marine Biology *142*, 949-958.

Fasham, M.J.R., Ducklow, H.W., and McKelvie, S.M. (1990). A nitrogen-based model of plankton dynamics in the oceanic mixed layer. Journal of Marine Research *48*, 591-639.

Ferrier-Pages, C., and Rassoulzadegan, F. (1994). N Remineralization in Planktonic Protozoa. Limnology and Oceanography *39*, 411-419.

Fischer, U.R., Weisz, W., Wieltschnig, C., Kirschner, A.K.T., and Velimirov, B. (2004). Benthic and pelagic viral decay experiments: a model-based analysis and its applicability. Applied & Environmental Microbiology *70*, 6706-6713.

Fisher, T.R., Gustafson, A.B., Radcliffe, G.M., Sundberg, K.L., and Stevenson, J.C. (2003). A Long-term Record of Photosynthetically Available Radiation (PAR) and Total Solar Energy at 38.6°N, 78.2°W. Estuaries *26*, 1450-1460.

Fisher, T.R., Hagy, J.D., and Rochelle-Newall, E.J. (1998). Dissolved and Particulate Organic Carbon in Chesapeake Bay. Estuaries *21*, 215-229.

Fisher, T.R., Harding, L.W.J., Stanely, D.W., and Ward, L.G. (1988). Phytoplankton, Nutrients, and Turbidity in the Chesapeake, Delaware, and Hudson Estuaries. Estuarine, Coastal and Shelf Science *27*, 61-93.

Flynn, K.J., Clark, D.R., and Xue, Y. (2008). Modeling the release of dissolved organic matter by phytoplankton. Journal of Phycology *44*, 1171-1187.

Fuhrman, J.A. (1992). Bacterioplankton Roles In Cycling Of Organic Matter: The Microbial Food Web. In Primary Productivity and Biogeochemical Cycles in the Sea, P.G. Falkowski, and A.D. Woodhead, eds. (New York, Plenum), pp. 361-383.

Fuhrman, J.A. (1999). Marine viruses and their biogeochemical and ecological effects. Nature *399*, 541-548.

Fukuda, R., Ogawa, H., Nagata, T., and Koike, I. (1998). Direct Determination of Carbon and Nitrogen Contents of Natural Bacterial Assemblages in Marine Environments. Applied & Environmental Microbiology *64*, 3352-3358.

Gasol, J.M., Giorgio, P.A.d., and Duarte, C.M. (1997). Biomass distribution in marine planktonic communities. Limnology and Oceanography *42*, 1353-1363.

Glibert, P.M. (1998). Interactions of top-down and bottom-up control in planktonic nitrogen cycling. Hydrobiologia *363*, 1-12.

Glibert, P.M., Dennett, M.R., and Caron, D.A. (1988). Nitrogen uptake and NH_4^+ regeneration by pelagic microplankton and marine snow from the North Atlantic. Journal of Marine Research *46*, 837-852.

Gobler, C.J., Hutchins, D.A., Fisher, N.S., Cosper, E.M., and Sanudo-Wilhelmy, S.A. (1997). Release and bioavailablility of C, N, P, Se, and Fe following viral lysis of a marine chrysophyte. Limnology and Oceanography *42*, 1492-1504.

Gobler, C.J., and Sañudo-Wilhelmy, S.A. (2003). Cycling of colloidal organic carbon and nitrogen during an estuarine phytoplankton bloom. Limnology and Oceanography *48*, 2314-2320.

Hamm, C.E. (2000). Architecture, ecology and biogeochemistry of *Phaeocystis* colonies. Journal of Sea Research *43*, 307-315.

Hansell, D.A. (2002). DOC in the Global Ocean Carbon Cycle. In Biogeochemistry of Marine Dissolved Organic Matter, D.A. Hansell, and C.A. Carlson, eds. (Elsevier Science (USA)), pp. 685-715.

Hansell, D.A., and Carlson, C.A. (1998). Deep ocean gradients in dissolved organic carbon concentrations. Nature *395*, 263-266.

Hansell, D.A., and Carlson, C.A., eds. (2002). Biogeochemistry of Marine Dissolved Organic Matter (Academic Press).

Hansen, B., Bjornsen, P.K., and Hansen, P.J. (1994). The Size Ratio Between Planktonic Predators and Their Prey. Limnology and Oceanography *39*, 395-403.

Hansen, D.V., and Rattray, M. (1965). Gravitational circulation in straits and estuaries. Journal of Marine Research *23*, 104-122.

Harding, L.W. (1994). Long-term trends in the distribution of phytoplankton in Chesapeake Bay: roles of light, nutrients and streamflow. Marine Ecology Progress Series *104*, 267-291.

Harding, L.W., Mallonee, M.E., and Perry, E.S. (2002). Toward a Predictive Understanding of Primary Productivity in a Temperate, Partially Stratified Estuary. Estuarine Coastal And Shelf Science *55*.

Harding, L.W., Meeson, B.W., and Fisher, T.R. (1986). Phytoplankton Production in Two East Coast Estuaries: Photosynthesis-Light Functions and Patterns of Carbon Assimilation in Chesapeake and Delaware Bays. Estuarine, Coastal and Shelf Science *23*, 773-806.

Harrison, W.G., Harris, L.R., and Irwin, B.D. (1996). The Kinetics of Nitrogen Utilization in the Oceanic Mixed Layer: Nitrate and Ammonium Interactions at Nanomolar Concentrations. Limnology and Oceanography *41*, 16-32.

Hartman, K.J., Howell, J., and Sweka, J.A. (2004). Diet and daily ration of bay anchovy in the Hudson River, New York. Transactions of the American Fisheries Society *133*, 762-771.

Hedges, J.I., Eglinton, G., Hatcher, P.G., Kirchman, D.L., Arnosti, C., Derenne, S., Evershed, R.P., Kogel-Knabner, I., de Leeuw, J.W., Littke, R.*, et al.* (2000). The molecularly-uncharacterized component of nonliving organic matter in natural environments. Organic Geochemistry *31*, 945-958.

Heinle, D.R., and Flemer, D.A. (1975). Carbon requirements of a population of the estuarine copepod *Eurytemora affinis*. Marine Biology *31*, 235-247.

Hood, R.R., Bates, N.R., Capone, D.G., and Olson, D.B. (2001). Modeling the effect of nitrogen fixation on carbon and nitrogen fluxes at BATS. Deep-Sea Research II *48*, 1609-1648.

Hopkinson, C.S., Buffam, I., Hobbie, J.E., Vallino, J.J., Perdue, M., Eversmeyer, B., Prahl, F., Covert, J., Hodson, R., Moran, M.A.*, et al.* (1998). Terrestrial inputs of organic matter to coastal ecosystems: An intercomparison of chemical characteristics and bioavailability. Biogeochemistry *43*, 211-234.

Horrigan, S.G., Montoya, J.P., Nevins, J.L., McCarthy, J.J., Ducklow, H., Goericke, R., and Malone, T.C. (1990). Nitrogenous Nutrient Transformations in the Spring and Fall in the Chesapeake Bay. Estuarine, Coastal And Shelf Science *30*, 369-391.

Hummel, H., Moerland, G., and Bakker, C. (1988). The concomitant existence of a typical coastal and a detitus food chain in the Westerschelde estuary. Hydrobiological Bulletin *22*, 35-41.

Huntley, M.E., and Lopez, M.D.G. (1992). Temperature-dependent production of marine copepods - a global synthesis. American Nature *140*, 210-242.

Irigoien, X., Meyer, B., Harris, R., and Harbour, D. (2004). Using HPLC pigment analysis to investigate phytoplankton taxonomy: the importance of knowing your species. Helgoland Marine Research *58*, 77-82.

Jeffrey, S.W. (1974). Profiles of photosynthetic pigments in the ocean using thin-layer chromatography. Marine Biology *26*, 101-110.

Jeffrey, S.W. (1980). Algal pigment systems. In Primary Productivity in the Sea, P.G. Falkowski, ed. (New York, Plenum Press), pp. 33-58.

Jeffrey, S.W., and Hallegraeff, G.M. (1986). Chlorophyllase distribution in ten classes of phytoplankton: a problem for chlorophyll analysis. Marine Ecology Progress Series *35*, 293-304.

Jeong, H.J., Park, J.Y., Nho, J.H., Park, M.O., Ha, J.H., Seong, K.A., Jeng, C., Seong, C.N., Lee, K.Y., and Yih, W.H. (2005). Feeding by red-tide dinoflagellates on the cyanobacterium *Synechococcus*. Aquatic Microbial Ecology *41*, 131-143.

Ji, R., and Franks, P.J.S. (2007). Vertical migration of dinoflagellates: model analysis of strategies, growth, and vertical distribution patterns. Marine Ecology Progress Series *344*, 49-61.

Johnson, M.D., Rome, M., and Stoecker, D.K. (2003). Microzooplankton grazing on *Prorocentrum minimum* and *Karlodinium micrum* in Chesapeake Bay. Limnology and Oceanography *48*, 238-248.

Joiris, C., Billen, G., Lancelot, C., Daro, M.H., Mommaerts, J.P., Bertels, A., Bossicart, M., Nijs, J., and Hecq, J.H. (1982). A budget of carbon cycling in the Belgian coastal zone: relative roles of zooplankton, bacterioplankton and benthos in the utilization of primary production. Netherlands Journal of Sea Research *16*, 260-275.

Jonas, R.B., and Tuttle, J.H. (1990). Bacterioplankton and Organic Carbon Dynamics in the Lower Mesohaline Chesapeake Bay. Applied & Environmental Microbiology *56*, 747-757.

Keller, D.P. (personal observation in 2007 and 2008).

Keller, D.P., and Hood, R.R. (2010). Modeling the Seasonal Cycle of Dissolved Organic Carbon and Nitrogen at Station CB3.3C in the Upper Chesapeake Bay. Journal of Marine Systems *submitted*.

Kemp, W.M., Smith, E.M., Marvin Di Pasquale, M., and Boynton, W.R. (1997a). Organic carbon balance and net ecosystem metabolism in Chesapeake Bay. Marine Ecology Progress Series *150*, 229-248.

Kemp, W.M., Smith, E.M., Marvin-DiPasquale, M., and Boynton, W.R. (1997b). Organic carbon balance and net ecosystem metabolism in Chesapeake Bay. Marine Ecology Progress Series *150*, 229-248.

Kimmel, D.G., and Roman, M.R. (2004). Long-term trends in mesozooplankton abundance in Chesapeake Bay USA: influence of freshwater input. Marine Ecology Progress Series *267*, 71-83.

Kiørboe, T., Møhlenberg, F., and Hamburger, K. (1985). Bioenergetics of the planktonic copepod *Acartia tonsa*: relation between feeding, egg production and respiration, and composition of specific dynamic action. Marine Ecology Progress Series *26*, 85-97.

Kleppel, G.S. (1993). On the diets of calanoid copepods. Marine Ecology Progress Series *99*, 183-195.

Koopmans, D.J., and Bronk, D.A. (2002). Photochemical production of dissolved inorganic nitrogen and primary amines from dissolved organic nitrogen in waters of two estuaries and adjacent surficial groundwaters. Aquatic Microbial Ecology *26*, 295-304.

Kragh, T., and Søndergaard, M. (2009). Production and decomposition of new DOC by marine plankton communities: carbohydrates, refractory components and nutrient limitation. Biogeochemistry *96*, 177-187.

Lancelot, C., Keller, M.D., Rousseau, V., Smith, W.O., and Mathot, S. (1998). Autoecology of the marine haptophyte *Phaeocystis* sp. In Physiological ecology of harmful algal blooms, D.M. Anderson, A.D. Cembella, and G.M. Hallegraeff, eds. (Berlin, Springer-Verlage), pp. 209-224.

Lancelot, C., and Mathot, S. (1987). Dynamics of a *Phaeocystis*-dominated spring bloom in Belgian coastal waters. I. Phytoplanktonic activities and related parameters. Marine Ecology Progress Series *37*, 239-248.

Landry, M.R., and Calbet, A. (2004). Microzooplankton production in the oceans. ICES Journal of Marine Science *61*, 501-507.

Lennon, J.T., and Martiny, J.B.H. (2008). Rapid evolution buffers ecosystem impacts of viruses in a microbial food web. Ecology Letters *11*, 1178-1188.

Levy, M., Memery, L., and Andre, J.-M. (1998). Simulation of primary production and export fluxes in the Northwestern Mediterranean Sea. Journal of Marine Research *56*, 197-238.

Lewis, V.P., and Peters, D.S. (1994). Diet of juvenile and adult atlantic menhaden in estuarine and coastal habitats. Transactions of the American Fisheries Society *123*, 803-810.

Lewitus, A.J., White, D.L., Tymowski, R.G., Geesey, M.E., Hymel, S.N., and Noble, P.A. (2005). Adapting the CHEMTAX method for assessing phytoplankton taxonomic composition in southeastern US estuaries. Estuaries *28*, 160-172.

Li, A., Stoecker, D.K., and Adolf, J.E. (1999). Feeding, pigmentation, photosynthesis and growth of the mixotrophic dinoflagellate *Gyrodinium galatheanum*. Aquatic Microbial Ecology *19*, 163-176.

Li, A., Stoecker, D.K., Coats, D.W., and Adam, E.J. (1996). Ingestion of fluorescently labeled and phycoerythrin-containing prey by mixotrophic dinoflagellates. Aquatic Microbial Ecology *10*, 139-147.

Loh, A.N., Bauer, J.E., and Canuel, E.A. (2006). Dissolved and particulate organic matter source-age characterization in the upper and lower Chesapeake Bay: A combined isotope and biochemical approach. Limnology and Oceanography *51*, 1421-1431.

Lomas, M.W., Trice, T.M., Glibert, P.M., Bronk, D.A., and McCarthy, J.J. (2002). Temporal and Spatial Dynamics of Urea Uptake and Regeneration Rates and Concentrations in Chesapeake Bay. Estuaries *25*, 469-482.

Louda, W.J., Li, J., Liu, L., Winfree, M.N., and Baker, E.W. (1998). Chlorophyll-*a* degradation during cellular senescence and death. Organic Geochemistry *29*, 1233-1251.

Mackey, M.D., Mackey, D.J., Higgins, H.W., and Wright, S.W. (1996). CHEMTAX - a program for estimating class abundances from chemical markers: application to HPLC measurements of phytoplankton. Marine Ecology Progress Series *144*, 265-283.

Malone, T.C. (1980). Size-Fractionated Primary Productivity of Marine Phytoplankton. In Primary Productivity in the Sea, P.G. Falkowski, ed. (New York, Plenum Press), pp. 301-319.

Malone, T.C., Conley, D.J., Fisher, T.R., Glibert, P.M., and Harding, L.W. (1996). Scales of Nutrient-Limited Phytoplankton Productivity in Chesapeake Bay. Estuaries *19*, 371-385.

Malone, T.C., Crocker, L.H., Pike, S.E., and Wendler, B.W. (1988). Influences of river flow in the dynamics of phytoplankton production in a partially stratified estuary. Marine Ecology Progress Series *48*, 235-249.

Malone, T.C., Ducklow, H.W., Peele, E.R., and Pike, S.E. (1991). Picoplankton carbon flux in Chesapeake Bay. Marine Ecology Progress Series *78*, 11-22.

Mannino, A., and Harvey, H.R. (2000). Biochemical composition of particles and dissolved organic matter along an estuarine gradient: Sources and implications for DOM reactivity. Limnology and Oceanography *45*, 775-788.

Marshall, H.G. (1994). Chesapeake Bay Phytoplankton: I. Composition. Proceedings of the Biological Society of Washington *107*, 573-585.

Marshall, H.G., Burchardt, L., and Lacouture, R.V. (2005). A review of phytoplankton composition within Chesapeake Bay and its tidal estuaries. Journal of Plankton Research *27*, 1083-1102.

Marshall, H.G., Lacouture, R.V., Buchanan, C., and Johnson, J.M. (2006). Phytoplankton assemblages associated with water quality and salinity regions in Chespeake Bay, USA. Estuarine Coastal And Shelf Science *69*, 10-18.

Martin, A.P., and Pondaven, P. (2006). New primary production and nitrification in the western subtropical North Atlantic: A modeling study. Global Biogeochemical Cycles *20*, GB4014.

Mayer, L., Schick, L.L., Hardy, K.R., and Estapa, M.L. (2009). Photodissolution and other photochemical changes upon irradiation of algal detritus. Limnology and Oceanography *54*, 1688-1698.

Mazzone, H.M. (1998). CRC handbook of viruses: mass-molecular weight values and related properties (CRC Press).

McCreary, J.P., Jr., Kohler, K.E., Hood, R.R., and Olson, D.B. (1996). A four-component ecosystem model of biological activity in the Arabian Sea. Progress in Oceanography *37*, 193-240.

McManus, G.B., and Ederington-Cantrell, M.C. (1992). Phytoplankton pigments and growth rates, and microzooplankton grazing in a large temperate estuary. Marine Ecology Progress Series *87*, 77-85.

Meon, B., and Kirchman, D.L. (2001). Dynamics and molecular composition of dissolved organic material during experimental phytoplankton blooms. Marine Chemistry *75*, 185-199.

Metzler, P., Glibert, P.M., Gaeta, S.A., and Ludlam, J.M. (1997). New and regenerated production in the South Atlantic off Brazil. Deep-Sea Research I *44*, 363-384.

Miller, W.L., and Zepp, R.G. (1995). Photochemical production of dissolved inorganic carbon from terrestrial organic matter: Significance to the oceanic carbon cycle. Geophysical Research Letters *22*, 417-420.

Møller, E.F. (2005). Sloppy feeding in marine copepods: prey-size-dependent production of dissolved organic carbon. Journal of Plankton Research *27*, 27-35.

Møller, E.F. (2007). Production of dissolved organic carbon by sloppy feeding in the copepods Acartia tonsa, Centropages typicus, and Temora longicornis. Limnology and Oceanography *52*, 79-84.

Møller, E.F., and Nielsen, T.G. (2001). Production of bacterial substrate by marine copepods: Effect of phytoplankton biomass and cell size. Journal of Plankton Research *23*, 527-536.

Mopper, K., and Kieber, D.J. (2002). Photochemistry and the Cycling of Carbon, Sulfur, Nitrogen and Phosphorus. In Biogeochemistry of Marine Dissolved Organic Matter, D.A. Hansell, and C.A. Carlson, eds. (Elsevier Science (USA)), pp. 455-508.

MOVE. Microbial Observatory for Virioplankton Ecology website. In wwwdbiudeledu/MOVE/MO_indexhtm.

Mulholland, M.R., Gobler, C.J., and Lee, C. (2002). Peptide hydrolysis, amino acid oxidation, and nitrogen uptake in communities seasonally dominated by *Aureococcus anophagefferens*. Limnology and Oceanography *47*, 1094-1108.

Mulholland, M.R., Lee, C., and Glibert, P.M. (2003). Extracellular enzyme activity and uptake of carbon and nitrogen along an estuarine salinity and nutrient gradient. Marine Ecology Progress Series *258*, 3-17.

Müller, H., and Geller, W. (1993). Maximum growth rates of aquatic ciliated protozoa: The dependence on body size and temperature reconsidered. Archives of Hydrobiology *126*, 315-327.

Muylaert, K., and Sabbe, K. (1999). Spring phytoplankton assemblages in and around the maximum turbidity zone of the estuaries of the Elbe (Germany), the Schelde (Belgium/The Netherlands) and the Gironde (France). Journal of Marine Systems *22*, 133-149.

Nagata, T. (2000). Production Mechanisms of Dissolved Organic Matter. In Microbial Ecology of the Oceans, D.L. Kirchman, ed. (Wiley-Liss, Inc.), pp. 121-152.

Nagata, T., and Kirchman, D.L. (1991). Release of dissolved free and combined amino acids by bacterivorous marine flagellates. Limnology and Oceanography *36*, 433-443.

Nakamura, Y., Suzuki, S.-y., and Hiromi, J. (1995). Growth and grazing of a naked heterotrophic dinoflagellate, *Gyrodinium dominans*. Aquatic Microbial Ecology *9*, 157-164.

Nelson, J.R. (1993). Rates and possible mechanism of light-dependent degradation of pigments in detritus derived from phytoplankton. Journal of Marine Research *51*, 155-179.

North, E.W., and Houde, E.D. (2001). Retention of White Perch and Stripped Bass Larvae: Biological-Physical Interactions in Chesapeake Bay Estuarine Turbidity Maximum. Estuaries *24*, 756-769.

North, E.W., and Houde, E.D. (2003). Linking ETM physics, zooplankton prey, and fish early-life histories to stripped bass *Morone saxatilis* and white perch *M. americana* recruitment. Marine Ecology Progress Series *260*, 219-236.

Obernosterer, I., Sempéré, R., and Herndl, G.J. (2001). Ultraviolet radiation induces reversal of the bioavailability of DOM to marine bacterioplankton. Aquatic Microbial Ecology *24*, 61-68.

Ogawa, H., Amagai, Y., Koike, I., Kaiser, K., and Benner, R. (2001). Production of Refractory Dissolved Organic Matter by Bacteria. Science *292*, 917-920.

Owen, M.J. (1976). Determination of the settling velocities of cohesive sands. Hydraulics Research Report No IT161.

Paerl, H.W., Valdes, L.M., Peierls, B.L., Adolf, J.E., and Harding Jr., L.W. (2006). Anthropogenic and climatic influences on the eutrophication of large estuarine ecosystems. Limnology and Oceanography *51*, 448-462.

Peperzak, L. (1993). Daily irradiance governs growth rate and colony formation of *Phaeocystis* (Prymnesiophyceae). Journal of Plankton Research *15*, 809-821.

Peperzak, L., Duin, R.N.M., Colijn, F., and Gieskes, W.W.C. (2000). Growth and mortality of flagellates and non-flagellate cells of *Phaeocystis globosa* (Prymnesiophyceae). Journal of Plankton Research *22*, 107-119.

Platt, T., Gallegos, C.J., and Harrison, W.G. (1980). Photoinhibiton of photosynthesis in natural assemblages of marine phytoplankton. Journal of Marine Research *38*, 678-701.

Press, W.H., Teukolsky, S.A., Vetterling, W.T., and Flannery, B.P. (1992). Numerical Recipes in FORTRAN: the Art of Scientific Computing, 2 edn (Cambridge, New York, Cambridge University Press).

Purcell, J.E. (1992). Effects of predation by the scyphomedusan *Chrysaora quinquecirrha* on zooplankton populations in Chesapeake Bay, USA. Marine Ecology Progress Series *87*, 65-76.

Raven, J.A., and Kübler, J.E. (2002). New light on the scaling of metabolic rate within the size of algae. Journal of Phycology *38*, 11-16.

Raymond, P.A., and Bauer, J.E. (2001). DOC cycling in a temperate estuary: A mass balance approach using natural C-14 and C-13 isotopes. Limnology and Oceanography *46*, 655-667.

Repeta, D.J., and Aluwihare, L.I. (2006). High molecular weight dissolved organic carbon cycling as determined by radiocarbon measurements of neutral sugars. Limnology and Oceanography *51*, 1045-1053.

Rochelle-Newall, E.J., and Fisher, T.R. (2002). Chromophoric dissolved organic matter and dissolved organic carbon in Chesapeake Bay. Marine Chemistry *77*, 23-41.

Roman, M.R., Holliday, D.V., and Sanford, L.P. (2001). Temporal and spatial patterns of zooplankton in the Chesapeake Bay turbidity maximum. Marine Ecology Progress Series *213*, 215-227.

Ross, O.N., and Sharples, J. (2008). Swimming for survival: A role of phytoplankton motility in a stratified turbulent environment. Journal of Marine Systems *70*, 248-262.

Ruardij, P., Veldhuis, M.J.W., and Brussaard, C.P.D. (2005). Modeling the bloom dynamics of the polymorphic phytoplankter *Phaeocystis globosa*: impact of grazers and viruses. Harmful Algae *4*, 941-963.

Saito, M.A., Goepfert, T.J., and Ritt, J.T. (2008). Some thoughts on the concept of colimitation: Three definitions and the importance of bioavailability. Limnology and Oceanography *53*, 276-290.

Sanford, L.P., Suttles, S.E., and Halka, J.P. (2001). Reconsidering the Physics of the Chesapeake Bay Estuarine Turbidity Maximum. Estuaries *24*, 655-669.

Santschi, P.H., Guo, L.D., Baskaran, M., Trumbore, S., Southon, J., Bianchi, T.S., Honeyman, B., and Cifuentes, L. (1995). Isotopic evidence for the contemporary origin of high-molecular-weight organic-matter in oceanic environments. Geochmica et Cosmochimica Acta *59*, 625-631.

Sarthou, G., Timmermans, K.R., Blane, S., and Tréguer, P. (2005). Growth physiology and fate of diatoms in the ocean: a review. Journal of Sea Research *53*, 25-42.

Schoemann, V., Becquevort, S., Stefels, J., Rousseau, V., and Lancelot, C. (2005). *Phaeocystis* blooms in the global ocean and their controlling mechanisms: a review. Journal of Sea Research *53*, 43-66.

Schubel, J.R. (1968). Turbidity maximum of the northern Chesapeake Bay. Science *161*, 1013-1015.

Schubel, J.R., and Pritchard, D.W. (1986). Responses of Upper Chesapeake Bay to Variations in Discharge of the Susquehanna River. Estuaries *9*, 236-249.

Seitzinger, S.P., and Sanders, R.W. (1999). Atmospheric inputs of dissolved organic nitrogen simulate estuarine bacteria and phytoplankton. Limnology and Oceanography *44*, 721-730.

Sellner, K.G., Lacouture, R.V., Cibik, S.J., Brindley, A., and Brownlee, S.G. (1991). Importance of a Winter Dinoflagellate-Microflagellate Bloom in the Patuxent River Estuary. Estuarine Coastal And Shelf Science *32*, 27-42.

Shen, J., and Wang, H.V. (2007). Determining the age of water and long-term transport timescale of the Chesapeake Bay. Estuarine, Coastal and Shelf Science *74*, 585-598.

Sherr, E.B., and Sherr, B.F. (2002). Significance of predation by protists in aquatic microbial food webs. Antonie van Leeuwenhoek *81*, 293-308.

Sherr, E.B., and Sherr, B.F. (2007). Heterotrophic dinoflagellates: a significant component of microzooplankton biomass and major grazers of diatoms in the sea. Marine Ecology Progress Series *352*, 187-197.

Shiah, F.-K., and Ducklow, H.W. (1994a). Temperature and substrate regulation of bacterial abundance, production and specific growth rate in Chesapeake Bay, USA. Marine Ecology Progress Series *103*, 297-308.

Shiah, F.-K., and Ducklow, H.W. (1994b). Temperature regulation of heterotrophic bacterioplankton abundance, production, and specific growth rate in Chesapeake Bay. Limnology and Oceanography *39*, 1243-1258.

Shoji, J., North, E.W., and Houde, E.D. (2005). The feeding ecology of Morone americana larvae in the Chesapeake Bay estuarine turbidity maximum: the influence of physical conditions and prey concentrations. Journal Of Fish Biology *66*, 1328-1341.

Shuman, F.R., and Lorenzen, C.J. (1975). Quantitative degradation of chlorophyll by a marine herbivore. Limnology and Oceanography *20*, 580-586.

Six, K.D., and Maier-Reimer, E. (1996). Effects of plankton dynamics on seasonal carbon fluxes in an ocean general circulation model. Global Biogeochemical Cycles *10*, 559-583.

Smayda, T.J. (1970). The suspension and sinking of phytoplankton in the sea. Oceanography and Marine Biology Annual Review *8*, 353-414.

Smith, D.C., Simon, M., Alldredge, A.L., and Azam, F. (1992). Intense hydrolytic enzyme activity on marine aggregates and implications for rapid particle dissolution. Nature *359*, 139-141.

Smith, E.M., and Benner, R. (2005). Photochemical transformation of riverine dissolved organic matter: effects on estuarine bacterial metabolism and nutrient demand. Aquatic Microbial Ecology *40*, 37-50.

Smith, E.M., and Kemp, W.M. (1995). Seasonal and Regional Variations in Plankton Community Production and Respiration for Chesapeake Bay. Marine Ecology Progress Series *116*, 217-231.

Solomon, C.M., Lessard, E.J., Keil, R.G., and Foy, M. (2003). Characterization of extracellular polymers of *Phaeocystis globosa* and *P. antarctica*. Marine Ecology Progress Series *250*, 81-89.

SooHoo, J.B., and Kiefer, D.A. (1982a). Vertical distribution of phaeopigments - I. A simple grazing and photooxidative scheme for small particles. Deep-Sea Research A *29*, 1539-1551.

SooHoo, J.B., and Kiefer, D.A. (1982b). Vertical distribution of phaeopigments - II. Rates of production and kinetics of photooxidation. Deep-Sea Research A *29*, 1553-1563.

Steele, J.H., and Henderson, E.W. (1992). The role of predation in plankton models. Journal of Plankton Research *14*, 157-172.

Stefels, J., Steinke, M., Turner, S., Malin, G., and Belviso, S. (2007). Environmental constraints on the production and removal of the climatically active gas dimethylsulphide (DMS) and implications for ecosystem modelling. Biogeochemistry *83*, 245-275.

Steinberg, D.K., Carlson, C.A., Bates, N.R., Goldthwait, S.A., Madin, L.P., and Michaels, A.F. (2000). Zooplankton vertical migration and the active transport of dissolved organic and inorganic carbon in the Sargasso Sea. Deep-Sea Research I *47*.

Steinberg, D.K., Goldthwait, S.A., and Hansell, D.A. (2002). Zooplankton vertical migration and the active transport of dissolved organic and inorganic nitrogen in the Sargasso Sea. Deep-Sea Research I *49*.

Stickney, H.L., Hood, R.R., and Stoecker, D.K. (2000). The impact of mixotrophy on planktonic marine systems. Ecological Modelling *125*, 203-230.

Stoecker, D.K., and Gustafson, D.E. (2002). Predicting grazing mortality of an estuarine dinoflagellate, Pfiesteria piscicida. Marine Ecology Progress Series *233*, 31-38.

Stoecker, D.K., Michaels, A.E., and Davis, L.H. (1987). Grazing by the jellyfish, *Aurelia aurita*, on microzooplankton. Journal of Plankton Research *9*, 901-915.

Stolte, W., McCollin, T., Noordeloos, A.A.M., and Reigman, R. (1994). Effect of nitrogen source on the size distribution within marine phytoplankton populations. Journal of Experimental Marine Biology and Ecology *184*, 83-97.

Stow, C.A., Jolliff, J., McGillicuddy Jr., D.J., Doney, S.C., Allen, J.I., Friedrichs, M.A.M., Rose, K.A., and Wallhead, P. (2009). Skill assessment for coupled biological/physical models of marine systems. Journal of Marine Systems *76*, 4-15.

Suttle, C.A. (2007). Marine viruses - major players in the global ecosystem. Nature Reviews Microbiology *5*, 801-812.

Szybalski, W. (1974). Genetic and molecular map of *Escherichia coli* bacteriophage lambda. In Handbook of Microbiology (USA, CRC Press, Inc.).

Tang, K.W., Jakobsen, H.H., and Visser, A.W. (2001). *Phaeocystis globosa* (Prymnesiophyceae) and the planktonic food web: Feeding, growth, and trophic interactions among grazers. Limnology and Oceanography *46*, 1860-1870.

Tang, K.W., and Simó, R. (2003). Trophic uptake and transfer of DMSP in simple planktonic food chains. Aquatic Microbial Ecology *31*, 193-202.

Tanoue, E., Nishiyama, S., Kamo, M., and Tsugita, A. (1995). Bacterial membranes: Possible source of a major dissolved protein in seawater. Geochimica et Cosmochimica Acta *59*, 2643-2648.

Taylor, A.H., and Joint, I. (1990). A steady-state analysis of the 'microbial loop' in stratified systems. Marine Ecology Progress Series *59*, 1-17.

Thingstad, T.F. (2000). Control of Bacterial Growth In Idealized Food Webs. In Microbial Ecology of the Oceans, D.L. Kirchman, ed. (Wiley-Liss, Inc), pp. 229-260.

Thingstad, T.F., Havskum, H., Zweifel, U.L., Berdalet, E., Sala, M.M., Peters, F., Alcaraz, M., Scharek, R., Perez, M., Jacquet, S.*, et al.* (2007). Ability of a "minimum" microbial food web model to reproduce response patterns observed in mesocosms manipulated with N and P, glucose, and Si. Journal of Marine Systems *64*, 15-34.

Thornton, D.C.O. (2002). Diatom aggregation in the sea: mechanisms and ecological implications. European Journal of Phycology *37*, 149-161.

Thorp, J.H., and Delong, M.D. (2002). Dominance of autochthonous autotrophic carbon in food webs of heterotrophic rivers. Oikos *96*, 543-550.

Tian, R.C., Vezina, A.F., Legendre, L., Ingram, R.G., Klein, B., Packard, T., Roy, S., Savenkoff, C., Silverberg, N., Therriault, J.-C.*, et al.* (2000). Effects of pelagic food-web interactions and nutrient remineralization on the biogeochemical cycling of carbon: a modeling approach. Deep-Sea Research II *47*, 637-662.

Tillmann, U. (2004). Interactions between Planktonic Microalgae and Protozoan Grazers. Journal of Eukaryotic Microbiology *51*, 156-168.

Tyler, M.A., and Seliger, H.H. (1978). Annual subsurface transport of a red tide dinoflagellate to its bloom area: Water circulation patterns and organism distributions in the Chesapeake Bay. Limnology and Oceanography *23*, 227-246.

Tyler, M.A., and Seliger, H.H. (1981). Selection for a red tide organism: Physiological responses to the physical environment. Limnology and Oceanography *26*, 310-324.

Tyler, M.A., and Seliger, H.H. (1989). Time scale variations of estuarine stratification parameters and impact on the food chains of the Chesapeake Bay. In Estuarine Circulation, B.J. Neilson, J. Brubaker, and A. Kuo, eds. (Clifton, NJ, The Humana Press Inc.).

Tzortziou, M., Neale, P.J., Osburn, C.L., Megonigal, J.P., Maie, N., and Jaffé, R. (2008). Tidal marshes as a source of optically and chemically distinctive colored dissolved organic matter in the Chesapeake Bay. Limnology and Oceanography *53*, 148-159.

U.S.G.S. http://va.water.usgs.gov/chesbay/RIMP/adaps.html (streamflow database).

Valdes-Weaver, L.M., Piehler, M.F., Pinckney, J.L., Howe, K.E., Rossignol, K., and Paerl, H.W. (2006). Long-term temporal and spatial trends in phytoplankton biomass and class-level taxonomic composition in the hydrologically variable Neuse-Pamlico estuarine continuum, North Carolina, USA. Limnology and Oceanography *51*, 1410-1420.

Vallino, J.J., Hopkinson, C.S., and Hobbie, J.E. (1996). Modeling Bacterial Utilization of Dissolved Organic Matter: Optimization Replaces Monod Growth Kinetics. Limnology and Oceanography *41*, 1591-1609.

Van Heukelem, L., and Thomas, C.S. (2001). Computer-assisted high-performance liquid chromatography method development with applications to the isolation and analysis of phytoplankton pigments. Journal of Chromatography A *910*, 31-49.

Varela, M.M., Bode, A., Fernández, E., Gónzalez, N., Kitidis, V., Varela, M., and Woodward, E.M.S. (2005). Nitrogen uptake and dissolved organic nitrogen release in planktonic communities characterized by phytoplankton size-structure in the Central Atlantic Ocean. Deep-Sea Research I *52*, 1637-1661.

Veldhuis, M.J.W., Colijn, F., and Venekamp, L.A.H. (1986). The spring bloom of *Phaeocystis pouchetii* (Haptophyceae) in Dutch coastal waters. Netherlands Journal of Sea Research *20*, 37-48.

Verdugo, P., Alldredge, A.L., Azam, F., Kirchman, D.L., Passow, U., and Santschi, P.H. (2004). The oceanic gel phase: a bridge in the DOM-POM continuum. Marine Chemistry *92*, 67-85.

Verity, P.G. (2000). Grazing experiments and model simulations of the role of zooplankton in *Phaeocystis* food webs. Journal of Sea Research *43*, 317-343.

Verity, P.G., Brussaard, C.P.D., Nejstgaard, J.C., van Leeuwe, M.A., Lancelot, C., and Medlin, L.K. (2007). Current understanding of *Phaeocystis* ecology and biogeochemistry, and perspectives for future research. Biogeochemistry *83*, 311-330.

Weinbauer, M.G. (2004). Ecology of prokaryotic viruses. FEMS Microbiology Reviews *28*, 127-181.

Weisse, T., and Scheffel-Möser, U. (1990). Growth and grazing loss in single-celled *Phaeocystis* sp. (Prymnesiophyceae). Marine Biology *106*, 153-158.

Wetz, M.S., Hales, B., and Wheeler, P.A. (2008). Degradation of phytoplankton-derived organic matter: Implications for carbon and nitrogen biogeochemistry in coastal ecosystems. Estuarine Coastal And Shelf Science *77*, 422-432.

White, J.R., and Roman, M.R. (1992). Seasonal study of grazing by metazoan zooplankton in the mesohaline Chesapeake Bay. Marine Ecology Progress Series *86*, 251-261.

Wilhelm, S.W., and Suttle, C.A. (1999). Viruses and Nutrient Cycles in the Sea. BioScience *49*, 781-788.

Winkler, G., Dodson, J.J., Bertrand, N., Thivierge, D., and Vincent, W.F. (2003). Trophic coupling across the St. Lawrence River estuarine transition zone. Marine Ecology Progress Series *251*, 59-73.

Wommack, E.K., and Colwell, R.R. (2000). Virioplankton: Viruses in Aquatic Ecosystems. Microbiology and Molecular Biology Reviews *64*, 69-114.

Wommack, E.K., Hill, R.T., Kessel, M., Russek-Cohen, E., and Colwell, R.R. (1992). Distribution of Viruses in the Chesapeake Bay. Applied & Environmental Microbiology *58*, 2965-2970.

Xu, J., and Hood, R.R. (2006). Modeling biogeochemical cycles in Chesapeake Bay with a coupled physical-biological model. Estuarine, Coastal and Shelf Science *69*, 19-46.

Xu, J.T., Hood, R.R., and Chao, S.Y. (2005). A simple empirical optical model for simulating light attenuation variability in a partially mixed estuary. Estuaries *28*, 572-580.

Yeager, C.L.J., Harding, L.W., and Mallonee, M.E. (2005). Phytoplankton production, biomass and community structure following a summer nutrient pulse in Chesapeake Bay. Aquatic Ecology *39*, 135-149.

Zhang, X., Roman, M.R., Kimmel, D., McGilliard, C., and Boicourt, W. (2006). Spatial variability in planktonic biomass and hydrographic variables along an axial transect in Chesapeake Bay. Journal of Geophysical Research *111*.